REPORT DOCUMENTATION PAGE

Form Approved OMB NO. 0704-0188

1. REPORT DATE (DD-MM-YYYY)	2. REPORT TYPE	3. DATES COVERED (From - To)
19-12-2015	Ph.D. Dissertation	-

4. TITLE AND SUBTITLE
Dancing to a different tune: adaptive evolution fine-tunes protein dynamics

5a. CONTRACT NUMBER
W911NF-11-1-0481

5b. GRANT NUMBER

5c. PROGRAM ELEMENT NUMBER
611102

6. AUTHORS
Katherine A. Donovan

5d. PROJECT NUMBER

5e. TASK NUMBER

5f. WORK UNIT NUMBER

7. PERFORMING ORGANIZATION NAMES AND ADDRESSES
University of Canterbury
20 Kirkwood Ave
Ilam
-

8. PERFORMING ORGANIZATION REPORT NUMBER

9. SPONSORING/MONITORING AGENCY NAME(S) AND ADDRESS (ES)
U.S. Army Research Office
P.O. Box 12211
Research Triangle Park, NC 27709-2211

10. SPONSOR/MONITOR'S ACRONYM(S)
ARO

11. SPONSOR/MONITOR'S REPORT NUMBER(S)
59767-LS.4

12. DISTRIBUTION AVAILIBILITY STATEMENT
Approved for public release; distribution is unlimited.

13. SUPPLEMENTARY NOTES
The views, opinions and/or findings contained in this report are those of the author(s) and should not contrued as an official Department of the Army position, policy or decision, unless so designated by other documentation.

14. ABSTRACT
The molecular mechanisms that underpin adaptive evolution are not well understood. This is largely because few studies relate evolved alleles (genotype) with their physiological changes (phenotype), which moves a population to better fit its environment (adaptation). The work described in this thesis provides a case study exploring the molecular changes underlying adaptive evolution in a key allosteric enzyme. It builds upon a long-term evolution experiment by Richard Lenksi, where twelve replicate populations of Escherichia coli have adapted in parallel to better fit their low glucose environment. I focus on the allosteric enzyme pyruvate kinase type 1, since has been

15. SUBJECT TERMS
pyruvate kinase

16. SECURITY CLASSIFICATION OF:			17. LIMITATION OF ABSTRACT	15. NUMBER OF PAGES	19a. NAME OF RESPONSIBLE PERSON
a. REPORT	b. ABSTRACT	c. THIS PAGE			Renwick Dobson
UU	UU	UU	UU		19b. TELEPHONE NUMBER +64-336-4298

Report Title

Dancing to a different tune: adaptive evolution fine-tunes protein dynamics

ABSTRACT

The molecular mechanisms that underpin adaptive evolution are not well understood. This is largely because few studies relate evolved alleles (genotype) with their physiological changes (phenotype), which moves a population to better fit its environment (adaptation). The work described in this thesis provides a case study exploring the molecular changes underlying adaptive evolution in a key allosteric enzyme. It builds upon a long-term evolution experiment by Richard Lenksi, where twelve replicate populations of Escherichia coli have adapted in parallel to better fit their low-glucose environment. I focus on the allosteric enzyme pyruvate kinase type 1, since has been shown to adapt to this environment.

First, I used X-ray crystallography to determine a higher resolution structure (2.2 Å) of the wild-type enzyme for comparison with the evolved enzymes. I resolved the ambiguous space-group problem that affects these crystals, and demonstrated that the kinetic function of the recombinant enzyme is the same as previously reported. In addition, I propose a new model for allosteric activation: a combination of structural and dynamic analyses determined that the allosteric signal is transferred by a series of dynamic changes between the allosteric site, upon fructose-1,6-bisphosphate binding, and the active site for increased substrate binding.

The functional analyses demonstrated that all eight evolved enzymes have a reduced activity compared to the wild-type at physiological substrate concentrations. Not only did the evolved enzymes show a parallel decrease in activity, but they all showed changes to substrate binding affinity and seven of the eight showed an altered allosteric activation mechanism. These results suggest that natural selection has selected for enzymes with a reduced activity by altering the functional mechanism of the evolved enzymes. However, in crystal and in solution structure characterisation determined that all of the evolved enzymes have maintained the same structural fold as the wild-type. Although the fold is the same, substrate binding promiscuity suggested a change in the flexibility of the enzyme, allowing substrates of different sizes and shapes to bind. Computational and experimental dynamics studies determined that natural selection has selected for altered dynamics in all of the evolved enzymes, and it has used altered dynamics to change the allostery of the enzymes. Therefore, this study provides the first example of adaptive evolution fine-tuning protein dynamics to alter allostery.

This thesis describes the molecular mechanisms underlying the adaptation of Escherichia coli to the low-glucose environment in Lenski's long-term evolution experiment. The adaptive mutations in Escherichia coli's pyruvate kinase type 1 serve to increase the availability of phosphoenolpyruvate for glucose uptake. From a molecular perspective, natural selection has selected for adaptive mutations that alter the dynamics to produce an enzyme with reduced catalytic activity at low phosphoenolpyruvate concentrations, thus decreasing phosphoenolpyruvate consumption. In addition, the adaptive mutations have altered the enzymes' affinity for the allosteric activator (fructose-1,6-bisphosphate), fine- tuning them to match the concentration of fructose-1,6-bisphosphate in the cell at the point of glucose re-introduction.

Overall, this work describes the intricate relationship between genetic changes and the resulting phenotype and demonstrates the parallel nature of adaptation for this particular case study. Whereby, parallel changes are mapped from organismal fitness, to enzyme function and to enzyme structure. The dynamic changes, however, are not parallel thus making predicting adaptive evolution difficult.

Dancing to a different tune: adaptive evolution fine-tunes protein dynamics

---

A thesis submitted in partial fulfilment of the

requirements for the degree of

Doctor of Philosophy in Biochemistry

in the School of Biological Sciences

by Katherine Aleisha Donovan

University of Canterbury

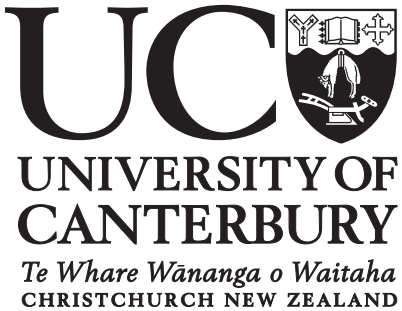

September 2015

Abstract

The molecular mechanisms that underpin adaptive evolution are not well understood. This is largely because few studies relate evolved alleles (genotype) with their physiological changes (phenotype), which moves a population to better fit its environment (adaptation). The work described in this thesis provides a case study exploring the molecular changes underlying adaptive evolution in a key allosteric enzyme. It builds upon a long-term evolution experiment by Richard Lenksi, where twelve replicate populations of *Escherichia coli* have adapted in parallel to better fit their low-glucose environment. I focus on the allosteric enzyme pyruvate kinase type 1, since has been shown to adapt to this environment.

First, I used X-ray crystallography to determine a higher resolution structure (2.2 Å) of the wild-type enzyme for comparison with the evolved enzymes. I resolved the ambiguous space-group problem that affects these crystals, and demonstrated that the kinetic function of the recombinant enzyme is the same as previously reported. In addition, I propose a new model for allosteric activation: a combination of structural and dynamic analyses determined that the allosteric signal is transferred by a series of dynamic changes between the allosteric site, upon fructose-1,6-bisphosphate binding, and the active site for increased substrate binding.

The functional analyses demonstrated that all eight evolved enzymes have a reduced activity compared to the wild-type at physiological substrate concentrations. Not only did the evolved enzymes show a parallel decrease in activity, but they all showed changes to substrate binding affinity and seven of the eight showed an altered allosteric activation mechanism. These results suggest that natural selection has selected for enzymes with a reduced activity by altering the functional mechanism of the evolved enzymes. However, *in crystal* and *in solution* structure characterisation determined that all of the evolved enzymes have maintained the same structural fold as the wild-type. Although the fold is the same, substrate binding promiscuity suggested a change in the flexibility of the enzyme, allowing substrates of different sizes and shapes to bind. Computational and

experimental dynamics studies determined that natural selection has selected for altered dynamics in all of the evolved enzymes, and it has used altered dynamics to change the allostery of the enzymes. Therefore, this study provides the first example of adaptive evolution fine-tuning protein dynamics to alter allostery.

This thesis describes the molecular mechanisms underlying the adaptation of *Escherichia coli* to the low-glucose environment in Lenski's long-term evolution experiment. The adaptive mutations in *Escherichia coli*'s pyruvate kinase type 1 serve to increase the availability of phosphoenolpyruvate for glucose uptake. From a molecular perspective, natural selection has selected for adaptive mutations that alter the dynamics to produce an enzyme with reduced catalytic activity at low phosphoenolpyruvate concentrations, thus decreasing phosphoenolpyruvate consumption. In addition, the adaptive mutations have altered the enzymes' affinity for the allosteric activator (fructose-1,6-bisphosphate), fine-tuning them to match the concentration of fructose-1,6-bisphosphate in the cell at the point of glucose re-introduction.

Overall, this work describes the intricate relationship between genetic changes and the resulting phenotype and demonstrates the parallel nature of adaptation for this particular case study. Whereby, parallel changes are mapped from organismal fitness, to enzyme function and to enzyme structure. The dynamic changes, however, are not parallel thus making predicting adaptive evolution difficult.

Acknowledgements

First of all, I owe my biggest thank you to my fantastic supervisor Renwick Dobson, for your unwavering support, enthusiasm, humour and great ideas. Thank you for all that you have taught me, and all of the amazing opportunities that you have provided me. I am so grateful to have had the opportunity to work with you. Thanks also to the other members of my PhD committee; Juliet, Tim, Sarah and Jack for your interest in my project, keeping me on track and for asking the tough questions.

A huge thanks to Rachel − I don't know how I would have made it through the emotional PhD rollercoaster without you, I am so grateful to have had you by my side throughout the entire process. Thank you to everyone else who has passed through the Dobson, Gerrard and Pearce labs over the last 4 years, especially Jeremy, Amy1, Amy2, Jen, Eric, Moe, Arvy, Chris and Akshita – you are all amazing people and even better friends. Each of you contributed to making my PhD days brighter, happier and so much more fun. Thank you to Juliet, Susie, Grant and Chris for always being available to answer my many questions and for providing excellent science and life advice, and Jackie for keeping me in line.

Thank you to all of the collaborators who helped to make this project such a great success. Tim and Fen, for the fitness data; Ash and Ben, for the MD simulations; Mike and Geoff, for crystallography guidance; and Derek, Shaolong and Peter for allowing me to join your lab and teaching me all about HDX.

Thank you to the various organisations that have provided financial assistance over the years: to the Marsden Fund and Army Research Office for a Doctoral scholarship; the Maurice Wilkins Centre, Journal of Cell Science, New Zealand Federation for Graduate Woman, New Zealand Society for Biochemistry and Molecular Biology and Royal Society for providing funds for travel to conferences and collaborating labs. Thanks to the New Zealand Synchrotron Group for supporting all of the tron trips, and to the Biomolecular Interaction Centre for providing access to a great range of equipment.

Thank you to my amazing supportive friends (Shari, Lynda, Penel, Melanie and Brock) for showing a genuine interest in my research, understanding my long periods of absence and encouraging me to succeed – I could not ask for better friends.

Thank you to my family, especially my parents for your everlasting love, support and encouragement − your positivity and words of wisdom made all the difference. And finally, lots of love and thanks to Josh, for being there for me at the best and worst of times. You made the last couple of years so much easier and more enjoyable.

Table of contents

Abbreviations

a	slope of the curve within T_m
ADP	adenosine diphosphate
ANOVA	analysis of variance
atm	atmospheric pressure
ATP	adenosine triphosphate
AtzA	atrazine chlorohydrolase
B-factor	temperature factor
BTP	bis-tris propane
CDP	cytodine diphosphate
Chi	discrepancy of the fit
C^{α}	alpha carbon
Da	dalton
d	spacing between layers of atoms
ddH_2O	double distilled water
dH_2O	distilled water
DSF	differential scanning fluorometry
DM25	davis minimal 25
DNA	deoxyribonucleic acid
D_{max}	maximum particle diameter
EDTA	ethylenediaminetetraacetic acid
ESI	electrospray ionisation
FBP	fructose-1,6-bisphosphate
fs	femtosecond
GDP	guanosine diphosphate
H	mass of a proton
HDX	hydrogen-deuterium exchange
HEPES	4-(2-hydroxyethyl)-1-piperazineethanesulfonic acid
HIC	hydrophobic interaction chromatography

*hok*B/*sok*B	toxin-antitoxin
HPLC	high pressure liquid chromatography
HSD	Honest Significant Difference
I	scattering intensity
ID	inside diameter
I(0)	forward scattering intensity
IDP	inosine diphosphate
IEC	anion exchange chromatography
IS	insertion sequence
K	kelvin
*K*d	dissociation constant
kcal	kilo calorie
kDa	kilo dalton
*K*i	inhibition constant
k_{cat}	catalytic turnover number
K_m	Michaelis-Menten constant
KCl	potassium chloride
KOH	potassium hydroxide
LB	Luria Bertani
LDH	lactate dehydrogenase
LL	minimum intensities
MalT	transcriptional activator of *E. coli* maltose regulon
MES	2-(*N*-morpholino)ethanesulfonic acid
mg	milligram
min	minute
mL	millilitre
mm	millimetre
mM	millimolar
MM	molecular mass
MgCl	magnesium chloride
MOPS	3-(N-morpholino)propanesulfonic acid
ms	millisecond
MS	mass spectrometry
MX1	macromolecular crystallography beamline 1

MX2	macromolecular crystallography beamline 2
m/z	mass-to-charge
n	integer number on the ion
NaCl	sodium chloride
NAD^+	nicotinamide adenine dinucleotide
NADH	nicotinamide adenine dinucleotide, reduced form
NADPH	nicotinamide adenine dinucleotide phospahte
*nad*R	gene codes for nicotinamide adenine dinucleotide
NCS	non crystallographic symmetry
*n*H	Hill coefficient
$(NH_4)_2SO_4$	ammonium sulphate
nL	nanolitre
nm	nanometre
ns	nanosecond
OD	outside diameter
OD_{600}	optical density at 600 nm
PAGE	polyacrylamide gel electrophoresis
*pbp*A-*rod*A	genes responsible for rod shape of *E. coli*
PDBePISA	Protein Interfaces, Surfaces and Assemblies service at the European Bioinformatics Institute
PDZ	second postsynaptic density-95/discs large/zonula occludens-1
PEP	phosphoenolpyruvate
PEG	polyethylene glycol
PK	pyruvate kinase
PK1	*Escherichia coli* pyruvate kinase type 1
PMMA	polymethyl methacrylate
ps	picosecond
PTFE	polytetrafluoroethylene
*pyk*F	gene codes for *E. coli* PK1
QqTOF	QSTAR Elite hybrid Quadrupole Time-of-Flight
RFU	relative fluorescence units
*R*g	radius of gyration
RMSD	root mean square deviation
RMSF	root mean square fluctuation

R-state	relaxed-state
R_{factor}	residual factor
R_{free}	free R_{factor}
s	second
s	momentum transfer
SAXS	small-angle X-ray scattering
SEC	size exclusion chromatography
SEM	standard error of the mean
SOC	super optimal broth with catabolic repressor
$S_{0.5}$	substrate concentration at half V_{max}
TRESI	time-resolved electrospray ionisation
TriA	melamine deaminase
T-state	tensed-state
T_m	melting temperature
UDP	uridine diphosphate
UL	maximum intensities
UV	ultraviolet
V	volts
v/v	volume to volume
V_{max}	maximum velocity
V_0	initial velocity
WT	wild-type
w/v	weight to volume
θ	scattering angle
[*ES*]	concentration of enzyme substrate complex
[*S*]	substrate concentration
µL	microlitre
µm	micrometre
λ	wavelength
Å	angstrom
°	degree
°C	degree Celsius
%	percent
σ	sigma

Chapter One

Introduction

The work described in this thesis focuses on the molecular adaptation of *Escherichia coli's* pyruvate kinase type 1 (PK1) enzyme, which adapted to produce a fitness benefit for the host, *E. coli*. Identifying the connection between altered alleles (genotype) and the resulting physiological properties (phenotype) is a major challenge in the study of evolutionary adaptation.[1] Characterising this connection is essential for developing an understanding of how adaptive mutations facilitate beneficial phenotypic changes. The work in this thesis provides a case study for investigating the molecular mechanisms that drive adaptation. This thesis describes the functional, structural and dynamic behaviours of eight adaptively evolved *E. coli* PK1 enzymes to probe the molecular mechanism of their action.

1.1 Enzyme evolution

1.1.1 Evolvability of enzymes

Natural selection, occurring over billions of years, refined generalist enzyme activities to be catalytically specialised for their metabolic role, allowing precise control of fluxes through metabolic pathways.[2] Today, the evolvability (a measure of ability to generate adaptive variation) of enzymes and the molecular mechanisms by which new catalytic functions arise is a 'hot topic', with studies suggesting that new enzymatic functions are the result of the promiscuous activities of specialist enzymes, such as substrate ambiguity.[2-4] For example, Seffernick *et al*.[5] proposed that substrate binding promiscuity and the

introduction of new chemical compounds enabled the divergence of melamine deaminase (TriA) and atrazine chlorohydrolase (AtzA) enzymes in *Pseudomonas* strains. The TriA and AtzA enzymes have a 98% sequence identity, corresponding to 9 of 475 different amino acids, yet they catalyse different reactions in different metabolic pathways. Therefore, Seffernick *et al*.[5] suggested that natural selection acted on the slight difference in sequence and fine-tuned the 'slight difference' into something more, a different function. The same is true for cytochrome P450 enzymes, which have been recognised as evolvable due to their natural functional diversity.[6] These enzymes are from a functionally diverse enzyme family with more than 11,000 members that produce large numbers of secondary metabolites. Laboratory studies have been successful in generating new activities in cytochrome P450 enzymes due to their mutational robustness and ability to accept new substrates, providing another example of enzyme diversification by exploiting substrate promiscuity.[6]

Promiscuous activities were recognised as important early on by Jensen, because they provide a selection of activities that can be recruited to assist the host in surviving changing environments.[4, 7] Jensen stated, "*broad substrate specificity provides a kind of biochemical leakiness [...], which is exploitable for gain of function*".[3, 7] If a host organism is exposed to an environment in which the promiscuous activity is beneficial, natural selection will act to increase the promiscuous activity and increase survival of subsequent generations, because natural selection acts on functions that either impair or improve host fitness and reproduction.

1.1.2 Adaptive enzyme evolution

Adaptation is the process by which a population moves towards a phenotype that represents a better fit to the environment. The variety of enzymatic functions found in nature is astonishing and the on going evolution of new enzymatic functions continues, as host organisms adapt to environmental perturbations.[2, 3] Point mutations appear randomly, but are rarely maintained in a population because their fitness consequences are often neutral or detrimental to the host's survival. However, mutations that are beneficial to the host can be selected for and will persist in subsequent generations, improving enzyme function to increase host survival in fluctuating environments.[4]

The ease with which populations adapt is exemplified when they evolve to survive our (human) interventions against them.[8] For instance, therapeutic agents, such as antibiotics, are introduced as a treatment for bacterial infections. Unfortunately, the overuse of antibiotics has provided a selection pressure for the success of antibiotic resistant phenotypes among bacterial strains.[9, 10] Also, the continual use of pesticides to protect crops has caused pesticide resistance in insects and plant pathogens.[8] For example, the introduction of insecticides in the 20th century has led to the evolution of phosphotriesterases to release phosphate from organophosphate insecticides in various bacteria, including *Pseudomonas diminuta*.[2, 11]

There are also many examples of adaptation to physiological challenges imposed by changing environments in nature. For example, studies into high altitude vertebrates identified modified haemoglobin function as an adaptive response to the hypoxic environment.[12, 13] A comparison of the high altitude bar-headed goose and its lowland sibling, the greylag goose demonstrated that a three amino acid substitution in haemoglobin enables the bar-headed goose an exceptionally high haemoglobin affinity to survive in the hypoxic high altitude environment.[12] The same increase in haemoglobin affinity for oxygen is found in deer mice that are living in hypoxic conditions.[13] Haemoglobin proteins from highland deer mice from the Rocky Mountains were compared to that of lowland deer mice from the Great Plains, revealing twelve amino acid substitutions that increase the oxygen binding affinity of the haemoglobin protein, thus increasing survival of highland deer mice in the hypoxic environment.[13]

Studies using laboratory-based enzyme evolution[14, 15] have identified the importance of factors such as the trade-off between catalytic function and stability,[15-17] and enzymatic promiscuity.[18, 19] However, one study carried out by Arnold *et al*.[20] used directed evolution to probe the extent to which the thermostability of subtilisin S41 can be increased without damaging the enzymes catalytic activity. The results determined that the trade-off between stability and catalytic ability is not unavoidable. This is demonstrated by the uncompromised catalytic efficiency at low temperatures when the enzymes from mesophilic bacteria were evolved to have stabilities as high as their thermophilic homologs. The work by Arnold *et al*. suggests that naturally evolved enzymes display a trade-off between stability and catalytic function because of the rarity of mutations that increase stability while maintaining catalytic function.[15, 20, 21] Unfortunately, the molecular

mechanisms underlying adaptive evolution is a relatively untouched field due to the time and difficulties required to evolve an organism to adapt to a specific selection pressure. This thesis uses adaptive evolution to investigate the molecular basis of a series of adaptive mutations in a key allosteric enzyme.

1.2 Linking genotype to phenotype

Adaptive forces such as natural selection select mutations that alter a population's genotype to enhance competitive fitness and reproduction within an environment. Barrett and Hoekstra described an adaptive allele as "*an allele that has functional effects on a phenotypic trait that produce an increase in fitness*".[22] A major challenge in the study of evolutionary adaptation is identifying the connection between the altered allele (genotype) and the subsequent physiological properties (phenotype),[1] to understand how adaptive mutations facilitate beneficial phenotypic changes.

Adaptive evolutionary changes are often difficult to identify because key events happen over long timescales. However, evolutionary experiments using viruses or bacterial populations allow us to witness genotypic and phenotypic changes as they occur in real time and the use of replicates provides a measure of the repeatability of evolutionary outcomes. Bacterial populations provide the ideal system for studying evolution because they allow us to circumvent many of the problems involved in studying evolution. They have large population sizes and short generation times,[23] and the bacterial system allows us to freeze and regenerate cells providing an opportunity to observe the effects of natural selection by investigating the mutations that prevail in the presence of specific selection pressures. Understanding an adaptive mutation requires identifying the relationship between genetic changes (genotype), physiological changes (phenotype) and fitness through functional effects.[22]

The study presented in this thesis investigates key facets of enzyme evolution by taking advantage of a long-term evolution experiment in *E. coli* to study the molecular mechanisms driving adaptation. In a long-term evolution experiment, twelve *E. coli* populations evolved a mutated genotype, altered phenotype and increased fitness to survive the implemented low-glucose selection pressure (Section 1.3). Therefore, this evolution experiment is identified as the perfect opportunity to ask key questions regarding enzyme

evolution because the study provides a model system for investigating the molecular mechanisms that drive evolutionary change in bacterial hosts.

1.3 Lenski's long-term evolution experiment

In the 1990's, Lenski *et al*.[24] decided to take advantage of the seemingly 'perfect' bacterial system to study both adaptation and divergence in natural selection using a long-term evolution experiment. Lenski began his study by creating twelve identical replicate populations of *E. coli* from a single asexual clone. These twelve replicates have been grown in identical low glucose Davis Minimal 25 (DM25) media at 37 °C for over 60,000 generations.[24, 25] The glucose concentration in the culture environment is controlled by a serial transfer regime, whereby each of the populations is diluted 100-fold each day into new glucose limited medium, permitting 6.64 generations of binary fission before the limiting glucose resource is exhausted.[25]

Examination of the populations at 10,000 generations revealed that all twelve replicate populations independently evolved larger cells (altered morphology),[25] which is unusual because under nutrient depleted conditions, bacteria generally show morphological changes such as reduced cell size.[23] Figure 1.1a shows that when the replicate populations (at 20,000 generations) were competed against the ancestor under the same conditions that were present during the evolution experiment,[24, 25] they show an overall increase in mean fitness of approximately 70%.[26] Moreover, the growth kinetics of the ancestral and replicate populations indicate that the derived genotypes have a shorter lag phase upon transfer into new medium (Figure 1.1b) as well as a faster growth rate (Figure 1.1c).[26, 27] Lenski's experimental system shows that all twelve populations independently evolved in parallel to produce a similar increased fitness in the minimal glucose medium compared to their common ancestor. Therefore, it seems that the parallel evolution is due to the appearance and fixation of beneficial mutations in all twelve replicate populations, a process commonly known as natural selection.[28]

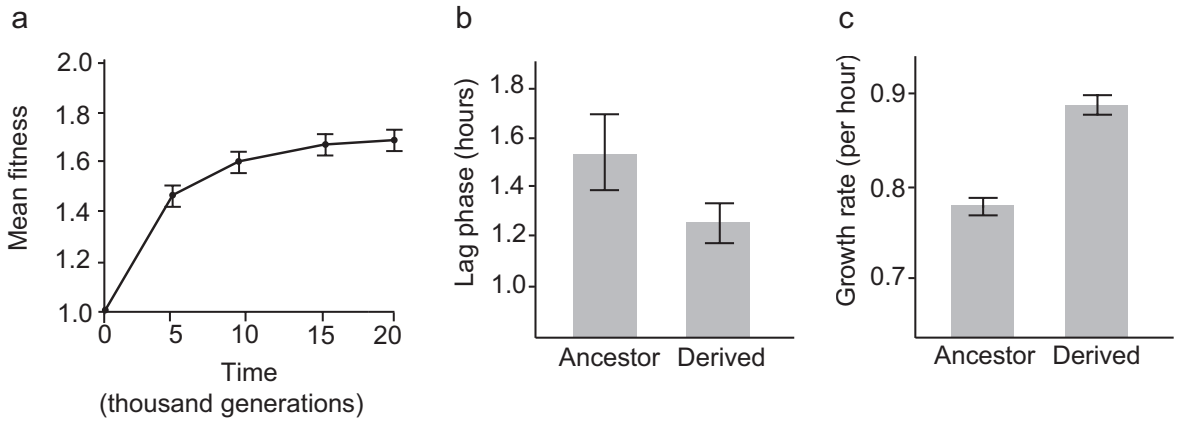

Figure 1.1 Increased fitness, decreased lag phase and increased growth rate of *E. coli* derived populations compared to ancestral populations during 20,000 generations in a glucose-limited medium. **(a)** Trajectory for mean fitness. Each point represents the mean of all twelve populations, and fitness of each population relative to the ancestor was measured with five-fold replication.[27] **(b)** Lag phase of ancestral and derived genotypes.[26] **(c)** Growth rate of ancestral and derived genotypes.[26] Error bars are 95% confidence intervals. Images replicated from referenced publications.[26, 29]

Genotypic analysis, suggested all descendants shared several fixed mutations. Remarkably, the genetic changes were concentrated in a small number of genes: *pyk*F, *nad*R, *hok*B/*sok*B and *pbp*A-*rod*A.[30, 31] Further analysis using four distinct statistical tests indicated that natural selection was probably the driving force behind the parallel evolution identified in the four candidate genes.[30] These tests measured: 1) the substitution rates between candidate genes and random genes; 2) the number of non-synonymous mutations relative to synonymous mutations; 3) substitution rate for beneficial mutations relative to neutral mutations and 4) the distribution of mutations across the twelve populations.

The mutations in *pyk*F occurred independently and were fixed in all twelve replicate populations, which is a strong indicator that the mutations in this gene are adaptive. Non-synonymous point mutations were identified in ten of the twelve populations, and the two other populations had an IS*150* and a frameshift mutation (Figure 1.2). Why does *pyk*F serve as an adaptive focus in the long-term evolution experiment? To answer this question, a molecular understanding of the effect of the genotypic changes upon the gene product and phenotype needs to be created.

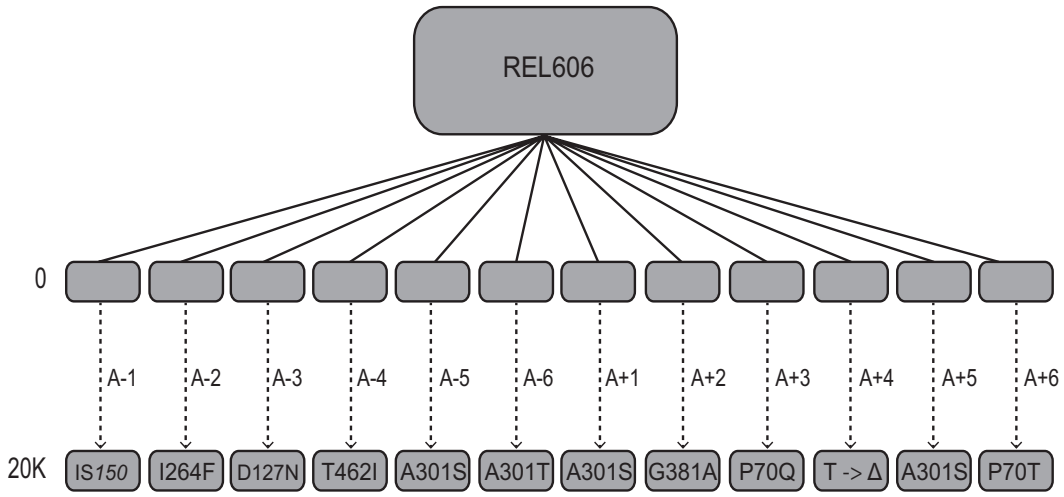

Figure 1.2 *pyk*F mutations identified from the long-term evolution experiment at 20,000 generations. Twelve replicate populations (numbered A-1 to A+6) were derived from the ancestor, REL606, and independently evolved in parallel in a glucose-limited environment. At 20,000 generations, one clone was isolated from each population and sequenced at candidate genes, identifying mutations in *pyk*F in all twelve populations. Point mutations were found in ten populations and the other two had an IS*150* and a frameshift mutation. The A301S mutation was identified in three independent populations. This image was created by Fen Peng.[32]

1.4 The influence of genetic background upon adaptation

The following work (Section 1.4) was carried out by Fen Peng, University of Houston. Fen and I were working in parallel on the same project, but with different roles. Fen's studies tested how similar the phenotypic effects of mutations in the same gene are, and whether the genetic background influences the phenotypic effect. To do this, two series of strains were created to allow direct comparison of the effect of independently evolved mutations in *pyk*F in a common genetic background and the evolved genetic background. The results conclude that mutations in the same gene present similar benefits, i.e. the genes are phenotypically parallel in the ancestral background, but have variable effects in their evolved background due to epistatic interactions with different sets of mutations that are fixed in each evolved population.[32]

1.4.1 Mutations in *pyk*F increase fitness in the isogenic ancestral background

Firstly, Fen wanted to assess how similar the phenotypic effects of mutations in the same gene are so she placed each of the eight evolved point mutation alleles and a deletion allele (to represent the IS*150* and frameshift) into the ancestral genetic background and measured the fitness effect relative to the ancestor. The results confirm that each of the mutations have a fitness benefit in and of themselves. Transfer of the evolved alleles into the ancestral background (common background) provided a strain series whereby the only fitness contribution is from the evolved gene. It was found that all eight of the non-synonymous evolved *pyk*F alleles produce similar fitness effects in the ancestral background, showing increases in fitness of 8% to 12% (Figure 1.3a). Interestingly, the fitness benefit caused by the evolved alleles is significantly different to that of the deletion allele, suggesting that the evolved enzymes retain some function for the benefit of the *E. coli*. These findings are consistent with other studies that found that different mutations in the same gene have similar fitness effects.[1]

1.4.2 Mutations in *pyk*F produce a varied fitness benefit in the evolved background

Next, the evolved alleles were placed into the evolved backgrounds at 20,000 generations to determine if the mutations have different fitness effects in their own evolved clones due to epistatic interactions with the genetic background. Movement of the evolved alleles into the evolved backgrounds is important because "*epistatic interactions are revealed when the contribution of a mutation to an organism's phenotype depends on the genetic background in which it occurs*"—Cooper *et al.*[33] Therefore, epistasis in these evolved populations will present as a different fitness effect to that observed when the evolved alleles were placed in the ancestral background. Any difference in fitness effect would be a result of the evolved *pyk*F alleles interacting with other mutations in the evolved background.

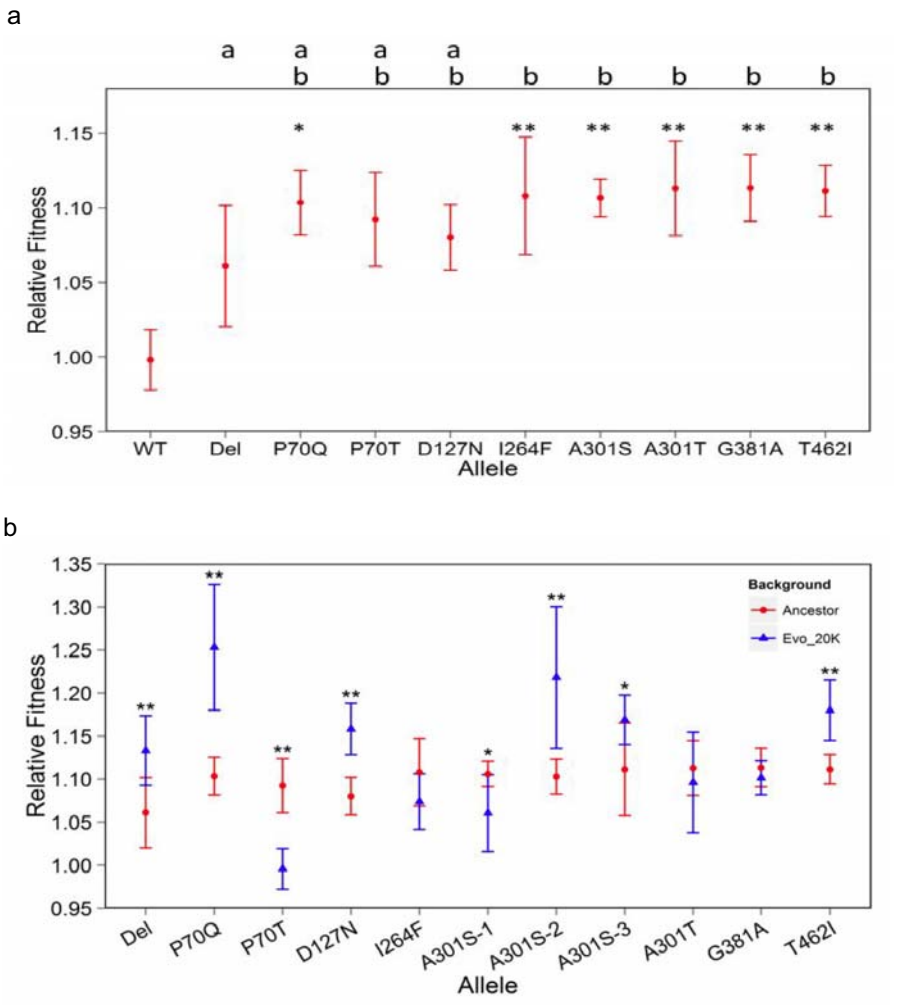

Figure 1.3 ***pykF* mutations isolated from independently evolved populations were added to the ancestor background and their fitness effect was measured relative to the ancestor (red) and their own evolved background (blue). (a)** The eight non-synonymous alleles and the deletion allele were added to the ancestral strain and competed against the ancestor. WT indicates a control fitness marker and was used as a reference in all fitness competitions. Symbols indicate mean and error bars are 95% confidence interval of four independent fitness measurements (except the A301S mutation effect was estimated with twelve replicates). One-way ANOVA found no detectable fitness difference ($F_{7, 32} = 1.67$, $P = 0.15$) among point mutations, but did identify a significant difference between effects if the Del mutation was included in the analysis ($F_{8, 35} = 3.71$, $P < 0.01$). Points sharing common letters indicate no significant difference was detected between the alleles (Tukey's HSD test). Asterisks reflect results of Dunnett's test comparing fitness conferred by point mutations against the Del mutation: ** $P < 0.01$, * $P < 0.05$. **(b)** The eight non-synonymous alleles and the deletion allele were added to the evolved strains and competed against the ancestor. The A301S mutation occurred independently in three populations and thus was measured in three backgrounds. Symbols indicate mean and error bars are 95% confidence interval of four independent fitness measurements. Significant differences in fitness between ancestor and evolved background are indicated by asterisks: ** $P < 0.001$ and * $P < 0.05$ by t-tests. Eight pair-wise comparisons were significantly different. Of these, six remained so after sequential Bonferroni correction. This image was created by Fen Peng.[32]

The results display fitness effects that are generally higher and much more variable, ranging from 0% to 25% (Figure 1.3b). These results determine that the effects of focal mutations are not constant, but often depend on the presence of additional mutations as they arise during evolution.

Comparison of fitness effects in the evolved backgrounds suggests that the adaptive mutations in *pyk*F are dependent upon the background in which they arose. The results show that even though the mutations are spread across the gene, their fitness effect is likely to be similar (Figure 1.3a). Therefore, the adaptive mutations *can* be parallel in their fitness effect, although only when assessed in a common genetic background (Figure 1.3b). I focus on testing whether the evolved enzymes also show a parallel change in function, i.e. catalysis and allostery.

1.5 *E. coli* pyruvate kinase type 1

The *pyk*F gene codes for the enzyme pyruvate kinase type 1 (PK1) in *E. coli*, which is important for carbohydrate metabolism, as it controls the flux through the glycolytic pathway.

1.5.1 Low-glucose selection pressure

The eight *pyk*F alleles were selected for under the low-glucose selection pressure, which was used in Lenski's long-term evolution experiment (Section 1.3). Since pyruvate kinase catalyses the final step of glycolysis, selection for mutated alleles is proposed to shorten the lag time until glucose import of the limiting resource, glucose, into cells.[30] This hypothesis was drawn based upon a study of PEP carboxylase regulation, which like pyruvate kinase is shown to convert PEP into intermediates that feed the citric acid cycle. In the study, Xu *et al*.[34] demonstrates that high levels of phosphoenolpyruvate (PEP) are necessary for driving the import of glucose into the cells for metabolism.[34] In the study, Xu *et al*. shows that when glucose is exhausted from the media, the cellular concentrations of fructose-1,6-bisphosphate (FBP) drop, causing a rapid decrease in PEP carboxylase activity. This decrease in activity stops the consumption of PEP, thus allowing the PEP

concentration to build up, enabling a rapid uptake of glucose into the cells once glucose is reintroduced into the culture medium.[34]

1.5.2 Glycolysis

Pyruvate kinase (PK; EC 2.7.1.40) is a regulatory enzyme in the glycolytic pathway, a ten-step pathway that breaks down glucose to form two molecules of pyruvate[35, 36] (Figure 1.4). Pyruvate is a key molecule that acts as a branch point in metabolism because it is an intermediate in several different pathways, e.g. under aerobic conditions, pyruvate is shuttled into the citric acid cycle and under anaerobic conditions, it is used in either alcoholic or lactic acid fermentation, depending on the organism. Pyruvate is also involved in amino acid metabolism, e.g. lysine biosynthesis.[37]

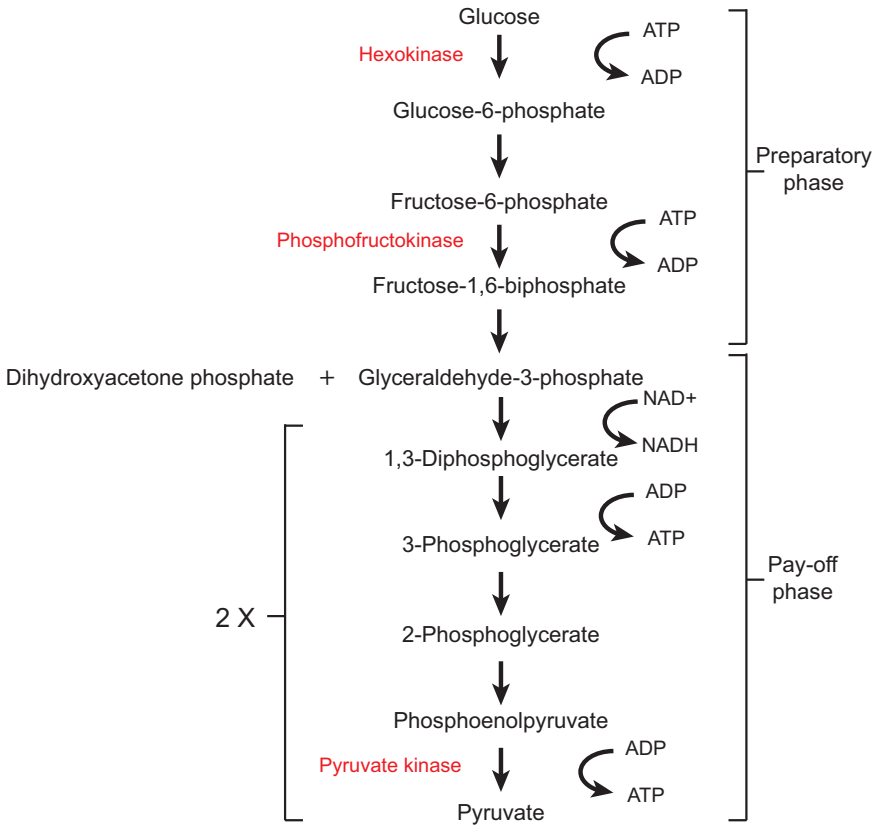

Figure 1.4 Overview of glycolysis emphasising the three regulatory steps. Regulatory enzymes are coloured red. Pyruvate kinase is the only regulatory enzyme in the second phase of glycolysis, the 'pay-off phase'.

The glycolytic pathway can be divided between a 'preparatory phase' where energy is consumed and a 'pay-off phase' where net energy is generated in two forms, adenosine triphosphate (ATP) and NADH. Three regulatory steps control the glycolytic pathway and these are catalysed by the enzymes hexokinase, phosphofructokinase and PK (Figure 1.4).[38] These three enzymes have a large negative free energy, making them essentially irreversible under physiological conditions.[39] However, PK is the only regulatory enzyme present in the second phase, the 'pay-off phase' of glycolysis, which suggests it is important for regulating energy production.[40]

1.5.3 Pyruvate kinase

Pyruvate kinase catalyses the final step of glycolysis, producing pyruvate from phosphoenolpyruvate (PEP), coupled to the synthesis of ATP. The reaction catalysed by PK is critical in the control of metabolic flux from PEP to pyruvate.[41] Pyruvate is a 'hub' metabolite that is utilised by a number of metabolic pathways to synthesise sugars, amino acids, cofactors, and lipids.

The PK reaction involves a phosphate transfer from PEP to adenosine diphosphate (ADP) to produce ATP and pyruvate. The reaction requires one monovalent cation, normally K^+, and two bivalent cations, often Mg^{2+} or Mn^{2+}, to provide efficient activity to carry out the reaction (Figure 1.5).[42]

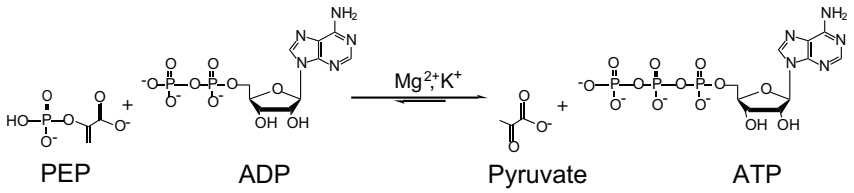

Figure 1.5 The reaction catalysed by pyruvate kinase. Pyruvate kinase catalyses the conversion of PEP and ADP into pyruvate and ATP.

In mammals, there are four tissue-related PK enzymes, which come from the two genes, M and L. The M gene encodes both the M1 (skeletal muscle) and M2 (kidney, intestine, stomach and testis) isozymes.[43] The L gene encodes both the L isozyme, which is found in the liver, and the R isozyme, found in red blood cells.[44] Pyruvate kinase isozymes are also present in plants, yeast and bacteria. Most bacteria contain only one isozyme of PK,

except for *E. coli*, which is known to have two (type 1 and type 2). The *E. coli* type 1 pyruvate kinase (PK1) isozyme will be the focus of this thesis.

1.5.4 Structure of pyruvate kinase

Crystal structures of PK enzymes from mammalian, bacterial and parasitic organisms have been reported,[42, 44-49] and are commonly homotetrameric in structure, although monomer,[50] dimer,[51] hexamer[52] and decamer[53] forms have also been found. Typically, each 50−60 kDa monomer is folded into three or four domains: A-, B- and C-domains, and the N-terminal domain is only present in mammalian enzymes (Figure 1.6).[49] The A-domain is a $(\beta/\alpha)_8$-barrel, housing the active site at the top of the barrel. The B-domain is also known as the 'lid domain' as it is thought to close over the active site upon substrate binding. The active site is located in the cleft between the A- and B-domains, and this is where the essential monovalent and divalent cations bind for activity.[54] The C-domain is the allosteric domain and this consists of five α-helices and five strands of mixed β-sheets, creating the site where the activator binds to activate the enzyme.[42, 55] Finally, the N-terminal domain is a short α-helical extension preceding the $(\beta/\alpha)_8$-barrel domain, whose role is less defined (Figure 1.6b).[49]

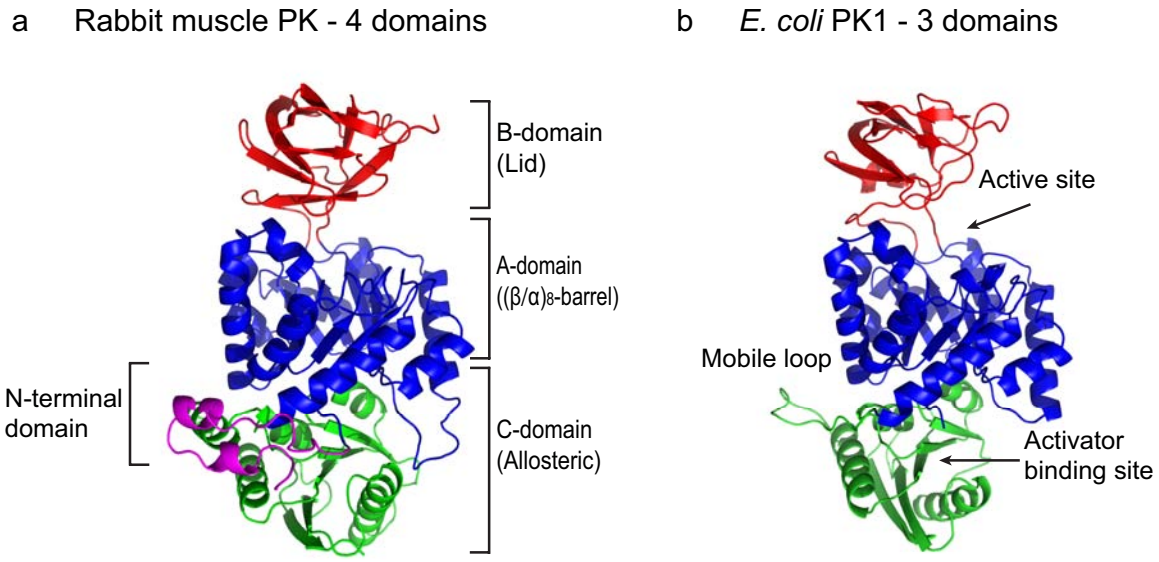

Figure 1.6 **Crystal structures of PK isozymes.** **(a)** Rabbit muscle PK (PDB ID: 1PKN) showing a 4-domain subunit. **(b)** *E. coli* PK1 (PDB ID: 1PKY) showing a 3-domain subunit. Subunits are coloured by domain: A (blue), B (red), C (green) and N (magenta).

The crystal structure of *E. coli* PK1 has been solved and refined to 2.50 Å resolution (PDB ID: 1PKY).[42, 56] The enzyme is a tetramer of four identical subunits (Figure 1.7a), each consisting of 470 amino acid residues. Electron density for residues 346−351 is not defined in the subunits, and additionally, electron density is insufficiently defined for residues 70−105 of the B-domain (lid domain) in one subunit (chain C) (Figure 1.7b). Therefore a higher resolution and more complete structural model would provide a more detailed understanding of the PK1 enzyme.

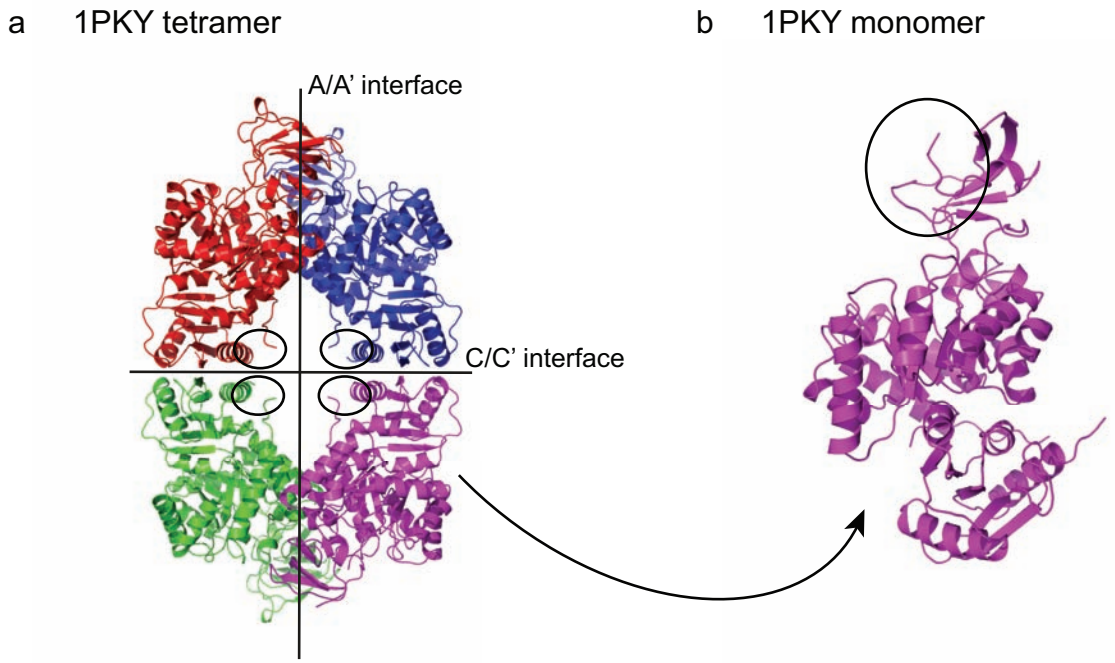

Figure 1.7 **Crystal structure of the *E. coli* PK1 enzyme.** **(a)** 1PKY tetramer coloured by subunit: subunit 1 (red), 2 (blue), 3 (magenta) and 4 (green). All four missing mobile loop regions (residues 346−351) are circled. **(b)** 1PKY subunit 3 showing that residues 70−105 are missing from the lid domain (circled).

1.5.4.1 The active site and catalytically important residues

The active site of *E. coli* PK1 is located at the C-terminal end of the $(\beta/\alpha)_8$-barrel. Structural information regarding the binding positions of substrates and catalytic ions are limited to that from *Leishmania mexicana* PK (Figure 1.8),[55, 57] because there are no bound structures of *E. coli* PK1 available.

Sequence comparison of the *L. mexicana* and *E. coli* PK type 1 active site regions (A- and B-domains) show a high sequence identity of >45%. Moreover, a structural alignment of the $(\beta/\alpha)_8$-barrels shows a 100% alignment of the specific active site residues involved in catalysis (Figure 1.8b), indicating that substrate and catalytic ion binding in *E. coli* PK1 is expected to be consistent with *L. mexicana* PK.

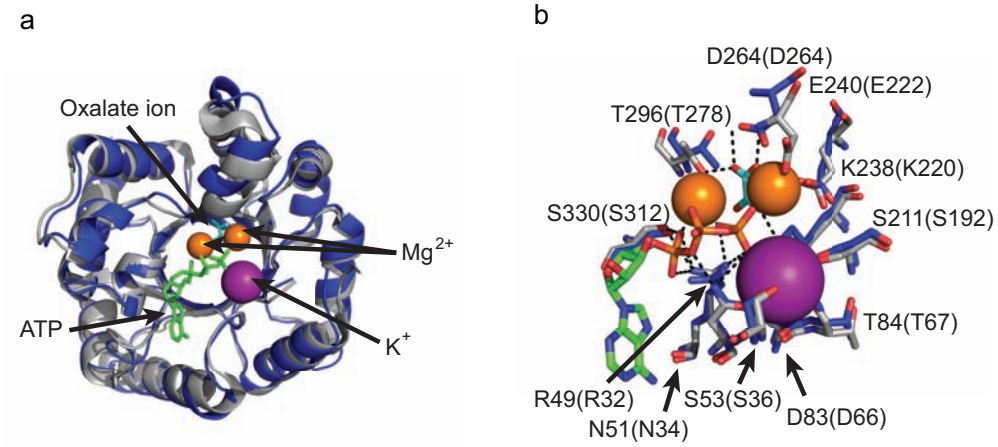

Figure 1.8 ***L. mexicana*** **PK aligned with PK1 showing substrate and catalytic ions bound in the active site.** **(a)** Active site showing the substrate and catalytic ion binding positions Coloured: ATP, green; oxalate, cyan; Mg^{2+}, orange and K^+, purple. **(b)** Substrate and catalytic ion binding interactions. Relevant residues are labelled (*L. mexicana* first with PK1 in parenthesis) and interactions are shown as dashed lines. *L. mexicana* PDB ID: 3HQP (grey) and PK1 (blue).

The reaction catalysed by PK is shown to occur by direct transfer of a phosphoryl group from the PEP donor to the ADP acceptor, producing ATP and pyruvate.[58] Various studies have demonstrated that PK catalysis has an absolute requirement for a monovalent cation and two divalent cations.[59, 60] Substrate binding within the *L. mexicana* PK active site requires a complex network of interactions involving mono- and divalent cations. The oxalate ion (PEP analogue) forms interactions with side chains and backbones of loops $\beta_5\alpha_5$, $\beta_6\alpha_6$ and $\beta_7\alpha_7$. Additionally, the oxalate ion interacts with a Mg^{2+} ion, which is bonded to side chains from loops $\beta_5\alpha_5$ and $\beta_6\alpha_6$. The α- and γ-phosphates of ATP interact with side chains from loops $\beta_2\alpha_2$, $\beta_3\alpha_3$, $\beta_4\alpha_4$, $\beta_5\alpha_5$ and $\beta_8\alpha_8$. All three phosphates (α, β and γ) of the ATP molecule interact with a second Mg^{2+} ion within the active site. Moreover, the γ-phosphate forms further interactions with the first Mg^{2+} ion, as well as the K^+ ion.

Many studies have shown that kinase enzymes have a metal ion requirement for catalysis of phosphate transfer, however the precise role of these metal ions is largely speculative. A study by Kerns *et al*. demonstrated that the metal cofactor helps to anchor the donor phosphoryl group for a more favourable attack by the oxygen of the acceptor molecule.[61] One common issue for kinases is the presence of water molecules within the active site, because the enzyme needs to successfully catalyse phosphoryl transfer, while avoiding the more favourable hydrolysis side reaction. Investigation into the mechanism that adenylate kinase employs to suppress the side hydrolysis reaction determines that the enzyme tightly coordinates the water molecules from the phosphoryl groups, into positions that are incapable of nucleophilic attack.[61] The similar phosphoryl-transfer role of kinases and the similar architecture of their active sites suggest that PK enzymes follow a similar catalytic mechanism to that of adenylate kinase.

1.5.4.2 Allosteric activation

The simplest kinetic behaviour can be described by the Michaelis-Menten function, where a curve of velocity in relation to substrate concentration forms a hyperbolic shape.[62] The mammalian M1 PK follows this 'simple' kinetic behaviour, as it has no cooperative properties or allosteric regulation.[44] However, the mammalian M2 isozyme exhibits the more 'complex', sigmoidal kinetics,[44, 62] which indicates that the enzyme has cooperative behaviour, where there is cooperative binding of ligands to multiple binding sites.[63] The binding of a ligand to one subunit often causes an increased affinity for a ligand at the next subunit's binding site. Thus, the sigmoidal curve is the result of the increased affinity with increasing saturation of ligand.[64]

Figure 1.9 displays the results of kinetic analyses of *E. coli* PK1 by Valentini *et al.*,[41] providing an example of sigmoidal and Michaelis-Menten kinetics. The *E. coli* PK1 enzyme is homotropically activated when it displays sigmoidal kinetics towards PEP in the absence of FBP (Figure 1.9a).[65, 66] This reaction has a Hill coefficient (n_H) of 3.2 (strong positive cooperativity), confirming that the binding of one PEP molecule to one subunit increases the enzyme's affinity for additional PEP molecules to bind to subsequent subunits. However, heterotropic activation is shown when the binding of FBP has a K-type effect on *E. coli* PK1 catalysis, whereby it increases the enzyme's affinity for the substrate, PEP,[67] resulting in the typical hyperbolic Michaelis-Menten kinetics (Figure 1.9b).[68] When FBP is present, PEP has no additional impact on the maximum capacity of

the enzyme.[41] This is confirmed with n_H of 1.0 (no cooperativity), demonstrating that FBP is the only ligand that is kinetically significant.[69]

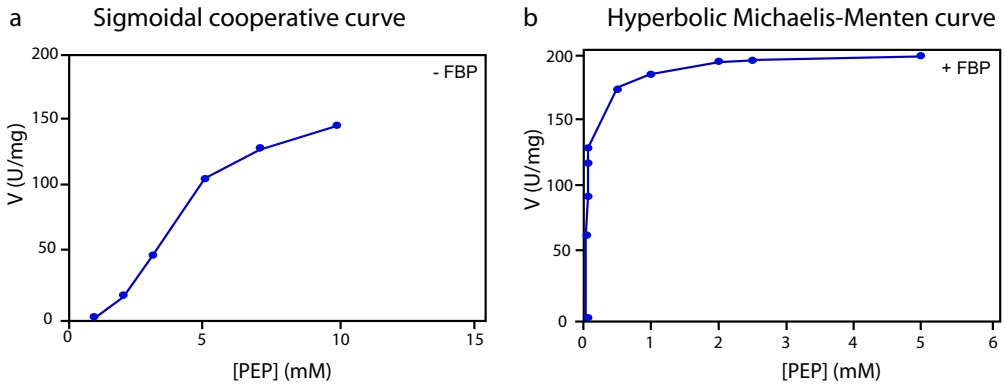

Figure 1.9 PEP titration curves for *E. coli* PK1 demonstrating the sigmoidal cooperative curve and the hyperbolic Michaelis-Menten curve. The enzyme activity was assayed at 25 °C, pH 7.5. ADP was present at a concentration of 2 mM. **(a)** Titrations were performed in the absence of FBP. **(b)** Titrations were performed in the presence of 2 mM FBP. Images were replicated from Valentini *et al*.[41]

1.5.4.3 The FBP binding site

FBP bound structures reveal that the allosteric activator binding site is located entirely within the C-domain and must transmit a signal over a 40 Å distance to the active site in the same subunit. The binding site is located in a pocket formed from an effector loop and the first two turns of the Cα5'-helix in *Saccharomyces cerevisiae*[49] (Figure 1.10) and human liver[70] PK's.

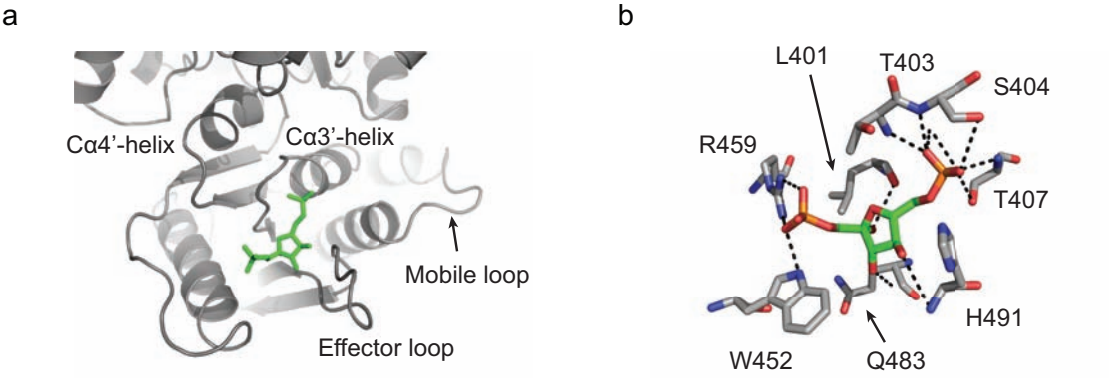

Figure 1.10 *S. cerevisiae* PK with FBP bound in the allosteric site depicting the binding position. **(a)** Allosteric site showing the FBP binding position. Important regions have been labelled. **(b)** FBP binding interactions in the allosteric site. Relevant residues are labelled and interactions are shown as dashed lines. *S. cerevisiae* PK, PDB ID: 1A3W.

Ligand binding in the allosteric site is facilitated by residue Arg459 in *S. cerevisiae* PK, forming a strong electrostatic interaction with the 1'-phosphate group of FBP. In addition, the 6'-phosphate forms a series of hydrogen bonds with side chains from the sequence Ser402-Thr-Ser-Gly-Thr-Thr407 (Thr378-Gln-Gly-Gly-Lys382 are *E. coli* equivalent residues) and the sugar ring of the FBP forms interactions with residues Gln483 and His491.[49]

1.6 Allosteric control of *E. coli* PK1

Pyruvate kinase enzymes are almost always allosterically regulated. Moreover, a range of different effectors that depend on the cell type mediate allostery, and in many cases multiple isozymes that respond to different allosteric effectors are expressed. Pyruvate kinase isozymes are all homotropically regulated by the substrate PEP to allow regulation of the glycolytic flux in response to elevated PEP levels.[46] In addition, they are often heterotropically regulated by allosteric activators, whose chemical nature depends on the organism or tissue.[42, 49]

Heterotropic allosteric regulation is proposed to involve a conformational reorganisation of the tetramer,[46] transitioning between an inactive T-state (tensed) and an active R-state (relaxed). The binding of the allosteric activator, FBP, to the allosteric domains of *E. coli* PK1 controls the regulatory switch between T-states and R-states. The current structural model of *E. coli* PK1 is in the inactive T-state (Figure 1.7) and attempts to gain a structure in the R-state by co-crystallisation have failed. Moreover, additional attempts to soak FBP into the grown crystals resulted in immediate cracking,[42] suggesting a significant structural rearrangement may be involved in the activation of the enzyme.

Fortunately, three-dimensional crystal structures of both T- and R-state PK enzymes have been solved for several organisms[46, 49, 55] and these structures reveal important details about the structural shift that occurs during the allosteric transition. The isozyme structural data provides evidence supporting two possible allosteric regulation mechanisms that could apply to *E. coli* PK1. The first is the domain and subunit rotation mechanism proposed by Mattevi *et al*., in 1995.[42, 71] More recently, a rigid-body rotation mechanism has been used to describe allosteric regulation in PK isozymes by Morgan *et al*.[46, 55]

1.6.1 Domain and subunit rotation model

A structural comparison of the unbound *E. coli* PK1 (T-state) to the non-allosteric rabbit M1 PK (R-like state) provides a domain and subunit rotation model for the allosteric activation mechanism (Figure 1.11).[42, 71] If domain A is taken as a reference point between the two structures, the transition to the R-like state involves a ~17° rotation of the lid domain, narrowing the substrate binding cleft. Moreover, the C-domain of M1 rotates ~15° relative to the *E. coli* PK1, widening the allosteric binding pocket in the active, R-like state. In addition to the domain rotations, a 16° rotation of subunits reorganises the A/A' interface and is coupled to a rotation of B-domains. The A/A' interface of the T-state shows a salt bridge formed between Arg292 and Asp297' of the Aα7'-helix from the opposing subunit. However, the R-like state causes a restructuring of the interface, where Arg292 reorients to form a salt bridge with Asp127' of the B-domain from the opposing subunit.

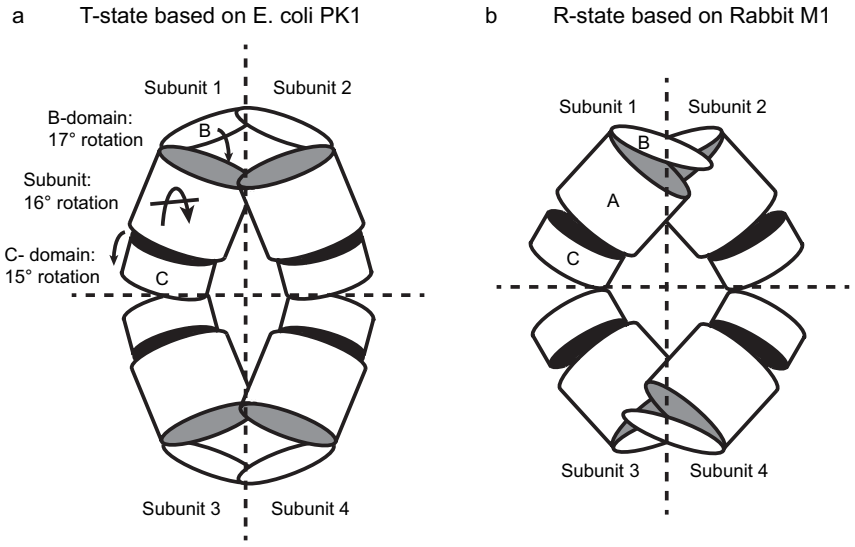

Figure 1.11 Schematic representation of the domain and subunit rotations proposed for the allosteric activation mechanism. The model proposes that FBP binding causes a 16° subunit rotation and rotations of the B- (17°) and C-domains (15°). **(a)** T-state structure from *E. coli* PK1.[42] **(b)** R-like state structure from rabbit M1 PK.[72] Figure replicated from Mattevi *et al.*[71]

The allosteric activation mechanism of PK therefore shows a combination of domain rotations within subunits and subunit rotations within the tetramer of the enzyme.

1.6.2 Rigid-body rotation model

Allosteric transition studies using both T- and R-state PK's from *Leishmania mexicana*[55] and *Trypanosoma cruzi*[46] suggest a symmetrical rigid domain rocking motion of the AC-domain cores to produce the active R-state. Allosteric activation by FBP causes each of the subunits to rotate around the Cα4'-helix (residues 430−433) pivot point, located at the interface between the A- and C-domains. Moreover, FBP binding 'locks' the active R-state by salt bridge formation across the two C/C' interfaces, demonstrated by an increase in thermal stability when FBP is bound.[46, 55] Although activation by substrate binding in the active site also causes the rigid-body rotations, the substrates do not have the same 'locking' effect as FBP binding; instead they cause a stabilisation of the active site region by B-domain rotations to close the lid over the bound substrates.[46, 55]

The two allosteric models describe the transition between T- and R-states to involve a binding event that causes subunit rotations, whereby the C-terminal end of the subunit rotates towards the tetramer centre (increasing A/A' surface area) and the N-terminal end rotates outwards. The major difference between the proposed models is the flexibility created by activation. The rigid-body model involves a 'rigidification' and increase in stability upon transition to the R-state, whereas transition to the R-state in the domain and subunit rotation model includes twelve independent rotations, suggesting increased flexibility between domains and subunits within the enzyme.

Obtaining a structure of the *E. coli* PK1 enzyme in the R-state, with FBP bound, would be helpful for confirming the allosteric mechanism of the *E. coli* PK1 enzyme.

1.7 Eight adaptive non-synonymous mutations in *E. coli* PK1

Investigations into the *pyk*F mutations have shown that all eight non-synonymous evolved alleles produce a fitness benefit (Section 1.3), however, the underlying cause of the benefit is unknown. The mutated genotype goes in, and the enhanced phenotype comes out, but what is happening in between? How have these mutations changed the *E. coli* PK1 protein? To investigate the changes at a protein level, we first need to locate each of the

substitution mutations on the structure to gauge the structural and functional effects that they may have.

Eight single substitution mutations were identified at six different residue sites across the twelve replicate *E. coli* populations from Lenski's evolutionary study (Figure 1.12).[30] In two cases, the same residue was independently mutated in more than one population (P70T, P70Q and A301T, A301Sx3).[30] Mapping the six mutation sites onto the *E. coli* PK1 structure reveals that they are scattered across the enzyme, but are clustered into three hot spots: active site, A/A' interface and allosteric binding site (Figure 1.12b). Three mutations are identified in the active site (P70Q, P70T and D127N), three are located at the A/A' interface (I264F, A301S and A301T), and two mutations are found within the allosteric activator, FBP, binding site (G381A and T462I).

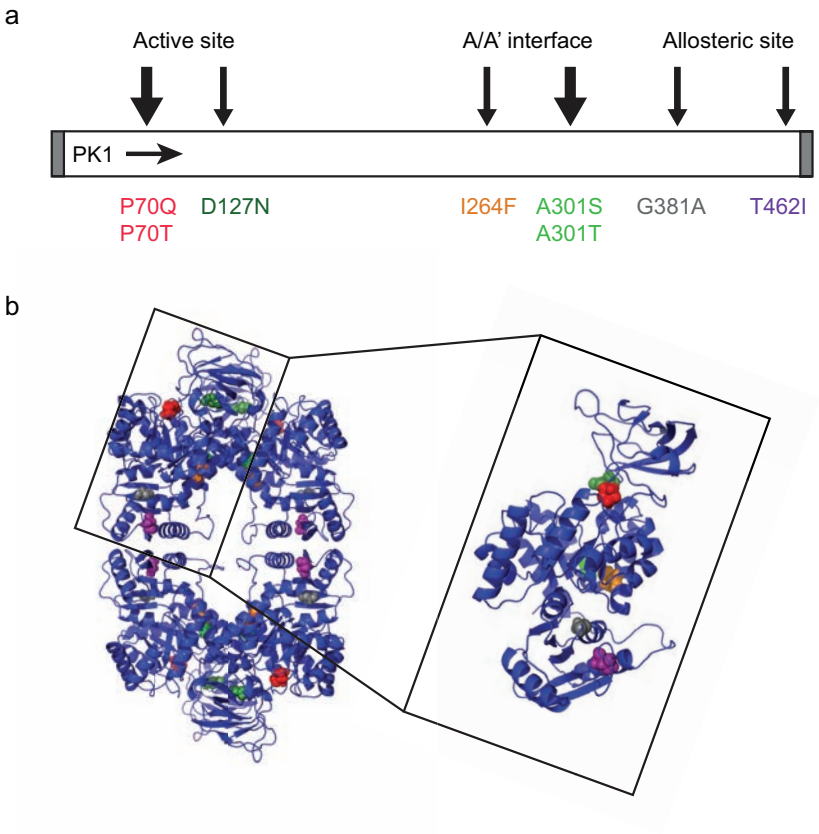

Figure 1.12 **Six different mutation sites are mapped onto the *E. coli* PK1 structure.** **(a)** The eight mutations are labelled by residue substitution and arrows indicate the six mutation sites. **(b)** The six mutation sites are mapped onto the *E. coli* PK1 structure to show their positions. Mutations are coloured as follows: P70 (red), D127 (olive), I264 (orange), A301 (green), G381 (grey) and T462 (purple).

1.7.1 Active site mutations

Residues in the active site have an important role in binding both substrate and catalytic metal ions (Section 1.5.4.1). Structural studies have shown that active site binding events control the movement of the B-domain (lid domain), by closing it over the active site for catalysis.[55, 73, 74] Thus, mutation of residues involved in the control of the lid domain opening and closing would likely be detrimental to the catalytic function of the enzyme. This study provides three examples of such mutations: P70Q, P70T and D127N. It is predicted that mutating these residues will have a significant impact upon the substrate binding efficiency and the enzymes' ability to catalyse reactions.

1.7.2 A/A' interface mutations

A/A' interface residues are highly conserved across PK enzymes and mutation of these residues can have a significant impact upon catalysis and allosteric regulation of the enzyme. One study mutated A/A' interface residue, Arg292 in *E. coli* PK1, causing a reorganisation of the interface, as well as destabilisation of two substrate binding loops at the active site, inactivating the enzyme.[41] This study established a link between interface and active site and confirmed the importance of A/A' interface residues for enzymatic activity. Other studies have shown that mutating A/A' interface residues can have a dramatic effect upon the allosteric regulation of the enzyme,[75] whereby heterotropic activation is reduced, resulting in a more cooperative enzyme.[41, 68] Likewise, the three A/A' interface mutations (I264F, A301S and A301T) in this thesis are predicted to induce changes to allosteric regulation and catalysis of *E. coli* PK1. Furthermore, disrupting interactions at the A/A' interface could alter function by disturbing the oligomeric state of the enzyme.

1.7.3 Allosteric site mutations

Mutation of residues involved in binding the allosteric activator, FBP, could have a dramatic negative effect upon *E. coli* PK1 function. There are two mutations identified in the FBP binding pocket, and they are both suspected to be involved in binding FBP (Section 1.5.4.3). Residue G381 is likely involved in binding the 6'-phosphate, and T462 is situated within bonding distance of the sugar ring of FBP.[49] The mutation of these

residues (G381A and T462I) is predicted to have a significant impact upon the binding affinity of FBP. Subsequently, heterotropic regulation and activity may also be altered.

1.7.4 Impact of mutations on *E. coli* PK1

All eight single substitution mutations in *E. coli* PK1 are located in positions that could have a significant impact upon the regulation and catalytic efficiency of the enzyme. Altering the enzyme behaviour could be responsible for, or at least contribute to the fitness changes identified in Section 1.4. Moreover, structural changes caused by these mutations could also affect the behaviour of the enzymes. However, quaternary analysis of the evolved enzyme structures have confirmed a single tetrameric species, similar to wild-type *E. coli* PK1.[76]

1.8 Summary and hypotheses

The overall aim of this research is to investigate the molecular mechanisms underlying natural selection, that is, the relationship between altered alleles (genotype) and the resulting physiological properties (phenotype). Identifying and characterising this connection is essential for developing an understanding of how adaptive mutations in a gene facilitate beneficial phenotypic changes, such as the altered *pyk*F alleles causing increased fitness in *E. coli*.

The work contained in this thesis provides a case study for investigating the molecular mechanisms that underlie adaptation. It builds on Lenski's long-term evolution experiment as a model system because the experiment identifies a series of adaptive mutations that have evolved as a response to the low-glucose selection pressure. The evolved *E. coli* populations have previously been studied from a genetic and phenotypic perspective, so it provided the ideal study for investigating the molecular basis of adaptation.

This thesis describes the functional, structural and dynamic behaviours of the eight adaptively evolved *E. coli* PK1 enzymes in order to probe the molecular mechanism of their adaptation. All eight mutations in *pyk*F are independently found to produce a fitness benefit to the *E. coli* populations. Analysis of the interactions between evolved genes determined different fitness effects compared to that produced by the evolved *pyk*F alleles

alone. This result suggests that epistatic interactions are present between the evolved *pyk*F alleles and other genes within the evolved background. Since the fitness analysis confirmed that the mutations in *pyk*F are producing a fitness benefit, I hypothesise that the selected mutations decrease the activity of the pyruvate kinase enzyme. This, in turn, increases the intracellular concentration of PEP, which decreases the lag phase upon glucose reintroduction into the media and subsequently generates rapid uptake of glucose into cells.

To investigate the molecular basis of adaptation and determine the relationship between selected genotype and altered phenotype, the evolved pyruvate kinase enzymes will be studied.

Chapter Two will structurally and functionally describe the *E. coli* PK1 enzyme to provide a reference for comparative studies against the eight evolved enzymes. In order to investigate the consequences of the evolved mutations on the structural and functional properties of *E. coli* PK1, a comparative model of the wild-type needs to be created first. This chapter will investigate the functional response of the wild-type enzyme to its substrates and allosteric activator, followed by atomic and solution structure analysis which will provide a detailed model of what the protein looks like.

Chapter Three will investigate the allosteric activation mechanism of *E. coli* PK1 by investigating how the binding of FBP in the allosteric domain facilitates changes in substrate binding in the active site, 40 Å away. I will test the two currently proposed models; the domain rotation model proposed by Mattevi *et al*.,[42, 71] or the rigid-body rotation model proposed by Morgan *et al*.[46, 55] Structure and dynamic analyses will measure the effect of FBP binding upon the wild-type enzyme to investigate the mechanism of allosteric activation, which will be used as a reference for comparison with the evolved enzymes in subsequent chapters.

Chapter Four will consider the function and stability of each of the eight evolved enzymes to test two key hypotheses: 1) the activity of each of the evolved enzymes will be lower than the wild-type; 2) the evolved enzymes will have parallel functional responses, i.e. they will have accomplished their goal in the same way. Since the evolved enzymes demonstrate a fitness benefit compared to the wild-type, it is likely that the molecular

mechanism behind this benefit is an altered function, therefore functional analyses will test this theory.

Chapter Five will investigate whether each of the single substitution mutations changes the atomic structures of the eight evolved enzymes. The three-dimensional fold of a protein is driven by non-covalent interactions between the constituent amino acids, and one single change can have dramatic effects upon the structure. For this reason, atomic and solution structures of each of the eight evolved enzymes will be determined and compared to the wild-type to assess whether a change in structure is responsible for the fitness benefit in the *E. coli* populations.

Finally, *Chapter Six* will assess whether the substitution mutations altered the dynamic behaviour of the enzymes. Similar to the investigations into the structures of the evolved enzymes in Chapter Five, the dynamic behaviours of each of the evolved enzymes will be tested using computational, and experimental techniques to determine whether the mutations have altered the conformational flexibility of the enzymes.

1.8 References

[1] Ostrowski, EA, Woods, RJ, and Lenski, RE. (2008) The genetic basis of parallel and divergent phenotypic responses in evolving populations of *Escherichia coli*, *Proc. Biol. Sci. 275*, 277-284.

[2] Copley, SD. (2012) Toward a systems biology perspective on enzyme evolution, *J. Biol. Chem. 287*, 3-10.

[3] Kaltenbach, M, and Tokuriki, N. (2014) Dynamics and constraints of enzyme evolution, *J. Exp. Zool. B Mol. Dev. Evol. 322*, 468-487.

[4] Copley, SD. (2014) An evolutionary perspective on protein moonlighting, *Biochem. Soc. Trans. 42*, 1684-1691.

[5] Seffernick, JL, de Souza, ML, Sadowsky, MJ, and Wackett, LP. (2001) Melamine deaminase and atrazine chlorohydrolase: 98 percent identical but functionally different, *J. Bacteriol. 183*, 2405-2410.

[6] Jung, ST, Lauchli, R, and Arnold, FH. (2011) Cytochrome P450: taming a wild type enzyme, *Curr. Opin. Biotechnol. 22*, 809-817.

[7] Jensen, RA. (1976) Enzyme recruitment in evolution of new function, *Annu. Rev. Microbiol. 30*, 409-425.

[8] Carroll, SP, Jorgensen, PS, Kinnison, MT, Bergstrom, CT, Denison, RF, Gluckman, P, Smith, TB, Strauss, SY, and Tabashnik, BE. (2014) Applying evolutionary biology to address global challenges, *Science 346*, 1245993.

[9] Davies, J, and Davies, D. (2010) Origins and evolution of antibiotic resistance, *Microbiol. Mol. Biol. Rev. 74*, 417-433.

[10] Lenski, RE. (1998) Bacterial evolution and the cost of antibiotic resistance, *Int. Microbiol. 1*, 265-270.

[11] Tokuriki, N, Jackson, CJ, Afriat-Jurnou, L, Wyganowski, KT, Tang, R, and Tawfik, DS. (2012) Diminishing returns and tradeoffs constrain the laboratory optimization of an enzyme, *Nat. Commun. 3*, 1257.

[12] Storz, JF, and Moriyama, H. (2008) Mechanisms of hemoglobin adaptation to high altitude hypoxia, *High. Alt. Med. Biol. 9*, 148-157.

[13] Natarajan, C, Inoguchi, N, Weber, RE, Fago, A, Moriyama, H, and Storz, JF. (2013) Epistasis among adaptive mutations in deer mouse hemoglobin, *Science 340*, 1324-1327.

[14] Tracewell, CA, and Arnold, FH. (2009) Directed enzyme evolution: climbing fitness peaks one amino acid at a time, *Curr. Opin. Chem. Biol. 13*, 3-9.

[15] Peisajovich, SG, and Tawfik, DS. (2007) Protein engineers turned evolutionists, *Nat. Methods. 4*, 991-994.

[16] Noor, S, Taylor, MC, Russell, RJ, Jermiin, LS, Jackson, CJ, Oakeshott, JG, and Scott, C. (2012) Intramolecular epistasis and the evolution of a new enzymatic function, *PLoS One 7*, e39822.

[17] Tokuriki, N, Stricher, F, Serrano, L, and Tawfik, DS. (2008) How protein stability and new functions trade off, *PLoS Comput. Biol. 4*, e1000002.

[18] Khanal, A, Yu McLoughlin, S, Kershner, JP, and Copley, SD. (2015) Differential effects of a mutation on the normal and promiscuous activities of orthologs: implications for natural and directed evolution, *Mol. Biol. Evol. 32*, 100-108.

[19] Copley, SD. (2012) Moonlighting is mainstream: paradigm adjustment required, *Bioessays 34*, 578-588.

[20] Arnold, FH, Wintrode, PL, Miyazaki, K, and Gershenson, A. (2001) How enzymes adapt: lessons from directed evolution, *Trends Biochem. Sci. 26*, 100-106.

[21] Miyazaki, K, Wintrode, PL, Grayling, RA, Rubingh, DN, and Arnold, FH. (2000) Directed evolution study of temperature adaptation in a psychrophilic enzyme, *J. Mol. Biol. 297*, 1015-1026.

[22] Barrett, RD, and Hoekstra, HE. (2011) Molecular spandrels: tests of adaptation at the genetic level, *Nat. Rev. Genet. 12*, 767-780.

[23] Philippe, N, Crozat, E, Lenski, RE, and Schneider, D. (2007) Evolution of global regulatory networks during a long-term experiment with *Escherichia coli*, *Bioessays 29*, 846-860.

[24] Lenski, RE, Rose, MR, Simpson, SC, and Tadler, SC. (1991) Long-term experimental evolution in *Escherichia coli.* I. Adaptation and divergence during 2000 generations, *Am. Nat. 138*, 1315-1341.

[25] Lenski, RE, and Travisano, M. (1994) Dynamics of adaptation and diversification: a 10,000-generation experiment with bacterial populations, *Proc. Natl. Acad. Sci. U. S. A. 91*, 6808-6814.

[26] Lenski, RE, Mongold, JA, Sniegowski, PD, Travisano, M, Vasi, F, Gerrish, PJ, and Schmidt, TM. (1998) Evolution of competitive fitness in experimental populations of *E. coli*: What makes one genotype a better competitor than another?, *Antonite van Leeuwenhoek 73*, 35-47.

[27] Cooper, VS, and Lenski, RE. (2000) The population genetics of ecological specialization in evolving *Escherichia coli* populations, *Nature 407*, 736-739.

[28] Travisano, M, and Lenski, RE. (1996) Long-term experimental evolution in *Escherichia coli*. IV. Targets of selection and the specificity of adaptation, *Genetics 143*, 15-26.

[29] Cooper, TF, Rozen, DE, and Lenski, RE. (2003) Parallel changes in gene expression after 20,000 generations of evolution in *Escherichia coli*, *Proc. Natl. Acad. Sci. U. S. A. 100*, 1072-1077.

[30] Woods, R, Schneider, D, Winkworth, CL, Riley, MA, and Lenski, RE. (2006) Tests of parallel molecular evolution in a long-term experiment with *Escherichia coli*, *Proc. Natl. Acad. Sci. U. S. A. 103*, 9107-9112.

[31] Lenski, RE, Winkworth, CL, and Riley, MA. (2003) Rates of DNA sequence evolution in experimental populations of *Escherichia coli* during 20,000 generations, *J. Mol. Evol. 56*, 498-508.

[32] Peng, F. (2015) Molecular basis of adaptive evolution of pyruvate kinase in *Escherichia coli*, In *Biology and Biochemistry*, University of Houston.

[33] Cooper, TF, Remold, SK, Lenski, RE, and Schneider, D. (2008) Expression profiles reveal parallel evolution of epistatic interactions involving the CRP regulon in *Escherichia coli*, *PLoS Genet 4*, e35.

[34] Xu, YF, Amador-Noguez, D, Reaves, ML, Feng, XJ, and Rabinowitz, JD. (2012) Ultrasensitive regulation of anapleurosis via allosteric activation of PEP carboxylase, *Nat. Chem. Biol. 8*, 562-568.

[35] Ponce, E, Flores, N, Martinez, A, Valle, F, and Bolívar, F. (1995) Cloning of the two pyruvate kinase isoenzyme structural genes from *Escherichia coli*: the relative roles of these enzymes in pyruvate biosynthesis, *J. Bacteriol. 177*, 5719-5722.

[36] Li, XB, Gu, JD, and Zhou, QH. (2015) Review of aerobic glycolysis and its key enzymes - new targets for lung cancer therapy, *Thorac Cancer 6*, 17-24.

[37] Garrett, RH, and Grisham, CM. (2012) *Biochemistry*, Brooks/Cole Publishing Company.

[38] Allert, S, Ernest, I, Poliszczak, A, Opperdoes, FR, and Michels, PA. (1991) Molecular cloning and analysis of two tandemly linked genes for pyruvate kinase of *Trypanosoma brucei*, *Eur. J. Biochem. 200*, 19-27.

[39] Haarasilta, S, and Oura, E. (1975) On the activity and regulation of anaplerotic and gluconeogenetic enzymes during the growth process of baker's yeast. The biphasic growth, *Eur. J. Biochem. 52*, 1-7.

[40] Ganapathy-Kanniappan, S, and Geschwind, JF. (2013) Tumor glycolysis as a target for cancer therapy: progress and prospects, *Mol. Cancer 12*, 152.

[41] Valentini, G, Chiarelli, L, Fortini, R, Speranza, ML, Galizzi, A, and Mattevi, A. (2000) The allosteric regulation of pyruvate kinase: A site-directed mutagenesis study, *J. Biol. Chem. 275*, 18145-18152.

[42] Mattevi, A, Valentini, G, Rizzi, M, Speranza, ML, Bolognesi, M, and Coda, A. (1995) Crystal structure of *Escherichia coli* pyruvate kinase type I: Molecular basis of the allosteric transition, *Structure 3*, 729-741.

[43] Noguchi, T, Inoue, H, and Tanaka, T. (1986) The M1- and M2-type isozymes of rat pyruvate kinase are produced from the same gene by alternative RNA splicing, *J. Biol. Chem. 261*, 13807-13812.

[44] Muirhead, H, Clayden, D, Barford, D, Lorimer, C, Fothergill-Gilmore, L, Schiltz, E, and Schmitt, W. (1986) The structure of cat muscle pyruvate kinase, *EMBO J. 5*, 475-481.

[45] Fothergill-Gilmore, LA, and Michels, PA. (1993) Evolution of glycolysis, *Prog. Biophys. Mol. Biol. 59*, 105-235.

[46] Morgan, HP, Zhong, W, McNae, IW, Michels, PAM, Fothergill-Gilmore, LA, and Walkinshaw, MD. (2014) Structures of pyruvate kinases display evolutionarily divergent allosteric strategies, *R. Soc. Open. Sci. 1*, 140120.

[47] Allen, SC, and Muirhead, H. (1996) Refined three-dimensional structure of cat-muscle (M1) pyruvate kinase at a resolution of 2.6 Å, *Acta Crystallogr. D Biol. Crystallogr. 52*, 499-504.

[48] Morgan, HP, McNae, IW, Hsin, KY, Michels, PA, Fothergill-Gilmore, LA, and Walkinshaw, MD. (2010) An improved strategy for the crystallization of *Leishmania mexicana* pyruvate kinase, *Acta Crystallogr. Sect. F Struct. Biol. Cryst. Commun. 66*, 215-218.

[49] Jurica, MS, Mesecar, A, Heath, PJ, Shi, W, Nowak, T, and Stoddard, BL. (1998) The allosteric regulation of pyruvate kinase by fructose-1,6-bisphosphate, *Structure 6*, 195-210.

[50] Knowles, VL, Dennis, DT, and Plaxton, WC. (1989) Purification of a novel pyruvate kinase from a green alga, *FEBS Lett. 259*, 130-132.

[51] Pawluk, A, Scopes, RK, and Griffiths-Smith, K. (1986) Isolation and properties of the glycolytic enzymes from *Zymomonas mobilis*. The five enzymes from glyceraldehyde-3-phosphate dehydrogenase through to pyruvate kinase, *Biochem. J. 238*, 275-281.

[52] Plaxton, WC, Dennis, DT, and Knowles, VL. (1990) Purification of leucoplast pyruvate kinase from developing castor bean endosperm, *Plant Physiol. 94*, 1528-1534.

[53] Lin, M, Turpin, DH, and Plaxton, WC. (1989) Pyruvate kinase isozymes from the green alga, *Selenastrum minutum.* I. Purification and physical and immunological characterization, *Arch. Biochem. Biophys. 269*, 219-227.

[54] Kumar, S, and Barth, A. (2011) Effects of ions on ligand binding to pyruvate kinase: mapping the binding site with infrared spectroscopy, *J. Phys. Chem. B 115*, 6784-6789.

[55] Morgan, HP, McNae, IW, Nowicki, MW, Hannaert, V, Michels, PAM, Fothergill-Gilmore, LA, and Walkinshaw, MD. (2010) Allosteric mechanism of pyruvate kinase from *Leishmania mexicana* uses a rock and lock model, *J. Biol. Chem. 285*, 12892-12898.

[56] Mattevi, A, Valentini, G, Speranza, ML, Sartori, P, Bolognesi, M, and Coda, A. (1995) Crystallization and preliminary X-ray analysis of pyruvate kinase type I from *Escherichia coli*, *Acta Crystallogr. D Biol. Crystallogr. 51*, 1089-1091.

[57] Morgan, HP, O'Reilly, FJ, Wear, MA, O'Neill, JR, Fothergill-Gilmore, LA, Hupp, T, and Walkinshaw, MD. (2013) M2 pyruvate kinase provides a mechanism for nutrient sensing and regulation of cell proliferation, *Proc. Natl. Acad. Sci. U. S. A. 110*, 5881-5886.

[58] Reynard, A, Hass, L, Jacobsen, D, and Boyer, P. (1961) The correlation of reaction kinetics and substrate binding with the mechanism of pyruvate kinase, *J. Biol. Chem. 236*, 2277-2283.

[59] Gupta, RK, and Oesterling, RM. (1976) Dual divalent cation requirement for activation of pyruvate kinase; essential roles of both enzyme- and nucleotide-bound metal ions, *Biochemistry 15*, 2881-2887.

[60] Bygrave, FL. (1966) Studies on the interaction of metal ions with pyruvate kinase from Ehrlich ascites-tumour cells and from rabbit muscle, *Biochem. J. 101*, 488-494.

[61] Kerns, SJ, Agafonov, RV, Cho, YJ, Pontiggia, F, Otten, R, Pachov, DV, Kutter, S, Phung, LA, Murphy, PN, Thai, V, Alber, T, Hagan, MF, and Kern, D. (2015) The energy landscape of adenylate kinase during catalysis, *Nat. Struct. Mol. Biol. 22*, 124-131.

[62] Cardenas, ML. (2013) Michaelis and Menten and the long road to the discovery of cooperativity, *FEBS Lett. 587*, 2767-2771.

[63] Friesen, RHE, Castellani, RJ, Lee, JC, and Braun, W. (1998) Allostery in rabbit pyruvate kinase: Development of a strategy to elucidate the mechanism, *Biochemistry 37*, 15266-15276.

[64] Fersht, A. (1999) *Structure and mechanism in protein science: a guide to enzyme catalysis and protein folding*, WH Freeman.

[65] Boiteux, A, Markus, M, Plesser, T, Hess, B, and Malcovati, M. (1983) Analysis of progress curves. Interaction of pyruvate kinase from *Escherichia coli* with fructose 1,6-bisphosphate and calcium ions, *Biochem. J. 211*, 631-640.

[66] Muñoz, M, and Ponce, E. (2003) Pyruvate kinase: Current status of regulatory and functional properties, *Comp. Biochem. Physiol. Biochem. Mol. Biol. 135*, 197-218.

[67] Monod, J, Wyman, J, and Changeux, JP. (1965) On the nature of allosteric transitions: a plausible model, *J. Mol. Biol. 12*, 88-118.

[68] Fenton, AW, and Blair, JB. (2002) Kinetic and allosteric consequences of mutations in the subunit and domain interfaces and the allosteric site of yeast pyruvate kinase, *Arch. Biochem. Biophys. 397*, 28-39.

[69] Coval, ML. (1970) Analysis of Hill interaction coefficients and the invalidity of the Kwon and Brown equation, *J. Biol. Chem. 245*, 6335-6336.

[70] Ishwar, A, Tang, Q, and Fenton, AW. (2015) Distinguishing the interactions in the fructose-1,6-bisphosphate binding site of human liver pyruvate kinase that contribute to allostery, *Biochemistry 54*, 1516-1524.

[71] Mattevi, A, Bolognesi, M, and Valentini, G. (1996) The allosteric regulation of pyruvate kinase, *FEBS Lett. 389*, 15-19.

[72] Larsen, TM, Laughlin, LT, Holden, HM, Rayment, I, and Reed, GH. (1994) Structure of rabbit muscle pyruvate kinase complexed with Mn2+, K+, and pyruvate, *Biochemistry 33*, 6301-6309.

[73] Zhong, W, Morgan, HP, Nowicki, MW, McNae, IW, Yuan, M, Bella, J, Michels, PA, Fothergill-Gilmore, LA, and Walkinshaw, MD. (2014) Pyruvate kinases have an intrinsic and conserved decarboxylase activity, *Biochem. J. 458*, 301-311.

[74] Fenton, AW, Williams, R, and Trewhella, J. (2010) Changes in small angle X-ray scattering parameters observed upon ligand binding to rabbit muscle pyruvate kinase are not correlated with allosteric transitions, *Biochemistry 49*, 7202-7209.

[75] Lovell, SC, Mullick, AH, and Muirhead, H. (1998) Cooperativity in *Bacillus stearothermophilus* pyruvate kinase, *J. Mol. Biol. 276*, 839-851.

[76] Zhu, T. (2008) Evolution of pyruvate kinase in the long-term evolution experiment of *Escherichia coli*: A structure/function study, In *Biological Sciences*, University of Canterbury.

Chapter Two

Structural and functional characterisation of the *Escherichia coli* pyruvate kinase type 1 enzyme

The work presented in Section 2.5 has been provisionally accepted for publication in Acta Crystallographica. Section D: Biological Chemistry:

Donovan, K.A., Atkinson, S.C., Kessans, S.A., Peng, F., Cooper, T.F., Griffin, D.W., Jameson, G.B., Dobson, R.C.J. (2015) Grappling with Anisotropic Data, Pseudo-merohedral Twinning and Pseudo-translational Non-crystallographic Symmetry: A Case Involving Pyruvate Kinase. Provisional acceptance to Acta Cryst. D.

2.1 Introduction

The glycolytic role of pyruvate kinase type 1 (PK1) from *Escherichia coli* has been well studied, especially in terms of its structure and function.[1-3] In this chapter, the *E. coli* PK1 enzyme was biophysically, functionally and structurally characterised to provide a detailed reference for comparative studies with the eight adaptively evolved *E. coli* PK1 enzymes from Lenski's long term evolution experiment (Section 1.3).

In order to investigate the consequences of the evolved mutations on the properties of *E. coli* PK1, the structure and function of the wild-type enzyme was determined first, to allow a direct comparison of the wild-type data established in this chapter and the eight evolved enzymes that are described in Chapters 3 to 6.

Functional analysis of the wild-type enzyme was carried out using a lactate dehydrogenase (LDH) coupled assay, which allows analysis of the kinetic properties of the enzyme with respect to substrates, phosphoenolpyruvate (PEP) and adenosine diphosphate (ADP), as well as the allosteric activation effect of the activator, fructose-1,6-bisphosphate (FBP). Additional functional analysis investigated the substrate specificity of the enzyme using an alternative substrate, guanosine diphosphate (GDP). Structural analysis of the enzyme was performed in a static crystal form and in solution. Both techniques confirm the enzyme adopts an elongated globular shape consisting of four identical subunits which form a homotetramer.

2.2 Over-expression and purification of wild-type PK1

Wild-type PK1 was overexpressed and purified according to methods adapted from Mattevi *et al.*[3] for structural and functional characterisation (Section 8.2.1 and 8.2.2). The wild-type enzyme was then purified using a three step purification procedure. Initially, the crude protein (Figure 2.1, lane 2) was applied to an anion-exchange column (IEC) to separate the proteins based upon charge. Negatively charged proteins bound to the anion resin and were eluted with a linear increasing salt gradient, eluting the tightly bound, less positive charged proteins last.

The fractions containing wild-type enzyme (Figure 2.1, lane 3) were subsequently applied to a hydrophobic interaction chromatography (HIC) column containing Phenyl-Sepharose. Hydrophobic interaction chromatography separated the remaining proteins based upon their hydrophobicity. The fractions containing wild-type from the HIC step (Figure 2.1, lane 4) were desalted and purified by size exclusion chromatography (SEC) (Figure 2.1, lane 5). Finally, the purified protein was snap cooled in liquid nitrogen and stored at -80

°C in the desalting buffer (10 mM Tris, pH 7.5, 1 mM ethylenediaminetetraacetic acid (EDTA) and 2 mM β-mercaptoethanol).

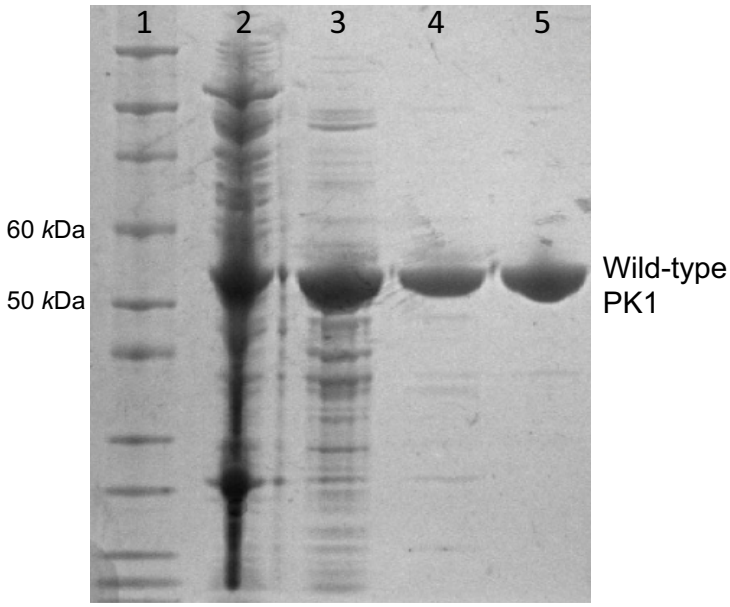

Figure 2.1 Sodium dodecyl sulfate polyacrylamide gel electrophoresis (SDS-PAGE) purification gel. SDS-PAGE gel following the purification of wild-type. Lanes: 1, Molecular weight marker; 2, Crude cell extract; 3, Eluent from Q-Sepharose column; 4, Eluent from Phenyl-Sepharose column; 5, Eluent from Gel Filtration column.

It was important that the final wild-type enzyme sample was pure with minimal contaminants, since structural characterisation using X-ray crystallography and small angle X-ray scattering (SAXS) requires a clean homogenous sample. The increase in purity of the enzyme is evident by the clear single band at ~50 kDa after the final purification step (Figure 2.1).

2.3 Functional studies

Steady-state kinetic analysis of the wild-type enzyme was carried out following the conditions outlined in Speranza *et al.*[4] to provide a reference for comparison with the evolved enzymes. Spectrophotometric assays allow enzyme reactions to be monitored by measuring the change in the absorbance of light. The kinetic analysis performed in this

thesis uses a coupled assay to measure the initial velocity of wild-type PK1 reactions. This specific coupled assay utilises pyruvate, the product of the *E. coli* PK1 reaction, as a substrate for a second reaction involving a coupling enzyme, LDH. The second reaction uses LDH to oxidise reduced nicotinamide adenine dinucleotide (NADH) to NAD^+. The oxidation of NADH is monitored using an ultraviolet (UV)-visible spectrophotometer at a wavelength of 340 nm (Section 8.3.1).[5]

The final concentrations of PEP, ADP and FBP varied by experiment. The 4-(2-hydroxyethyl)-1-piperazineethanesulfonic acid (HEPES) buffer concentration used in Speranza's work was low (10 mM),[4] therefore trials were carried out to test the effect of higher buffer concentrations on the activity of wild-type enzyme.

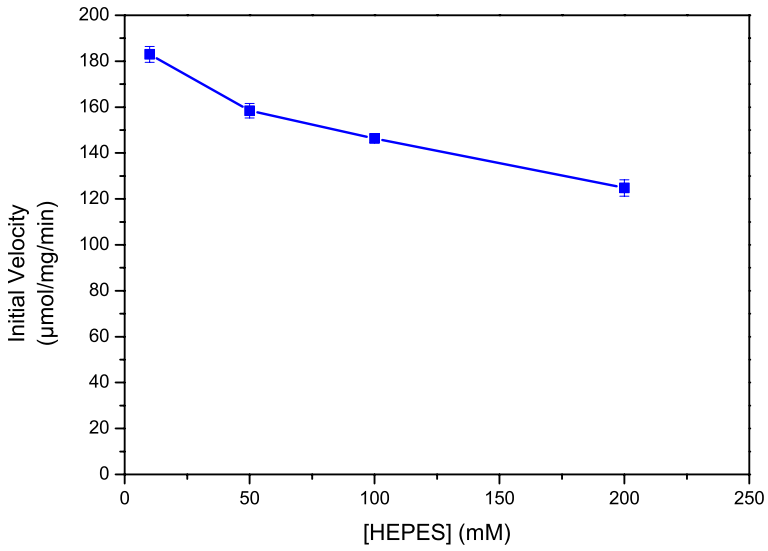

Figure 2.3 The activity of wild-type PK1 with respect to HEPES concentration. The activity of wild-type was measured at varying concentrations of HEPES buffer showing a decrease in velocity as the concentration of buffer inreases. Error bars represent the standard error of the mean (SEM) for two technical replicates.

Enzyme activity was retained as the concentration of HEPES increased in the reaction mixture (Figure 2.3). About 87% of activity was retained at a final concentration of 50 mM HEPES, and this decreased to 80% activity at 100 mM and decreased further to 68% at a final concentration of 200 mM HEPES. It was decided that a small amount of enzyme activity would be sacrificed to enhance the buffering capacity of the system. Therefore, the final HEPES concentration in the reaction mixture was increased to 100 mM. As an

additional pH measure, the PEP stock solution was pre-adjusted to a neutral pH (as judged by universal pH testing strips) using a concentrated potassium hydroxide solution (KOH).

Assay reactions were carried out at a physiologically relevant temperature of 37 °C to reflect the conditions of the Lenski experiment.[6] To determine whether temperature had a significant effect on enzyme activity, wild-type PK1 activity was tested as a function of temperature (Figure 2.4). The results show that the activity of wild-type increases relative to the increasing reaction temperature until the reaction reaches 50 °C, where it starts to decline. Temperatures above 60 °C cause the activity to decline rapidly, probably because 62 °C represents the temperature that causes the enzyme to denature (Figure 2.7).

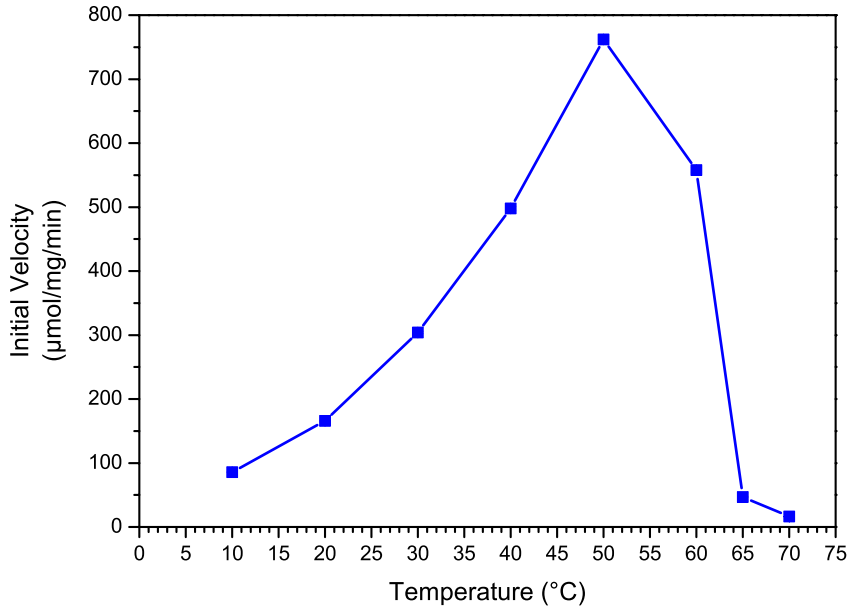

Figure 2.4 The activity of wild-type PK1 with respect to temperature. The activity of wild-type was measured at varying temperatures demonstrating an increase in velocity with increasing temperature until ~50 °C, where activity starts to decline. Activity is lost after ~60 °C, which is the point at which the enzyme unfolds. Error bars represent the standard error of the mean (SEM) for two technical replicates.

The subsequent loss of activity upon reaching the enzymes unfolding temperature suggests that the loss of quaternary, tertiary or secondary structure reduces the ability for substrates to bind to the active site, thus the activity measured at 37 °C is not compromised by temperature.

2.3.1 Kinetic analysis

Kinetic analysis of enzyme activity offers information about enzyme specificity and mechanism, providing valuable insight into the function of an enzyme. Substrate concentration plays a significant role in the rate of enzyme catalysis and it decreases over time once a reaction has started due to the conversion of substrate to product. It is therefore imperative that the initial rate, V_0 is measured, since this is where substrate concentration is known and it avoids the complication of a reversible reaction.

A steady-state analysis provides key information about the reaction mechanism, including the Michaelis constants (K_m) and turnover number (k_{cat}). An enzyme is considered to be in steady-state when the rate of formation of the enzyme substrate complex [*ES*] is equal to its rate of breakdown. When excess substrate is mixed with enzyme it is assumed that the concentration of [*ES*] quickly increases to reach a steady-state, whose concentration does not change significantly during the initial part of a reaction for which the V_0 is measured.

E. coli PK1 is an allosterically regulated protein that can be activated via two different activation mechanisms (Section 1.6). Previous studies of *E.coli* PK1 have revealed that in the presence of the allosteric activator, FBP, and with respect to varying PEP concentrations, the enzyme follows a typical Michaelis-Menten type kinetic pattern displaying a hyperbolic curve (Hill coefficient (n_H) = 1).[7, 8] However, in the absence of activator, the enzyme displays a sigmoidal shaped curve because it has positive cooperative activation, caused by its substrate PEP (n_H = >1).

Equations for the two kinetic models are shown below:

Michaelis-Menten model: $$V_0 = \frac{k_{cat}[S]}{K_m + [S])}$$ **(Equation 2.1a)**

Hill cooperativity model: $$V_0 = \frac{k_{cat}[S]^n}{(S_{0.5}{}^n) + ([S]^n)}$$ **(Equation 2.1b)**

k_{cat}	Turnover number
$[S]$	Substrate concentration
$S_{0.5}$	Substrate concentration when half of the V_{max} is reached
V_0	Initial velocity
n_H	Hill coefficient

In this thesis, the data are fitted to Equations 2.1a and b and the $S_{0.5}$ is measured as both $S_{0.5}{}^{PEP}$, $S_{0.5}{}^{ADP}$ and $S_{0.5}{}^{FBP}$.

Kinetic analysis of wild-type PK1 was performed by measuring the V_0 at various PEP, ADP and FBP concentrations (Section 8.3). The collected data was processed and all relevant kinetic parameters were calculated (V_{max}, $S_{0.5}$, k_{cat}, n_H) using the program, OriginPro (Origin Lab, version 8.5.1).

The wild-type kinetic parameters relative to substrates PEP and ADP; and allosteric activator, FBP were determined at 37 °C. To determine the V_0 values of each of the substrates, the concentration of one was varied, while the other was fixed at a predetermined excess concentration (to ensure changes in rate were caused by the varied substrate), both in the absence and presence of FBP. To determine the FBP parameters, the V_0 was measured as a function of the effect when both substrates were at fixed concentrations.

Fitting the data to the Hill cooperative model allows the turnover number (k_{cat}), substrate concentration at half V_{max} ($S_{0.5}$) and the Hill coefficient (n_H) to be calculated (Table 2.1).[7]

Table 2.1 Kinetic parameters for wild-type PK1 determined by fitting the Hill equation (Equation 2.1b).[7] The results are fitted values from two technical replicates ± standard errors from the fit.

PEP							
- FBP				**+ FBP (2 mM)**			
k_{cat} s^{-1}	$S_{0.5}^{PEP}$ mM	n_H	$k_{cat}/S_{0.5}$ s^{-1}/ mM	k_{cat} s^{-1}	$S_{0.5}^{PEP}$ mM	n_H	$k_{cat}/S_{0.5}$ s^{-1}/ mM
243±4	4.27±0.05	5.2±0.3	57±1	266±3	0.090±0.002	1.51±0.03	2956±72
ADP							
- FBP				**+ FBP (2 mM)**			
k_{cat} s^{-1}	$S_{0.5}^{ADP}$ mM	n_H	$k_{cat}/S_{0.5}$ s^{-1}/ mM	k_{cat} s^{-1}	$S_{0.5}^{ADP}$ mM	n_H	$k_{cat}/S_{0.5}$ s^{-1}/ mM
345±31	1.0±0.2	1.05±0.07	338±73	329±11	0.57±0.06	1.31±0.06	577±64

The absence of FBP in solution produces a sigmoidal kinetic curve which is representative of positive cooperativity in PEP (n_H = 5.24 ± 0.26) (Figure 2.5a). These results are consistent with the PEP being a homotropic regulator of *E. coli* PK1. The k_{cat} of the PEP titrations are similar both with (266 ± 3 s^{-1}) and without (243 ± 4 s^{-1}) FBP in solution, however there is a dramatic decrease in the $S_{0.5}^{PEP}$ in the presence of FBP (0.090 ± 0.002 mM) in comparison to the results without FBP (4.27 ± 0.05 mM). This suggests that there is no loss of activity when FBP is not present, however the enzyme requires a higher concentration of PEP to reach maximum velocity (V_{max}).

Comparison of the ADP titration plots in the presence and absence of FBP do not reveal any major differences in maximum activity or ADP affinity ($S_{0.5}$) (Figure 2.5b). The presence of FBP causes a minor decrease in $S_{0.5}^{ADP}$ (-FBP, 1.02 ± 0.20 mM; +FBP, 0.57 ± 0.06 mM) and a small increase in the Hill coefficient n_H^{ADP} = 1.31, suggesting slight positive cooperativity. The small changes noted are not significant enough to propose an effect of FBP upon ADP binding. However, the data do imply that FBP binding influences PEP binding by heterotropic regulation as discussed in previous studies.[8]

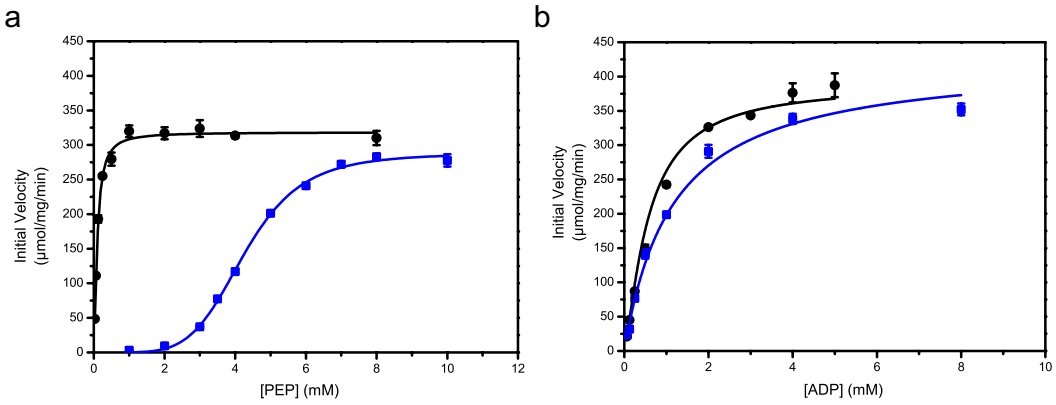

Figure 2.5 **Kinetic properties of wild-type PK1.** The activity of wild-type was measured at varying concentrations of substrates (PEP and ADP), in the absence (■) and presence (●) of FBP. **(a)** To obtain PEP response plots, the PEP concentration was varied and the ADP concentration was fixed (4 mM ADP). **(b)** To obtain ADP response plots, the ADP concentration was varied and the PEP concentration was fixed (-FBP, 8 mM PEP; +FBP, 2 mM PEP). Plots represent the best fit by a non-linear regression to the Hill equation.[7] Error bars represent the standard error of the mean (SEM) for two technical replicates.

The results presented confirm that FBP binding does not influence k_{cat}, however it does appear to affect the mechanism of PEP binding and activation.

2.3.2 Kinetic analysis with an alternative substrate, GDP

E. coli PK1 has been shown to be promiscuous, capable of transferring phosphates from PEP to several nucleoside diphosphate acceptors: adenosine, guanosine, uridine, inosine and cytidine diphosphates (ADP, GDP, UDP, IDP and CDP). Kinetic experiments suggest that GDP may be the best substrate for the enzyme, with a K_m value of only 0.05 mM.[9] However, *E. coli* PK1 starts to show signs of product inhibition at GDP concentrations higher than 0.04−0.05 mM, unlike ADP, which does not show any signs of inhibition even at concentrations of up to 10 mM ADP.

The substrate specificity of wild-type PK1 was tested following the same methods used previously (Section 2.3.1), however using GDP as a substrate in place of ADP.

The fitting of the data to the Hill cooperative model allows the turnover number (k_{cat}), the substrate concentration at half V_{max} ($S_{0.5}$) and the Hill coefficient n_H to be calculated (Table 2.2).[7]

Table 2.2 Kinetic parameters for wild-type PK1, using GDP as a substrate determined by fitting the Hill equation (Equation 2.1b).[7] The results are fitted values for two technical replicates ± standard errors of the fit.

PEP							
- FBP				**+ FBP (2 mM)**			
k_{cat} s^{-1}	$S_{0.5}^{PEP}$ mM	n_H	$k_{cat}/S_{0.5}$ s^{-1}/mM	k_{cat} s^{-1}	$S_{0.5}^{PEP}$ mM	n_H	$k_{cat}/S_{0.5}$ s^{-1}/mM
205±7	2.9±0.1	4.4±0.8	71±3	229±3	0.060±0.003	1.5±0.1	3817±199
GDP							
- FBP				**+ FBP (2 mM)**			
k_{cat} s^{-1}	$S_{0.5}^{GDP}$ mM	K_i mM	$k_{cat}/S_{0.5}$ s^{-1}/mM	k_{cat} s^{-1}	$S_{0.5}^{GDP}$ mM	K_i mM	$k_{cat}/S_{0.5}$ s^{-1}/mM
297±28	0.07±0.01	3±1	4243±728	384±10	0.090±0.003	2.0±0.2	4266±181

The absence of FBP in solution results in a sigmoidal kinetic curve, consistent with the PEP titrations using ADP as the substrate (Section 2.3.1). This sigmoidal curve is representative of positive cooperativity in PEP ($n_H = 4.4 \pm 0.8$) (Figure 2.6). These results are consistent with PEP acting as a homotropic regulator of *E. coli* PK1, irrespective of the phosphate acceptor. The k_{cat} of the PEP titrations are similar both with (229 ± 3 s^{-1}) and without (205 ± 7 s^{-1}) FBP in solution, however there is a significant decrease in the $S_{0.5}^{PEP}$ in the presence of FBP (0.060 ± 0.003 mM) compared to the results without FBP (2.9 ± 0.1 mM). This suggests that there is no loss of activity when FBP is absent, however the enzyme requires a higher concentration of PEP to reach maximum velocity (V_{max}).

Comparison of the GDP titration plots with and without FBP do not reveal any major differences. The presence of FBP causes a slight increase in maximum velocity, however, overall the trend is very similar. As expected, increased concentrations of GDP result in substrate inhibition[9] which is apparent by the decrease in activity at concentrations over 0.5 mM GDP.

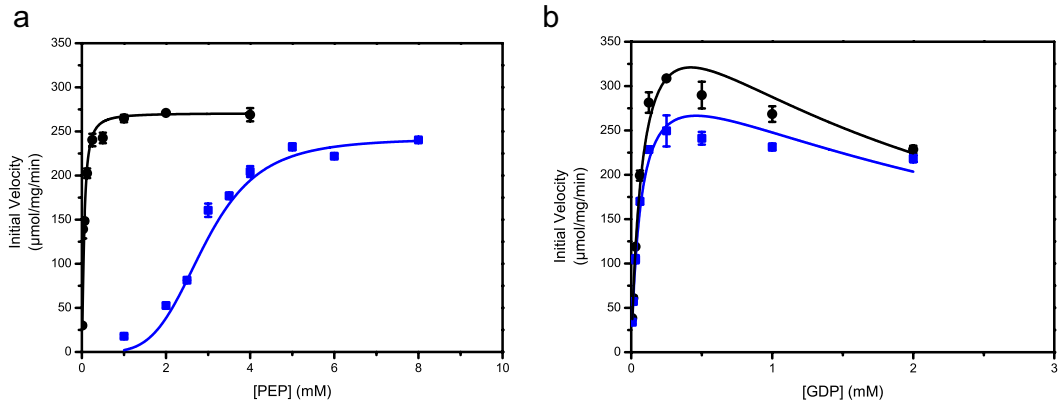

Figure 2.6 **Kinetic properties of wild-type PK1.** The activity of wild-type was measured at varying concentrations of substrates (PEP and GDP), in the absence (■) and presence (●) of FBP. **(a)** To obtain PEP response plots, the PEP concentration was varied and the GDP concentration was fixed (0.25 mM GDP). **(b)** To obtain GDP response plots, the GDP concentration was varied and the PEP concentration was fixed (-FBP, 8 mM PEP; +FBP, 2 mM PEP). Plots represent the best fit by a non-linear regression to the Hill equation.[7] Error bars represent the SEM of two technical replicates.

The inhibitor constant (K_i) provides an indication of how potent an inhibitor is. The K_i is calculated based on the concentration of inhibitor that is required to reduce the enzyme activity to half of the maximal rate. In this case, the K_i is 2 mM in the presence of FBP, however in the absence of the activator, a higher concentration of GDP ($K_i = 3 \pm 1$ mM) is required to inhibit the enzyme.

The results presented confirm that with an alternative substrate (GDP), FBP binding does not affect the k_{cat}, however it does appear to affect the mechanism of PEP binding and activation. Using the non-conventional GDP as a substrate instead of ADP provides an eight-fold higher specificity constant ($k_{cat}/S_{0.5}$), suggesting that GDP is a better substrate for the enzyme. However, GDP inhibits enzyme activity at very low concentrations, which could explain why ADP is the preferred substrate within the cell.[10]

2.4 Wild-type PK1 mass and thermal stability

2.4.1 Mass spectrometry

Mass spectrometry is an analytical chemistry technique that can provide quantitative molecular mass information on molecules, such as proteins upon their conversion to ions. Electrospray ionisation is the source used to ionise the molecules. A high voltage is applied to a solution of molecules (or proteins), which produces a gaseous phase of charged molecules to be sprayed into the mass spectrometer. The ions move through the mass analyser, to the detector, at a speed determined by their mass to charge (m/z) ratio. The data produced is analysed by first identifying the charge state of the ions and then identifying the mass based upon the m/z ratio (Section 8.4.1).[11]

Mass estimation of wild-type from *E. coli* K12 using ExPASy's ProtParam tool[12] provided a theoretical mass of 50,729.4 Da.[12] This mass is consistent with the deconvoluted mass of 50,729.5 Da derived from the mass spectrometer, confirming the wild-type protein is intact.

2.4.2 Thermal stability of wild-type PK1

Differential scanning fluorometry (DSF) was used to determine the unfolding temperature of wild-type. Thermal shift assays, such as DSF, work by binding a fluorescent dye to the hydrophobic regions of proteins, commonly the core region and measuring the increase in fluorescence as the protein unfolds and the dye is exposed. Denaturation is controlled by slowly heating the protein from an ambient temperature of around 20 °C to 100 °C. This heating induces changes in the hydration shells and the breaking of hydrogen bonds which leads to conformational restructuring of the protein and eventually results in denaturation and unfolding.[13] Interactions between the hydrophobic residues and the dye cause the dye to emit an increased fluorescence, which can be measured and recorded.[14] A higher unfolding temperature suggests more hydrogen bonds and types of interactions, thus a more stable protein and vice versa.

The DSF results provide an unfolding temperature (T_m) of 62 °C for the wild-type enzyme. This unfolding temperature is relatively high for a non-thermophilic enzyme,[15] as mesophilic enzymes typically unfold below 60 °C,[16, 17] however this value is consistent with other PK enzymes, such as *Trypanosoma cruzi*, 56 °C and *Trypanosoma brucei*, 45 °C.[18]

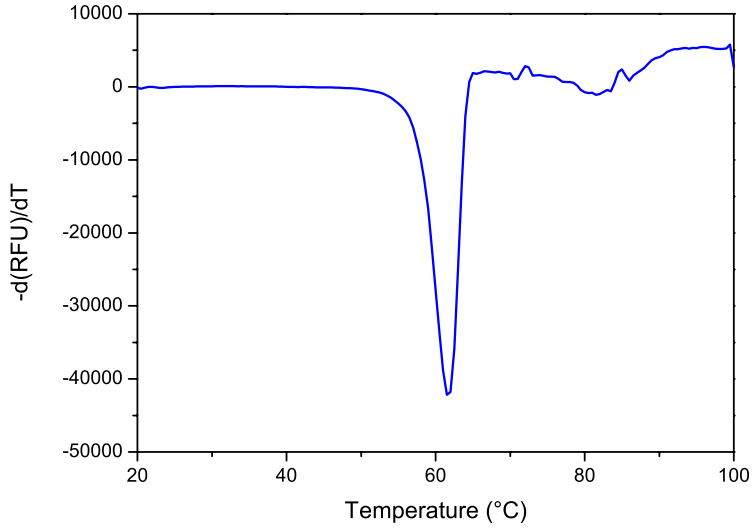

Figure 2.7 Unfolding temperature of the wild-type PK1 enzyme is 62 °C. The T_m peak is shown as a negative derivative of relative fluorescence units (RFU). The curves depict the mean of three technical replicates.

2.5 Crystal structure of wild-type PK1 with improved resolution

A high resolution structure of the wild-type PK1 enzyme is important to provide an accurate reference for comparison with the evolved enzymes. X-ray crystallography was employed to determine a more complete structural model of the *E. coli* PK1 enzyme, since the original structure (PDB ID: 1PKY) was missing a mobile loop region (residues 344−351) in all four of the subunits, and 30 residues from the lid domain of subunit 3.

X-ray crystallography is a valuable tool that uses X-ray diffraction to identify the average structure of macromolecules for rational inhibitor design and mechanistic understanding.[19] The first step of X-ray crystallography involves crystallisation, which requires driving a supersaturated solution of macromolecules (in this case proteins) out of solution to form an ordered array of atoms – the crystal. The vapour diffusion method used in this work was performed using a sealed hanging drop growth plate, housing a small protein-precipitant drop and a larger reservoir of a higher concentration precipitant. The closed system results in the movement of water from the supersaturated protein drop into the reservoir until the concentration of crystallant is equivalent in both solutions.[20] This slowly decreases the size of the protein drop which increases the concentration of protein molecules in the drop, forcing the protein molecules into close proximity where they begin to pack together.[21]

Crystal formation requires two steps: firstly a nucleation event, which creates the seed wherefrom the crystal will grow, and secondly crystal growth, which is the attachment of new molecules to the surface of the growing crystal.[20]

The crystallised protein is then flash cooled in a cryo-protectant to reduce X-ray radiation damage[19] and mounted onto the X-ray beamline goniometer. The protein crystal is exposed to monochromatic collimated X-rays while it is rotated, which creates a diffraction pattern of regularly spaced reflections (or spots) based upon the ordered array of atoms within the crystal.

Crystal diffraction is the incidence of X-rays hitting the ordered array of atoms in a crystal. Bragg's Law determines where a diffraction spot will be observed, and the spacing of the measured spots is inversely proportional to the spacing of planes within the crystal.[22]

Braggs Law: $2d \sin\theta = n\lambda$ **(Equation 2.2)**

λ	Wavelength
θ	Scattering angle
d	Spacing between layers of atoms

The intensity of the diffraction spot is dependent on how many atoms lie on the specific plane in the unit cell.

After data collection, the raw intensities are indexed, scaled and merged, and lastly the phases are determined. Indexing produces the dimensions of the unit cell and symmetry information (space group). Merging and scaling involves combining all of the information from ~360 images and normalising their intensities.[23] The final step to solving a crystal structure is phasing. Unfortunately the phase information can not be directly recorded during the diffraction experiment, this is referred to as the phase problem. Both amplitude and phase information are necessary for solving a crystal structure, therefore there are several methods available to determine the phases of a structure. Molecular replacement was the phasing method used in this work; it requires using a similar or related structure as a search model to determine the orientation and position of molecules within the unit cell.[24]

Crystal structural refinement involves fitting the model atoms into the electron density to create a reliable and accurate representation of the true crystal structure.[19] As the model improves, the theoretical amplitudes calculated from the model should converge with the observed amplitudes; this is followed by the crystallographic *R*-factors.

2.5.1 Data collection and processing

Multiple data sets were collected on crystals from various drops; one of which produced a crystal that diffracted to 2.19 Å. This crystal came from a co-crystallisation drop containing 2 mM PEP. However, co-crystallisation with PEP was unsuccessful due to the lack of clear electron density consistent with a PEP molecule in the active site of the final refined model. Given the presence of a long axis (c = 241 Å), the crystal to detector distance was optimised to minimise overlapping reflections at the cost of resolution, such that completeness in the outermost shell (2.25−2.22 Å) was only 51% despite a signal:noise ratio of 4.0. Notwithstanding the lack of electron density for PEP, the 2.19 Å dataset was processed and evaluated for structure determination and refinement.

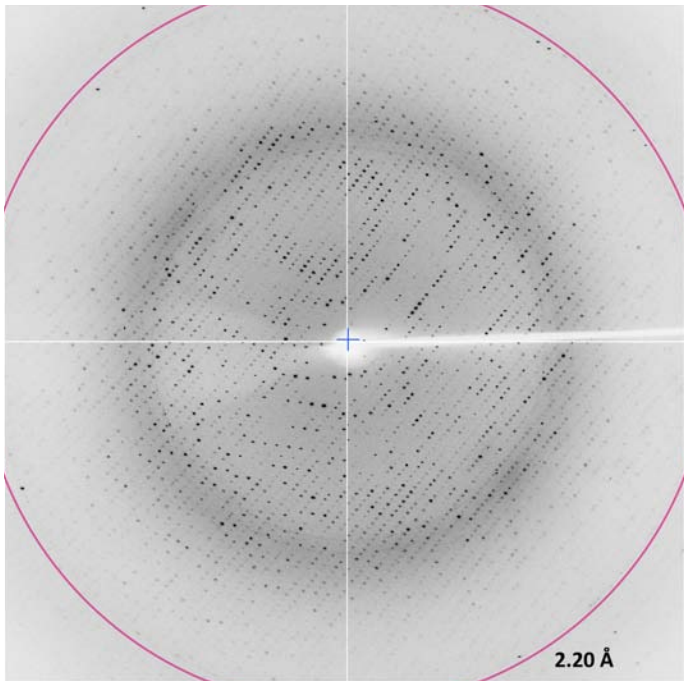

Figure 2.8 X-ray diffraction of wild-type PK1, displaying one of the 360 images merged for structure determination. Diffraction to 2.20 Å is marked with a ring.

2.5.2 Structure determination and refinement

All relevant data collection and processing parameters are provided in Table 2.3. The diffraction data exhibits mild anisotropy, with weaker reflections found in the c* direction resulting in a 2.28 Å resolution limit (Figure 2.9).[25] Initial space group analysis suggested a primitive orthorhombic ($P2_12_12_1$) space group and data quality assessment using *XTRIAGE* from the *PHENIX* package[26] revealed that the crystal had pseudo-translational symmetry (Figure 2.10). Molecular replacement was performed with the program *PHASER*[27] from the *CCP4* suite of programmes[28] using the monomer of *E. coli* PK1 as a search model (PDB ID: 1PKY).[2] Initial rounds of refinement were carried out in *REFMAC5* [29] from the *CCP4* program suite. Refinement of data in the $P2_12_12_1$ space group resulted in the lid domain of one subunit having unresolved electron density; however, careful inspection allowed the lid to be modelled as two separate conformations. Continued refinement provided R_{free} values that would not decrease below 30%. At this stage, it was suspected that the space group might have been misassigned.

Table 2.3 X-ray data collection statistics. Statistical values for the highest resolution shells are given in parentheses. The Matthews coefficient and solvent content are based on eight monomers, with a molecular weight of 50,729 Da each in the asymmetric unit.

	Escherichia coli PK1
Data-collection statistics	
Wavelength (Å)	0.9537
Number of images	360
Oscillations (°)	0.5
Space group	$P2_1$
Cell parameters *a*, *b*, *c*, β (Å; º)	130.1, 74.6, 241.8; 90.14
Mol/asym. unit	8
Resolution range (Å)	45.32-2.28 (2.32-2.28)
Unique reflections	201,780 (8,896)
Mean I/σ(I)	9.7 (3.0)
Completeness (%)	95.2 (85.6)
R_{merge} †	0.078 (0.273)
Multiplicity	3.3 (2.5)
Refinement details	
Resolution (Å)	2.28
R_{work}/R_{free} ‡ (%)	21.7/24.5
No. of atoms §	
Total	30,508
Macromolecules	27,987
Ligands	12
Water	2461
Protein residues	3720
*B*factors (Å^2)	
Macromolecules	28.8
Ligands	32.2
Water	26.6
Ramachandran plot, residues in (%)	
Most favoured regions	95.80
Additionally allowed regions	3.25
Disallowed regions	0.95
All-atom clashscore	2.43

† $R_{merge} = \sum_{hkl}\sum_i |I_i\,(hkl) - \langle I(hkl)\rangle| / \sum_{hkl}\sum_i I_i\,(hkl)$ where $I_i\,(hkl)$ is the *i*th intensity measurement of reflection *hkl*, $\langle I(hkl)\rangle$ is its average and *N* is the redundancy of a given reflection.
‡ $R = \sum_{hkl} ||F_{obs}| - |F_{calc}|/\sum_{hkl} |F_{obs}|$. R_{free} is calculated using reflections belonging to a test set of randomly selected data comprising 5% of the data.
§ Not including riding H atoms.

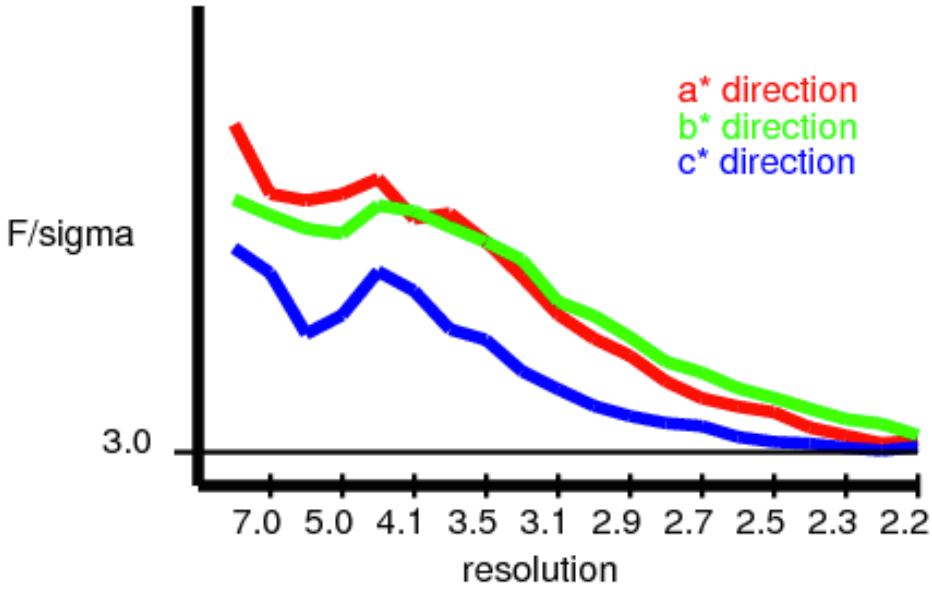

Figure 2.9 F/sigma was plotted for the three principal directions of the crystal, a*, b* and c*. The anisotropic analysis suggests resolution limits of 2.2 Å along the a*, b* and c* directions.[25]

Scaling in a lower symmetry primitive monoclinic space group ($P2_1$) was successful and the newly scaled data was assessed in *XTRIAGE,* revealing one pseudo-merohedral twin operator that had been masked by the pseudo-translation. The twin fraction was estimated to be 0.457 by the cumulative distribution of H[30] and 0.43 by the Britton plot (Figure 2.11).[31] Analysis of the native Patterson map in $P2_1$ showed the presence of one significant off-origin peak that is 41% of the origin peak, centred at coordinates 0.000, 0.442, 0.500; strongly suggesting pseudo-translational symmetry (Figure 2.10).

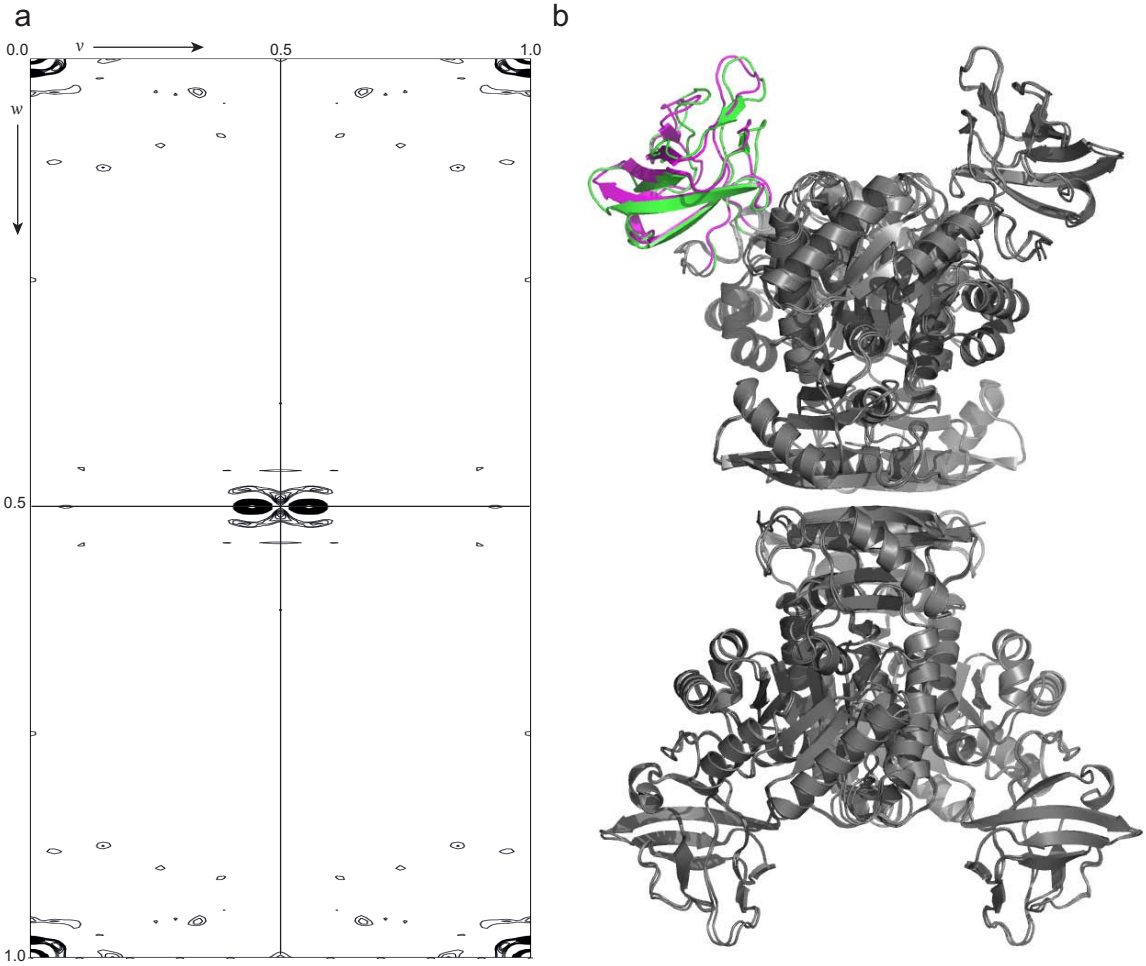

Figure 2.10 Detection of pseudo-translation in wild-type PK1 crystals. (a) The plot shows the native Patterson calculated for the unit cell at 2.28 Å resolution at section $u = 0.0$. Contoured at every 1σ starting from 2σ. There is a visible peak at coordinates 0.000, 0.442, 0.500, corresponding to the translation vector between the two wild-type tetramers in the asymmetric unit. **(b)** Near perfect translational non-crystallographic symmetry. The two tetramers are superimposed revealing one lid domain, subunit 3 (coloured) in an altered conformation. The regions of the structures that align well are in grey.

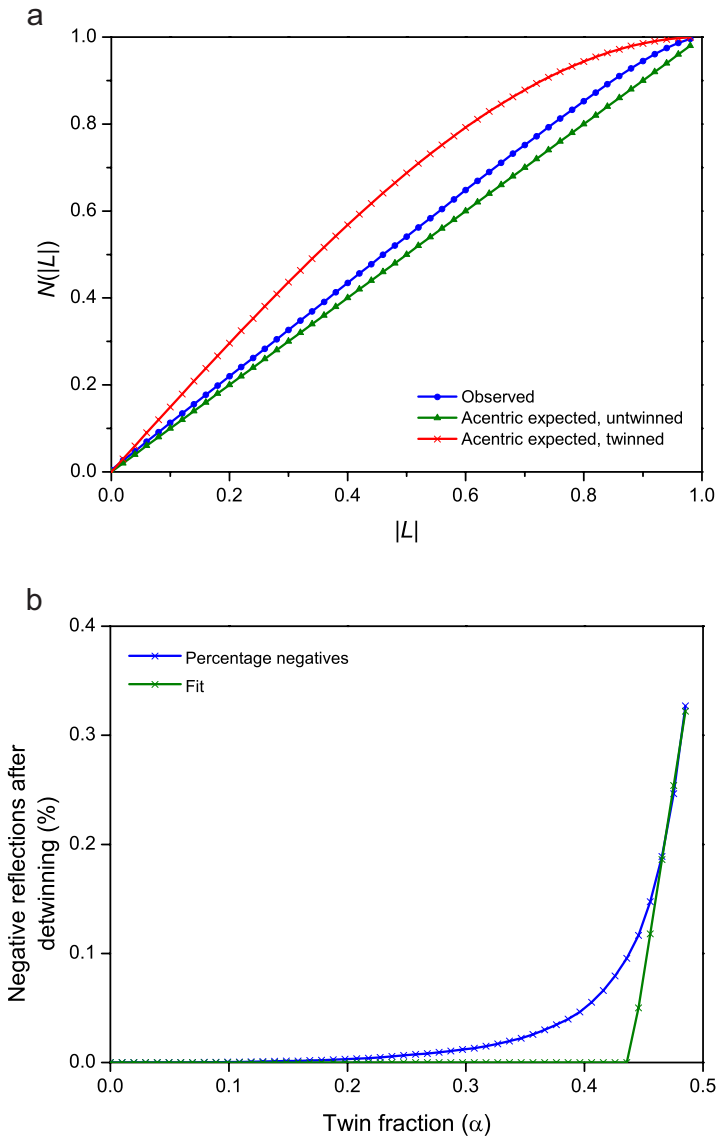

Figure 2.11 **Twinning detection in wild-type PK1 crystal.** **(a)** Twinning detection using the *L*-test: $|L|$ is plotted against $N(|L|)$. L is given by $(I_1-I_2)/(I_1+I_2)$, where I_1 and I_2 are the intensities of unrelated reflections and $N(|L|)$ is the cumulative probability distribution of L. The *L*-test suggests the acentric data could be twinned (0.466). **(b)** The Britton plot: percentage of twin fractions. Extrapolation of the curve (green line) yields a twin fraction of 0.438.[31]

Simulated annealing and subsequent iterative adjustments were performed using *REFINE* from the *PHENIX* package,[26] including NCS restraints. Identification and inclusion of the twinning operator (*h*, *-k*, *-l*) in *REFINE* reduced the final refined R_{factor} (21.7%) and R_{free} (24.5%) and a final refined twinning fraction $\alpha = 0.49$. This model includes all residues except some of those within the disordered mobile loop (residues 354–351) for seven of the eight chains; however, these residues could be modelled in at 0.5 σ $2F_o–F_c$ maps.

2.5.3 Crystal structure results

The previously reported work on *E. coli* PK1 in the unliganded T-state (tensed) concluded that the space group was $P2_12_12_1$,[2] despite preliminary structure determination in the $C222_1$ space group.[32] The 2.50 Å resolution primitive orthorhombic *E. coli* PK1 structure has a R_{free} value of 30.7% coupled with a large gap between the R_{factor} and R_{free} (20.5% and 30.7%, respectively), suggesting some ambiguity or incompleteness in the structure determination.

Here, the structure of wild-type PK1 was determined at 2.28 Å resolution in space group $P2_1$, as described above (Section 2.5.2). The wild-type PK1 model in its final development contains two tetramers in the asymmetric unit with 3720 residues and a high number of water molecules (2461) given the resolution (see Table 2.3 for model refinement statistics). Superimpositions of the $(\beta/\alpha)_8$-barrel and C-domain regions of the subunits of the two tetramers reveals that one mobile lid domain of each tetramer adopts a slightly different conformation to that of the six other well-ordered lid domains (Figure 2.12). Overlays of the new wild-type PK1 structure and the original 1PKY model were created by aligning the structures at the $(\beta/\alpha)_8$-barrel and C-domain regions. These overlays confirm that the secondary, tertiary and quaternary features are very similar between the old (1PKY) and new models. All three domains: the $(\beta/\alpha)_8$-barrel, C-domain and the lid domains are tightly packed with the exception of the lid domain with relatively high atomic displacement parameters. A putty diagram shows the relative atomic displacements of the tetramer, highlighting the flexibility of backbone atoms in one lid domain of each tetramer (Figure 2.12).

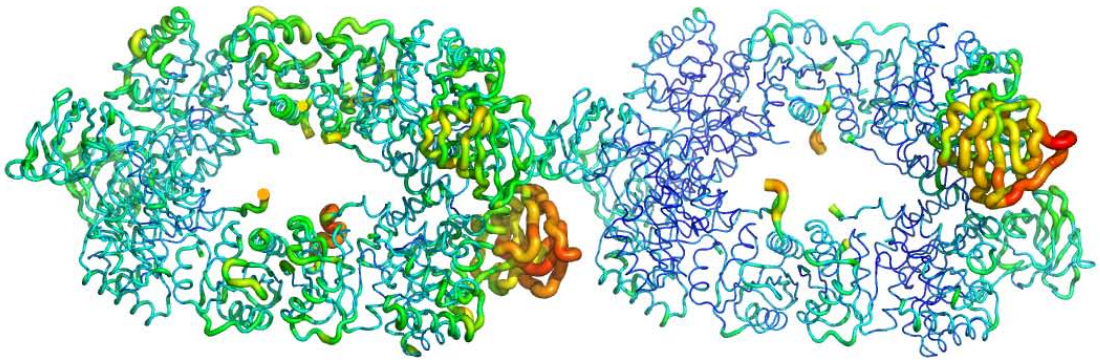

Figure 2.12 Wild-type PK1 two tetramers in the asymmetric unit displayed by B-factor putty model to highlight the relative atomic displacements. (*Red*: high B-factor to *Blue*: low B-factor).

The 2.28 Å resolution limit of the data is substantially better than the previous 2.50 Å published structure. However, the presence of mild anisotropy in one direction (*c** axes) and the long axis that necessitated a long crystal-detector separation that limited the resolution due to a sharp drop-off in completeness as higher resolution reflections were confined to corners of the detector (Figure 2.9). Nonetheless, the outer shell statistics, including an excellent signal:noise ratio of 3.0, coupled with an R_{merge} of 0.078 and adequate redundancy of 2.5, meant that a larger portion of the structure was able to be modelled, including ~30 residues in a previously unmodelled lid domain and allowed clear identification of the tetrahedral electron density in the FBP binding site. This latter density was modelled as sulphate, which was present in the crystallisation medium. The sulphate is buried in a hydrophobic pocket and hydrogen bonded to residues Thr378, Gln379, Gly380, Ser383 and Gly460. Although there is not yet a structure of the activated *E. coli* PK1 with FBP bound, the sulphate ion in the activator pocket suggests a possible binding position of the 6'-phosphate of FBP (Figure 2.13).[33, 34]

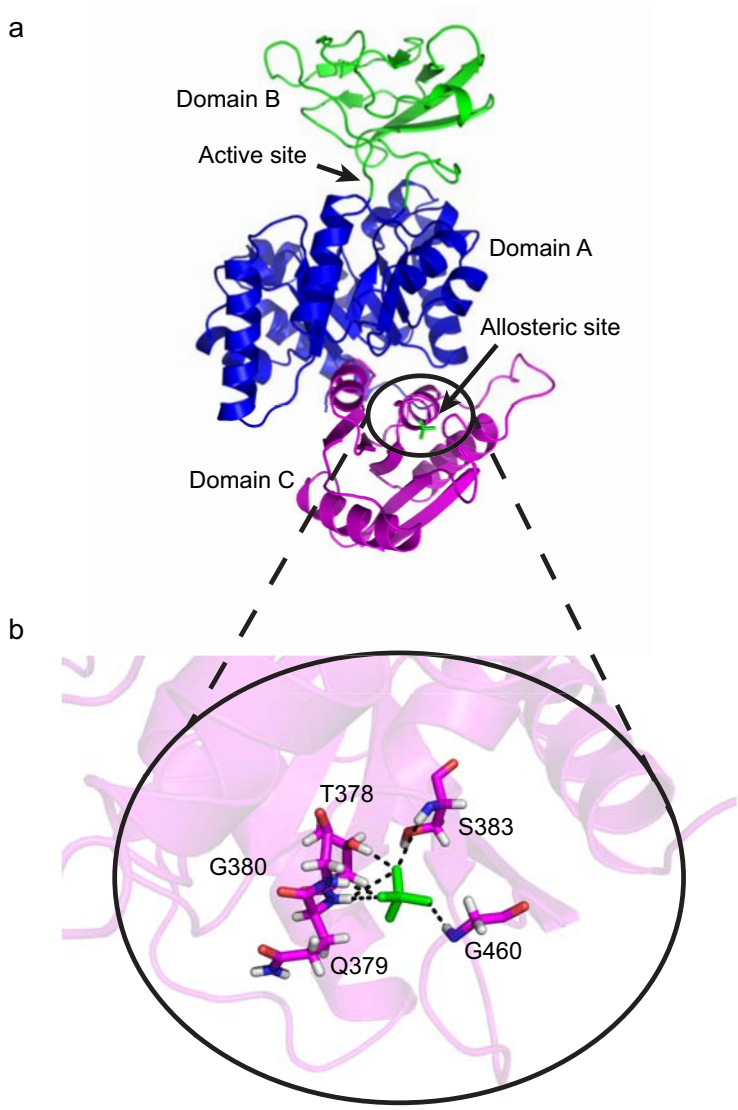

Figure 2.13 Wild-type PK1 structural model showing a sulphate bound in the allosteric binding pocket. **(a)** Static view of a single wild-type PK1 subunit with sulphate (green) bound in the activator-binding pocket. The A domain is coloured blue, and the B and C domains are coloured green and magenta, respectively. **(b)** Static view of the allosteric site with sulphate bound in the phosphate-binding pocket. Hydrogen bonds are formed between the sulphate and residues T378, Q379, G380, S383 and G460 and are denoted with dashed lines.

This work demonstrates the determination of a higher resolution crystal structure in a new twinned space group that provides a model for the T-state of PK1 from *E. coli* with new, as well as improved, information about the structure and dynamics. The final refined tetramer with labelled interfaces is presented below (Figure 2.14).

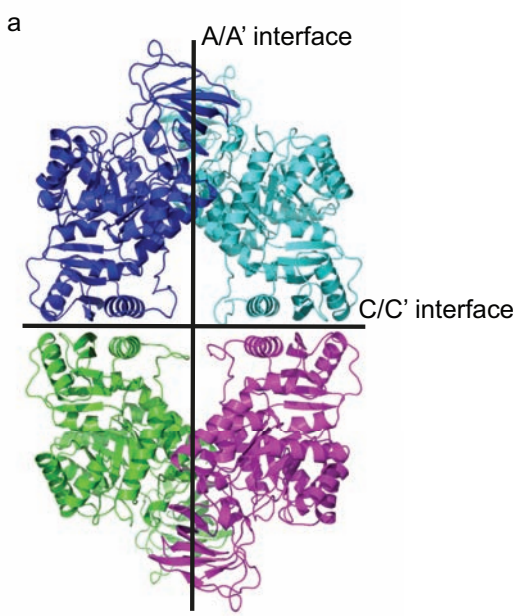

Figure 2.14 Wild-type PK1 tetramer with the A/A' and C/C' interfaces labelled. The four subunits of the tetramer are coloured differently.

Interface interactions have been shown to be extremely important for the activation and consequential conformational changes in several PK isomers.[18, 33, 34] X-ray structure analyses have shown FBP binding causes a rigid-body subunit rotation where the allosteric domains rotate away from each other and the $(\beta/\alpha)_8$-barrel domains rotate inwards, increasing their surface area.

Crystal structure analysis of the A/A' and C/C' interfaces using the online PDBePISA server (version 1.51)[35] found the surface areas to be 1152 Å and 925 Å, respectively. More specific analysis suggests that the A/A' interface is much more stable with a significantly higher number of bonds forming across the interface. PDBePISA[35] identified ten potential hydrogen bonds and eleven potential salt bridges across the A/A' interface, whereas seven potential hydrogen bonds and one potential salt bridge are found spanning the C/C' interface. Moreover, the average solvation energy for the A/A' interface is -6.9 kcal/mol and -9.6 kcal/mol for the C/C' interface, suggesting that the C/C' interface is more hydrophobic and therefore a more favourable protein-protein interaction site than the A/A' interface.[35, 36]

2.6 SAXS confirms the structure in solution

Small-angle X-ray scattering provides a means of studying the low resolution (10−50 Å) structure and interactions of biological macromolecules in solution. SAXS can provide insight into the behaviour of proteins in solution, such as large conformational changes and protein-protein interactions. Furthermore, these changes can be investigated as a function of solution condition (i.e. ligand concentration, temperature, pH, salt adducts).[37, 38]

The basic concept of SAXS is the elastic scattering of X-rays, when a collimated monochromatic X-ray beam hits molecules in solution.[39, 40] The scattering intensity (I) is recorded by a detector as a function of the momentum transfer (s),[38]

Momentum transfer: $$s = \frac{4\pi \sin(\theta)}{\lambda}$$ **(Equation 2.3)**

s	Momentum transfer
λ	Wavelength
θ	Scattering angle

Where 2θ is the angle between the incident and scattered beam, and λ the X-ray wavelength. The recorded scattering profile is presented as a one-dimensional scattering curve, providing information about the global structure (size, oligomeric state, shape) of the molecules in solution.[39] Several parameters can be extracted from a SAXS profile, including: the radius of gyration (R_g), estimated moleculer mass (MM), maximum particle diameter (D_{max}) and the forward scattering intensity ($I(0)$). The Guinier analysis is the most straightforward method of extracting the R_g and $I(0)$,[38, 41]

Guinier equation: $I(s) = I(0) \exp(-(1/3)R_g^2 s^2)$ **(Equation 2.4)**

I	Scattering intensity
s	Momentum transfer
$I(0)$	Forward scattering intensity
R_g	Radius of gyration

In addition, Guinier analysis plots provide a measure of sample quality. A non-linear Guinier indicates poor sample quality that could be due to inaccurate background substraction, sample polydispersity or the presence of inter-particle effects. For example, samples that contain a large proportion of non-specific aggregates produce scattering curves and Guinier plots with an increase in intensity at small q values, whereas samples containing inter-particle repulsion produce curves and Guinier plots with a decrease in intensity at lower q values.[40]

Here, SAXS has been used to investigate the size and shape information of wild-type PK1 in solution.

2.6.1 Wild-type PK1 is a tetramer in solution

SAXS analysis was employed to validate the crystal structure of wild-type in solution. The sample quality was firstly assessed by Guinier analysis. The linear Guinier plot below (Figure 2.15) confirmed the sample was of a high quality without any significant aggregate or inter-particle interactions.

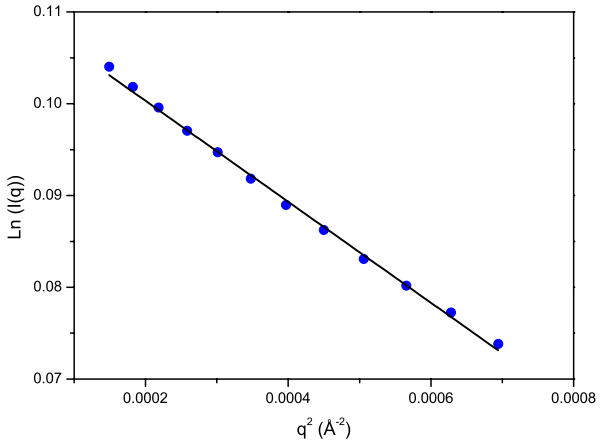

Figure 2.15 Guinier analysis of wild-type PK1, the linear fit demonstrates very good sample quality. Linear fit with an R-Square of 0.998.

Scattering data are presented as both an intensity plot and a *P*(*r*) plot (Figure 2.16). The bell shape of the *P*(*r*) plot confirms the protein is a large globular shape in solution.[42] The elongated tail observed in the real space distance distribution (*P*(*r*)) plot is consistent with a slightly elongated shape in solution, [44] supporting the description of the wild-type crystal structure, which has an elongated r-axis (Figure 2.14).[2, 42]

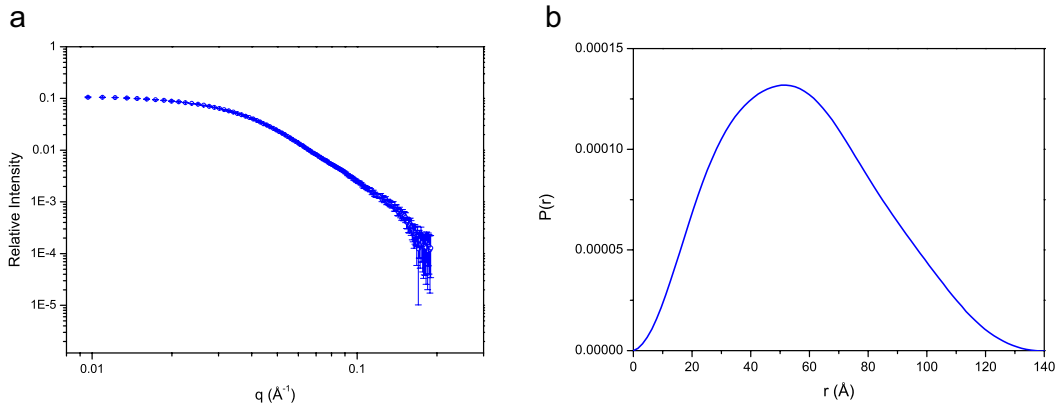

Figure 2.16 SAXS analysis of wild-type PK1 descibes a globular protein in solution. (a) Experimental scattering profile of the wild-type enzyme presented as an intensity plot with error bars. **(b)** *P*(r) plot of wild-type.

Radius of gyration (R_g) calculations using *GNOM*[43] were determined to be 44.5 Å (Table 2.4). In addition, the maximum dimension of the scattering particle (D_{max}) for wild-type

PK1 in solution was determined to be 141.9 Å using *AUTOPOROD* and 146.8 Å for the structural envelop determined using *CRYSOL*.[37]

Table 2.4 Wild-type PK1 parameters calculated from SAXS values.

	Radius of gyration[a] Å	$I(0)$[a]	D_{max}[b] Å	Molecular mass[b] kDa
Wild-type	44.5 ± 0.1	0.114	141.9	190

[a] Calculated using *GNOM*.

[b] Calculated using *AUTOPOROD*.

Direct comparisons of the experimentally determined SAXS scattering curves and the theoretical scattering generated from the X-ray crystal structure were performed using *CRYSOL*.[37] The scattering profile in solution is in agreement with the scattering profile created from the crystal structure (Chi (discrepancy of the fit) = 0.791) confirming that the structure *in crystal* is a good representation of the enzyme structure *in solution* (Figure 2.17). The overlay is a very good fit at low q regions (lower resolution) and a good fit at the higher q regions. Any minor differences could be due to crystal packing or the presence of precipitants and cryo-protectants, such as polyethylene glycol (PEG).

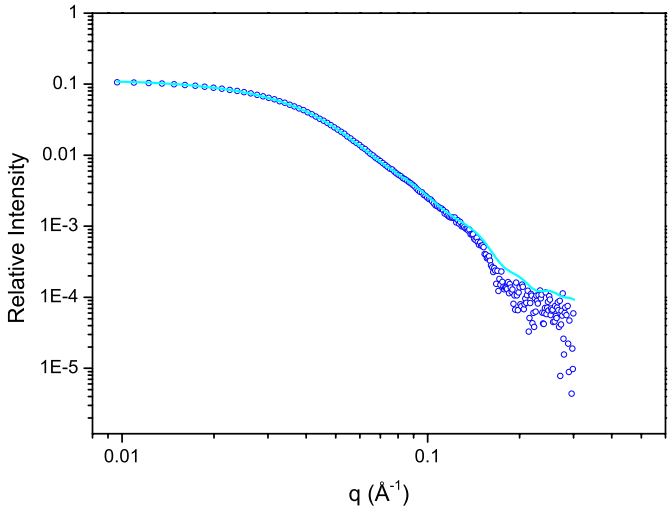

Figure 2.17 SAXS comparison of wild-type solution and crystal structural scatter. Experimental scattering profile of the wild-type enzyme (o) and theoretical scatter generated from the wild-type crystal structure (cyan line). The theoretical scattering profiles were generated from crystallographic coordinates using *CRYSOL*.[37]

2.7 Summary

Here, the *E. coli* wild-type PK1 enzyme was successfully purified and functionally/structurally characterised to provide a reference for comparison against the eight evolved *E. coli* PK1 enzymes investigated in Chapters Three to Six.

Functional analysis is in line with previous studies,[4, 8, 44] confirming that the wild-type is heterotropically activated by its allosteric activator, FBP producing classic Michaelis-Menten kinetics, and homotropically activated by its substrate PEP, producing cooperative binding.

Crystal and solution structural analyses were performed to confirm that the enzyme is an elongated globular shape consisting of four identical subunits which form a homotetramer. The atomic detail gained in the wild-type crystal structure provides a complete structural model for comparison with the evolved enzymes and identification of a sulphate bound in the allosteric domain delivered the first evidence identifying the activator binding site in the *E. coli* PK1 enzyme.

The wild-type PK1 functional and high resolution structural data presented in this chapter enables accurate investigation of the functional and structural consequences of the eight mutations by comparison with the ancestral reference.

2.8 References

[1] Muñoz, M, and Ponce, E. (2003) Pyruvate kinase: Current status of regulatory and functional properties, *Comp. Biochem. Physiol. Biochem. Mol. Biol. 135*, 197-218.

[2] Mattevi, A, Valentini, G, Rizzi, M, Speranza, ML, Bolognesi, M, and Coda, A. (1995) Crystal structure of *Escherichia coli* pyruvate kinase type I: Molecular basis of the allosteric transition, *Structure 3*, 729-741.

[3] Mattevi, A, Bolognesi, M, and Valentini, G. (1996) The allosteric regulation of pyruvate kinase, *FEBS Lett. 389*, 15-19.

[4] Speranza, ML, Valentini, G, and Malcovati, M. (1990) Fructose-1,6-bisphosphate-activated pyruvate kinase from *Escherichia coli.* Nature of bonds involved in the allosteric mechanism, *Eur. J. Biochem. 191*, 701-704.

[5] Malcovati, M, and Valentini, G. (1982) AMP- and fructose 1,6-bisphosphate-activated pyruvate kinases from *Escherichia coli*, *Methods Enzymol. 90*, 170-179.

[6] Lenski, RE, and Travisano, M. (1994) Dynamics of adaptation and diversification: a 10,000-generation experiment with bacterial populations, *Proc. Natl. Acad. Sci. U. S. A. 91*, 6808-6814.

[7] Hill, A. (1910) The possible effects of the aggregation of the molecules of haemoglobin on its dissociation curves, *J. Phys. 40*, i-vii.

[8] Valentini, G, Chiarelli, L, Fortini, R, Speranza, ML, Galizzi, A, and Mattevi, A. (2000) The allosteric regulation of pyruvate kinase: A site-directed mutagenesis study, *J. Biol. Chem. 275*, 18145-18152.

[9] Waygood, EB, Rayman, MK, and Sanwal, B. (1975) The control of pyruvate kinases of *Escherichia coli*. II. Effectors and regulatory properties of the enzyme activated by ribose 5-phosphate, *Can. J. Biochem. 53*, 444-454.

[10] Saito, T, Nishi, M, Lim, MI, Wu, B, Maeda, T, Hashimoto, H, Takeuchi, T, Roos, DS, and Asai, T. (2008) A novel GDP-dependent pyruvate kinase isozyme from *Toxoplasma gondii* localizes to both the apicoplast and the mitochondrion, *J. Biol. Chem. 283*, 14041-14052.

[11] Banerjee, S, and Mazumdar, S. (2012) Electrospray ionization mass spectrometry: a technique to access the information beyond the molecular weight of the analyte, *Int. J. Anal. Chem. 2012*, 282574.

[12] Wilkins, MR, Gasteiger, E, Bairoch, A, Sanchez, JC, Williams, KL, Appel, RD, and Hochstrasser, DF. (1999) Protein identification and analysis tools in the ExPASy server, *Methods Mol. Biol. 112*, 531-552.

[13] Vollrath, F, Hawkins, N, Porter, D, Holland, C, and Boulet-Audet, M. (2014) Differential Scanning Fluorimetry provides high throughput data on silk protein transitions, *Sci. Rep. 4*, 5625.

[14] Niesen, FH, Berglund, H, and Vedadi, M. (2007) The use of differential scanning fluorimetry to detect ligand interactions that promote protein stability, *Nat. Protoc. 2*, 2212-2221.

[15] Ku, T, Lu, P, Chan, C, Wang, T, Lai, S, Lyu, P, and Hsiao, N. (2009) Predicting melting temperature directly from protein sequences, *Comput. Biol. Chem. 33*, 445-450.

[16] Jaenicke, R, and Bohm, G. (1998) The stability of proteins in extreme environments, *Curr. Opin. Struct. Biol. 8*, 738-748.

[17] Cardenas, ML. (2013) Michaelis and Menten and the long road to the discovery of cooperativity, *FEBS Lett. 587*, 2767-2771.

[18] Morgan, HP, Zhong, W, McNae, IW, Michels, PAM, Fothergill-Gilmore, LA, and Walkinshaw, MD. (2014) Structures of pyruvate kinases display evolutionarily divergent allosteric strategies, *R. Soc. Open. Sci. 1*, 140120.

[19] Garman, EF. (2014) Developments in X-ray crystallographic structure determination of biological macromolecules, *Science 343*, 1102-1108.

[20] McPherson, A, and Gavira, JA. (2014) Introduction to protein crystallization, *Acta Crystallogr. Sect. F Struct. Biol. Cryst. Commun. 70*, 2-20.

[21] Rhodes, G. (2006) *Crystallography made crystal clear*, Third Edition ed., Burlington, Academic Press.

[22] Bragg, WB, WL. (1915) *X-rays and crystal structure*, London, G. Bell and Sons, Ltd.

[23] Evans, PR. (2011) An introduction to data reduction: space-group determination, scaling and intensity statistics, *Acta Crystallogr. D Biol. Crystallogr. 67*, 282-292.

[24] Rossmann, MG. (1990) The molecular replacement method, *Acta Crystallogr. A 46 (Pt 2)*, 73-82.

[25] Strong, M, Sawaya, MR, Wang, S, Phillips, M, Cascio, D, and Eisenberg, D. (2006) Toward the structural genomics of complexes: crystal structure of a PE/PPE protein complex from *Mycobacterium tuberculosis*, *Proc. Natl. Acad. Sci. U. S. A. 103*, 8060-8065.

[26] Adams, PD, Afonine, PV, Bunkóczi, G, Chen, VB, Davis, IW, Echols, N, Headd, JJ, Hung, L-W, Kapral, GJ, and Grosse-Kunstleve, RW. (2010) PHENIX: a comprehensive Python-based system for macromolecular structure solution, *Acta Crystallogr. D Biol. Crystallogr. 66*, 213-221.

[27] McCoy, AJ, Grosse-Kunstleve, RW, Adams, PD, Winn, MD, Storoni, LC, and Read, RJ. (2007) Phaser crystallographic software, *J. Appl. Crystallogr. 40*, 658-674.

[28] Winn, MD, Ballard, CC, Cowtan, KD, Dodson, EJ, Emsley, P, Evans, PR, Keegan, RM, Krissinel, EB, Leslie, AGW, and McCoy, A. (2011) Overview of the CCP4 suite and current developments, *Acta Crystallogr. D Biol. Crystallogr. 67*, 235-242.

[29] Murshudov, GN, Vagin, AA, and Dodson, EJ. (1997) Refinement of macromolecular structures by the maximum-likelihood method, *Acta Crystallogr. D Biol. Crystallogr. 53*, 240-255.

[30] Yeates, T. (1988) Simple statistics for intensity data from twinned specimens, *Acta Crystallogr. A 44*, 142-144.

[31] Britton, D. (1972) Estimation of twinning parameter for twins with exactly superimposed reciprocal lattices, *Acta Crystallogr. A 28*, 296-297.

[32] Mattevi, A, Valentini, G, Speranza, ML, Sartori, P, Bolognesi, M, and Coda, A. (1995) Crystallization and preliminary X-ray analysis of pyruvate kinase type I from *Escherichia coli*, *Acta Crystallogr. D Biol. Crystallogr. 51*, 1089-1091.

[33] Jurica, MS, Mesecar, A, Heath, PJ, Shi, W, Nowak, T, and Stoddard, BL. (1998) The allosteric regulation of pyruvate kinase by fructose-1,6-bisphosphate, *Structure 6*, 195-210.

[34] Morgan, HP, McNae, IW, Nowicki, MW, Hannaert, V, Michels, PAM, Fothergill-Gilmore, LA, and Walkinshaw, MD. (2010) Allosteric mechanism of pyruvate kinase from *Leishmania mexicana* uses a rock and lock model, *J. Biol. Chem. 285*, 12892-12898.

[35] Krissinel, E, and Henrick, K. (2007) Inference of macromolecular assemblies from crystalline state, *J. Mol. Biol. 372*, 774-797.

[36] Fiorucci, S, and Zacharias, M. (2010) Prediction of protein-protein interaction sites using electrostatic desolvation profiles, *Biophys. J. 98*, 1921-1930.

[37] Svergun, D, Barberato, C, and Koch, M. (1995) CRYSOL-a program to evaluate X-ray solution scattering of biological macromolecules from atomic coordinates, *J. Appl. Crystallogr. 28*, 768-773.

[38] Putnam, CD, Hammel, M, Hura, GL, and Tainer, JA. (2007) X-ray solution scattering (SAXS) combined with crystallography and computation: defining accurate macromolecular structures, conformations and assemblies in solution, *Q. Rev. Biophys. 40*, 191-285.

[39] Skou, S, Gillilan, RE, and Ando, N. (2014) Synchrotron-based small-angle X-ray scattering of proteins in solution, *Nat. Protoc. 9*, 1727-1739.

[40] Mertens, HD, and Svergun, DI. (2010) Structural characterization of proteins and complexes using small-angle X-ray solution scattering, *J. Struct. Biol. 172*, 128-141.

[41] Guinier, A. (1939) La diffraction des rayons X aux tres petits angles; application a l'etude de phenomenes ultramicroscopiques., *Annals of Physics (Paris) 12*, 161-237.

[42] Mertens, HDT, and Svergun, DI. (2010) Structural characterization of proteins and complexes using small-angle X-ray solution scattering, *J. Struct. Biol. 172*, 128-141.

[43] Svergun, DI. (1992) Determination of the regularization parameter in indirect-transform methods using perceptual criteria, *J. Appl. Crystallogr. 25*, 495-503.

[44] Boiteux, A, Markus, M, Plesser, T, Hess, B, and Malcovati, M. (1983) Analysis of progress curves. Interaction of pyruvate kinase from *Escherichia coli* with fructose 1,6-bisphosphate and calcium ions, *Biochem. J. 211*, 631-640.

Chapter Three

Allosteric activation mechanism of *Escherichia coli* pyruvate kinase type 1

Part 1 – Structure

Developing an indepth understanding of the mechanism of allosteric activation is essential, not only for understanding how the *Escherichia coli* pyruvate kinase type 1 (PK1) enzyme functions, but also for identifying and interpreting the functions of the eight adaptively evolved *E. coli* PK1 enzymes (Section 1.7). This chapter uses structural techniques as well as dynamic analyses to investigate the allosteric activation mechanism of *E. coli* PK1. Part 1 provides the first structural evidence for the allosteric activator binding position and consequent conformational changes in an evolved *E. coli* PK1 enzyme. Furthermore, Part 2 describes a detailed dynamic analysis, creating a strong experimental illustration of intra-domain conformational flexibility during the allosteric activation of the wild-type PK1 enzyme.

3.1 Introduction

Allostery is the effect that the binding of a ligand has on the chemistry (binding properties and/or reaction mechanism) at a second topographically distinct site in a macromolecule.[1-5] For enzymes, allostery provides immediate control of reaction flux in response to cellular signals (e.g. the feedback regulation of a branch point enzyme by the concentration of the pathway product). As such, allostery is critical for the modulation of cellular metabolism and is ubiquitous across all forms of life. Not surprisingly, pyruvate kinase (PK) enzymes are almost always allosterically regulated.[6]

Key to unravelling allosteric mechanisms are the structures of the enzyme with and without bound allosteric effectors. Atomic resolution X-ray structures of PK enzymes have been reported from mammalian, bacterial and parasitic organisms.[6-13] As is common in allosterically controlled enzymes, PK is oligomeric and is usually a homotetramer. Each monomer comprises three or four domains: A-, B- and C-domains and the N-terminal domain is only present in mammalian enzymes.[11] To unpick the molecular mechanism(s) by which PK achieves allosteric control upon fructose-1,6-bisphosphate (FBP) binding, several groups have the three-dimensional crystal structures of various isozymes in both the allosteric activator bound and unbound states.[8, 11-13]

Currently, there is no structure available of the wild-type *E. coli* PK1 isozyme with FBP bound. Previous attempts to soak FBP into wild-type PK1 crystals have caused them to crack.[6] This indicates that FBP binding causes conformational changes that affect crystal packing. Moreover, attempts to co-crystallise FBP and wild-type PK1 have not yielded crystals, despite employing large and sparse matrix screens that can trial >1000 different conditions, and successfully obtaining unbound enzyme crystals in various conditions. One explanation for this is that the FBP bound protein is heterogeneous in some way.

Part 1 of this chapter provides the first allosteric activator bound structure of an *E. coli* PK1 enzyme, albeit the evolved A301S enzyme. The FBP binding position and subsequent conformational changes are expected to be similar in wild-type PK1.

3.2 Crystallisation and structure determination of the unbound and FBP bound states

Previous structural studies have identified structures of PK enzymes in an inactive T(tense)-state (unbound) and an active R(relaxed)-state (bound), suggesting that the allosteric activation of PK involves a switch between the two states.[8, 11, 12] The allosteric switch is governed by the binding of the allosteric activator, FBP. A comparison of the enzyme in both states is required to gauge the conformational changes that occur during the allosteric transition. Here, crystals of the evolved form of the *E. coli* PK1, A301S, were soaked with FBP and used to successfully determine the first structure of an *E. coli* PK1 in the active bound state.

3.2.1 Crystallisation of A301S in the unbound state

A crystal was taken from drop D4 (The PACT Suite; 281 K) and soaked in a cryoprotectant solution that did not contain FBP. Data was collected from this crystal resulting in a 2.7 Å crystal structure of A301S in the unbound state. However, the data quality proved inadequate for detailed structure analysis (R_{factor}/R_{free} = 35.5/37.8) due to the low resolution and low completeness (see Table 3.1 for full data statistics). Therefore, an optimisation screen based on The PACT Suite condition D4 was carried out at the Collaborative Crystallisation Centre to enhance the resolution of the crystal structure and provide a more detailed structural analysis. Fortunately, a higher resolution (2.1 Å) crystal structure of the A301S enzyme in the unbound state was collected from a crystal condition grown from a 10 mg/mL preparation of A301S in: 18.6% w/v PEG 1500 and 10% v/v DL-malate-MES-tris at pH 6. This higher resolution structure is in the same space group and has the same cell dimensions as the 2.7 Å structure, which alleviates the possibility of lattice artefacts affecting the structure.

The higher resolution crystal structure is a much better representation of the structure of unbound A301S. However, to ensure that any structural changes were not a result of crystal growth in different crystallisation drops, the higher resolution (optimised) unbound A301S structure was compared to the low-resolution unbound A301S structure using PyMOL (The PyMOL Molecular Graphics System, Version 1.5.0.4 Schrödinger, LLC).

This comparison confirmed that the structures have the same structural fold (Figure 3.2a and b) and the key activator-binding loop is in the same orientation (Figure 3.2c), with a root mean square deviation (RMSD) of 0.710. The RMSD provides a measure of the average distance between C^{α} backbone atoms of superimposed proteins. The higher resolution structure is superior and thus is used for all further structural comparison in this chapter.

3.2.2 Crystallisation of A301S in the bound state

A301S crystals were crystallised according to Section 8.6.1.2 at the Collaborative Crystallisation Centre, producing crystals with a diamond-like morphology (Figure 3.1). The crystals were grown in the absence of activators, phosphoenolpyruvate (PEP) and FBP, resulting in the protein being crystallised in the unbound state. A crystal from drop D4 (PACT suite; 281 K) was soaked for approximately one minute in a cryoprotectant solution containing 85% crystal condition (25% w/v PEG 1500 and 10% v/v DL-malate-MES-tris at pH 7), 15% of a 50:50 ethylene glycol:glycerol combination and 18 mM FBP. This crystal provided the first crystal structure of the *E. coli* PK1 in the bound state – data statistics can be found in Table 3.1.

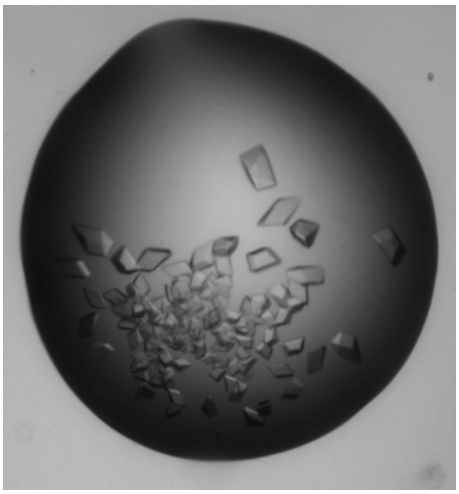

Figure 3.1 A301S crystals with diamond-like morphology.

Table 3.1 X-ray data collection statistics of A301S structures. Statistical values for the highest resolution shells are given in parentheses.

	Unbound	Unbound (optimised)	Bound
Data-collection statistics			
Space group	P_12_11	P_12_11	$C222_1$
Twin law	h, -k-h, -l	h, -k, -l	-
Twin fraction	0.38	0.5	-
Cell dimensions *a*, *b*, *c* (Å); β (º)	130.1, 74.6, 241.8; 90.15	129.3, 74.5, 240.8; 90.04	74.2, 238.2, 128.9 90.00
Resolution range (Å)	44.52-2.70 (2.79-2.70)	48.17-2.10 (2.14-2.10)	43.74-2.50 (2.59-2.5)
Unique reflections	53,762 (6,219)	263,984 (12,877)	39,38 (4,438)
Mean I/σ(I)	6.0 (2.1)	11.6 (2.1)	7.9 (1.5)
$CC_{1/2}$	0.989 (0.849)	0.998 (0.754)	
Completeness (%)	84.7 (88.3)	98.7 (97.8)	99.6 (97.2)
R_{merge} †	0.083 (0.294)	0.087 (0.631)	0.117 (0.817)
R_{meas}	0.215 (2.912)	0.179 (1.148)	0.167 (1.207)
R_{pim}	0.150 (2.059)	0.090 (0.577)	0.092 (0.664)
Multiplicity	1.9 (1.9)	7.7 (7.8)	5.4 (5.4)
Refinement details			
Resolution (Å)	2.70	2.00	2.50
R_{factor}/R_{free} ‡ (%)	35.5/37.8	18.0/20.3	22.6/26.0
No. of atoms §			
Macromolecules	14,180	28,198	7,030
Ligands	5	40	45
Water	98	3360	69
B-factors (Å^2)			
Macromolecules	48.6	26.8	80.2
Ligands	34.9	28.1	70.3
Solvent	33.3	30.7	60.6
Ramachandran plot, residues in (%)			
Favoured regions	86.38	94.47	96.37
Allowed regions	9.19	4.81	3.09
Disallowed regions	4.44	0.72	0.53
All-atom clash-score	30.88	14.17	11.17

† $R_{merge} = \sum_{hkl}\sum_i |I_i(hkl) - \langle I(hkl)\rangle| / \sum_{hkl}\sum_i I_i(hkl)$ where $I_i(hkl)$ is the *i*th intensity measurement of reflection *hkl*, $\langle I(hkl)\rangle$ is its average and *N* is the redundancy of a given reflection.

‡ $R = \sum_{hkl} ||F_{obs}| - |F_{calc}|/\sum_{hkl} |F_{obs}|$. R_{free} is calculated using reflections belonging to a test set of randomly selected data comprising 5% of the data.

§ Not including riding H atoms.

3.3 Allosteric mechanism in *E. coli* PK1

With the bound and unbound structures in hand, the structures were compared to determine if the *E. coli* PK1 enzyme binds FBP in the same position as seen in other PK isozymes, and to investigate the resulting mechanism of allostery. Bound crystal structures of several PK isozymes reveal the allosteric activator, FBP, binds entirely within the C-domain and transmits an allosteric signal over a 40 Å distance to the active site in the same subunit.[8, 11, 12, 14] The FBP binding site is located in a pocket formed from an effector loop and the first two turns of the Cα5'-helix in PK from *Saccharomyces cerevisiae*[11] and human liver.[14] Similarly, fructose-2,6-bisphosphate binds in the equivalent pocket in *Leishmania mexicana*,[12] *Trypanosoma cruzi*[8] and *Trypanosoma brucei*[15]. In *S. cerevisiae* PK, FBP binding in the allosteric site is facilitated by residue Arg459 that forms a strong electrostatic interaction with the 1'-phosphate group of FBP. In addition, the 6'-phosphate makes a series of hydrogen bonds with side chains of residues Ser402-Thr-Ser-Gly-Thr-Thr407 (Thr378-Gln-Gly-Gly-Lys382 are the *E. coli* equivalent residues) and the sugar ring of the FBP forms interactions with residues Gln483 and His491.[11]

3.3.1 Confirmation of FBP in the bound structure

Although the allosteric activator binding site is well established in several PK isozymes,[8, 11, 12] there is no structural evidence confirming the binding site in *E. coli* PK1. However, the higher resolution X-ray structure of wild-type PK1 in the unbound state has identified sulphate anions bound (Figure 2.13, Chapter Two) in the site where the 6'-phosphate of FBP is observed in *S. cerevisiae* PK.[11] The polar nature of the binding pocket is well known for its strong phosphate binding ability.[11] However, the absence of phosphate in the crystallisation media, and the presence of sulphate suggest that sulphate is instead sequestered within the pocket (Figure 3.3a). The sulphate ion forms electrostatic interactions with residues Gln379, Gly380, Lys382, Ser383 and Ser459, which together form a very tight binding pocket.

Analysis of the FBP-soaked A301S crystal structure (Section 3.2.1) using *COOT* identifies FBP bound completely within the C-domain of each subunit of the enzyme. The electron density for each FBP molecule was strong and unambiguous, as observed in the F_o-F_c difference maps (Figure 3.3b). Surprisingly, the FBP molecule is oriented the opposite way to the *S. cerevisiae* PK. The orientation was confirmed by refinement testing both orientations, i.e. with the 6'-phosphate bound in the sulphate pocket (as with *S. cerevisiae* PK), and with the 1'-phosphate bound in the sulphate pocket (Figure 3.3b and c, respectively). The refinement confirmed that the latter orientation is a better fit to the electron density.

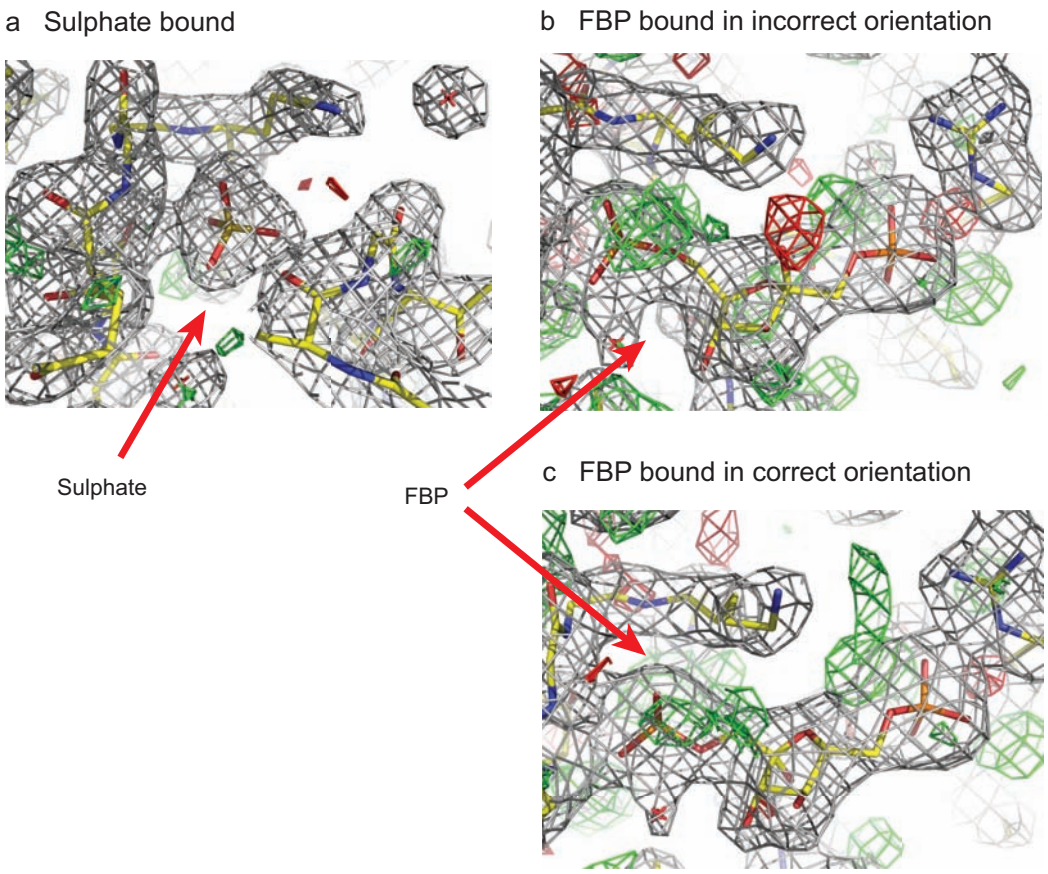

Figure 3.3 A301S enzyme depicting a sulphate and FBP bound in the same location within the allosteric pocket. **(a)** Unbound A301S with a sulphate anion bound in the allosteric pocket. **(b)** A301S with the 6'-phosphate of FBP bound in the allosteric pocket, with negative difference density suggesting the orientation is incorrect. **(c)** A301S with the 1'-phosphate of FBP bound in the allosteric pocket. Electron density ($2F_o$-F_c) is shown at 1 σ contour level and F_o-F_c is shown at 2 and -2 σ contour level.

3.3.2 FBP binds in a secure binding site

Analysis of the allosteric site in the FBP bound structure determined that FBP binds in a pocket formed by the loops preceding the Cα3'-helix and the Cβ5'-strand, as well as the first turn of the Cα2'-helix (Figure 3.4 and Figure 3.5c). The 6'-phosphate group of FBP makes strong 2.6 Å hydrogen bonds with Arg353 and Thr355 side chains from the first turn of the Cα2'-helix. The 1'-phosphate forms a series of hydrogen bonds with side and main chain atoms of Thr378, Gln379, Gly380, Lys382 and Ser383 residues. The sugar ring of FBP molecule forms hydrogen contacts with side and main chain atoms of two threonine residues, Thr355 and Thr462 from the loop preceding the Cβ5'-strand (Figure 3.4).

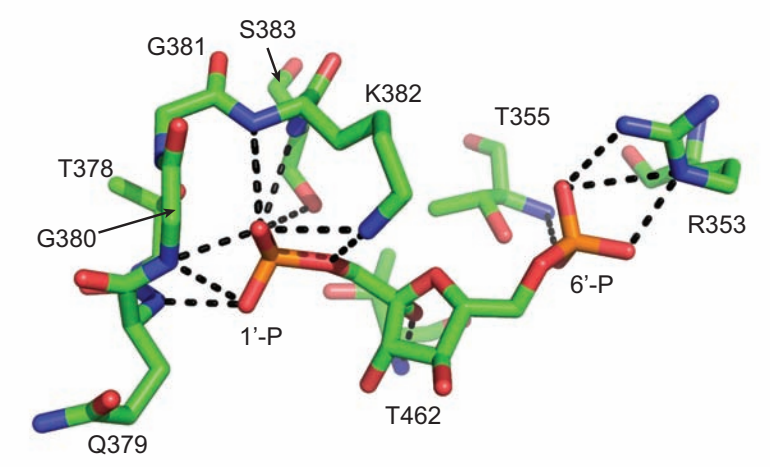

Figure 3.4 FBP bound in the A301S allosteric site displaying interactions with surrounding residues. The binding pocket and FBP molecule are shown as green stick representations. FBP's 1'-phosphate forms interactions with T378, Q379, G380, K382 and S383. The 6'-phosphate forms hydrogen bonds with residues R353 and T355, while the sugar ring interacts with T355 and T462. The interactions are denoted as dashed black lines.

Now that the FBP binding site has been located in the evolved *E. coli* PK1 (A301S), the next step is to investigate any structural changes induced by activation. Previous structural analysis of PK isozymes have identified various conformational changes upon FBP binding.[8, 11, 12] It is therefore important to analyse the bound A301S to identify any changes that could help to explain the mechanism of allosteric regulation in PK enzymes.

3.3.3 Allosteric transition involves subunit rotations

The tetramers of the A301S in the unbound and bound states were aligned (Figure 3.5) to investigate potential activation induced conformational changes that have been identified previously in other PK isozymes.[8, 12] Crystal structures of *L. mexicana* PK and *T. cruzi* PK in the unbound and bound states show 6° and 8° rotation of the subunits upon activation by FBP, respectively. The lid domains were excluded from the analysis because of their extreme flexibility. They were found to be irrelevant to the allosteric activation by FBP, instead they are thought to be controlled by the binding of substrate in the active site.[12]

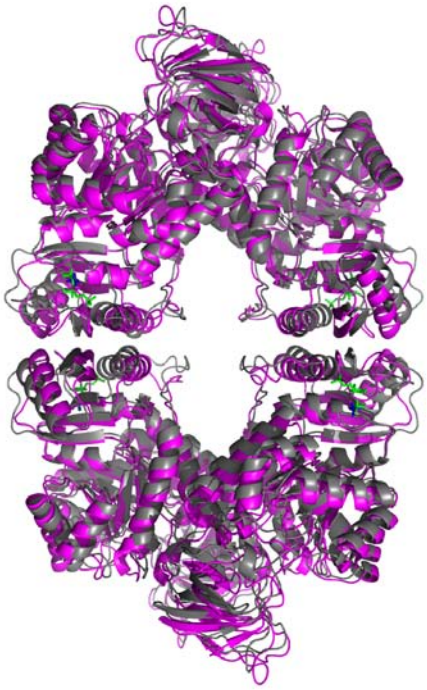

Figure 3.5 A301S unbound and bound tetramer alignment showing the same overall structural fold but a slight change in subunit conformations. The tetramers were aligned by the AC cores. The unbound state structure is coloured magenta and the bound structure is coloured grey.

The C^{α} RMSD fit from the unbound to bound state structural alignment is 1.385 Å, suggesting a reorganisation of the backbone during the allosteric transition.

Additional structural analysis of the unbound and bound tetramers using the PDBePISA online server[16] identified a substantial change to the interface surface area upon transition to the active bound state: the A/A' interface surface area increases (1139 to 1363 Å), whereas the C/C' interface surface area decreases (1000 to 759 Å) during the allosteric transition (Figure 3.6). The surface area changes are consistent with the subunits rotating ~5°, not unlike the isozymes studied by Morgan *et al.*,[8, 12] which show rotation around a potential pivot point located at the base of the $(\beta/\alpha)_8$-barrel.

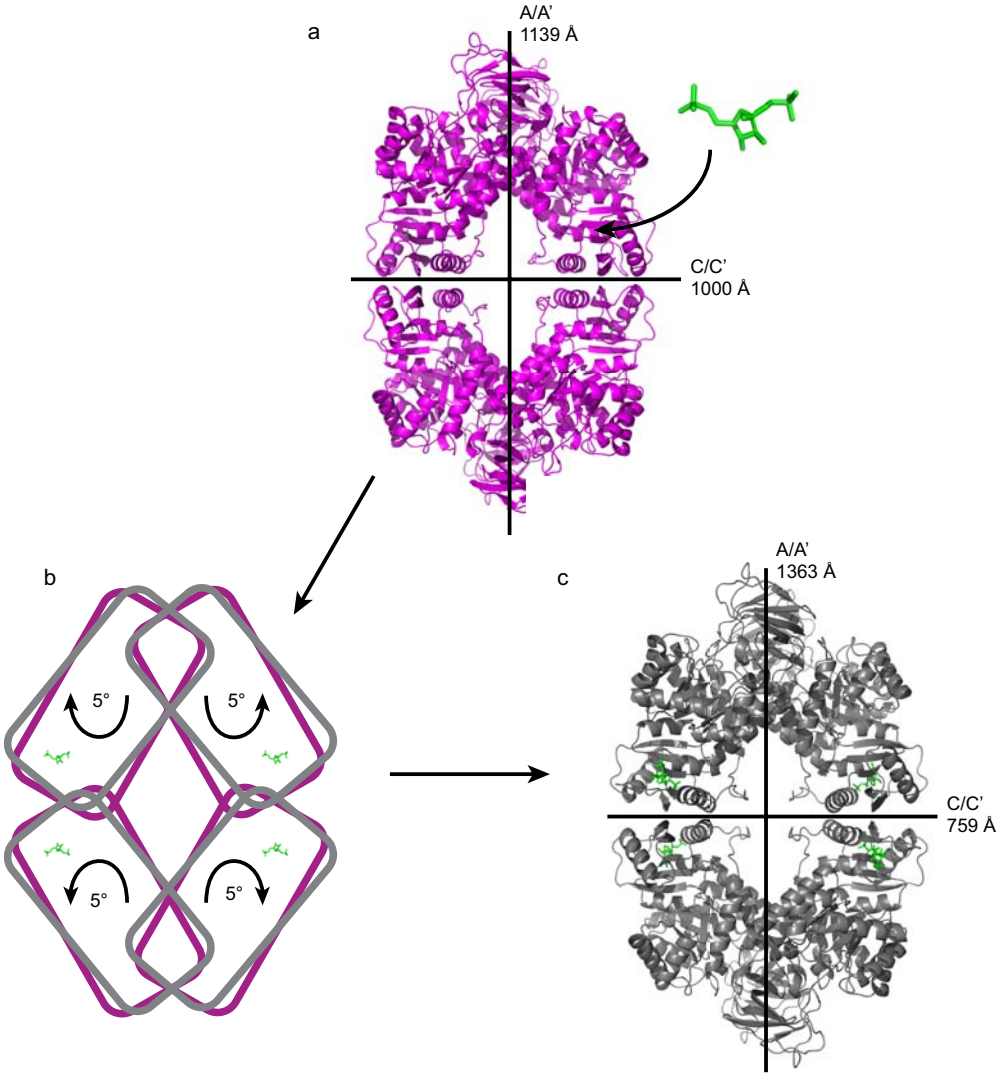

Figure 3.6 A301S crystal structures identify subunit rotations; increasing the A/A' interface surface area and decreasing the C/C' interface surface area upon allosteric activation. a) Unbound A301S tetramer (magenta) displaying A/A' and C/C' interface surface areas. **(b)** Schematic displaying the AC core ~5° rigid body rotation upon binding of the FBP activator (green). **(c)** Bound A301S tetramer (blue) displaying A/A' and C/C' interface surface areas.

As well as analysing the surface area of the interfaces, the PDBePISA server[16] provided a complete evaluation of the hydrogen bonds and salt bridges that could potentially form across the A/A' and C/C' interfaces of the tetramer. Details of the A/A' interface interactions are provided in Table 3.2, below:

Table 3.2 The number of potential interactions across one A/A' interface of unbound and bound A301S.

A/A' interface	A301S		A301S + FBP	
	Hydrogen bond	Salt bridge	Hydrogen bond	Salt bridge
Arg334 : Glu255'	2	4		3
Arg292 : Asp297'	1	2		
Arg292 : Gln279'	1			
Lys261 : Asn300'	1			
Glu255 : Arg334'	2	4		3
Gln279 : Arg292'	1			
Asp297 : Arg292'	1	3		
Arg244 : Arg292'			1	
Arg292 : Arg244'			1	
Arg292 : Asp127'				1
Asp127 : Arg292'				1
Gly128 : Arg289'			1	
Arg289 : Gly128'			1	
Arg289 : Asn148'			1	
Asn148 : Arg289'			1	
Total	9	13	6	8

The A/A' interface analysis indicates that the total number of potential hydrogen bond and salt bridge interactions across the interface are reduced when the enzyme is in the bound state. Therefore, FBP binding reduces the restraining forces connecting the opposing A-domains.

The A/A' interface analysis identifies Arg292 as important because FBP binding causes the residue to reorient across the interface, where it forms hydrogen bond contacts with the opposing subunit. Previous studies have identified Arg292 as essential for the allosteric mechanism of *E. coli* PK1 as mutation of this residue to an aspartate completely removes the activity of the enzyme, presumably by inhibiting transition to the active bound state.[17]

Moreover, allosteric studies using *E. coli* and *L. mexicana* PK's determine that the Arg292 (*L. mexicana*, Arg310) residue is critical for forming hydrogen bonds across the A/A' interface with the Aα6'-helix to lock the enzyme in the active bound state. The importance of residue Arg292 is confirmed for the *E. coli* A301S enzyme, as residue Arg292 is hydrogen bonded to Asp297' of the opposing subunit in the unbound state (Figure 3.7a). However, when FBP binds, Arg292 reorients across the A/A' interface, where it forms a hydrogen bond with Arg244' from the Aα6'-helix of the opposing subunit, locking the enzyme in the bound state. In addition to the hydrogen bond formed between Arg292 and the Aα6'-helix, the reorientation of Arg292 enables it to form a salt bridge with Asp127' from the underside of the lid domain of the opposing subunit (Figure 3.7b). This salt bridge formation seems to lock the lid domain off to the side in an open conformation to promote substrate binding within the active site of the $(\beta/\alpha)_8$-barrel.

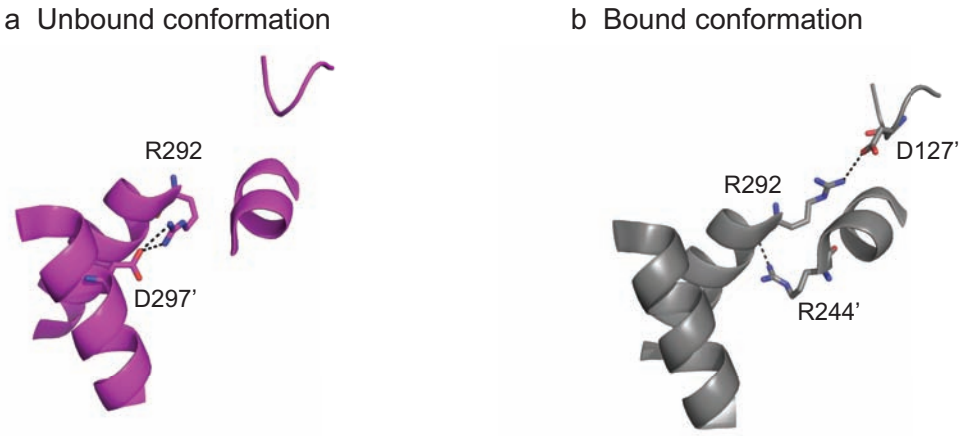

Figure 3.7 FBP binding in A301S enzyme alters A/A' interface interactions of residue R292. (a) Unbound (magenta)**:** R292 forms interactions with D297' of the opposing subunit. **(b)** Bound (grey): R292 forms interactions with D127' of the opposing subunit and R244' from the Aα6'-helix of the opposing subunit. Interactions are displayed as black dashed lines.

The conformational transition to the active bound state not only affects the A/A' interface, but also the smaller C/C' interface. The C/C' interface analysis found a reduction in total number of hydrogen bonds and salt bridges across the interface in the bound state. Details of the C/C' interface interactions are provided in Table 3.3. The rotation of the C-terminal end of each subunit inwards and the N-terminal end outwards (Figure 3.8) results in the contacts in the centre of the 'doughnut' hole (mobile loops) becoming closer together and

the contacts that were previously on the outside of the tetramer becoming too distant to interact. Figure 3.9 illustrates that FBP binding promotes a structural rearrangement whereby residues Lys351 and Asp370' of mobile loops from opposing subunits move closer together, allowing new interactions to form across the C/C' interface.

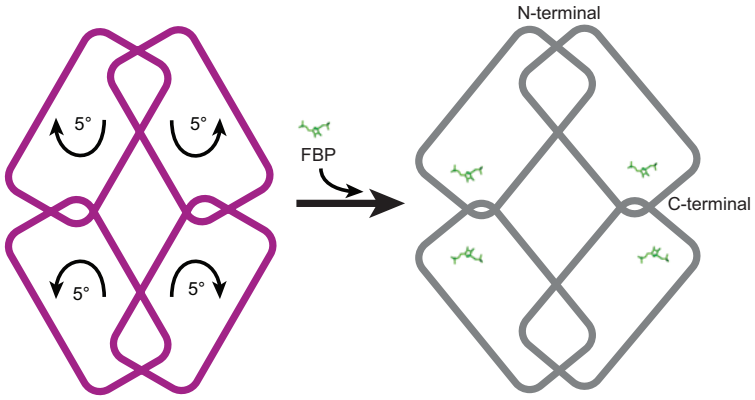

Figure 3.8 Conformational change upon FBP binding decreases the surface area contacts of the C/C' interface. The N-terminal end of the subunits rotate towards each other and the C-terminal ends rotate away from each other, upon FBP binding.

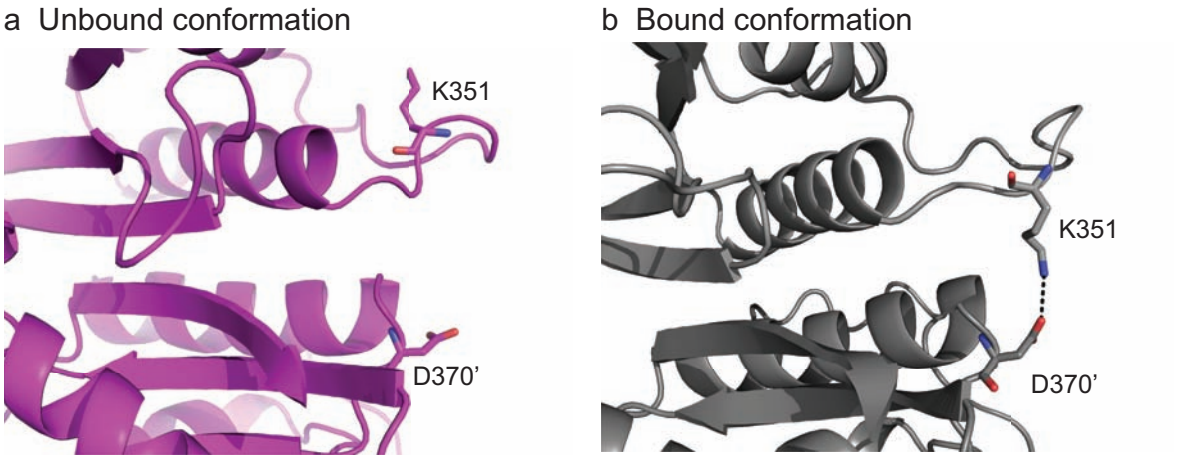

Figure 3.9 FBP binding introduces interaction between K351 and D370 across the C/C' interface of A301S. (a) Unbound (magenta) mobile loops are disordered and too far apart to form interactions across the C/C' interface. K351 and D370' are labelled for comparison with the bound state. **(b)** Bound (grey) mobile loops are ordered and within interaction distance. K351 and D370' form a salt bridge across the C/C' interface.

Table 3.3 C/C' interface interactions in unbound and bound A301S.

C/C' interface	A301S		A301S + FBP	
	Hydrogen bond	Salt bridge	Hydrogen bond	Salt bridge
Val467 : Asn463'	1		1	
Ala465 : Ala465'	2		2	
Asn463 : Val467'	1		2	
Asp427 : Thr426'	1			
Thr426 : Asp427'	1			
Arg350 : Asp370'		1		
Asp370 : Arg353'		1		
Lys351 : Asp370'				1
Ser466 : Asn463'	1			
Ser466 : Thr464'	1			
Arg360 : Glu364'		1		
Lys368 : Lys351'			2	
Total	8	3	7	1

3.3.4 FBP binding induces structural flexibility

Here, the structural changes associated with FBP binding have been investigated, demonstrating that the binding of FBP within the activator-binding site causes structural changes within the subunits of the enzyme. One major structural change is the movement of the effector loop involved in hydrogen bonding with the sugar ring of FBP (residues 453–462). In the absence of FBP this loop appears to be blocking the FBP binding site, as it is positioned over the FBP binding site (Figure 3.9a). However, when the FBP is present, there is a major structural rearrangement of this effector loop moving it out of the way creating a pocket for the FBP to bind (Figure 3.9b). Examination of the activator binding sites of the aligned unbound and bound state structures demonstrates the different positions of the effector loop. Movement of this loop preceding the Cβ5'-strand promotes effector binding and places the loop in the perfect position for hydrogen bond interactions with the sugar ring of FBP.

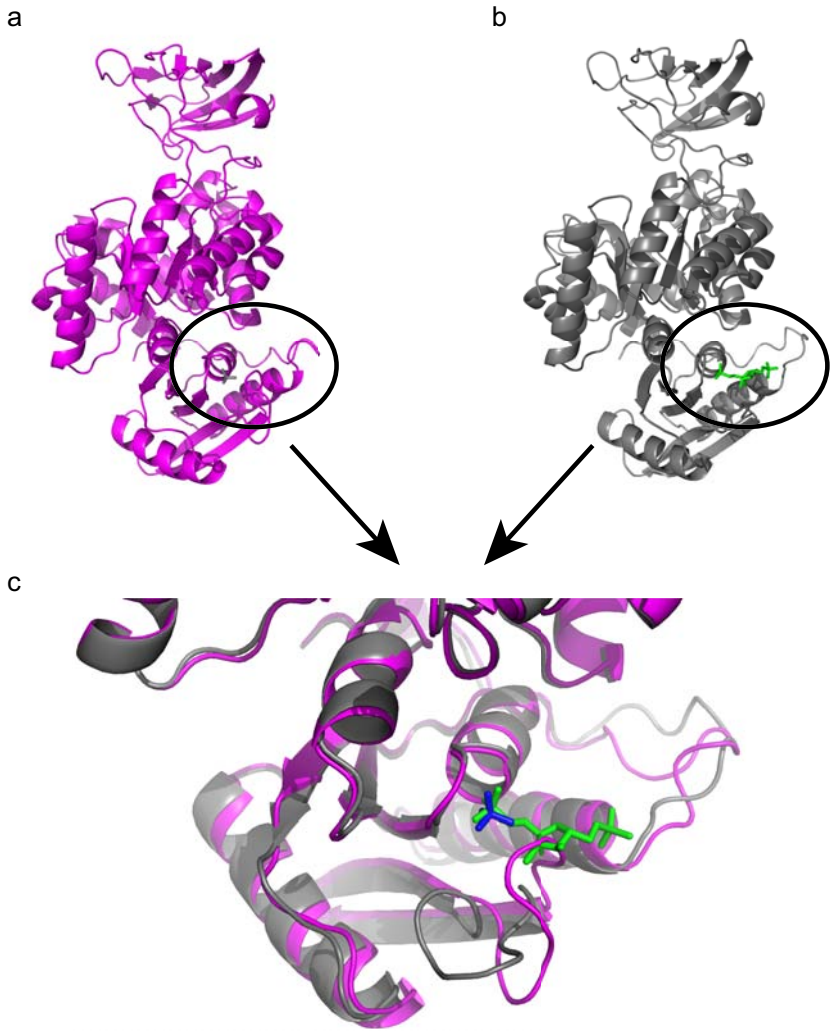

Figure 3.9 A301S unbound and bound state subunits depicting the difference in conformation of the effector loop. **(a)** Unbound subunit (magenta) with the sulphate ion (blue) bound in the FBP binding position (*E. coli* PK1) of the activator-binding pocket. **(b)** Bound subunit (grey) with the FBP molecule (green) bound in the activator-binding pocket. The binding pocket is circled in black. **(c)** A closer look at the circled activator-binding pocket of the aligned unbound and bound state subunits demonstrating the difference in conformation of the effector loop.

Residues 346−352 are highly disordered in the absence of FBP, forming the mobile loop that is often difficult to model in PK enzymes.[6, 11] This mobile loop is positioned before the Cα2'-helix and it forms no interactions with other residues, allowing it to move freely in solution.[11] X-ray crystal structures of PK enzymes in the unbound state rarely include this mobile loop due to the limited electron density resulting from disorder. Fortunately, the high-resolution 2.1 Å structure of A301S in the unbound state provided sufficient electron density to model in the disordered loop. Moreover, FBP binding in the allosteric

site causes a decrease in flexibility of this loop, which can be seen by the significant decrease in temperature factor (B-factor) for residues 346−352 (Figure 3.10).

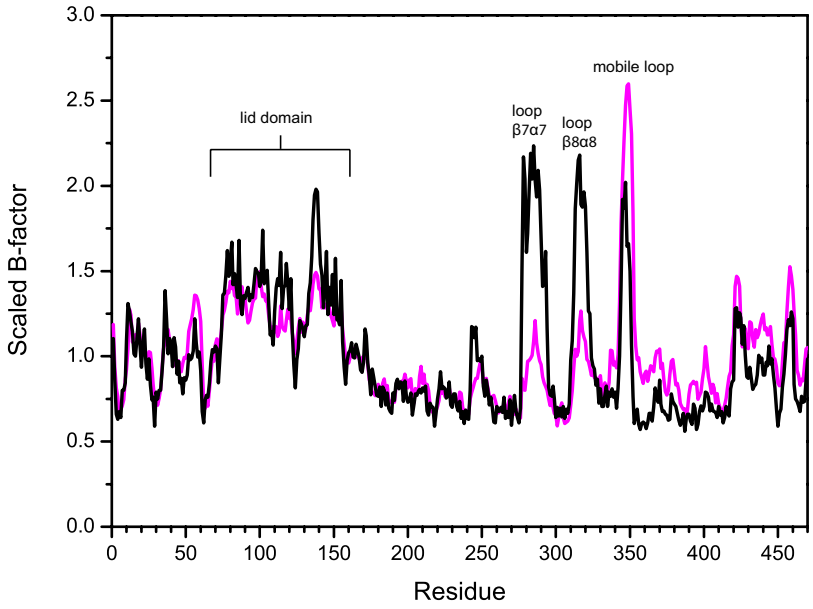

Figure 3.10 B-factor plot of scaled main chain residues for unbound and bound A301S displaying fluctuations in flexibility. The unbound A301S (magenta) is scaled with bound A301S (black) and important regions are labelled.

Next, the active site was examined to explore how FBP binding affects substrate binding for catalysis. Consideration of the B-factor plot (Figure 3.10) determined that two active site loops thought to be involved in substrate binding show a significant increase in disorder. The first loop precedes the Aα7'-helix (loop $\beta_7\alpha_7$; residues 275−295) and is located very near the PEP binding site. Analysis of *L. mexicana* PK with a PEP analogue (oxalate) bound shows that it is bonded primarily to the short Aα6'-helix, but it may also interact with Thr278 of loop $\beta_7\alpha_7$. The second loop precedes the Aα8'-helix (loop $\beta_8\alpha_8$; residues 311−320) and is located within binding distance of the ATP (or ADP) in *L. mexicana* PK, suggesting that it is involved in binding the substrate for phosphoryl-transfer during catalysis.[12] An increase in disorder of the βα-loops around the top of the $(\beta/\alpha)_8$-barrel is unsurprising as these loops are known to be involved in the catalysis and function of $(\beta/\alpha)_8$-barrel proteins, and increased flexibility of loop regions has been shown to enhance the ligand binding affinity in enzymes.[18] Therefore, B-factor analysis demonstrates that FBP binding induces conformational fluctuations of the active site loops to increase binding affinity and in turn catalysis.

3.4 Conformational changes cannot be identified using SAXS

The conformational changes identified in X-ray crystallography, although informative, are not true to the physiological behaviour of the enzyme. While crystals contain about 50% solvent, the cooling process and lattice environment limits the collection of 'dynamic' data to a measure of the ensemble-averaged protein conformations found within the crystal lattice.[19] This data essentially provides a structural image of the protein in its averaged conformational state. The ability to determine crystal structures with and without ligands bound enables comparisons of bound and unbound structures, which allows the conformational transitions that occur between states to be pieced together.

A complementary structural technique to X-ray crystallography is small-angle X-ray scattering (SAXS) (Section 2.6). SAXS compliments X-ray crystallography by supplying information about folding, dynamics, aggregation and assembly, although at the lower resolution range of approximately 10−50 Å.[20] Here, SAXS was applied to investigate the conformational changes of wild-type PK1 in solution, to observe the size and shape of the tetramer change when the enzyme is activated to its bound state.

SAXS analysis of wild-type PK1 in the absence and presence of 2 mM FBP was carried out according to Section 8.5. The experimental results were aligned as an intensity graph (Figure 3.11a), which provides information about the size and shape of the protein. In this case, the binding of FBP does not alter the wild-type enzyme's overall structural envelope, nor does it change the structural envelope of the evolved A301S enzyme (Figure 3.11c), despite A301S X-ray structures identifying a conformational change upon FBP binding (Section 3.3.3). The inability to see a major change caused by the activation could be because the resolution is too low (10−50 Å)[20] to identify the small conformational change (C^{α} RMSD of 1.358 Å) discovered in the A301S X-ray crystal structure (Section 3.3.3).

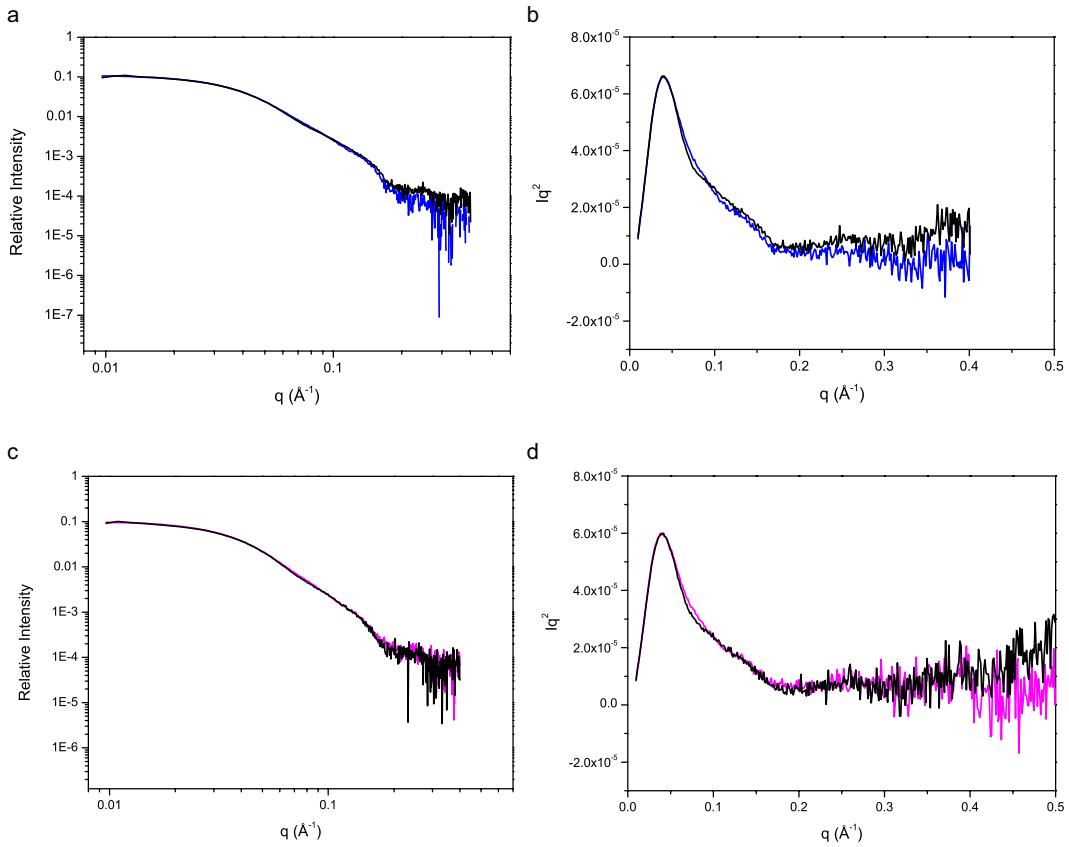

Figure 3.11 SAXS analysis of wild-type PK1 and A301S in the unbound and bound states confirms similar solution structural envelopes. Experimental scattering profiles of wild-type enzyme in the absence (blue) and presence (black) of FBP, presented as: **(a)** an intensity plot demonstrating that the solution structural envelopes are similar, **(b)** a Kratky plot showing that FBP binding causes differences at the high q region. Experimental scattering profiles of A301S in the absence (magenta) and presence (black) of FBP, presented as: **(c)** an intensity plot demonstrating the solution structural envelopes are similar, **(d)** a Kratky plot showing that FBP binding causes slight differences at the high q region.

The Kratky plot provides a more sensitive analysis of the effects of allosteric activation upon the sample molecule's folding and flexibility.[21] Folded globular proteins typically produce a prominent peak at low scattering angles, such as the prominent peaks seen for unbound and bound wild-type in Figure 3.11b and unbound and bound A301S in Figure 3.11d. Although the peaks of both unbound and bound states align reasonably well, there are some slight differences towards the high q region of the plots. The unbound wild-type enzyme shows a baseline of close to zero at the high q region. However, in the FBP bound state the baseline is slightly elevated (above zero) towards the high q region, consistent with the binding of FBP to the wild-type enzyme increasing the flexibility of the protein.[22] Although the Kratky analysis of the A301S enzyme also shows a slight baseline elevation

towards the high q region (Figure 3.11d), it is not quite as significant as the difference identified in the wild-type PK1 enzyme.

Unfortunately, SAXS does not provide high enough resolution information to identify the conformational changes of the enzyme upon transition between unbound and bound states, however it does insinuate that the presence of FBP increases the flexibility of the protein.

3.5 Summary of Part 1

The results presented here follow the description of allostery, in that the binding of one ligand affects catalysis or binding at a distant site (functional site).[1-5] In the case of *E. coli* PK1, the binding of the allosteric effector FBP in the allosteric domain causes structural changes not only to the binding region, but also at detached sites across the subunit.

These studies provide the first X-ray structure of *E. coli* PK1 in the bound state, confirming that the FBP binding position is similar to other PK isozymes.[8, 11, 12] Structural analysis of the bound structure provides evidence showing that FBP binding in the allosteric domain not only alters subunit conformations (also seen in *S. cerevisiae*, *T. cruzi* and *L. Mexicana* PK's), but it also causes changes to the active site, over 40 Å away. SAXS was employed as a complementary technique to crystallography to identify structural changes in solution, but as expected, little change was identified by the low-resolution technique.

The specific FBP binding mechanism includes a movement of the effector loop to allow access to the allosteric binding site and to promote binding with the FBP molecule. Residues Thr355 and Thr462 of the effector loop (preceding the Cβ5-strand) form interactions with the sugar ring of the FBP molecule. Additionally, the 6'-phosphate of FBP interacts with residues Arg353 and Thr355 of the Cα2'-helix and the 1'-phosphate forms a series of hydrogen bonds with residues Thr378, Gln379, Gly380, Lys382 and Ser383. The binding of FBP at the allosteric site transmits a signal through the structure to the active site, where substrate binding loops become more disordered to increase substrate binding efficiency for catalysis. Moreover, the subunits undertake a ~5° subunit conformational change, increasing the A/A' interface surface area and decreasing the C/C' interface surface area. The new tetramer conformation has reduced interactions across the

tetrameric interfaces, which differs from the ‘locking’ mechanism that is seen in the bound PK isozymes.[8, 12]

Although, the ensemble-averaged X-ray structure provides atomic detail of the unbound and bound states, it does not deliver information concerning the enzyme’s conformational sampling. It is therefore crucial that dynamic information is gathered to fully grasp the conformational transitions between substates of the active *E. coli* PK1 enzyme.

Chapter Three

Pyruvate kinase allosteric activation mechanism

Part 2 – Dynamics

The work presented in this chapter has been provisionally accepted for publication in the Journal of Biological Chemistry:

Donovan, K.A., Zhu, S., Liuni, P., Peng, F., Kessans, S.A., Cooper, T.F., Wilson, D.J., Dobson, R.C.J. (2015) Conformational Dynamics and Allostery in Pyruvate Kinase Activation. Provisional acceptance to JBC.

To build a detailed picture of the conformational and dynamic changes that drive *Escherichia coli* pyruvate kinase type 1 (PK1) heterotropic allosteric activation by fructose-1,6-bisphosphate (FBP), a time-resolved electrospray ionisation mass spectrometry coupled to hydrogen-deuterium exchange (TRESI-MS/HDX) study was performed. The 'new view' of allostery describes a dynamic process whereby a protein fluctuates within an ensemble of conformations.[23-26] Although the concept of allostery has evolved dramatically, allosteric mechanisms remain difficult to establish, since defining changes in protein dynamics is challenging even for small proteins.[25] Current models that explain allostery in PK are based largely on static crystal structures. Here, the HDX data

for the wild-type *E. coli* PK1 enzyme is presented; suggesting that the wild-type samples a larger conformational ensemble upon FBP binding. Mapping deuterium exchange to peptides within *E. coli* PK1 reveals regions that show significantly altered conformational dynamics upon the binding of FBP. Based on this data, a new mechanism is proposed, whereby FBP regulates *E. coli* PK1. This work extends previous knowledge of the allosteric activation mechanism by explaining how FBP promotes substrate binding, despite the allosteric binding site being 40 Å away from the active site.

3.6 Dynamic allosteric transition process

X-ray crystallography provides an atomic resolution model of the ensemble-averaged protein conformations found in a protein crystal lattice. The usually high solvent content of protein crystals allows for some dynamics and conformational heterogeneity. However, since dynamics and heterogeneity is inferred by an absence of electron density, modelling the heterogeneity can be difficult, so a single model averaged conformation with some variance can be described by temperature factors (B-factors).[19] Essentially all aspects of protein activity, folding, and interactions depend on the ability of the protein to sample an array of ensemble conformations.[19, 24] In order to fully grasp the conformational transitions between substates in an active protein, dynamic information is often needed.[27, 28]

Recent experimental advances in detecting and characterising protein dynamics (e.g. nuclear magnetic resonance relaxation dispersion and hydrogen-deuterium exchange (HDX)) paint allostery as a dynamic process. Proteins exist as an ensemble of conformers and conformational sampling allows proteins to fluctuate between different conformers.[27, 29, 30] The lowest energy state is the most favourable. Thus, a greater proportion of the population will exist in this state.[23, 31] In theory, all possible conformational states of a protein can be mapped and described by an energy landscape,[23, 28] although in practice detecting high energy conformers is more challenging owing to their small number in the population and their transient nature. In the dynamic view of allostery, the binding of the allosteric modulator remodels the energy landscape and triggers a shift in the relative occupancy of states in the conformational ensemble[23, 25, 27] – the conformation that represents the lowest energy state is changed, although many conformers may still be

sampled. Importantly, this shift increases how often a given (activated or inhibited) state is sampled.[23, 25, 28] For example, studies have suggested that the binding of reduced nicotinamide adenine dinucleotide phosphate (NADPH) increases how often dihydrofolate reductase samples the active 'R-state'.[26, 32]

Hydrogen-deuterium exchange coupled to mass spectrometry (HDX-MS) is widely recognised as a powerful technique for the study of function-related conformational changes in proteins.[33] Mass spectrometry provides a high sensitivity and high throughput method enabling HDX measurements on the millisecond to second timescale.[34] Unlike nuclear magnetic resonance, MS also offers the opportunity to analyse large intact proteins and protein complexes. Hydrogen-deuterium exchange can be implemented on a custom microfluidic device that incorporates all of the sample-handling processes required for a 'bottom-up' spatially resolved workflow.[35] 'Bottom-up' HDX involves digestion of labelled proteins using an acid protease prior to MS-analysis, allowing for the localisation of exchange differences. Another advantage of the microfluidic chip is the ability to use millisecond timescale HDX labelling times, i.e. time-resolved measurements, resulting in the ability to characterise weakly-ordered regions of proteins.[36] This approach is based upon the principal that solvent accessible backbone amide protons are protected from exchange with the solvent if they are involved in hydrogen bonding (as is the case in secondary structure). The level of protection reflects the strength of the hydrogen bond, and in turn, the stability of the secondary structure.[35]

The HDX results provide evidence to show that the allosteric activation signal is sent from the allosteric site to the active site via a series of destabilisation events, resulting in increased conformational sampling of active site loops. Moreover, destabilisation of tetrameric interfaces suggests a decoupling of subunits, inhibiting cooperative activation by the substrate, phosphoenolpyruvate (PEP).

All of the following HDX results (Part 2) were carried out on the wild-type *E. coli* PK1 enzyme and compared to the bound structural analysis of A301S from Part 1 of this chapter.

3.6.1 Protein and device preparation

Below is a brief description of the methods used to obtain dynamic data regarding the allosteric activation of the wild-type *E. coli* PK1 enzyme.

The wild-type *E. coli* PK1 enzyme was expressed and purified using a method adapted from the procedure used by Mattevi *et al*.,[37] (Section 8.2) and prepared according to Section 8.7.1. The rapid protein-deuterium mixing device was created according to Section 8.7.2, to provide a time-controlled protein deuteration device for measuring site-specific dynamic fluctuations in the enzyme.

In summary, the device works by mixing protein and deuterium, which results in exchange of the available amide protons for deuterium atoms, causing a mass increase corresponding to the amount of deuterium exchanged. Digestion of the deuterated protein localises the deuterium onto the peptides, which are then mass analysed to determine the exchange in specific regions.

3.7 FBP binding causes an increase in global protein flexibility

To gauge changes in global conformational dynamics, global HDX was measured as a time course (14 ms to 1.5 s) for wild-type PK1 with and without its allosteric activator, FBP. The data were fitted to an exponential function (Equation 3.1), generating a kinetic plot of overall protein deuterium exchange (Figure 3.12). Increases in deuterium exchange characteristically result from a loss of hydrogen bonds within and between secondary structure elements, leading to increased solvent access associated with destabilisation of secondary structure and tertiary structure. By the same token, decreases in deuterium exchange typically result from stable hydrogen bond formation within secondary structure elements and decreased solvent accessibility.

$$y = y0 + a(1-e^{-kt}) \qquad \textbf{(Equation 3.1)}$$

The global HDX kinetic plot (Figure 3.12) provides a measure of both amplitude and rate of deuterium uptake. The amplitude of deuterium uptake is a measure of the number of exchange sites that become available within the measured time-scale. Whereas, the rate of deuterium uptake is a measure of the frequency of hydrogen bond breakages, which roughly corresponds to how 'fast' the protein samples conformational space.[38]

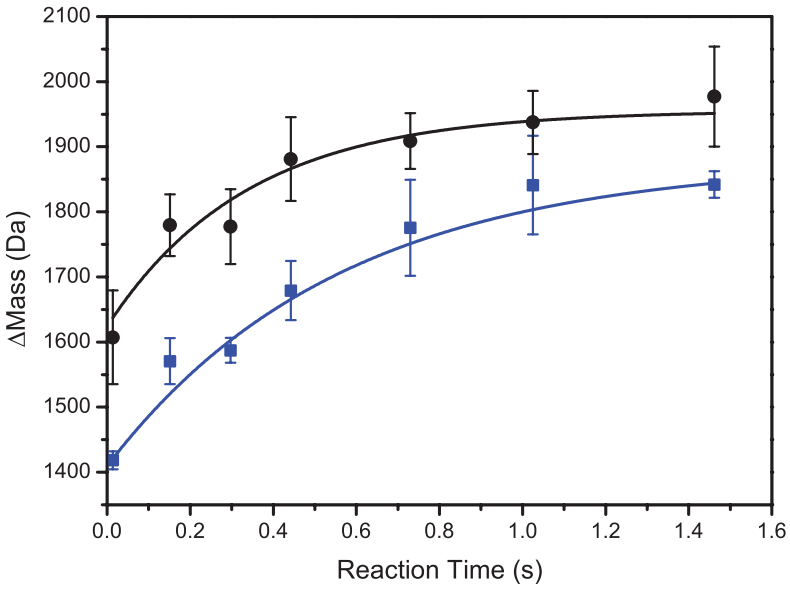

Figure 3.12 Global deuterium exchange kinetics of wild-type PK1. The global HDX kinetics determined the change in mass (ΔMass) from non-deuterated to deuterated, over time. The kinetics were measured in the absence (■) and presence (●) of FBP, providing uptake rates of 1.9 s^{-1} and 2.9 s^{-1}, respectively. Kinetic data was fitted using single exponential non-linear regression analysis ($y=y0 + a(1-e^{-kt})$). Error bars represent the standard error of the mean (SEM) of three replicates.

The results reveal that when FBP is present, the enzyme has a higher amplitude of deuterium exchange (~Δ1966 Da), which is evident in the increased change in mass change seen at 1−1.5 s. In the absence of FBP, the amplitude is ~Δ1884 Da. From this, it is inferred that the binding event causes a shift towards a more unstructured, heterogeneous protein.

In addition to a change in the amount of deuterium exchanged into the protein, the rate of exchange also increases upon FBP binding, from 1.9 ± 0.5 s^{-1} to 2.9 ± 0.8 s^{-1}. This is consistent with activator binding increasing the globally averaged dynamic conformational sampling the protein is undergoing over time, i.e. FBP increases how 'fast' the protein explores conformational space.

Combined, these data suggest that FBP binding causes a shift towards a globally more unstructured and dynamic ensemble of conformations. Moreover, it is consistent with other biophysical data and observations collected, including the SAXS Kratky plot (Section 3.4, Figure 3.11b), which indicates an increase in global flexibility. This may also explain the observation that treating crystals of *E. coli* PK1 with FBP results in crystal cracking and the lack of successful co-crystallisation[6] (Section 3.1).

3.8 Localised analysis of conformational flexibility

3.8.1 Efficiency of the localised TRESI-MS/HDX

Time-resolved electrospray ionisation mass spectrometry coupled to hydrogen-deuterium exchange was implemented to investigate the conformational changes in wild-type *E. coli* PK1 upon binding FBP (Section 8.7.4.). The continuous protein-deuterium mixing device provided rapid labelling times of 59 ms to 1 s for localised analysis, with on-chip digestion and electrospray generating an efficient system for measuring structural dynamics of protein backbones. Wild-type was pre-incubated with 2 mM FBP[17, 39, 40] (10 times the K_d of 0.2 mM)[41] of FBP to ensure the saturation of the allosteric binding sites. Digestion of wild-type was effective, resulting in a 64% sequence coverage corresponding to 36 distinctive peptides, which provided an average spatial resolution of 10 amino acid residues (Figure 3.13).

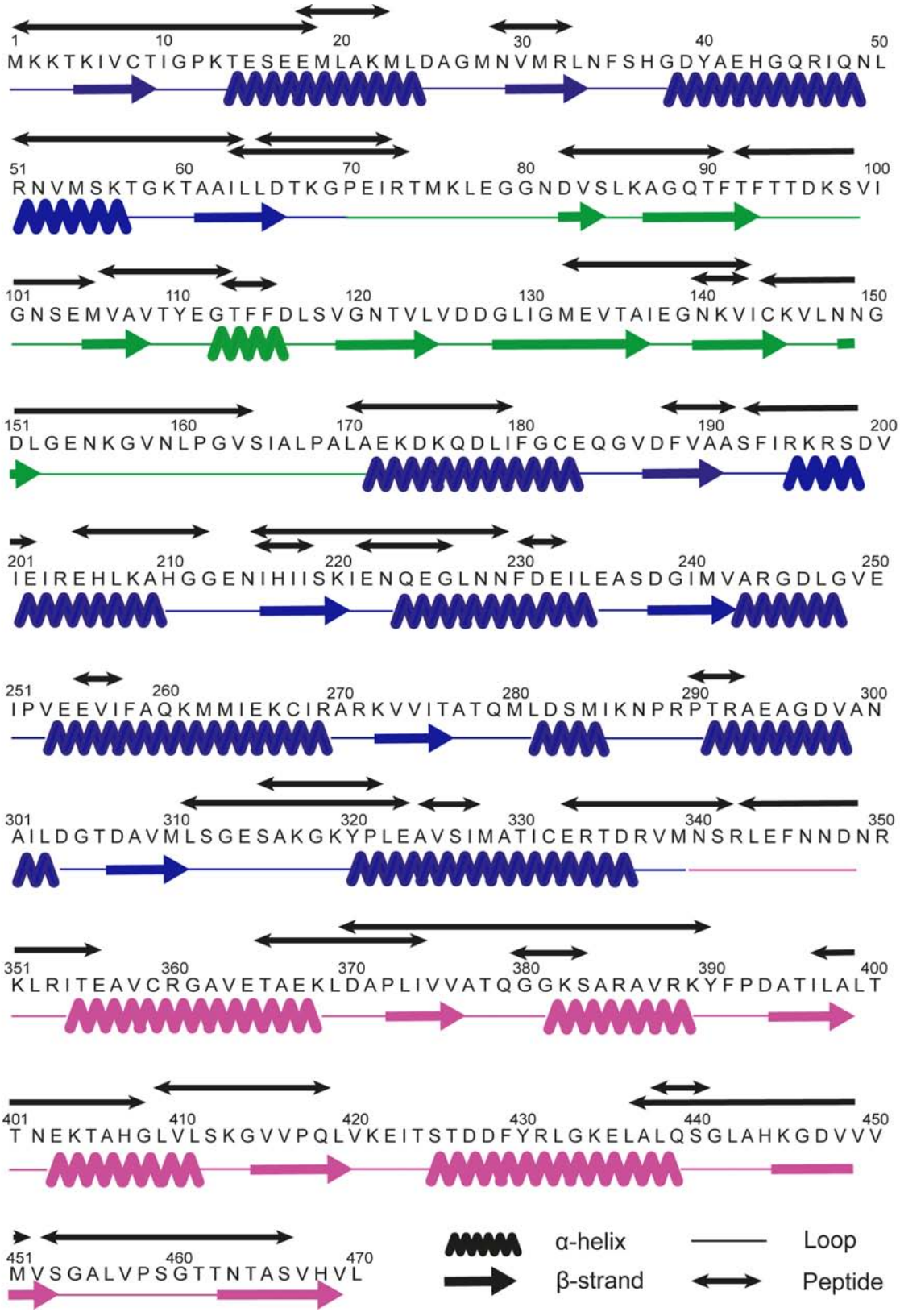

Figure 3.13 Primary protein sequence and secondary structure assignment of the wild-type PK1.

The above figure contains all 36 identified peptides that were resolved and analysed in the HDX experiments of both unbound and bound enzymes. The total sequence coverage for the experiment was 64%. A-domain (blue), B-domain (green) and C-domain (magenta).

3.8.2 Representative raw data

Typical raw HDX-MS data of three representative peptides is shown in Figure 3.14a, which reveal the mass shifts caused by deuteration of unbound and bound wild-type peptides. The theoretical isotopic distribution (black circles) was generated from a *FORTRAN* program that was developed in the Wilson Laboratory (York University, Toronto, Canada). The amount of deuterium exchanged was calculated as a percentage by fitting the observed isotopic distribution to the theoretical distribution using the *FORTRAN* program; these are shown as percentages on the graphs.

The raw data of the representative peptides (Figure 3.14) was used to develop kinetic plots of those same representative peptides in Figure 3.14b. To accurately characterise conformational dynamics of proteins, the deuterium uptake was monitored as a function of time, i.e. HDX kinetics. The 'percentage exchange' was plotted against time to show the amount of deuterium exchanged over time. Kinetic HDX profiles were fit with an exponential function (Equation 3.1) to illustrate a change in peptide deuterium uptake as a function of labelling time (Figure 3.14b). The kinetic profiles are representative of the 36 peptides identified and used in the analysis and illustrate that the loops of wild-type PK1 have different dynamic properties in the unbound and bound states.

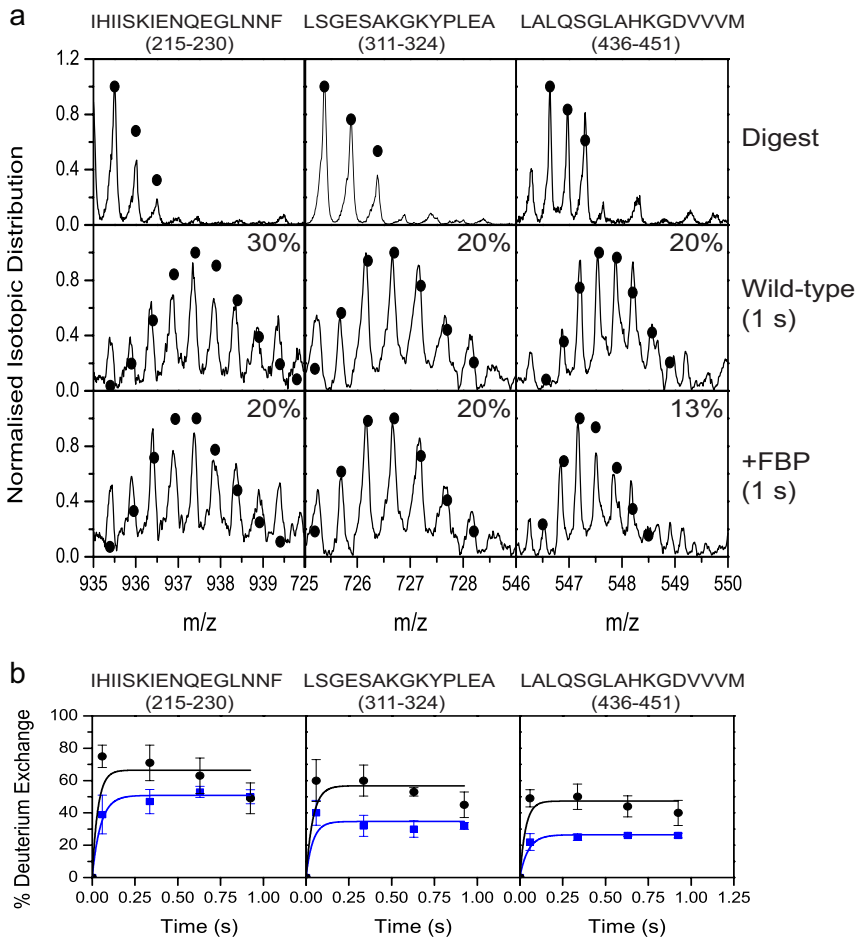

Figure 3.14 **Analysis of site-specific HDX analysis**. **(a)** Representative spectra for peptides derived from *E. coli* PK1 for non-deuterated wild-type (top row), deuterated wild-type from 1 s labeling time (second row) and deuterated wild-type with bound FBP from 1 s labeling time (third row). The raw spectra illustrate the observed shifts in isotopic distribution following HDX. The raw percentage of deuterium uptake for the illustrated replicate is indicated on each spectra. **(b)** HDX kinetic plots of representative peptides for wild-type in the absence (■) and presence (●) of FBP. Data represent an average of triplicate runs (error bars denote SEM). Kinetic data was fitted using single exponential non-linear regression analysis ($y=y0 + a(1-e^{-kt})$).

3.8.3 Overview of activation dynamics

Mapping the percentage of deuterium exchange for each peptide onto the wild-type structure uncovers regions that have significant changes in local backbone dynamics (Figure 3.15, the colour spectrum indicates the level of exchange: blue to red; low to high exchange, respectively).

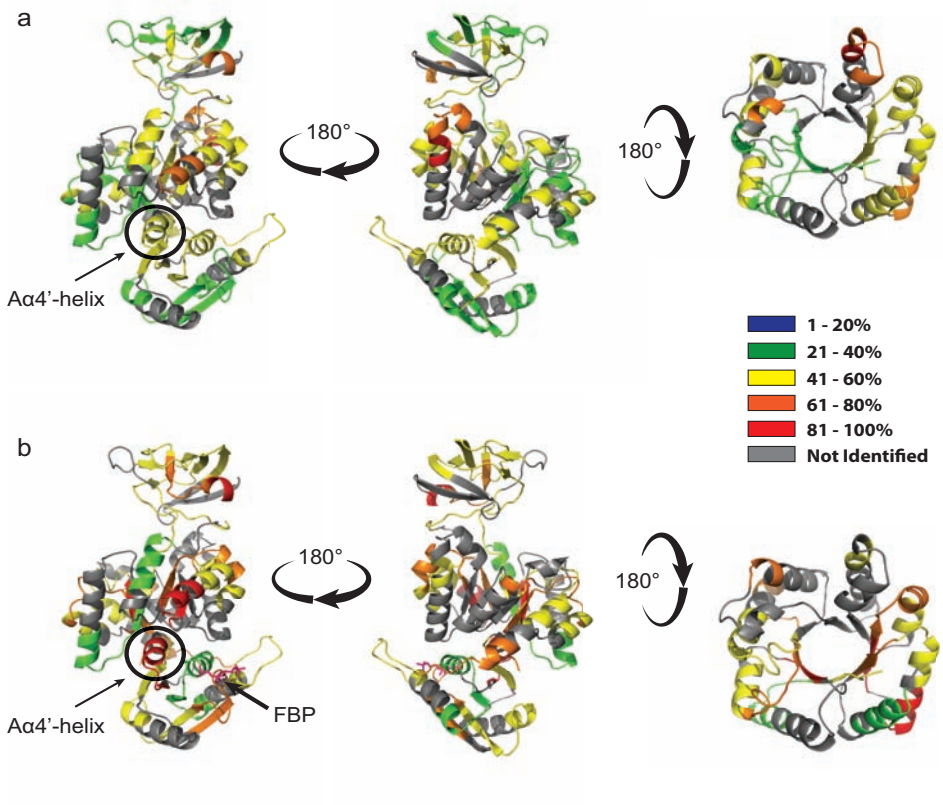

Figure 3.15 Amplitude of deuterium exchange mapped and colour-coded onto the wild-type *E. coli* PK1 structure (PDB ID: 4YNG). (a) Unbound wild-type viewing both sides of the subunit and looking down the $(\beta/\alpha)_8$-barrel. **(b)** Wild-type with the allosteric activator, FBP (magenta), modelled into the structure (based upon bound A301S) viewing both sides of the subunit and looking down the $(\beta/\alpha)_8$-barrel. The grey regions were not identified in the hydrogen-deuterium exchange experiment. The Aα4'-helix, residues 398−408, is circled in black. Only peptides that are identified in both experiments (with and without FBP) are displayed.

Qualitatively, the protein in the absence of FBP shows a generally low exchange of deuterium (20−60%), commensurate with a stable, globular structure. In particular, the peptides close to the tetrameric interfaces (A/A', peptide 291−294; and C/C', peptide 452−467) show low exchange, which is consistent with previous work demonstrating that wild-type is a very stable tetramer ($K_d^{4\text{-}1} < 10$ nM).[39] Moreover, the peptide at the A/C inter-domain interface (peptide 398−408, circled in Figure 3.16) has relatively low deuterium exchange (47%) compared to the same peptide in the presence of FBP (87%).

When mapping the degree of exchange in peptides derived from protein pre-treated with FBP and comparing this with peptides from the free enzyme, it is evident that the pattern of exchange is different (Figure 3.15a and 3.15b). Figure 3.16a shows only those peptides that exhibited a significant change in absolute deuterium exchange (>15% absolute

difference) when comparing peptides derived from unbound enzyme with those from FBP bound enzyme. To permit straightforward interpretation of the data, the absolute changes are noted only as an increase or decrease in exchange (Figure 3.16b). The percentage change in deuterium exchange upon FBP binding was then mapped to the structure to highlight regions of the protein that exhibited significant changes in backbone deuterium exchange (Figure 3.16c). Clearly, there are regions that show significant changes, which are addressed in the sections below.

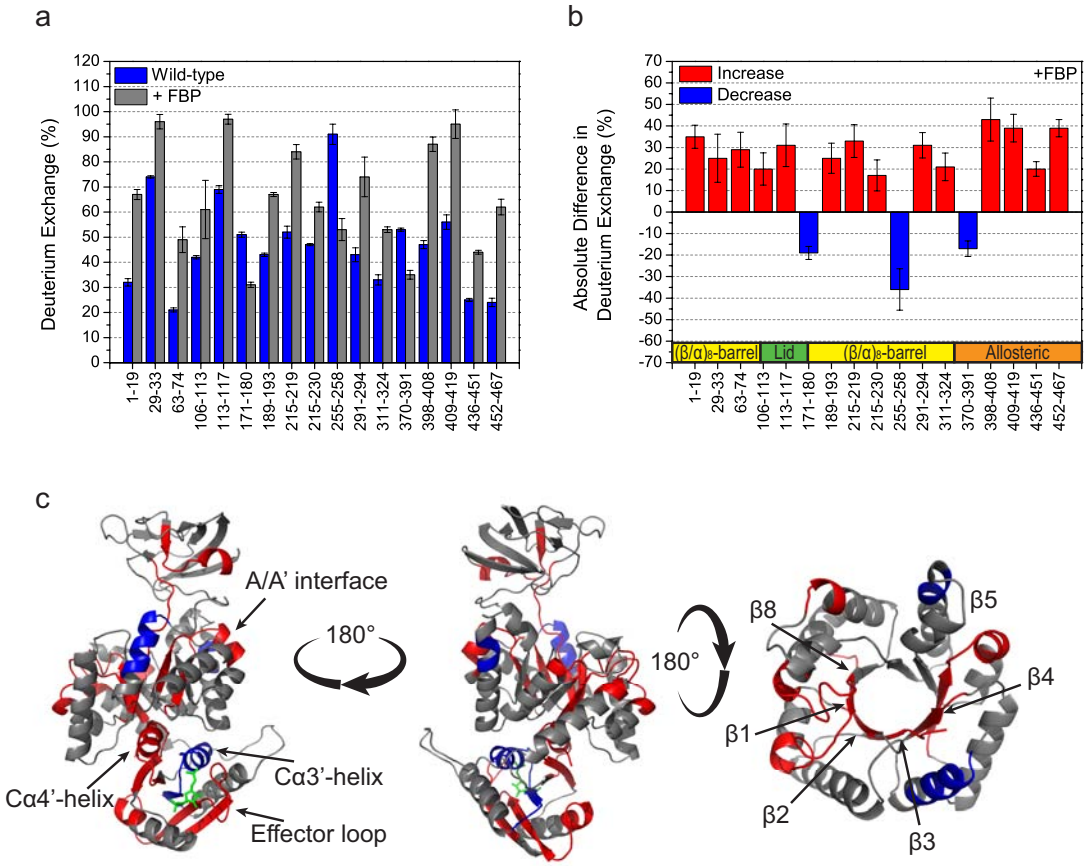

Figure 3.16 Change in average deuterium exchange between the unbound and bound wild-type PK1 peptides. **(a)** Amount of deuterium exchange in peptides derived from unbound (blue) and FBP bound (grey) wild-type. **(b)** Absolute difference (>15%) in deuterium exchange are plotted as an increase (red) or a decrease in exchange (blue) when in the presence of FBP. **(c)** Absolute differences (>15%) are mapped onto the wild-type subunit as an increase (red) or a decrease in exchange (blue). The allosteric activator FBP (green stick) has been modelled into the structure to show the binding position based upon the bound structure of PK1-A301S. Only peptides with a difference of >15% absolute differences in normalised deuterium exchange are plotted. Data represent an average of triplicate runs and error bars represent the SEM.

3.8.3.1 Dynamic changes to the allosteric domain upon FBP binding

The allosteric binding domain was examined to assess how FBP binding affects its conformational flexibility. From Figure 3.16, FBP binding resulted in clear changes in deuterium exchange in the allosteric C-domain. Since a structure of wild-type *E. coli* PK1 with bound FBP is not available, FBP is modelled into the allosteric binding domain based upon overlays with the bound A301S structure (Section 3.3.2; Figure 3.4). For A301S, FBP binding in the allosteric site is facilitated by Arg353 and Thr355 of the Cα2'-helix, forming electrostatic interactions with the 6'-phosphate. The 1'-phosphate forms a series of electrostatic interactions with side and main chain atoms of Thr378-Gln-Gly-Gly-Lys382 residues and the sugar ring of FBP forms hydrogen contacts with side and main chain atoms of two threonine residues, Thr355 and Thr462, from the loop preceding the Cβ5'-strand.

The FBP binding site in the allosteric domain shows key changes in conformational flexibility. Assuming FBP binds in the same pocket and in a similar orientation as bound A301S (Section 3.3.2), ligand binding requires a displacement of surface accessible water molecules and a change in the hydrogen bonding network of the pocket, including residues of the Cα3'- and Cα4'-helices and the effector loop (Figure 3.17c), so changes to the backbone flexibility in these regions were expected to be found. The first observation was that the surface that binds FBP has decreased exchange, consistent with FBP binding decreasing the availability of amides and reducing exchange. In addition, there is a large increase in deuterium exchange for the peptide containing the effector loop, residues 452−467 (Figure 3.17c). The effector loop is at the suspected activator-binding site and it shows a 38% increase in deuterium exchange. It has been implicated as the FBP binding loop,[8, 12] and in the unbound state it is located very near the position of suspected FBP binding. One interpretation of this result, which is supported by structural data of bound A301S (Figure 3.5), is that this loop detaches from the protein core in the presence of FBP, moving out of the way to allow binding. Figure 3.17a shows the position of the effector loop in the FBP bound A301S structure, while Figure 3.17b shows the same FBP bound A301S structure with the wild-type PK1 exchange changes mapped onto it to illustrate the change in conformation for this loop upon FBP binding.

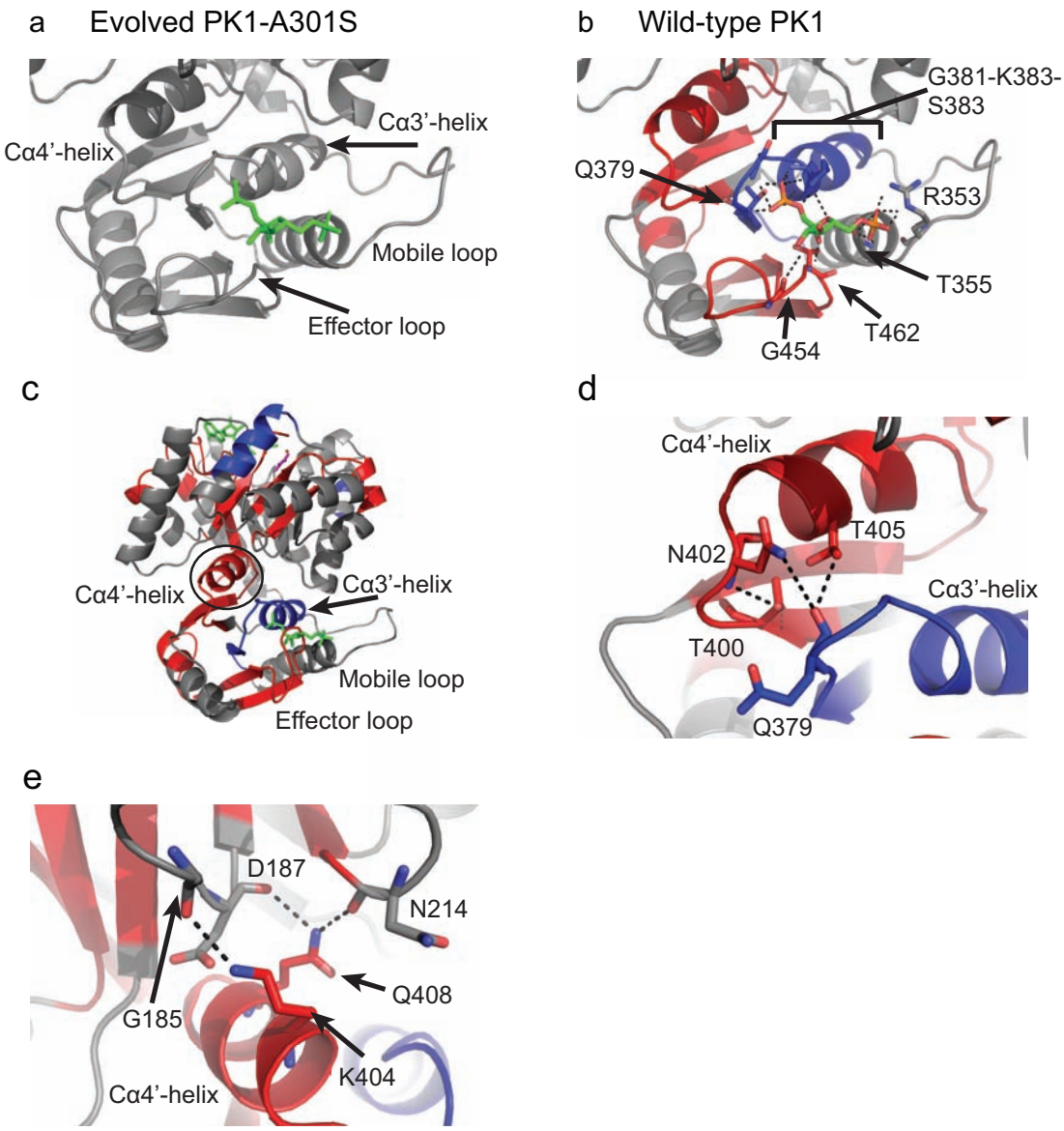

Figure 3.17 Dynamic changes to the wild-type PK1 allosteric domain. **(a)** A301S allosteric domain with FBP bound (green). **(b)** Change in deuterium exchange of wild-type PK1 mapped onto bound A301S showing binding interactions. **(c)** Wild-type PK1 with FBP modelled into the binding site from bound A301S. **(d)** Wild-type displaying the interactions between Cα3'- and Cα4'-helices, **(e)** Wild-type displaying the interactions between the Cα4'-helix and loops $\alpha_2\beta_2$ and $\alpha_3\beta_3$. Significant (>15% change in normalised deuterium uptake) changes are mapped onto the wild-type subunit as an increase in exchange (red) or a decrease in exchange (blue). Relevant residues are shown as sticks and key regions of the protein have been labelled. Interactions are displayed as dashed lines.

The wild-type exchange data shows that the neighbouring Cα3'-helix (residues 370−391) has a 17% decrease in deuterium exchange (Figure 3.17b and 3.17c). The decrease in dynamics for the Cα3'-helix may be due to hydrogen bonding with FBP, decreasing the number of amide hydrogen atoms available for exchange. The bound A301S structure

confirmed that residues Lys382 and Ser383 of the Cα3'-helix are involved in forming hydrogen bonds with the 1'-phosphate of FBP (Section 3.3.2). Hydrogen bond formation with FBP may cause a reorientation of residue Gln379, weakening its interactions with residues Asn402 and Thr405 of the Cα4'-helix (Figure 3.17d), located at the A/C interface.

Significantly, FBP binding causes destabilisation of the inter-domain interface that links the allosteric domain (C-domain) and the $(\beta/\alpha)_8$-barrel (A-domain) within the subunit (Figure 3.17). The interactions between the allosteric domain and the $(\beta/\alpha)_8$-barrel are largely mediated by the Cα4'-helix of the allosteric domain (circled in Figures 3.15b and 3.17c) and the N-terminal loops of the $(\beta/\alpha)_8$-barrel. The binding of FBP causes a 40% increase in deuterium exchange of the Cα4'-helix motif, strongly suggesting it may play an important role in the transition between inactive and active state populations. This result is inconsistent with the *L. mexicana* and *T. cruzi* PK crystal structures,[8, 12] which show rigid body rocking of the AC core domains.[8, 12] However, destabilisation of inter-domain (A/C) interfaces combined with destabilisation of subunit interfaces (Section 3.3.3) is consistent with the allosteric activation mechanism proposed in 1995 by Mattevi *et al*.,[6] which suggested a domain and subunit rotation model, implying increased conformational flexibility upon activation.

To summarise, FBP binding results in large changes in conformational flexibility of key elements within the allosteric domain. Firstly, the effector loop, which in the unbound wild-type structure lies across the FBP binding site, has increased conformational flexibility, consistent with its displacement upon binding. Secondly, the Cα3'-helix has decreased conformational flexibility, consistent with FBP binding to this helix (Figure 3.17b), as seen in the bound A301S structure. Finally, the Cα4'-helix has increased conformational flexibility (Figure 3.17d), which is supposedly due to weakening interactions between the Cα3'- and Cα4'-helices as the Cα3'-helix binds FBP (Figure 3.17d). The changes in conformational flexibility in the Cα3'- and Cα4'-helices at the A/C inter-domain interface, I propose, are important for communicating the allosteric signal to the active site.

Together, the dynamic results from the allosteric domain propose a structural rearrangement whereby: the FBP molecule binds to the Cα3'-helix, increasing its stability (Figure 3.17b), causing a breakage of bonds between the Cα3'- and Cα4'-helices (Figure

3.14d), resulting in destabilisation of inter-domain interfaces for signal transfer to the active site.

3.8.3.2 The tetrameric C/C' and A/A' interfaces are altered upon FBP binding

The tetrameric C/C' interface that is formed by the allosteric domains shows significantly increased conformational flexibility upon FBP binding, suggesting that the β-strand (Cβ5'-strand; residues 463−470) that forms this interface is destabilised. Figure 3.18a shows the C/C' interface interactions in the unbound wild-type. These interactions include hydrogen bonds between residues Ala465 and Ala465', Val467 and Asn463' and Asn463 and Val467'. FBP binding causes a 38% increase in deuterium exchange in the peptide that includes this strand.

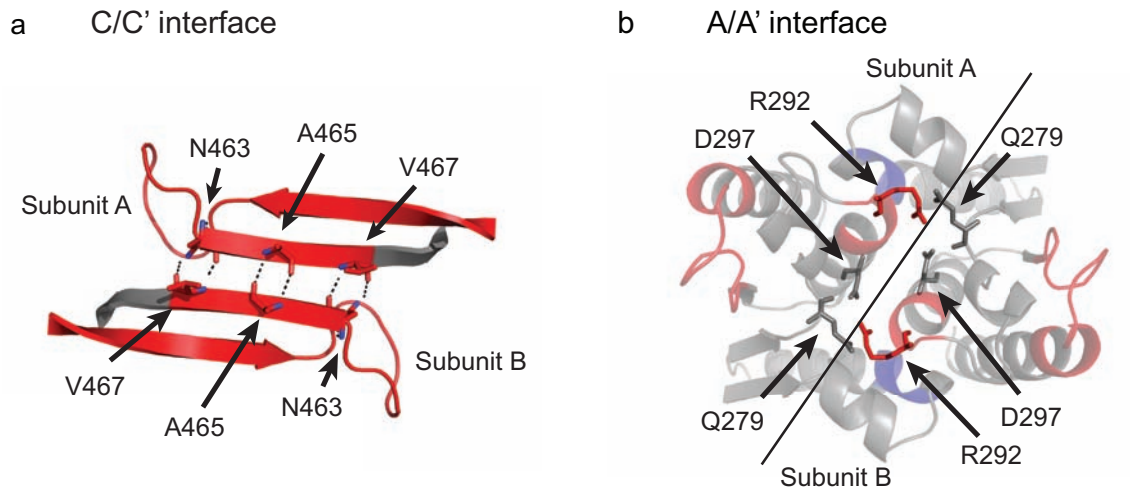

Figure 3.18 Changes in conformational flexibility within the C/C' and A/A' tetrameric interfaces. Change in deuterium exchange mapped on to the wild-type structure highlighting exchange changes at the **(a)** C/C' interface (interactions are shown as dashed lines) and **(b)** A/A' interface. Relevant residues are displayed as sticks and labelled.

Although peptide coverage across the A/A' interface is poor (7 of 26 residues in the FBP unbound monomer are within peptides that could be detected in both samples), several peptides show altered deuterium exchange (Figure 3.18a). The peptide containing residues 291−294 has an increase in deuterium exchange (difference of +31%) and is less structured. Pyruvate kinase structures have identified the conserved Arg292 as being key to both the allosteric transition of the enzyme and the activity of the enzyme,[12, 17] as it is involved in forming two hydrogen bonds with the backbone carbonyls belonging to the

PEP-stabilised Aα6'-helix.[12] Mutational studies in *E. coli* PK1 found that the substitution of this arginine to an aspartate removed the ability of the enzyme to transition to the active R-state, thus abolishing enzyme activity.[17] In contrast, the peptide containing residues 255−258, which is close to the A/A' interface, has decreased exchange (-38%) and is, therefore, significantly more structured upon FBP binding. The decreased exchange could be a result of reduced solvent accessibility due to activation induced subunit conformational changes (Section 3.3.3).

Overall, the peptides mapped to the tetrameric interfaces demonstrate increased conformational flexibility, indicating that the interfaces are destabilised upon FBP binding. Interestingly, this result, together with the increased conformational sampling evidenced from the global HDX experiment above, contradict the general hypothesis put forward by Morgan and co-workers,[8] that "*while the regulatory molecules and molecular mechanisms may vary between species, the underlying principle of tetrameric stabilisation in response to effector binding is conserved*." That study used thermal unfolding to infer conformation stability, whereas the data from the HDX directly assesses the degree of conformational flexibility, both globally and within specific regions within the protein. In any event, together with the dramatic destabilisation at the A/C inter-domain interface Cα4'-helix (peptide 398−408), these exchange results connect the domain and tetrameric interfaces, and in particular their destabilisation, to the allosteric mechanism of PK enzymes.[17]

Lastly, this result is also consistent with the effect that FBP has on PEP affinity. FBP binding blocks the homotropic allosteric mechanism by PEP; in the absence of FBP, titration of PEP results in a sigmoidal response, a signature of cooperativity, whereas in the presence of FBP a rectangular hyperbolic curve is observed, signalling a loss of cooperativity. Destabilisation of the domain and tetrameric interfaces, such that the active site-containing A-domains are decoupled from one another, is consistent with the loss of PEP cooperation between active sites. In other words, FBP binding destabilises the tetrameric interfaces, decoupling the subunits, which blocks the activation signal transfer between subunits and localises the signal transfer within subunits, i.e. between the allosteric site and the active site of a subunit.

3.8.3.3 Signalling the catalytic site for activation

Next, the changes in conformational flexibility associated with the active site $(\beta/\alpha)_8$-barrel domain were traced to understand the mechanism by which FBP binding affects catalysis (Figure 3.19).

Increased conformational flexibility of the β-strands within the $(\beta/\alpha)_8$-barrel accompanies destabilisation of the Cα4'-helix, which sits at the A/C inter-domain interface and interacts with the αβ-loops at the N-terminus of the $(\beta/\alpha)_8$-barrel. Residue Gln408 of the key Cα4'-helix forms interactions with Asp187 of loop $\alpha_3\beta_3$ and Asn214 of loop $\alpha_4\beta_4$, while Lys404 of the Cα4'-helix interacts with Gly185 of loop $\alpha_3\beta_3$ (Figure 3.17e). Given the large change in conformational flexibility of the Cα4'-helix, unsurprisingly the β-strands following the αβ-loops (β-strands 4 and 5, respectively) show an increase in deuterium exchange of 23% and 31%, respectively. Furthermore, β-strands 1, 2 and 3 also show some destabilisation (increase in deuterium exchange of 36%, 22% and 27%, respectively), resulting in a largely unstable $(\beta/\alpha)_8$-barrel core. The destabilisation of these β-strands suggests the allosteric signal is communicated through the core of the $(\beta/\alpha)_8$-barrel to the active site.

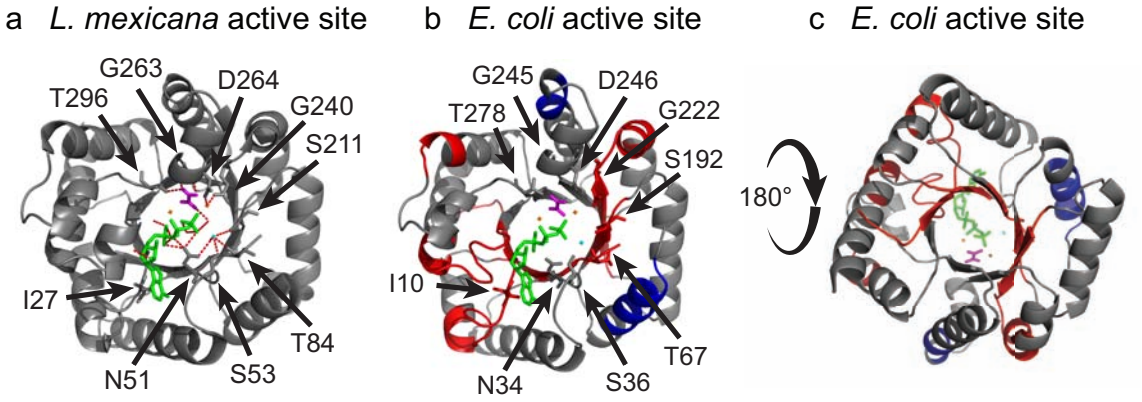

Figure 3.19 Dynamic changes to the catalytic site of the $(\beta/\alpha)_8$-barrel. (a) *L. mexicana* $(\beta/\alpha)_8$-barrel, showing the substrates bound in the active site (PDB ID: 3HQP). Hydrogen bonds between the substrates and residues are shown in red with interacting residues shown as sticks and labelled. **(b)** Wild-type $(\beta/\alpha)_8$-barrel (looking down the barrel). The active site substrates and equivalent interacting residues modelled from the *L. mexicana* crystal structure (PDB ID: 3HQP) are presented as sticks and labelled. **(c)** Wild-type $(\beta/\alpha)_8$-barrel (looking up the barrel). The substrates bound in the active site are coloured as follows: ATP (green), pyruvate (magenta), Mg^{2+} (orange) and K^+ (cyan).

Changes in deuterium exchange are also identified in the active site loops at the top of the $(\beta/\alpha)_8$-barrel (Figure 3.19). Exchange in the peptide containing loop $\beta_8\alpha_8$ (residues 311−324) increased by 20% and the peptide with the neighbouring $\beta_1\alpha_1$ loop (residues 1−19) increased by 36%. Furthermore, β-strands 1, 2, 3, 4 and 5 in the core of the $(\beta/\alpha)_8$-barrel, near the substrate binding sites, are also destabilised. Specific substrate binding regions are modelled from *L. mexicana* PK crystal structures (PDB ID: 3HQP) to determine which β-strands are near the bound substrates and catalytic ions. This reveals that the adenosine ring of the ATP (or ADP) is located within interaction distance of loops $\beta_1\alpha_1$, $\beta_2\alpha_2$, $\beta_3\alpha_3$ and $\beta_8\alpha_8$, while the oxalate molecule (PEP analogue) and catalytic ions are situated near β-strands 4 and 5 (Figure 3.19). Thus, many of the catalytically important residues show increased conformational flexibility. A caveat to this analysis is that the peptides, in addition to residues belonging to β-strands 1, 3 and 4, also include residues that are within the βα-loops, which are likely to be dynamic. Unfortunately, the resolution limits of this experiment are not high enough to confirm if the loop regions are experiencing high exchange, thus causing an averaged apparent high exchange of the peptide, or if the entire peptide is experiencing high exchange.

In addition to the wild-type *E. coli* PK1 exchange data demonstrating flexibility of substrate binding loops, structural analysis comparing temperature factors (B-factors) of the *L. mexicana* structures in the presence and absence of FBP identifies two active site loops ($\beta_7\alpha_7$, and $\beta_8\alpha_8$,) and their preceding β-strands (7 and 8), in the core of the $(\beta/\alpha)_8$-barrel that have increased B-factors upon FBP binding. The restricted movement of proteins in a crystalline environment reduces the likelihood of identifying most, if not all, conformational sampling within a protein. However, the results from *L. mexicana* PK and *E. coli* PK1 suggest the increased flexibility upon allosteric activation may be common to PK enzymes.

The binding of the allosteric activator can redistribute protein conformational ensembles and alter the rates of interchange between these populations; this can manifest as a change in flexibility at the active site.[26] The increased exchange can be explained by these loops having greater flexibility and therefore an increase in conformational sampling, which would increase the chances of substrate binding for catalysis.[42] Increased exchange in the active site at early labelling time-points is consistent with the 'intensification' model for catalysis-linked dynamics whereby the energy barrier between conformational substates is

lowered upon activator binding, presenting as an initial 'burst-phase' of exchange.[38] This supports the K-type binding mechanism, which proposes that allosteric activation increases the binding affinity of substrate in the active site.[5]

3.8.3.4 The flexible lid domain is not allosterically controlled by FBP

The exchange profiles of peptides derived from the lid domain (B-domain) of wild-type are largely unchanged when the enzyme is pre-treated with FBP, suggesting that ligand binding in the allosteric site has only a minor effect upon the secondary structure of the lid domain. This result is consistent with previous studies that have shown that the movement of the flexible lid domain is not allosterically controlled;[12, 15, 43] however, it is controlled by the presence, type and position of substrates bound within the active site.

3.9 Dynamic allosteric activation mechanism

The results presented here provide an experimental characterisation of site-specific dynamics for the allosteric activation of *E. coli* PK1, a central metabolic enzyme. The deuterium exchange data demonstrates that FBP binding alters the conformational flexibility of specific backbone amides, largely increasing the conformational sampling in the bound state. In addition, the data reveals altered dynamics in the allosteric binding region and also at the substrate binding site approximately 40 Å away.

The interpreted results suggest that the following scheme results in allosteric activation of wild-type *E. coli* PK1 upon FBP binding:

1) The presence of FBP destabilises the effector loop and causes a structural rearrangement, displacing it to allow binding.
2) The FBP then forms interactions with the Cα3'-helix, increasing the stability of the helix and weakening an interaction between the loop preceding Cα3'- and the Cα4'-helix.
3) Destabilisation of the Cα4'-helix results in destabilisation of the inter-domain interface that links the allosteric domain (C-domain) and the $(\beta/\alpha)_8$-barrel (A-domain) within the monomer.

4) Altered interactions of the destabilised Cα4'-helix at the interface between the A- and C-domains and loops $\alpha_2\beta_2$ and $\alpha_3\beta_3$ result in destabilised β-strands following the αβ-loops, consequently producing a more conformationally flexible $(\beta/\alpha)_8$-barrel core. This destabilisation is consistent with the β-strands being involved in allosteric signal transfer through the core of the $(\beta/\alpha)_8$-barrel, to the active site.

5) The signal transfer through the core of the $(\beta/\alpha)_8$-barrel destabilises the substrate binding loops at the active site. I propose that the active site loops then sample a greater number of conformations, some of which facilitate binding of the substrate and catalytic ions. This theory is supported by studies directly assessing the correlation between flexibility and binding, which demonstrate that increased loop flexibility does enhance ligand affinity.[18]

6) The destabilisation of the tetrameric interfaces (A/A' and C/C') decouples the monomers attenuating the PEP homotropic allosteric signal between active sites, explaining why FBP binding blocks the PEP allosteric mechanism.

In conclusion, the bound A301S structure supports the allosteric mechanism proposed by Mattevi *et al*.,[6, 44] where FBP binding causes domain and subunit rotations.[6, 44] Moreover, the wild-type *E. coli* PK1 exchange results are inconsistent with Morgan's rigid-body rotation model.[8, 12] Nevertheless, the results support and extend Mattevi's model by explaining how FBP promotes substrate binding and attenuates the PEP homotropic allosteric signal, despite the allosteric binding site being 40 Å away from the active site.

3.10 References

[1] Fenton, AW. (2008) Allostery: an illustrated definition for the second secret of life, *Trends Biochem. Sci. 33*, 420-425.

[2] Changeux, JP. (2013) 50 years of allosteric interactions: the twists and turns of the models, *Nat. Rev. Mol. Cell Biol. 14*, 819-829.

[3] Monod, J, Changeux, JP, and Jacob, F. (1963) Allosteric proteins and cellular control systems, *J. Mol. Biol. 6*, 306-329.

[4] Yuan, Y, Tam, MF, Simplaceanu, V, and Ho, C. (2015) New look at hemoglobin allostery, *Chem. Rev. 115*, 1702-1724.

[5] del Sol, A, Tsai, CJ, Ma, B, and Nussinov, R. (2009) The origin of allosteric functional modulation: multiple pre-existing pathways, *Structure 17*, 1042-1050.

[6] Mattevi, A, Valentini, G, Rizzi, M, Speranza, ML, Bolognesi, M, and Coda, A. (1995) Crystal structure of *Escherichia coli* pyruvate kinase type I: Molecular basis of the allosteric transition, *Structure 3*, 729-741.

[7] Fothergill-Gilmore, LA, and Michels, PA. (1993) Evolution of glycolysis, *Prog. Biophys. Mol. Biol. 59*, 105-235.

[8] Morgan, HP, Zhong, W, McNae, IW, Michels, PAM, Fothergill-Gilmore, LA, and Walkinshaw, MD. (2014) Structures of pyruvate kinases display evolutionarily divergent allosteric strategies, *R. Soc. Open. Sci. 1*, 140120.

[9] Muirhead, H, Clayden, D, Barford, D, Lorimer, C, Fothergill-Gilmore, L, Schiltz, E, and Schmitt, W. (1986) The structure of cat muscle pyruvate kinase, *EMBO J. 5*, 475-481.

[10] Allen, SC, and Muirhead, H. (1996) Refined three-dimensional structure of cat-muscle (M1) pyruvate kinase at a resolution of 2.6 Å, *Acta Crystallogr. D Biol. Crystallogr. 52*, 499-504.

[11] Jurica, MS, Mesecar, A, Heath, PJ, Shi, W, Nowak, T, and Stoddard, BL. (1998) The allosteric regulation of pyruvate kinase by fructose-1,6-bisphosphate, *Structure 6*, 195-210.

[12] Morgan, HP, McNae, IW, Nowicki, MW, Hannaert, V, Michels, PAM, Fothergill-Gilmore, LA, and Walkinshaw, MD. (2010) Allosteric mechanism of pyruvate kinase from *Leishmania mexicana* uses a rock and lock model, *J. Biol. Chem. 285*, 12892-12898.

[13] Levine, M, Muirhead, H, Stammers, DK, and Stuart, DI. (1978) Structure of pyruvate kinase and similarities with other enzymes: possible implications for protein taxonomy and evolution, *Nature 271*, 626-630.

[14] Ishwar, A, Tang, Q, and Fenton, AW. (2015) Distinguishing the interactions in the fructose-1,6-bisphosphate binding site of human liver pyruvate kinase that contribute to allostery, *Biochemistry 54*, 1516-1524.

[15] Zhong, W, Morgan, HP, Nowicki, MW, McNae, IW, Yuan, M, Bella, J, Michels, PA, Fothergill-Gilmore, LA, and Walkinshaw, MD. (2014) Pyruvate kinases have an intrinsic and conserved decarboxylase activity, *Biochem. J. 458*, 301-311.

[16] Krissinel, E, and Henrick, K. (2007) Inference of macromolecular assemblies from crystalline state, *J. Mol. Biol. 372*, 774-797.

[17] Valentini, G, Chiarelli, L, Fortini, R, Speranza, ML, Galizzi, A, and Mattevi, A. (2000) The allosteric regulation of pyruvate kinase: A site-directed mutagenesis study, *J. Biol. Chem. 275*, 18145-18152.

[18] Bauer, F, and Sticht, H. (2007) A proline to glycine mutation in the Lck SH3-domain affects conformational sampling and increases ligand binding affinity, *FEBS Lett. 581*, 1555-1560.

[19] DePristo, MA, de Bakker, PI, and Blundell, TL. (2004) Heterogeneity and inaccuracy in protein structures solved by X-ray crystallography, *Structure 12*, 831-838.

[20] Skou, S, Gillilan, RE, and Ando, N. (2014) Synchrotron-based small-angle X-ray scattering of proteins in solution, *Nat. Protoc. 9*, 1727-1739.

[21] Mertens, HDT, and Svergun, DI. (2010) Structural characterization of proteins and complexes using small-angle X-ray solution scattering, *J. Struct. Biol. 172*, 128-141.

[22] de Oliveira, LC, da Silva, VM, Colussi, F, Cabral, AD, de Oliveira Neto, M, Squina, FM, and Garcia, W. (2015) Conformational changes in a hyperthermostable glycoside hydrolase: enzymatic activity is a consequence of the loop dynamics and protonation balance, *PLoS One 10*, e0118225.

[23] Tsai, CJ, and Nussinov, R. (2014) A unified view of "how allostery works", *PLoS Comput. Biol. 10*, e1003394.

[24] Boehr, DD, Nussinov, R, and Wright, PE. (2009) The role of dynamic conformational ensembles in biomolecular recognition, *Nat. Chem. Biol. 5*, 789-796.

[25] Motlagh, HN, Wrabl, JO, Li, J, and Hilser, VJ. (2014) The ensemble nature of allostery, *Nature 508*, 331-339.

[26] Goodey, NM, and Benkovic, SJ. (2008) Allosteric regulation and catalysis emerge via a common route, *Nat. Chem. Biol. 4*, 474-482.

[27] Ma, B, Tsai, CJ, Haliloglu, T, and Nussinov, R. (2011) Dynamic allostery: linkers are not merely flexible, *Structure 19*, 907-917.

[28] Smock, RG, and Gierasch, LM. (2009) Sending signals dynamically, *Science 324*, 198-203.

[29] Kerns, SJ, Agafonov, RV, Cho, YJ, Pontiggia, F, Otten, R, Pachov, DV, Kutter, S, Phung, LA, Murphy, PN, Thai, V, Alber, T, Hagan, MF, and Kern, D. (2015) The energy landscape of adenylate kinase during catalysis, *Nat. Struct. Mol. Biol. 22*, 124-131.

[30] Frauenfelder, H, Sligar, SG, and Wolynes, PG. (1991) The energy landscapes and motions of proteins, *Science 254*, 1598-1603.

[31] Nussinov, R, and Tsai, CJ. (2014) Allostery without a conformational change? Revisiting the paradigm, *Curr. Opin. Struct. Biol. 30*, 17-24.

[32] Boehr, DD, McElheny, D, Dyson, HJ, and Wright, PE. (2006) The dynamic energy landscape of dihydrofolate reductase catalysis, *Science 313*, 1638-1642.

[33] Resetca, D, Haftchenary, S, Gunning, PT, and Wilson, DJ. (2014) Changes in signal transducer and activator of transcription 3 (STAT3) dynamics induced by complexation with pharmacological inhibitors of Src homology 2 (SH2) domain dimerization, *J. Biol. Chem. 289*, 32538-32547.

[34] Resetca, D, and Wilson, DJ. (2013) Characterizing rapid, activity-linked conformational transitions in proteins via sub-second hydrogen deuterium exchange mass spectrometry, *FEBS J. 280*, 5616-5625.

[35] Rob, T, Liuni, P, Gill, PK, Zhu, S, Balachandran, N, Berti, PJ, and Wilson, DJ. (2012) Measuring dynamics in weakly structured regions of proteins using microfluidics-enabled subsecond H/D exchange mass spectrometry, *Anal. Chem. 84*, 3771-3779.

[36] Rob, T, and Wilson, DJ. (2009) A versatile microfluidic chip for millisecond time-scale kinetic studies by electrospray mass spectrometry, *J. Am. Soc. Mass Spectrom. 20*, 124-130.

[37] Malcovati, M, and Valentini, G. (1982) AMP- and fructose 1,6-bisphosphate-activated pyruvate kinases from *Escherichia coli*, *Methods Enzymol. 90*, 170-179.

[38] Liuni, P, Jeganathan, A, and Wilson, DJ. (2012) Conformer selection and intensified dynamics during catalytic turnover in chymotrypsin, *Angew. Chem. Int. Ed. Engl. 51*, 9666-9669.

[39] Zhu, T, Bailey, MF, Angley, LM, Cooper, TF, and Dobson, RCJ. (2010) The quaternary structure of pyruvate kinase type 1 from *Escherichia coli* at low nanomolar concentrations, *Biochimie 92*, 116-120.

[40] Fenton, AW, and Blair, JB. (2002) Kinetic and allosteric consequences of mutations in the subunit and domain interfaces and the allosteric site of yeast pyruvate kinase, *Arch. Biochem. Biophys. 397*, 28-39.

[41] Boiteux, A, Markus, M, Plesser, T, Hess, B, and Malcovati, M. (1983) Analysis of progress curves. Interaction of pyruvate kinase from *Escherichia coli* with fructose 1,6-bisphosphate and calcium ions, *Biochem. J. 211*, 631-640.

[42] Urfer, R, and Kirschner, K. (1992) The importance of surface loops for stabilizing an eightfold βα barrel protein, *Protein Sci. 1*, 31-45.

[43] Fenton, AW, Williams, R, and Trewhella, J. (2010) Changes in small angle X-ray scattering parameters observed upon ligand binding to rabbit muscle pyruvate kinase are not correlated with allosteric transitions, *Biochemistry 49*, 7202-7209.

[44] Mattevi, A, Bolognesi, M, and Valentini, G. (1996) The allosteric regulation of pyruvate kinase, *FEBS Lett. 389*, 15-19.

Chapter Four

Escherichia coli PK1 enzymes with altered allostery and activity are selected

This chapter broadly investigates, at the level of enzyme function, the rationale for the fitness benefit that results from the adaptations in *Escherichia coli* pyruvate kinase type 1 (PK1). In particular, I test the parallel nature of evolution at the enzyme function level and probe which features of enzyme function (e.g. $S_{0.5}$, k_{cat}, allostery) are being selected for in the low glucose environment. In addition, the evolved enzymes, which have mutations in the active site, allosteric binding site and the tetrameric interface, provide a unique opportunity to learn more about the structure and function relationship of *E. coli* PK1, as seen through the light of evolution. To do this, enzyme kinetic experiments were carried out to investigate the functional responses of each of the evolved enzymes to their substrates, adenosine diphosphate (ADP) and phosphoenolpyruvate (PEP), as well as the effect of the allosteric regulator, fructose-1,6-bisphosphate (FBP). The results determined that the evolved enzymes exhibit a variety of kinetic responses, with all showing a parallel decrease in activity at physiological substrate concentrations compared to the wild-type enzyme. Moreover, seven of the eight evolved enzymes show an altered mechanism of allosteric activation. These results suggest that the key functional adaptations that are being selected are catalytic activity and allostery.

4.1 Introduction

Twelve replicate populations of *E. coli* were evolved in glucose-limited conditions, from which eight adaptive mutations in *E. coli* pyruvate kinase type 1 (PK1), a regulatory enzyme involved in metabolising glucose were selected. These adaptive mutations increase the fitness of the *E. coli* and increase host survival in the new glucose-limited environment.[1, 2]

Pyruvate kinase catalyses a phosphate transfer from PEP to ADP, to produce adenosine triphosphate (ATP) and pyruvate. PEP is not only the substrate for the reaction catalysed by PK, but is also used by the phosphotransferase system to import glucose across the cell membrane and into *E. coli* cells, as well as many other biosynthetic reactions within the cell.[3] Woods *et al*. proposed that the adaptive mutations resulted in a fitness benefit by slowing the conversion of PEP to pyruvate, making more PEP available to drive the phosphotransferase-mediated import of the limiting resource glucose.[4] Similar to Woods' hypothesis, a recent metabolomics study by Xu *et al*. demonstrated that if *E. coli* cells accumulated sufficient intra-cellular PEP upon glucose removal, they had an advantage for initiating glycolysis when the glucose was restored.[5] The higher PEP concentration is associated with a faster rate of glucose import and shorter lag times before the continuation of exponential growth.[5] The study determined that PEP accumulation is associated with the regulation of PEP carboxylase by FBP, similar to *E. coli* PK1 being allosterically activated by FBP. Therefore, following the study, I hypothesise that the evolved *E. coli* PK1 enzymes will have reduced activity, causing PEP accumulation as a response to glucose removal from the environment.

To investigate physiologically relevant functional activity of the enzymes, the concentrations of substrates, PEP, ADP and FBP were determined within the *E. coli* cells. Intracellular PEP and FBP concentrations for the ancestor strain (which contains the wild-type PK1 enzyme), and evolved strains (which is the ancestor background, but with the evolved PK1 inserted into the chromosome) were measured in the stationary phase by Sarah Kessans (University of Canterbury) in DM25 low glucose media. The PEP concentrations were found to be in the 0.08 to 0.12 mM range, in accordance with the 0.16 mM reported by Xu *et al*.[5] and the 0.18 mM reported by Bennett *et al*.,[6] and the FBP

concentrations were within the 1.1 to 1.8 mM range. Metabolite profiling of *E. coli* by Bennett *et al.* found the ADP to be 0.56 mM.[6]

Kinetic analysis of the wild-type PK1 enzyme in Chapter Two (Section 2.3.1) confirmed that the wild-type enzyme is homotropically activated by its substrate PEP. However, the presence of its allosteric activator, FBP, causes heterotropic activation of the enzyme, producing classic Michaelis-Menten kinetics with respect to PEP titration.[7, 8] Having established the kinetic properties and allosteric activation mechanism for *E. coli* PK1, the next question is whether the eight evolved enzymes are functionally and allosterically different. Answering this question is important for determining the feature of enzyme function that adaptation is selecting; i.e. is adaptation selecting for V_{max}, $S_{0.5}$ or allostery.

The eight evolved enzymes can be separated into three different groups based upon their location in the *E. coli* PK1 structure (Section 1.6); P70Q, P70T and D127N are located in the active site region of the protein, I264F, A301S and A301T are located around the A/A' interface between subunits, and G381A and T462I are located in the allosteric site and are directly involved in binding the FBP molecule (Section 3.3.2). It is predicted that the enzymes with mutations in the active site would display altered catalysis, mutations in the A/A' interface would affect regulation, and mutation of residues involved in binding FBP would alter the FBP binding affinity and activation efficiency of the enzyme (Section 1.2).

I hypothesise that the evolved populations adapted to the low glucose environment by altering the regulatory and functional properties of wild-type PK1, including altering catalysis and structure.[9] In this chapter, I investigate the molecular mechanism underlying the functional benefit produced by each of the eight single substitution mutations. Here, the function and stability of each of the evolved enzymes is assessed to answer the following questions: 1) Are the results of adaptive evolution parallel on the functional level, as they are on the genetic and physiological level? 2) Have the mutations altered the functional responses of the enzymes? What feature of the enzyme is being selected for? 3) What have we learned about the *E. coli* PK1 enzyme? 4) Has the stability of the enzymes changed?

4.2 Enzymes have evolved varied kinetic behaviours

Kinetic analysis of each enzyme's function starts here in Section 4.2, looking at the global kinetic parameters. Section 4.3 then analyses the detailed functional behaviours of each of the evolved enzymes compared to the wild-type enzyme.

Although the enzyme kinetics have been measured across a range of different substrate and activator concentrations, the concentrations of metabolites within *E. coli* cells are as follows: PEP, 0.08 to 0.12 mM; FBP, 1.1 to 1.8 mM and ADP, 0.56 mM.[6] These concentrations are important for determining the physiological relevance of the functional behaviours. Substrate concentrations will be marked on the respective kinetic plots to provide a guide for physiological relevance.

4.2.1 Evolved enzymes display varied response to ADP

This section assesses the catalysis of the evolved enzymes relative to ADP concentration (Figure 4.1 and Table 4.1), in the absence (Figure 4.1a) and presence (Figure 4.1b) of the allosteric activator FBP to identify the effect of allosteric activation upon the enzymes' response to ADP.

4.2.1.1 Effect on k_{cat}

The results indicate that the apparent k_{cat}'s are variable and all of the enzymes display different kinetic abilities compared to that of wild-type PK1. Four of the evolved enzymes (P70Q, A301S, G381A and T462I) have a higher activity than wild-type (>345 ± 30 s^{-1}) and four (P70T, D127N, I264F and A301T) have a lower activity than wild-type (<345 ± 30 s^{-1}). The differences in activity are a result of the substitution mutations altering the enzymes' ability to catalyse the conversion of substrates to products, resulting in varied enzyme activities, or turnover numbers (k_{cat}).

4.2.1.2 Effect on $S_{0.5}$

Next, the $S_{0.5}^{ADP}$ for all eight enzymes were determined and compared to the wild-type enzyme. The wild-type kinetic curve shifted slightly to the left upon the addition of FBP, decreasing the $S_{0.5}^{ADP}$ (1.0 ± 0.2 mM to 0.60 ± 0.06 mM), suggesting that FBP binding increases the binding affinity of ADP in the active site. All of the evolved enzymes show a similar effect of FBP binding upon the $S_{0.5}^{ADP}$ as the wild-type, demonstrating either a slight change or no observable change. I264F, G381A and T462I were the exceptions to this, as they showed 3-fold, 7-fold and 9-fold decreases, respectively, in $S_{0.5}^{ADP}$ upon FBP binding. Significant decreases such as these suggest that FBP binding in the allosteric sites of the enzymes is altering the binding affinity of ADP at the active site, over 40 Å away.

4.2.1.3 Effect of FBP on ADP titrations

Consistent with wild-type PK1, the presence of FBP does not alter the ADP binding effect of the evolved enzymes; however, I264F and A301T have reduced activity when the activator is not present. High concentrations of PEP were required to saturate these enzymes in the absence of FBP. This result suggests they have evolved weakened cooperative activation and/or decreased PEP binding affinity, so much so that A301T was considered inactive without FBP and was excluded from the ADP titrations without FBP.

The results of the ADP kinetic analysis recognises the difference in kinetic activity of each of the evolved enzymes compared to the wild-type and demonstrates that FBP binding does not majorly affect the binding of ADP. The results are displayed above in Figure 4.1 and the derived kinetic parameters are below in Table 4.1.

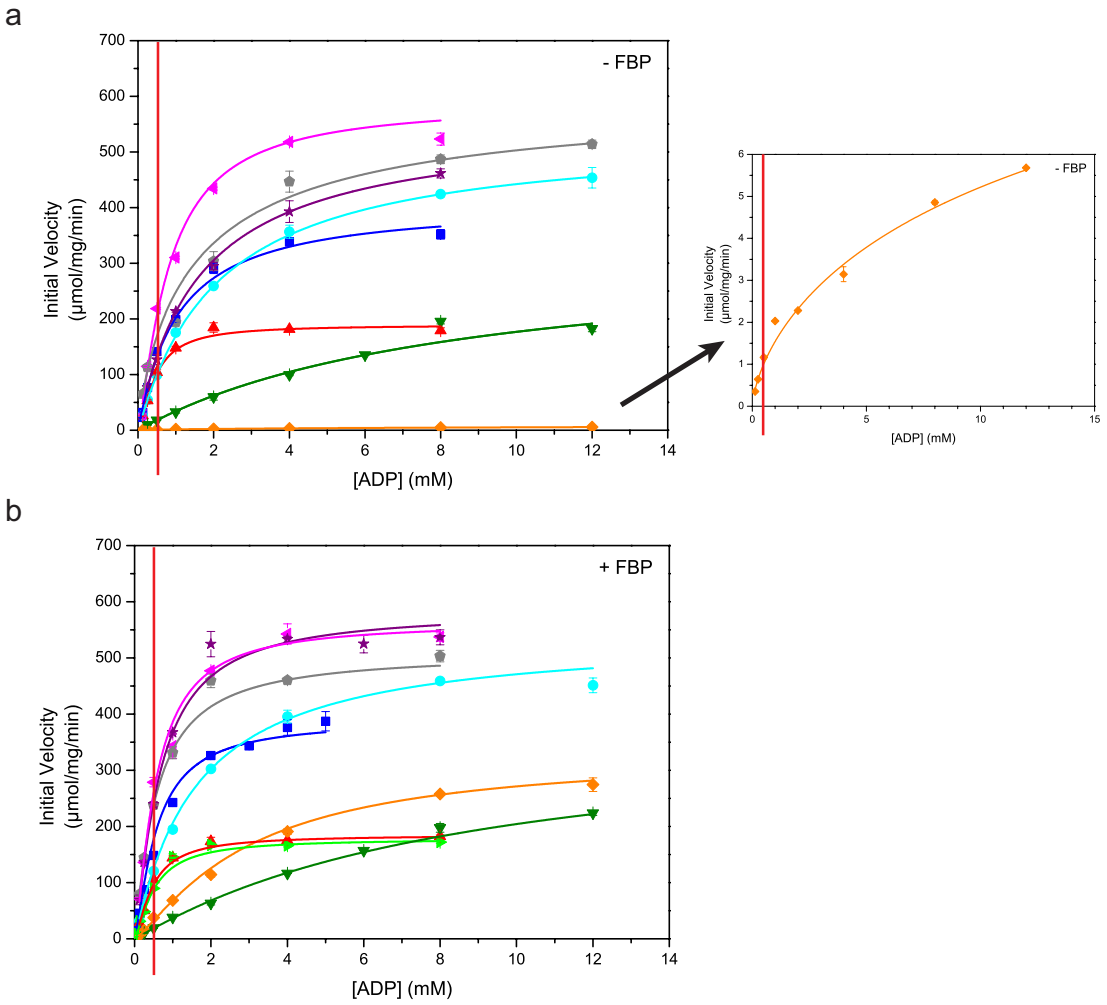

Figure 4.1 ADP titration curves for wild-type PK1 and eight evolved enzymes; P70Q, P70T, D127N, I264F, A301S, A301T, G381A and T462I. Enzyme activity was assayed at 37 °C and pH 7.5 as previously described in Section 2.3.1, with PEP present at saturating concentration for each respective enzyme. **(a)** The titration was performed in the absence of FBP. **(b)** The titration was performed in the presence of 2 mM FBP. Wild-type (■, blue), P70Q (●, cyan), P70T (▲, red), D127N (▼, olive), I264F (◆, orange), A301S (◄, magenta), A301T (►, green), G381A (⬟, grey), T462I (★, purple). Red line indicates the concentration of ADP (0.56 mM) in the cell. Error bars represent the standard error of the mean (SEM) for two technical replicates.

Table 4.1 Kinetic parameters of wild-type PK1 and eight evolved enzymes with ADP determined by fitting the Hill equation (Equation 2.1b).[10] Results are fitted values from two technical replicates ± errors derived from the kinetic fit.

ADP										
	- FBP					+ FBP (2 mM)				
Enzyme	k_{cat} s^{-1}	$S_{0.5}$ mM	n_H	$k_{cat}/S_{0.5}$ s^{-1}/ mM	*R*-square	k_{cat} s^{-1}	$S_{0.5}$ mM	n_H	$k_{cat}/S_{0.5}$ s^{-1}/ mM	*R*-square
Wild-type	345 ±30	1.0 ±0.2	1.05 ±0.07	338 ±70	0.990	329 ±10	0.57 ±0.06	1.31 ±0.06	577 ±60	1.000
P70Q	530 ±7	2.09 ±0.06	1.03 ±0.01	254 ±8	1.000	541 ±23	1.6 ±0.2	1.04 ±0.03	340 ±40	0.999
P70T	160 ±3	0.45 ±0.03	1.45 ±0.09	356 ±20	0.998	156 ±3	0.47 ±0.05	1.4 ±0.1	332 ±40	0.998
D127N	294 ±50	10 ±3	0.88 ±0.04	31 ±10	1.000	322 ±50	9 ±2	1.04 ±0.05	37 ±10	0.999
I264F	12 ±5	22 ±20	0.68 ±0.05	0.6 ±0.6	0.987	280 ±10	3.0 ±0.2	1.24 ±0.02	94 ±8	0.999
A301S	498 ±30	0.8 ±0.1	1.3 ±0.2	607 ±90	0.996	477 ±20	0.56 ±0.05	1.34 ±0.08	852 ±80	0.999
A301T	N/A	N/A	N/A	N/A	N/A	151 ±5	0.51 ±0.03	1.36 ±0.05	296 ±20	0.996
G381A	674 ±100	5 ±3	0.65 ±0.06	136 ±90	0.998	431 ±100	0.56 ±0.03	1.15 ±0.06	770 ±200	1.000
T462I	470 ±20	1.6 ±0.1	0.98 ±0.02	288 ±20	0.999	493 ±10	0.65 ±0.03	1.24 ±0.04	758 ±40	0.998

N/A, not able to be measured because the concentration of PEP required for activity was much too high and costly.

4.2.2 Evolved enzymes display an increased cooperative response to PEP

Next, the catalysis of the evolved enzymes relative to PEP concentration was assessed (Figure 4.2 and Table 4.2) in the absence and presence of FBP. PEP titrations in the absence of FBP allowed the homotropic activation response to PEP to be assessed, and the

presence of FBP allowed the heterotropic allosteric regulation response to FBP to be assessed.

4.2.2.1 Effect on k_{cat}

Within the physiologically relevant PEP concentrations (0.08–0.12 mM), all of the evolved enzymes (except P70Q and A301S) display a lower k_{cat} than the wild-type (Figure 4.2b inset). The P70Q and A301S enzymes maintain a lower k_{cat} until ~0.3 mM, above which they show a higher k_{cat} than wild-type. The intracellular concentration of PEP in *E. coli* was found to be within the range of 0.08–0.12 mM and studies by both Xu *et al*.,[5] and Bennett *et al*.,[6] demonstrated that *E. coli* have PEP concentrations of 0.16 and 0.18 mM, respectively. Therefore, at the physiological PEP concentration, all of the evolved enzymes have a lower activity than the wild-type enzyme. This result confirms my hypothesis that the evolved enzymes have a lower activity than the wild-type enzyme.

4.2.2.2 Effect on $S_{0.5}^{PEP}$

The kinetic results suggest that seven of the evolved enzymes display a preference for cooperative activation by their substrate PEP, demonstrated by the sigmoidal curves. Although these seven evolved enzymes have a reduced response to FBP, the FBP is still having an activating effect. Four of the evolved enzymes show more than a 25-fold decrease in the $S_{0.5}^{PEP}$ when FBP is present, confirming that FBP increases PEP binding affinity for catalysis. However, the presence of FBP only has a marginal effect upon the $S_{0.5}^{PEP}$ of I264F and T462I with the $S_{0.5}^{PEP}$ changing by only ~2-fold. Additionally, FBP alters the $S_{0.5}^{PEP}$ of A301T and G381A by 14- and 5-fold, respectively, indicating that FBP has a reduced influence upon increasing PEP binding affinity in these four enzymes.

4.2.2.3 Effect of FBP on PEP titrations

The PEP titrations reveal that all of the enzymes (except D127N) have evolved a different response to allosteric activation. Figure 4.2 clearly shows that four enzymes (I264F, A301T, G381A and T462I) have a sigmoidal cooperative activation curve in the presence of FBP. Although, the same sigmoidal curves cannot readily be identified in the other three altered enzymes (P70Q, P70T and A301S), Table 4.2 confirms they have positive cooperativity (n_H>1), confirming they too exhibit cooperative activation even in the presence of FBP.

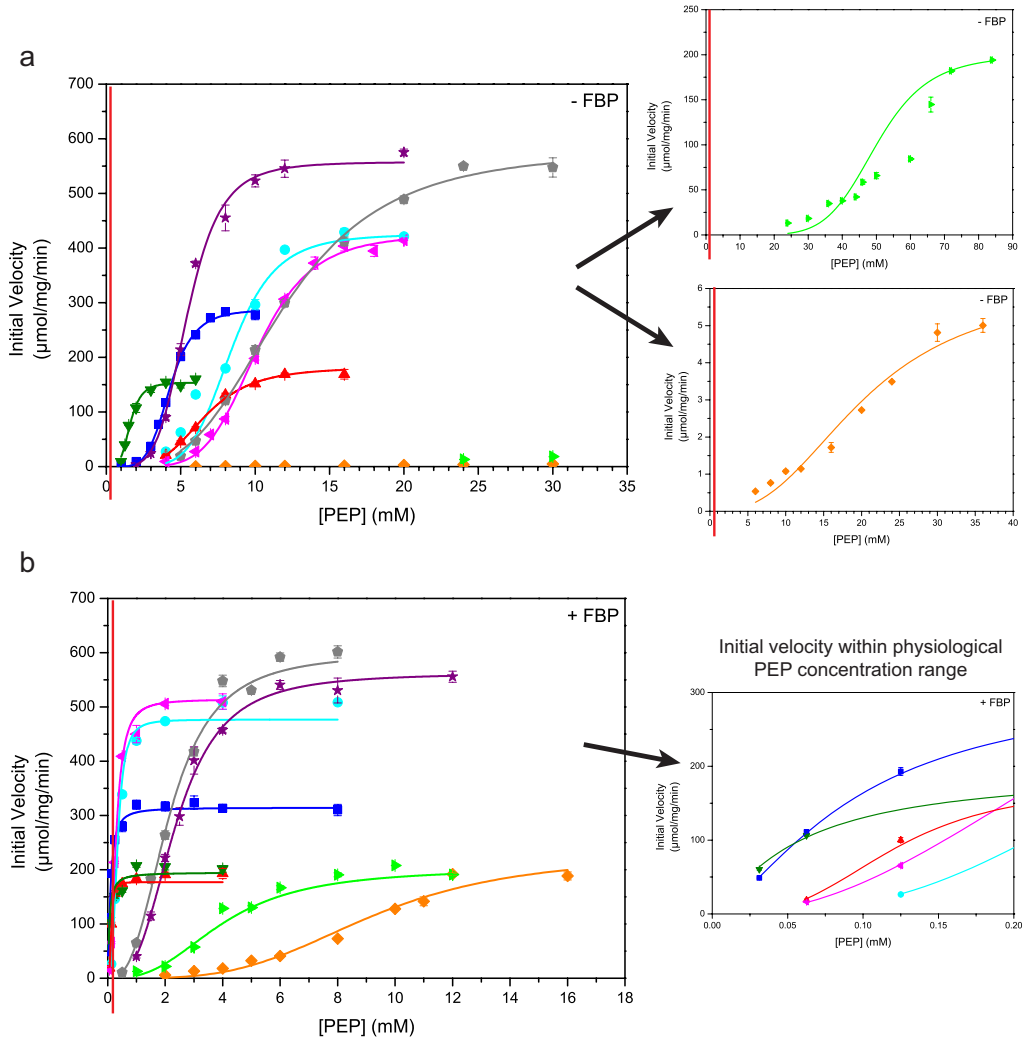

Figure 4.2 PEP titration curves for wild-type PK1 and eight evolved enzymes; P70Q, P70T, D127N, I264F, A301S, A301T, G381A and T462I. Enzyme activity was assayed at 37 °C and pH 7.5 as previously described Section 2.3.1, with ADP present at saturating concentration for each respective enzyme. **(a)** The titration was performed in the absence of FBP. **(b)** The titration was performed in the presence of 2 mM FBP. Inset displays the initial velocity of the enzymes within the physiologically relevant PEP concentrations (<0.2 mM). Wild-type (■, blue), P70Q (●, cyan), P70T (▲, red), D127N (▼, olive), I264F (◆, orange), A301S (◀, magenta), A301T (▶, green), G381A (⬟, grey), T462I (★, purple). Red line indicates the concentration of PEP (0.08–0.12 mM) in the cell. Error bars represent the SEM for two technical replicates.

The results of the PEP titrations (Figure 4.2 and Table 4.2) identify large differences in enzyme responses to PEP in the absence and presence of FBP. Homotropic activation by PEP seems to be preferred amongst the nine enzymes, with all except two (wild-type and D127N) showing cooperative activation in the presence of FBP. This result suggests that adaptation has altered the allosteric activation mechanism of seven of the eight evolved enzymes.

Table 4.2 Kinetic parameters of wild-type PK1 and eight evolved enzymes with PEP determined by fitting the Hill equation (Equation 2.1b).[10] Results are fitted values from two technical replicates ± errors derived from the kinetic fit.

PEP										
	- FBP					+ FBP (2 mM)				
Enzyme	k_{cat} s^{-1}	$S_{0.5}$ mM	n_H	$k_{cat}/S_{0.5}$ s^{-1}/ mM	*R*-square	k_{cat} s^{-1}	$S_{0.5}$ mM	n_H	$k_{cat}/S_{0.5}$ s^{-1}/ mM	*R*-square
Wild-type	243 ±3	4.27 ±0.05	5.2 ±0.3	57 ±1	0.998	266 ±3	0.090 ±0.002	1.51 ±0.03	2956 ±70	1.000
P70Q	360 ±6	8.4 ±0.2	6 ±1	43 ±1	0.992	477.0 ±0.9	0.33 ±0.01	2.9 ±0.2	1445 ±40	1.000
P70T	154 ±4	6.6 ±0.2	4.1 ±0.2	23.0 ±0.9	0.998	150 ±2	0.12 ±0.01	3.1 ±0.5	1250 ±100	0.995
D127N	130 ±4	1.59 ±0.06	4.3 ±0.6	82 ±4	0.996	165 ±10	0.06 ±0.01	1.2 ±0.3	2750 ±500	0.943
I264F	5.0 ±0.2	20[#] ±0	2.6 ±0.3	0.24 ±0.01	0.971	192 ±30	9 ±1	3.6 ±0.8	21 ±4	0.964
A301S	359 ±5	10.1 ±0.1	5.5 ±0.3	36.0 ±0.7	0.997	435 ±6	0.29 ±0.01	2.27 ±0.06	1500 ±60	0.999
A301T	169 ±4	50[#] ±0	6.5 ±0.9	3.00 ±0.08	0.987	162 ±2	3.51 ±0.06	2.7 ±0.2	46 ±1	0.994
G381A	490 ±10	11.9 ±0.3	3.4 ±0.3	41 ±1	0.997	507 ±10	2.2 ±0.1	2.74 ±0.08	236 ±10	0.998
T462I	47 ±10	5.5 ±0.1	4.9 ±0.5	86 ±3	0.993	475 ±8	2.36 ±0.05	2.9 ±0.1	201 ±5	0.999

[#] Parameters fixed to fit Hill function.

4.2.3 Enzymes display altered response to FBP titrations

The allosteric activation response to FBP was monitored (Figure 4.3 and Table 4.3) to assess each of the enzyme's affinity for FBP and the extent to which FBP influences PEP binding affinity.[11] The titrations were carried out using a fixed concentration of PEP and ADP that was less than or approximately equal to the $S_{0.5}^{PEP}$ in the PEP titrations without FBP: 10 mM PEP and ADP for I264F and A301T and 2 mM PEP and ADP for the remaining seven enzymes (wild-type, P70Q, P70T, D127N, A301S, G381A and T462I). The reason for the higher substrate concentrations in I264F and A301T is because these two enzymes were shown to require substantial concentrations of PEP for activation in the absence of FBP.

The FBP titration results confirm that all eight of the enzymes differ in their FBP binding and heterotropic activation responses compared to wild-type PK1.

4.2.3.1 Effect on activity

The percentage increase in activity as a response to FBP was determined by calculating the percentage increase from the rate at 0 mM FBP, to the derived V_{max} in the presence of FBP. The results determined that the D127N enzyme activity was least affected by FBP, with only a 2-fold increase in activity, suggesting that this enzyme has a relatively low FBP requirement for function. The response of D127N to FBP was two times lower than that of the wild-type enzyme, which has a 4-fold increase in activity in the presence of FBP. The G381A enzyme showed a dramatic response to FBP, with a 430-fold increase in activity upon the addition of ~2 mM FBP. The remaining evolved enzymes fall into the range between the wild-type (4-fold) and G381A (430-fold) confirming the importance of FBP for enzyme function.

Overall these evolved enzymes demonstrate the considerable effect that FBP has upon their activity. The wild-type PK1 is fully activated when the FBP concentration is 1 mM (100-fold greater than the $S_{0.5}^{FBP}$ of 0.01 mM), the evolved enzymes (except D127N) will be more sensitive to changes in FBP concentration since their $S_{0.5}^{FBP}$ (0.1−2.8 mM) is within the intracellular FBP concentration range (1.1−1.8 mM) in the stationary phase.

4.2.3.2 Effect on $S_{0.5}^{FBP}$

The results indicate that all of the evolved enzymes have a reduced FBP binding affinity compared to the wild-type. The wild-type has a very low $S_{0.5}^{FBP}$ of 0.010 ± 0.007 mM, and the D127N enzyme is similar with an $S_{0.5}^{FBP}$ of 0.017 ± 0.003 mM. The P70Q, P70T and A301S enzymes also display low $S_{0.5}^{FBP}$ values of ~0.1 mM, suggesting that they too have tight FBP binding affinity. However, the I264F, A301T, G381A and T462I enzymes show a considerable decrease in FBP binding affinity, with $S_{0.5}^{FBP}$ of >1 mM (except A301T, 0.57 ± 0.08 mM), this is demonstrated by the right-shifted curve compared to the wild-type.

4.2.3.3 Effect on n_H

The evolved enzymes all demonstrate a change in their n_H compared to the wild-type, with seven showing an increased n_H and one showing a decreased n_H. The wild-type enzyme displays the classic Michaelis-Menten curve for FBP binding (n_H =1.1 ± 0.9), indicating that FBP binding is not cooperative between the four FBP binding sites. However, all of the evolved enzymes show positive cooperativity with respect to FBP binding (1.5 ± 0.3 – 2.9 ± 0.3), except D127N, which shows a n_H of 0.7 ± 0.2, more similar to the wild-type enzyme.

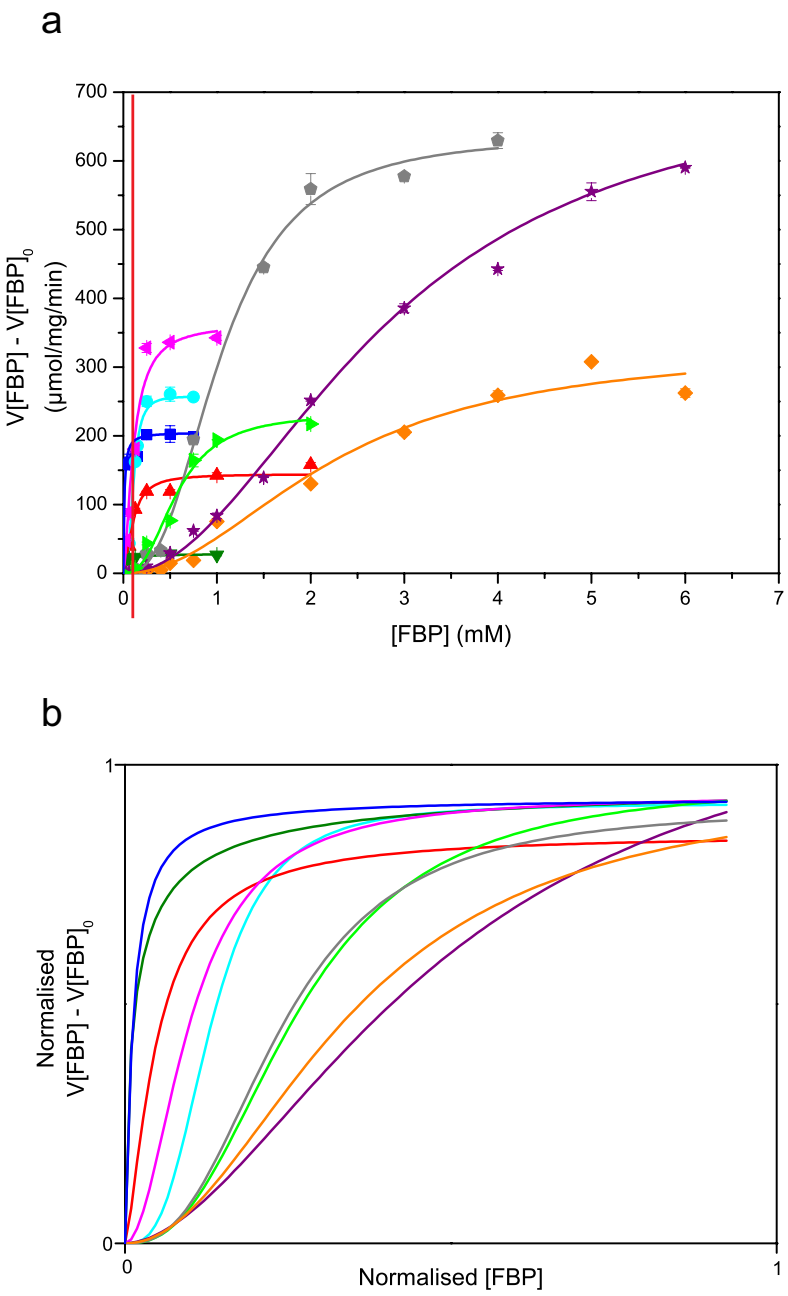

Figure 4.3 Enzyme activity relative to FBP for wild-type PK1 and eight evolved enzymes.
Enzyme activity was assayed at 37 °C and pH 7.5. PEP and ADP concentrations were present at 10 mM for I264F and A301T, and 2 mM for the remaining seven enzymes. **(a)** Displays the V-V_0 for FBP titrations of each of the nine enzymes, showing the effect of FBP upon the activity. Red line indicates the concentration of FBP (1.1–1.8 mM) in the cell **(b)** Displays the normalised V-V_0 for FBP titrations of each of the nine enzymes to highlight the relative shapes of the curves. The curves were normalised to the highest concentration (6 mM) and the highest velocity (629 µmol/mg/min). Wild-type (■, blue), P70Q (●, cyan), P70T (▲, red), D127N (▼, olive), I264F (◆, orange), A301S (◀, magenta), A301T (▶, green), G381A (⬟, grey), T462I (★, purple). Error bars represent the SEM for two technical replicates.

Table 4.3 Kinetic parameters with respect to FBP for wild-type PK1 and eight evolved enzymes determined by fitting the Hill equation (Equation 2.1b).[10] Results are the fitted values from two technical replicates ± errors derived from the kinetic fit.

Enzyme	V[FBP] - V[FBP]$_0$ μmol/mg/min	Response to FBP fold change	$S_{0.5}$ mM	n_H
Wild-type	205 ± 10	4	0.010 ± 0.007	1.1 ± 0.9
P70Q	258 ± 2	98	0.110 ± 0.003	2.9 ± 0.3
P70T	145 ± 10	14	0.10 ± 0.02	1.7 ± 0.4
D127N	29 ± 2	2	0.017 ± 0.003	0.7 ± 0.2
I264F	329 ± 30	274	2.3 ± 0.3	2.0 ± 0.4
A301S	363 ± 20	109	0.11 ± 0.02	1.6 ± 0.3
A301T	233 ± 20	238	0.57 ± 0.08	2.5 ± 0.7
G381A	637 ± 20	430	1.05 ± 0.05	2.6 ± 0.2
T462I	726 ± 30	282	2.8 ± 0.2	2.0 ± 0.1

A more detailed analysis of each evolved enzymes kinetic behaviour can be found below in Section 4.3.

4.3 Detailed functional properties of the evolved enzymes

The behaviour of the enzymes in the PEP and FBP titrations above (Section 4.2) provides a rationale for grouping the enzymes based upon their kinetic response to the activators, FBP and PEP (in the presence of FBP) (Figure 4.5). Comparison of each of the evolved enzymes to the wild-type allows them to be separated into four different groups:

1) Group one (red) contains P70T and D127N, these enzymes also have a $S_{0.5}^{PEP/FBP}$ of less than 0.5 mM, however their activity is lower than wild-type.
2) Group two enzymes (green), I264F and A301T, exhibit a lower level of activity than wild-type and have $S_{0.5}^{PEP/FBP}$ greater than 0.5 mM.
3) Group three (magenta) includes G381A and T462I, this group has a higher level of activity than wild-type, however the $S_{0.5}^{PEP/FBP}$ is greater than 0.5 mM.

4) Group four (cyan) contains P70Q and A301S, these two enzymes show a higher level of activity than wild-type and $S_{0.5}^{PEP/FBP}$ of less than 0.5 mM.

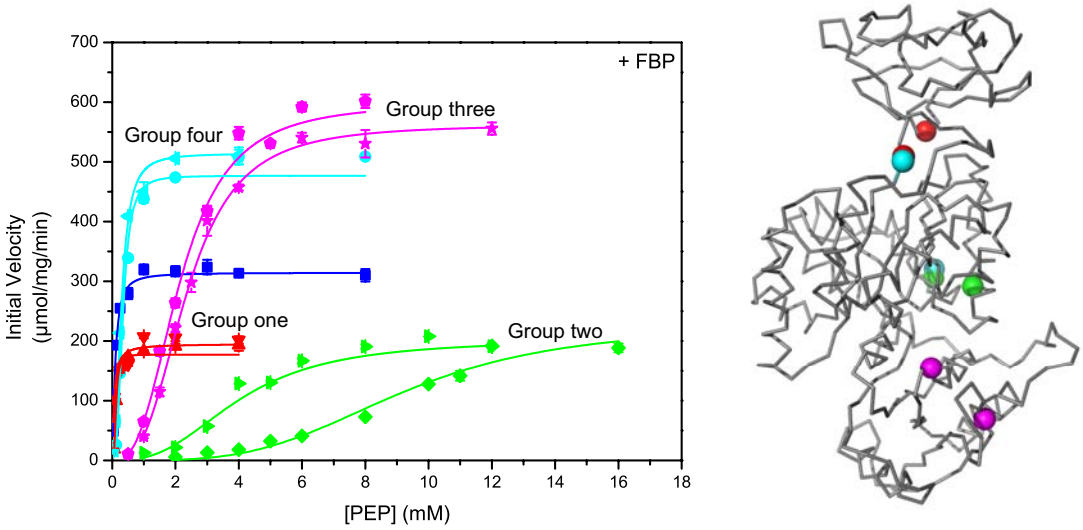

Figure 4.5 Evolved enzymes split into four groups based upon the kinetic response to PEP in the presence of FBP. **(a)** PEP titration curves for wild-type PK1 and eight evolved enzymes in the presence of FBP. The evolved enzymes are split into four groups based upon their kinetic behaviour. **(b)** Mutations are mapped onto the wild-type structure and coloured by grouping to compare behaviour to mutation site. Wild-type (■, blue), group one: P70Q (●, cyan) and A301S (◀, cyan); group two: P70T (▲, red) and D127N (▼, red); group three: G381A (⬟, magenta) and T462I (★, magenta); group four: I264F (◆, green) and A301T (▶, green).

4.3.1 Group one – P70T and D127N (red)

Mutation of active site residues P70 and D127 has significant effects upon the activity and functional properties of the enzymes. Residues P70 and D127 are both located within the active site region of *E. coli* PK1. Residue P70 forms the kink that acts as the hinge on the extended loop between the A- and B-domains. Mutation of P70 could interfere with the opening and closing of the lid domain, altering the catalytic efficiency of the enzyme. Residue D127 is located on the underside of the B-domain (lid domain), and is presumed to be important for 'locking' the lid in an open conformation upon activation with FBP.[7] Mattevi (1995) suggested that when FBP binds to *E. coli* PK1, D127 forms a salt bridge with residues of the Aα6'-helix from the opposing subunit, holding the lid domain in an open conformation to promote substrate binding within the active site. Mutation of residue

D127 may alter the 'lid-locking' ability, which would modify the substrate binding ability and catalytic efficiency of the enzyme. Both P70T and D127N evolved enzymes are predicted to have altered catalytic constants to that of the wild-type enzyme.

4.3.1.1 P70T and D127N effect on activation

Analysis of the activities of the P70T and D127N evolved enzymes demonstrates that they both have a lower activity than the wild-type (Figure 4.6). The wild-type shows a k_{cat} of ~300 s^{-1} and the two evolved enzymes show k_{cat}'s of ~200 s^{-1}, confirming the hypothesis that mutations in the active site region reduce enzyme catalysis.

4.3.1.2 P70T and D127N response to ADP titration

Next, the activation responses of P70T and D127N were measured relative to ADP concentrations and compared to the wild-type enzyme (Figure 4.6a, b and c), establishing that the addition of FBP does not significantly alter the response of either of the evolved enzymes to ADP. The wild-type enzyme has a 2-fold decrease in $S_{0.5}^{ADP}$ when FBP is present, and the P70T and D127N enzymes show 0-fold and 1-fold decreases, respectively.

4.3.1.3 P70T and D127N response to PEP titration

Although P70T and D127N enzymes both have mutations at the active site, D127N displays a similar response to PEP activation as the wild-type, whereas P70T has an altered activation response. These will be compared to the wild-type and described separately, below (Figure 4.6d, e and f),

Analysis of the P70T enzyme determined that FBP binding results in a 47-fold decrease in $S_{0.5}^{PEP}$ for wild-type and a similar 55-fold decrease in $S_{0.5}^{PEP}$ for P70T suggesting that FBP has a similar affect upon PEP binding in P70T compared to the wild-type enzyme. The difference in PEP binding affinity without FBP is exemplified in Figure 4.6d and e, where the titration curve for P70T is shifted to the right suggesting higher concentrations of PEP are required to activate the enzyme in the absence of FBP. P70T demonstrates cooperative activation behaviour even in the presence of FBP, with n_H values of 4.1 ± 0.2 in the absence and 3.1 ± 0.5 in the presence of FBP, compared to 5.2 ± 0.3 in the absence and 1.51 ± 0.03 in the presence of FBP for the wild-type enzyme. P70T shows a significantly smaller decrease in n_H compared to wild-type confirming that cooperative activation by PEP is still occurring.

Next, the D127N enzyme was examined and the results determined that it is the only evolved enzyme that does not display positive cooperativity with respect to PEP in the presence of FBP. Instead, it behaves similar to the wild-type by showing a change in n_H from cooperative in the absence of FBP (4.3 ± 0.6), to non-cooperative in the presence of FBP (1.2 ± 0.3). Analysis of the $S_{0.5}^{PEP}$ for D127N showed a 27-fold decrease in $S_{0.5}^{PEP}$ upon FBP binding, compared to the 47-fold decrease identified in the wild-type enzyme.

4.3.1.4 P70T and D127N response to FBP titration

The D127N enzyme displays a similar response to FBP as the wild-type, however, P70T demonstrates an altered response (Figure 4.6g, h and i).

The response of P70T relative to FBP was determined and showed that P70T has higher cooperative binding of FBP (n_H = 1.7 ± 0.4) compared to the wild-type enzyme (n_H = 1.1 ± 0.9). Moreover, P70T shows a 10-fold increase in $S_{0.5}^{FBP}$ (0.10 ± 0.02 mM) compared to the wild-type (0.010 ± 0.007 mM), suggesting decreased FBP binding affinity of the evolved enzyme. Analysis of the effect of FBP upon the activation of the P70T enzyme, determined that the presence of FBP causes a 14-fold increase in the activity, this is a significantly larger response to FBP than the 4-fold increase found in the wild-type enzyme.

Next, the response of D127N relative to FBP was measured and compared to the wild-type enzyme, demonstrating that they both have a similar behaviour with respect to FBP. The results show a similar $S_{0.5}^{PEP}$ for wild-type (0.010 ± 0.007 mM) and D127N (0.017 ± 0.003 mM) as well as similar n_H's of 1.1 ± 0.9 for the wild-type and 0.7 ± 0.2 for D127N. One notable difference is the effect that FBP has upon the activity of the D127N enzyme. The results show that D127N is the only evolved enzyme to have a smaller change in activity upon FBP binding (2-fold increase) than the wild-type (4-fold increase), suggesting that FBP has very little affect upon the activity of D127N.

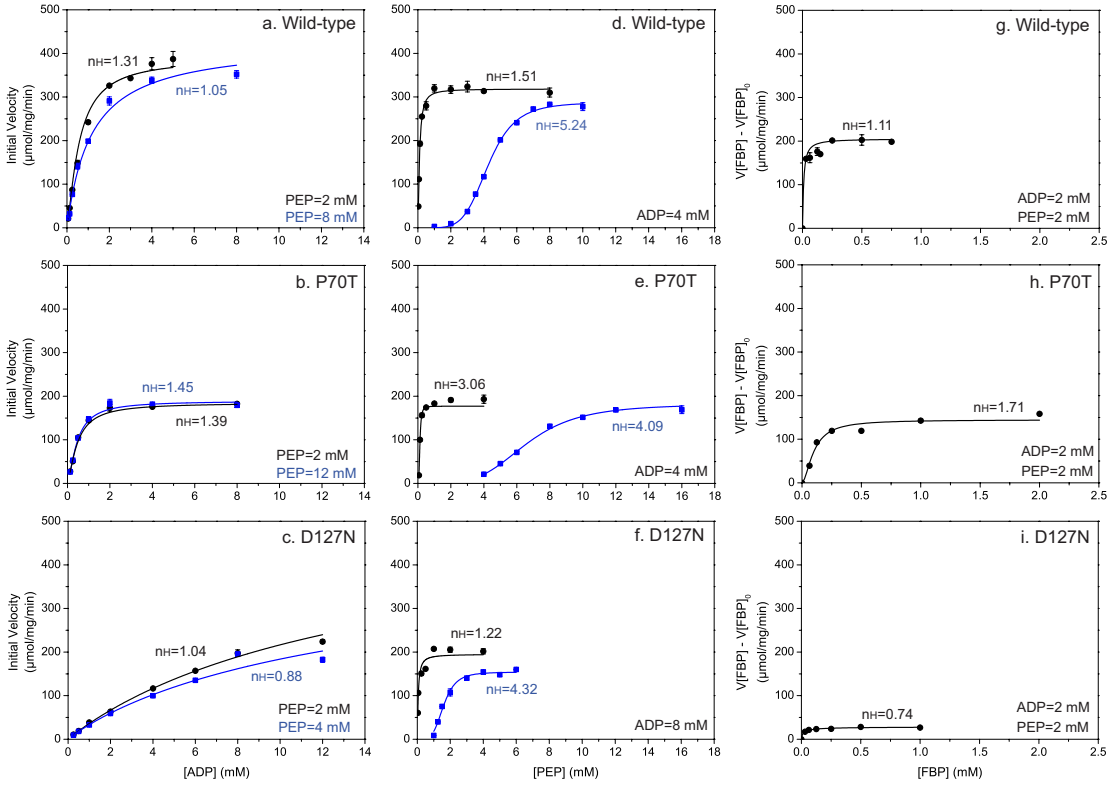

Figure 4.6 Kinetic properties of wild-type PK1, P70T and D127N enzymes demonstrating an altered allosteric activation response compared to the wild-type. ADP, PEP and FBP titrations for wild-type, P70T and D127N in the absence (■) and presence (●) of 2 mM FBP. Fixed substrate concentration for each titration is presented on each graph – two PEP concentrations are noted, one for the absence (blue) and one for the presence (black) of FBP. n_H values in the presence (black) and absence (blue) of FBP are depicted on each graph. Error bars represent the SEM for two technical replicates.

4.3.1.5 Summary of P70T and D127N results

Here, the results demonstrate that although the P70T and D127N mutations are located in a similar region of the enzyme, they actually display very different responses to the substrates and activator. The kinetic results from these mutations confirm that mutations in the active site alter the catalysis of the *E. coli* PK1 enzyme, in this case, lowering the activity. Since both of the mutations would have an effect upon opening and closing of the lid domain, the reduced activity suggests that the lid is involved in *E. coli* PK1 catalysis.

4.3.2 Group two – I264F and A301T (green)

Kinetic analysis of two interface mutations, I264F and A301T identifies significant decreases in both the FBP allosteric activation response and the PEP cooperative activation response. Residues I264 and A301 are located at the enzymes A/A' interface. Mutation of residues within the A/A' interface region have been shown to alter catalysis and allosteric regulation of pyruvate kinase enzymes.[11, 12] The kinetic properties of the I264F and A301T evolved enzymes are displayed below (Figure 4.7) for comparison with wild-type PK1.

4.3.2.1 I264F and A301T effect on activation

Analysis of the activities of the I264F and A301T evolved enzymes demonstrates that they both have a lower activity than the wild-type (Figure 4.7). The wild-type shows a k_{cat} of ~300 s^{-1} and the two evolved enzymes show k_{cat} values of ~200 s^{-1}, demonstrating the negative effect of interface mutations upon *E. coli* PK1 enzyme activity.

4.3.2.2 I264F and A301T responses to ADP titration

The responses of I264F and A301T were measured relative to ADP concentration and compared to the wild-type enzyme (Figure 4.7a, c and c). Unfortunately, ADP titrations of A301T in the absence of FBP were unable to be carried out because the concentration of PEP required to cooperatively activate the enzyme was much too costly (~60−80 mM per assay). However, analysis of the I264F ADP response shows a 7-fold decrease in $S_{0.5}^{ADP}$ when FBP is present, compared to the 2-fold change measured in the wild-type. This result determines that the I264F A/A' interface mutation shows a greater increase in ADP binding response to FBP than the wild-type enzyme.

4.3.2.3 I264F and A301T responses to PEP titration

Kinetic analyses were employed to measure the responses of I264F and A301T to PEP concentrations and these were then compared to the wild-type enzyme (Figure 4.7d, e and f). The results show that I264F and A301T display 2- and 14-fold decreases in $S_{0.5}^{PEP}$ (respectively) upon FBP binding compared to the wild-type's 47-fold decrease. The reduced PEP binding response of the evolved enzymes to FBP suggests that the A/A' interface mutations have altered the enzymes' response to allosteric activation. Furthermore, the PEP titrations with and without FBP determined that in physiologically relevant conditions (PEP concentrations <0.2 mM),[5, 6] I264F and A301T activity is dependent upon the presence of FBP. In addition, both evolved enzymes exhibited an

increase in cooperativity with respect to PEP, when FBP was bound. This is shown by n_H values of 3.6 ± 0.8 for I264F and 2.7 ± 0.2 for A301T, whereas the wild-type had a n_H of 1.51 ± 0.03.

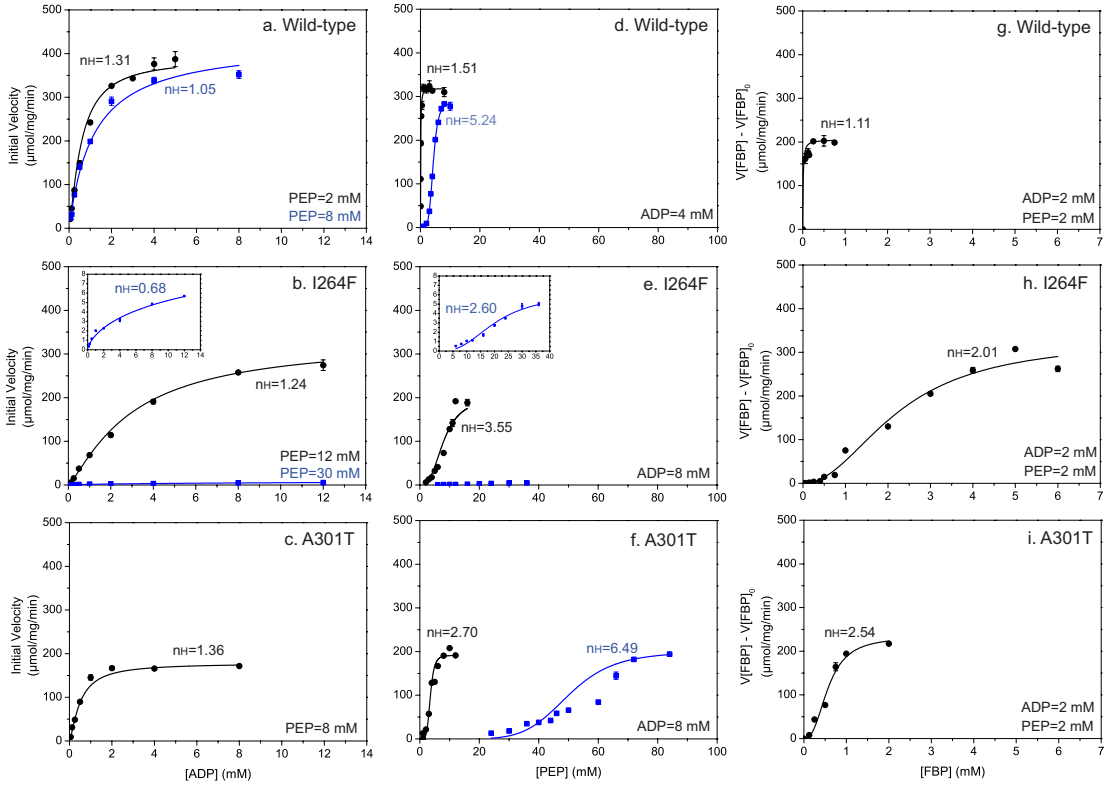

Figure 4.7 Kinetic properties of wild-type PK1, I264F and A301T enzymes demonstrating an altered allosteric activation response compared to the wild-type. ADP, PEP and FBP titrations for wild-type, I264F and A301T in the absence (■) and presence (●) of 2 mM FBP. Fixed substrate concentration for each titration is presented on each graph – two PEP concentrations are noted, one for the absence (blue) and one for the presence (black) of FBP. n_H values in the presence (black) and absence (blue) of FBP are depicted on each graph. Error bars represent the SEM for two technical replicates.

4.3.2.4 I264F and A301T response to FBP titration

Finally, the I264F and A301T enzymes were kinetically analysed to determine their response to FBP concentration. The FBP titrations determined that $S_{0.5}^{FBP}$ was decreased in the evolved enzymes, compared to the wild-type (Figure 4.7g, h and i). I264F was found to have a $S_{0.5}^{FBP}$ of 2.3 ± 0.3 mM and A301T was 0.57 ± 0.08 mM, compared to the wild-type's $S_{0.5}^{FBP}$ of 0.010 ± 0.007 mM. Although both evolved enzymes have a decreased FBP binding affinity compared to wild-type, the I264F enzyme decreases to a greater extent (228-fold versus 57-fold in A301T). Interestingly, I264F displays a similar

FBP binding affinity to the evolved enzymes with mutations directly involved in binding the FBP molecule, implying that the A/A' interface mutation is altering allosteric site binding. In addition, both I264F and A301T show ~2-fold increase in n_H for FBP compared to the wild-type, implying that these A/A' interface mutations are causing cooperative binding of FBP within the enzymes.

4.3.2.5 Summary of I264F and A301T results

Here, the I264F and A301T evolved enzymes confirm the importance of subunit interfaces within PK enzymes. These two single substitution mutations instigated a significant change to the allosteric regulation of *E. coli* PK1 by altering heterotropic activation by FBP.

4.3.3 Group three – G381A and T462I (magenta)

Mutation of the two allosteric activator binding residues causes changes not only to FBP binding at the allosteric site, but also to substrate binding at the active site over 40 Å away. These specific mutations produced a dramatic change to the allosteric regulation response and catalytic efficiency of the enzymes. From the structure of A301S in the presence of FBP (Section 3.3.2), residues G381 and T462 both proved to be directly involved in binding the allosteric activator. Mutation of these residues is predicted to alter FBP binding and the allosteric response of each enzyme. The ADP, PEP and FBP kinetic properties for G381A and T462I are displayed below for comparison against the wild-type PK1 enzyme (Figure 4.8).

4.3.3.1 G381A and T462I effect on activation

The activation of the two *E. coli* PK1 enzymes with mutations at the FBP binding site show higher activity than the wild-type enzyme (Figure 4.8). The wild-type enzyme has a k_{cat} of ~300 s^{-1}, whereas the G381A and T462I enzymes have k_{cat} values of ~600 s^{-1}, demonstrating that allosteric site mutations can increase enzyme activity.

4.3.3.2 G381A and T462I responses to ADP titration

The responses of G381A and T462I enzymes were measured relative to ADP concentration and compared to the wild-type enzyme (Figure 4.8a, b and c). T462I exhibits a similar ADP response as the wild-type enzyme, with $S_{0.5}^{ADP}$ decreasing 2-fold in the wild-type and 3-fold in T462I upon FBP binding. Alternatively, G381A demonstrates a $S_{0.5}^{ADP}$ change of

5 ± 3 mM to 0.56 ± 0.03 mM (9-fold decrease) upon FBP binding, implying that FBP binding in the allosteric site of this evolved enzyme alters ADP binding in the active site, 40 Å away, in contrast to the wild-type enzyme.

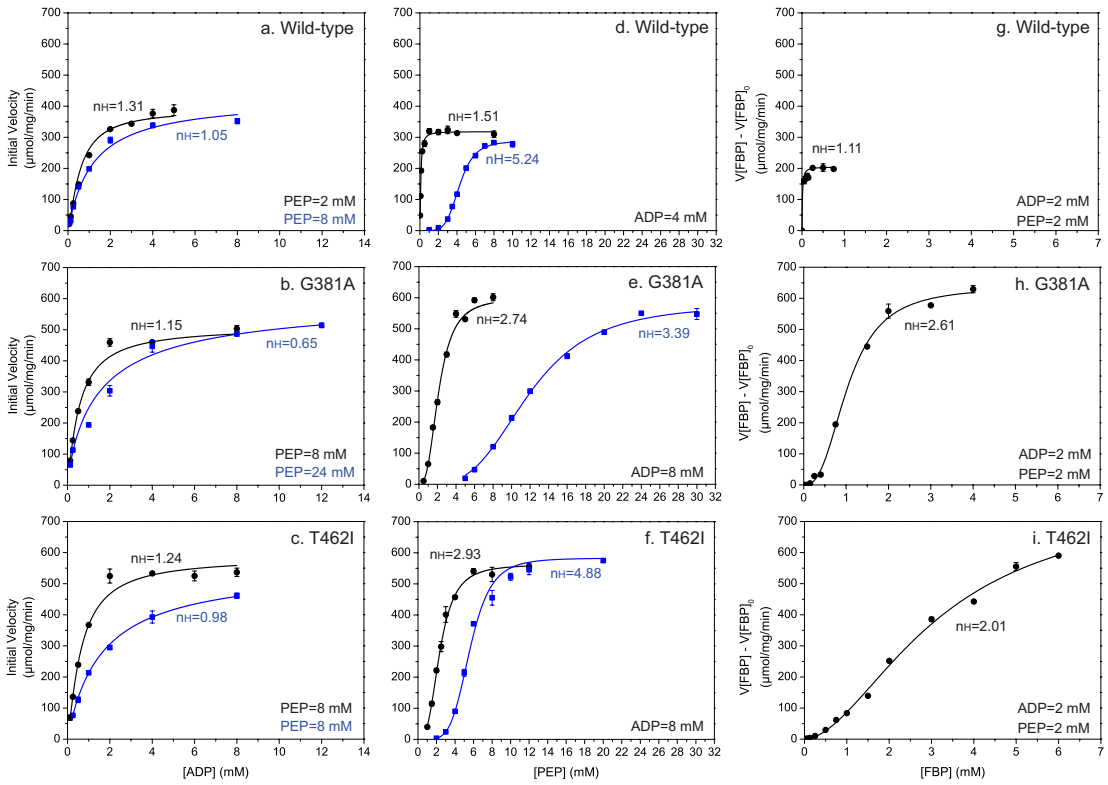

Figure 4.8 Kinetic properties of wild-type PK1, G381A and T462I enzymes demonstrating an altered allosteric activation response compared to the wild-type. ADP, PEP and FBP titrations for wild-type, G381A and T462I in the absence (■) and presence (●) of 2 mM FBP. Fixed substrate concentration for each titration is presented on each graph – two PEP concentrations are noted, one for the absence (blue) and one for the presence (black) of FBP. n_H values in the presence (black) and absence (blue) of FBP are depicted on each graph. Error bars represent the SEM for two technical replicates.

4.3.3.3 G381A and T462I responses to PEP titration

The allosteric activation responses of G381A and T462I were measured relative to PEP concentration and compared to the wild-type enzyme (Figure 4.8d, e and f). The results demonstrate that both G381A and T462I enzymes have a largely reduced change in $S_{0.5}^{PEP}$ between the FBP unbound and bound states compared to the wild-type. The wild-type enzyme shows a 47-fold decrease in $S_{0.5}^{PEP}$ when FBP is bound. However, G381A shows a 5-fold and T462I a 2-fold decrease in $S_{0.5}^{PEP}$ when FBP is bound. These results suggest that the mutations at the FBP binding site have reduced the enzymes' allosteric response to

FBP − this is likely due to reduced FBP binding at the allosteric site because of the mutation of residues (381 and 462) involved in binding FBP. Interestingly, the two evolved enzymes display sigmoidal response curves with respect to PEP, even in the presence of FBP, suggesting a preference for cooperative activation over allosteric activation. This cooperative result is demonstrated by n_H values above 1 in the presence of FBP (G381A, 2.74 ± 0.08 and T462I 2.9 ± 0.1), compared to wild-type, which has a rectangular hyperbola curve and a n_H of 1.51 ± 0.03 (Figure 4.8d, e and f).

4.3.3.4 G381A and T462I responses to FBP titration

Finally, the responses of G381A and T462I were measured relative to FBP concentration and compared to the wild-type enzyme (Figure 4.8g, h and i). The dramatic increase in $S_{0.5}^{FBP}$ of G381A (105-fold) and T462I (281-fold), confirms that FBP binding affinity is reduced compared to the wild-type enzyme. In addition, the sigmoidal response curves in Figure 4.8h and i confirm that the two evolved enzymes have a higher level of cooperative binding of FBP than that of the wild-type enzyme, suggesting that the binding of one FBP molecule increases binding of subsequent FBP molecules in other monomers of the tetramer.

4.3.3.5 Summary of G381A and T462I results

Kinetic analysis of the two enzymes with mutations at the allosteric site, G381A and T462I, reveals similar changes in both enzymes including a considerable change to the allosteric response to FBP. The altered FBP binding result confirms the importance of these two residues for binding FBP in the allosteric domain. In addition, the increased activity of these two evolved enzymes suggests structural differences not only at the allosteric site, but also at the active site, over 40 Å away.

4.3.4 Group four – P70Q and A301S (cyan)

P70Q and A301S may have evolved residue substitutions in different regions of the *E. coli* PK1 protein, but both mutations produce similar catalytic responses. Importantly, the evolved enzymes display altered activity and regulation compared to the wild-type enzyme. The residues P70 and A301 are not located in the same region of the protein. Residue P70 is located on one of two extended loops that connect the lid domain (B-domain) to the $(\beta/\alpha)_8$-barrel domain (A-domain). The proline introduces a kink into the loop, acting as a hinge for the opening and closing of the lid. Mutation of this residue is

predicted to have an affect upon the activity of the enzyme. Alternatively, residue A301 is located on the Aα7'-helix in the A/A' interface between adjacent subunits and mutation of this residue is predicted to alter the allosteric regulation of the enzyme. The kinetic properties for P70Q and A301S with respect to ligands, PEP, ADP and FBP are displayed below (Figure 4.9).

4.3.4.1 P70Q and A301S effect on activation

Comparison of the k_{cat} values for the two evolved enzymes determined that the evolved enzymes have increased activity compared to the wild-type (Figure 4.9). The k_{cat} for the wild-type enzyme is ~300 s^{-1}, whereas the P70Q and A301S enzymes have k_{cat}'s of ~450 s^{-1}. This increase in activity suggests that the evolved enzymes are more efficient catalysts than wild-type, the change could be attributed to a change in structure or dynamics of the enzyme.

4.3.4.2 P70Q and A301S response to ADP

The activation responses of P70Q and A301S were measured relative to ADP concentrations and compared to the wild-type enzyme (Figure 4.9a, b and c), establishing that the addition of FBP does not significantly alter the response of either of the evolved enzymes to ADP. The results show that the wild-type enzyme has a 1.8-fold increase in $S_{0.5}^{ADP}$ upon FBP addition, whereas P70Q has a 1.3-fold and A301S has a 1.4-fold increase in $S_{0.5}^{ADP}$ in the presence of FBP.

4.3.4.3 P70Q and A301S response to PEP

The allosteric activation response to PEP was measured for evolved enzymes, P70Q and A301S and compared to the wild-type PK1 enzyme (Figure 4.9a, b and c). The results demonstrate that both evolved enzymes show a larger curve shift to the right upon FBP presence, suggesting they have reduced PEP binding affinity, since more PEP is required for the enzymes to reach maximum velocity. The wild-type enzyme displays a 47-fold decrease in $S_{0.5}^{PEP}$ upon FBP binding, whereas P70Q shows a 26-fold and A301S a 35-fold decrease in $S_{0.5}^{PEP}$ upon FBP binding. Additionally, the evolved enzymes show an increase in PEP cooperative activation compared to wild-type. The wild-type has a n_H of 1.51 ± 0.03 in the presence of FBP, however P70Q and A301S have n_H's of 2.9 ± 0.2 and 2.27 ± 0.06, respectively.

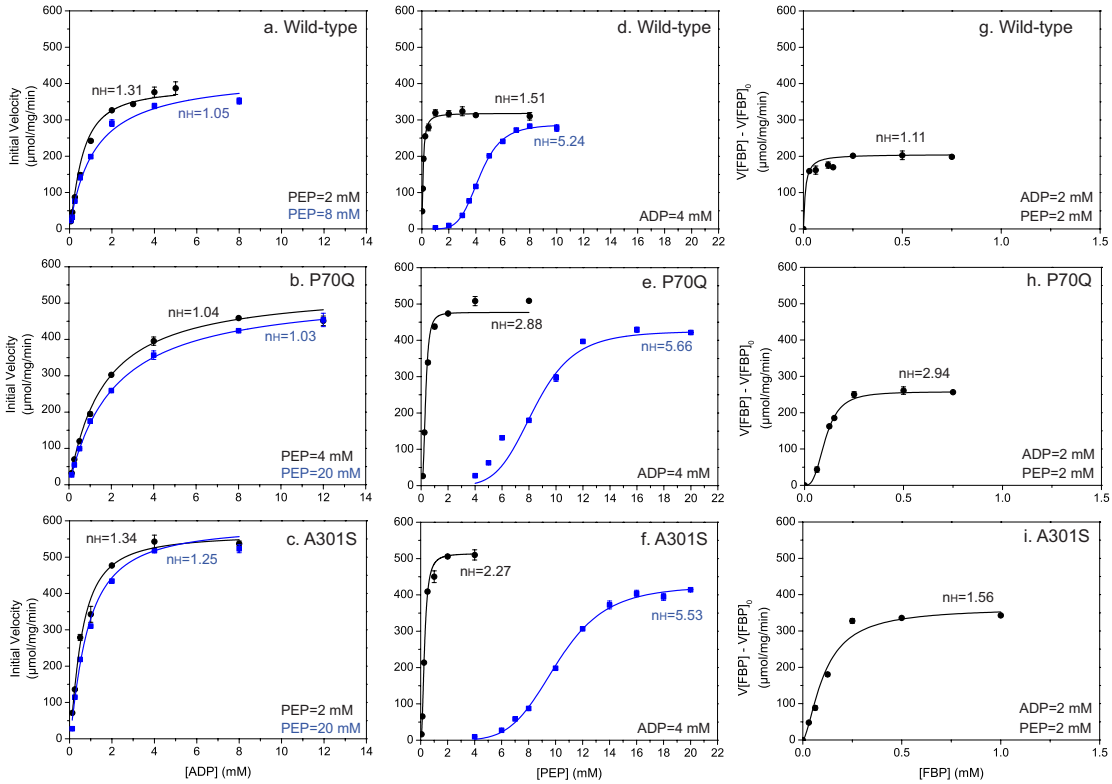

Figure 4.9 Kinetic properties of wild-type PK1, P70Q and A301S enzymes demonstrating an altered allosteric activation response compared to the wild-type. ADP, PEP and FBP titrations for wild-type, P70Q and A301S in the absence (■) and presence (●) of 2 mM FBP. Fixed substrate concentration for each titration is presented on each graph – two PEP concentrations are noted, one for the absence (blue) and one for the presence (black) of FBP. n_H values in the presence (black) and absence (blue) of FBP are depicted on each graph. Error bars represent the SEM for two technical replicates.

4.3.4.4 P70Q and A301S response to FBP

Finally, the response of evolved enzymes, P70Q and A301S were measured relative to FBP concentrations and compared to the response of the wild-type enzyme (Figure 4.9g, h and i). The results determine that both P70Q and A301S have increased $S_{0.5}^{FBP}$ values compared to the wild-type. The wild-type enzyme requires 0.010 ± 0.007 mM of FBP to reach half of the maximal velocity, whereas, P70Q requires 0.110 ± 0.003 mM and A301S needs 0.11 ± 0.02 mM to reach half of their maximal velocity, suggesting the enzymes may have evolved a lower FBP binding affinity.

4.3.4.5 Summary of P70Q and A301S results

Here, we observe a mutation at the active site and a mutation at the A/A' subunit interface showing increased catalytic efficiency and altered activation responses to both the

allosteric activator, FBP and the substrate PEP when compared to the kinetic behaviour of the wild-type enzyme.

4.4 Thermal stability of the evolved enzymes is largely unchanged

Sections 4.2 and 4.3 identified major differences in allosteric activation of the eight evolved enzymes compared to the wild-type. This suggests that the evolved enzymes have diverged from the typical *E. coli* PK1 kinetic behaviour. Often, function and stability are described as competing properties, with mutations that improve or alter function, decreasing stability and vice versa.[13] Thermal shift assays were performed for wild-type PK1 and the eight evolved enzymes to investigate whether the functional changes correlate to a change in stability, and whether changes in stability could indicate dynamic changes. Thermal shift assays provide insight into the dynamic nature of proteins because stability often reflects flexibility (Section 2.4.2). A protein with a higher unfolding temperature is considered to be more stable and rigid due to the large amount of thermal energy required to break the internal bonds for unfolding. A protein that unfolds at a lower temperature generally has less strength in its internal bonding and is often a less stable or more flexible protein.

4.3.1 Thermal shift assays

The thermal shift assay results determined that four of the eight enzymes evolved slight changes to their thermal stability. Two common laboratory buffers were used for the thermal shift assays, Tris and Bis-Tris Propane (BTP) (Figure 4.10). The use of two buffers provided a control to ensure the buffer composition was not influencing enzyme stability. The assays in both buffer conditions showed a similar trend in unfolding temperature. A301T revealed ~3 °C increase in T_m, and T462I, I264F and G381A displayed T_m decreases of ~4 °C, 5 °C and 7 °C, respectively. The remaining four evolved enzymes; P70T, P70Q, D127N and A301S presented with similar stability data to wild-type PK1. This is an important result as it demonstrates that the enzymes are likely to be

stable in the assay (37 °C) and that the change in activity is not a function of protein stability in the assay.

Overall, the changes to thermal stability are not consistent with the activity-stability theory, which states that mutations causing new or altered functions will be thermodynamically destabilising.[13, 14]

Table 4.4 Unfolding temperatures of wild-type and the eight evolved enzymes in both Tris and Bis-Tris-Propane buffers. The unfolding temperatures are the mean of three technical replicates.

	Wild-type	P70Q	P70T	D127N	I264F	A301S	A301T	G381A	T462I
Tris buffer (°C)	62	62	62	61	57	62	65	55	57
BTP buffer (°C)	61	60	60	59	45/53*	61	64	52	55

* I264F has a biphasic unfolding pattern

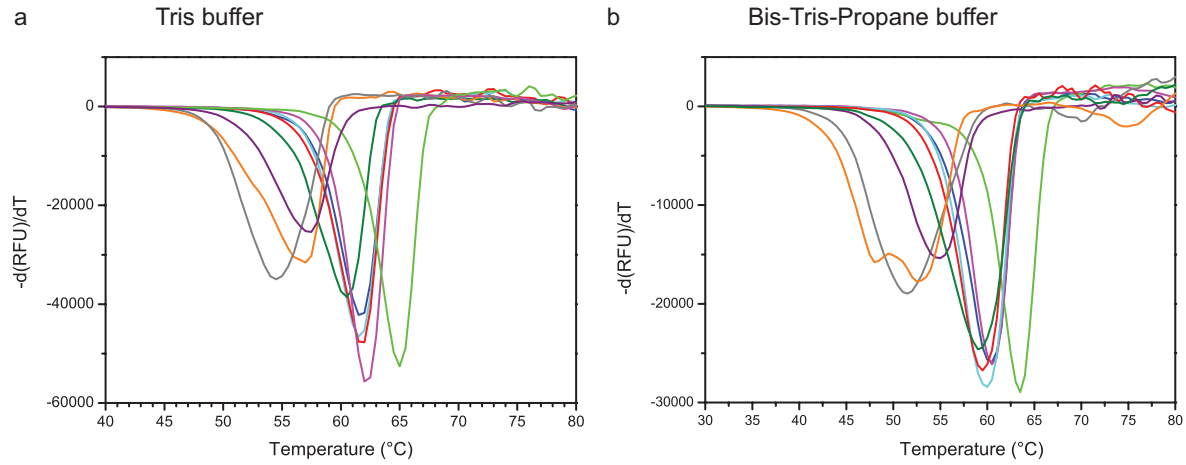

Figure 4.10 Thermal shift assays of wild-type PK1 and eight evolved enzymes displaying different unfolding temperatures in four evolved enzymes. The unfolding measurements were made with the enzymes (0.5 mg/mL) in two buffers: **(a)** Tris storage buffer (10 mM Tris, pH 7.5, 2 mM β-mercaptoethanol and 1 mM EDTA) and **(b)** BTP buffer (10 mM BTP, pH 7.5, 2 mM β-mercaptoethanol and 1 mM EDTA). Wild-type (blue), P70Q (cyan), P70T (red), D127N (olive), I264F (orange), A301S (magenta), A301T (green), G381A (grey) and T462I (purple). The curves depict the mean of three technical replicates.

Although the enzyme stability data is similar in both buffer conditions, one major change was recorded: in Tris buffer, I264F shows a smooth single unfolding peak at ~56 °C. However, in BTP buffer, the enzyme shows biphasic unfolding, with a secondary peak (45 °C) appearing before the original prominent peak (53 °C). The appearance of the secondary peak suggests that BTP may be binding to the enzyme and causing a 'pre-mature' unfolding event. This uncertainty is resolved in Chapter Five when the structure of I264F is assessed.

4.6 Discussion

Eight independently evolved mutations in the *E. coli* PK1 enzyme increase the fitness of the bacterial populations in the low glucose environment. Here, each of the evolved PK1 enzymes is functionally characterised to answer the following questions: 1) Are the results of adaptive evolution parallel on the functional level, as they are on the genetic and physiological level? 2) Have the mutations altered the functional responses of the enzymes? What feature of the enzyme is being selected for? 3) What have we learnt about the function of the *E. coli* PK1 enzyme?

To answer the first question, the kinetic results demonstrate that the results of adaptive evolution are parallel on a functional level, as well as on a genetic and physiological level. Analysis of the kinetic behaviours of all eight evolved enzymes shows that they all have a lower activity than the wild-type at physiological concentrations of PEP (<0.2 mM).[5, 6] This result supports the hypothesis by Woods *et al*.,[4] who proposed that the adaptive mutations cause a fitness benefit by slowing the conversion of PEP to pyruvate, making more PEP available to drive import of the limiting resource glucose in the cells.[4] Following this hypothesis, a study by Xu *et al*. demonstrated that if *E. coli* cells accumulated sufficient intra-cellular PEP upon glucose removal by lowered PEP carboxylase activity, they had an advantage for initiating glycolysis when the glucose was restored.[5] The higher PEP concentration is associated with a faster rate of glucose import and shorter lag times before the continuation of exponential growth.[5] Therefore, the reduced activity in the evolved enzymes compared to the wild-type is consistent with reduced catalysis of PEP substrate. This would allow PEP accumulation for driving rapid

glucose uptake into cells once glucose-containing media was reintroduced into the environment.

Analysis of the functional behaviours of each enzyme determined that the evolved enzymes have altered functional responses compared to the wild-type. Assessment of the enzyme behaviours in response to PEP shows that seven of the eight mutations alter the activation mechanism of *E. coli* PK1. The evolved enzymes are cooperatively activated in the presence of the allosteric activator, FBP, unlike the wild-type enzyme. The eighth enzyme, D127N, exhibits a Michaelis-Menten kinetic response to PEP when FBP is present. The D127N response is similar to the wild-type enzyme, but instead has changes to its binding affinity for ADP. This result suggests that the low-glucose selection pressure in Lenski's evolution experiment results in the selection for enzymes with an altered allosteric activation mechanism. The resulting mechanism includes preference for cooperative activation by the substrate PEP, over allosteric activation by FBP.

The reduced activity of all of the evolved enzymes in physiological substrate concentrations, as well as the altered activation responses of all of the enzymes (except D127N), confirms the importance of these mutated residues for catalysis and regulation.
Active site residues − since all three of the 'active site' mutations are suspected to alter the lid domain opening and closing, the reduced activity at physiological substrate concentrations confirms the importance of the lid domain for catalysis. In addition, the P70Q and P70T mutations have an altered activation mechanism, whereby the enzymes are cooperatively activated by PEP, even when FBP is present.
A/A' interface residues − the allosteric activation mechanism proposed in Chapter Three highlighted the importance of domain and subunit interfaces for relaying the allosteric signal between the regulatory and catalytic sites. The altered allosteric response of the three enzymes with mutations at the A/A' inter-subunit interface (I264F, A301S and A301T) confirms the importance of subunit interfaces for communicating the activation signal between sites. In addition, the I264F and A301T enzymes have a reduced response to PEP in the absence of FBP, with extremely large concentrations of PEP required to cooperatively activate the enzymes. The considerable reduction in activation potential of these two mutated enzymes confirms a strong link between A/A' interface residues and the catalytic site.

Allosteric site residues – mutation of residues G381A and T462I, involved in binding FBP in the allosteric site of the enzyme was found to significantly reduce FBP binding affinity, resulting in cooperative activation of the enzyme in the presence of FBP. Residue G381 is one of multiple residues that form a pocket for binding the 1'-phosphate of FBP and mutation of G381 to an alanine alters FBP binding. However, the decrease in $S_{0.5}^{PEP}$ when FBP is present shows that some allosteric activation is occurring. While, the T462I mutation also shows reduced FBP binding, this enzyme shows almost no change in $S_{0.5}^{PEP}$ when FBP is present, suggesting that FBP has only a small allosteric activation effect upon the enzyme.

Considerable changes to allosteric activation, such as those identified in the evolved enzymes, would suggest the structure or dynamic behaviour of the enzymes must be altered in a way that could cause the change. Thermal shift assays established that the stability of the enzymes is largely unchanged. However, four of the evolved enzymes (I264F, A301T, G381A and T462I) did show slight differences in unfolding temperatures, which could imply that the flexibility is altered. Likewise, the biphasic unfolding pattern of the I264F enzyme in BTP buffer, but not Tris buffer, suggests that this mutation has altered binding specificity, which could be a result of increased flexibility, producing two major unfolding events.

In summary, this chapter confirms that *E. coli* PK1 has adapted to produce changes in the kinetic function, regulation response, and stability. In the next chapter, atomic resolution structures of the evolved enzymes are could help to identify the source of the altered kinetic behaviours in the evolved *E. coli* PK1 enzymes.

4.7 References

[1] Lenski, RE, and Travisano, M. (1994) Dynamics of adaptation and diversification: a 10,000-generation experiment with bacterial populations, *Proc. Natl. Acad. Sci. U. S. A. 91*, 6808-6814.

[2] Cooper, VS, and Lenski, RE. (2000) The population genetics of ecological specialization in evolving *Escherichia coli* populations, *Nature 407*, 736-739.

[3] Escalante, A, Salinas Cervantes, A, Gosset, G, and Bolivar, F. (2012) Current knowledge of the *Escherichia coli* phosphoenolpyruvate-carbohydrate phosphotransferase system: peculiarities of regulation and impact on growth and product formation, *Appl. Microbiol. Biotechnol. 94*, 1483-1494.

[4] Woods, R, Schneider, D, Winkworth, CL, Riley, MA, and Lenski, RE. (2006) Tests of parallel molecular evolution in a long-term experiment with *Escherichia coli*, *Proc. Natl. Acad. Sci. U. S. A. 103*, 9107-9112.

[5] Xu, YF, Amador-Noguez, D, Reaves, ML, Feng, XJ, and Rabinowitz, JD. (2012) Ultrasensitive regulation of anapleurosis via allosteric activation of PEP carboxylase, *Nat. Chem. Biol. 8*, 562-568.

[6] Bennett, BD, Kimball, EH, Gao, M, Osterhout, R, Van Dien, SJ, and Rabinowitz, JD. (2009) Absolute metabolite concentrations and implied enzyme active site occupancy in Escherichia coli, *Nat. Chem. Biol. 5*, 593-599.

[7] Mattevi, A, Valentini, G, Rizzi, M, Speranza, ML, Bolognesi, M, and Coda, A. (1995) Crystal structure of *Escherichia coli* pyruvate kinase type I: Molecular basis of the allosteric transition, *Structure 3*, 729-741.

[8] Boiteux, A, Markus, M, Plesser, T, Hess, B, and Malcovati, M. (1983) Analysis of progress curves. Interaction of pyruvate kinase from *Escherichia coli* with fructose 1,6-bisphosphate and calcium ions, *Biochem. J. 211*, 631-640.

[9] Pendergrass, DC, Williams, R, Blair, JB, and Fenton, AW. (2006) Mining for allosteric information: natural mutations and positional sequence conservation in pyruvate kinase, *IUBMB Life 58*, 31-38.

[10] Hill, A. (1910) The possible effects of the aggregation of the molecules of haemoglobin on its dissociation curves, *J. Phys. 40*, i-vii.

[11] Fenton, AW, and Blair, JB. (2002) Kinetic and allosteric consequences of mutations in the subunit and domain interfaces and the allosteric site of yeast pyruvate kinase, *Arch. Biochem. Biophys. 397*, 28-39.

[12] Valentini, G, Chiarelli, L, Fortini, R, Speranza, ML, Galizzi, A, and Mattevi, A. (2000) The allosteric regulation of pyruvate kinase: A site-directed mutagenesis study, *J. Biol. Chem. 275*, 18145-18152.

[13] Wang, X, Minasov, G, and Shoichet, BK. (2002) Evolution of an antibiotic resistance enzyme constrained by stability and activity trade-offs, *J. Mol. Biol. 320*, 85-95.

[14] Tokuriki, N, Stricher, F, Serrano, L, and Tawfik, DS. (2008) How protein stability and new functions trade off, *PLoS Comput. Biol. 4*, e1000002.

Chapter Five

Evolved enzymes conserve structure, despite differences in function

Kinetic analyses demonstrate that the evolved *Escherichia coli* pyruvate kinase type 1 (PK1) enzymes have varying different activity compared to the wild-type enzyme (Chapter Four). Additionally, all of the evolved enzymes demonstrate a variety of different kinetic behaviours, including changes to substrate/allosteric activator binding and response. This chapter uses crystal and solution structure analyses to investigate whether evolved enzymes have different structures to the wild-type that could be responsible for their altered functional behaviour. The results demonstrate that the overall structural fold of each of the eight evolved enzymes is the same as the wild-type and is therefore not responsible for the altered functional behaviour. However, crystal soaks of two of the evolved enzymes identified 'foreign' molecules bound in the active site suggesting binding promiscuity, which, given the similar structures, is likely due to dynamic differences.

5.1 Introduction

Disruption to even a single amino acid within the protein sequence can have dramatic effects upon the structure and/or function of an enzyme. A well known example is that of sickle cell anaemia: a single substitution mutation from a glutamate to a valine in human haemoglobin results in a mutant called haemoglobin S., which is a genetic mutation that produces the inherited sickle cell anaemia disease.[1] This example describes how a very small change in sequence can make a huge difference to protein function.

The large changes to activity and functional behaviour exhibited in the evolved enzymes suggests that perhaps the enzyme structures have changed in a way that would contribute to (or cause) the identified functional changes. To investigate the affect of each substitution mutation upon the respective enzyme's structure, X-ray crystallography was employed to determine the atomic structures of the eight evolved enzymes for comparison with the wild-type. Are the mutations causing changes to the enzymes structure? Can structural changes explain the altered functional properties identified in Chapter Four?

Following X-ray structure determination, solution structure analysis using small-angle X-ray scattering (SAXS) was used to investigate protein conformational changes that are often unable to be identified in a crystalline environment. In addition, SAXS was used to verify that the X-ray structures complement the solution structural envelopes. Do the evolved enzymes behave the same as wild-type PK1 in a solution environment? Are the structural envelopes the same in solution as they are in structure?

The results determine that the evolved enzymes have retained the same structural fold as the wild-type enzyme. X-ray crystal structures combined with solution structures confirm that the altered kinetic properties can not entirely be explained by the enzyme structures because they are largely the same. However, crystallisation of one enzyme (I264F) and a small molecule crystal soak of another (T462I) produced structures with 'foreign' molecules bound in the active sites of the enzymes. Therefore, given the lack of structural differences between the evolved enzymes and the wild-type, binding promiscuity is proposed as a result of increased flexibility of the substrate binding loops.

5.2 The fold of the evolved enzymes is retained

The X-ray crystal structures of the eight evolved enzymes were determined and compared to the wild-type to assess whether the substitution mutations have changed the enzyme structures in a way that could be altering the kinetic properties (Chapter Four). The wild-type PK1 and eight evolved enzymes were crystallised according to the methods found in Section 8.6.1, with all of the enzymes favouring crystallisation in different conditions. The X-ray crystal structures were solved following the methods in Sections 8.6.2 and 8.6.3 using PDB ID: 4YNG as a molecular replacement model. The basic structural parameters

are listed in Table 5.1 and a more detailed analysis of the structural parameters can be found in the supplementary materials (Section 5.8).

Table 5.1 X-ray crystallographic *R*-values for wild-type PK1 and eight evolved enzyme structures. The refinement statistics presented are for the highest quality structure of each individual enzyme.

Enzyme	Space group	Resolution (Å)	R_{free} (%)	R_{factor} (%)	Twin law
Wild-type	$P2_1$	2.28	24.5	21.7	h, -k, -l
P70Q	$C222_1$	2.65	24.3	19.6	
P70T	$C222_1$	2.10	23.1	19.3	
D127N	$P2_1$	2.32	25.9	21.1	h, -k-h, -l
I264F	$C222_1$	2.88	24.0	18.4	
A301S	$P2_1$	2.10	20.3	18.0	h, -k, -l
A301T	$C222_1$	2.01	19.8	14.9	
G381A	$P2_1$	2.45	26.5	22.1	h, -k-h, -l
T462I	$C222_1$	2.25	23.3	18.5	

Comparison of each of the evolved enzymes to the wild-type determines that the substitution mutations have not altered the overall structural fold of the *E. coli* PK1 enzyme. Quaternary analysis of the wild-type and evolved enzymes (excluding T462I) carried out by Tong Zhu (University of Canterbury), demonstrated that all of the enzymes have a tight tetrameric structure in solution.[2] In addition, the evolved enzyme crystal structures were each superimposed with the wild-type by the AC cores to determine how well the C^{α} backbone atoms of the enzymes align (Figure 5.1). The alignment is measured by the root mean square deviation (RMSD), which describes the average distance between the C^{α} backbone atoms.[3] However, this measure has caveats: it can be difficult to determine the significance of an RMSD value because it varies depending on the number of residues in the protein (Irving *et al.* stated that "*the RMSD as a function of the number of residues aligned varies exponentially for large common sub-structures and linearly for small common sub-structures*").[4, 5]

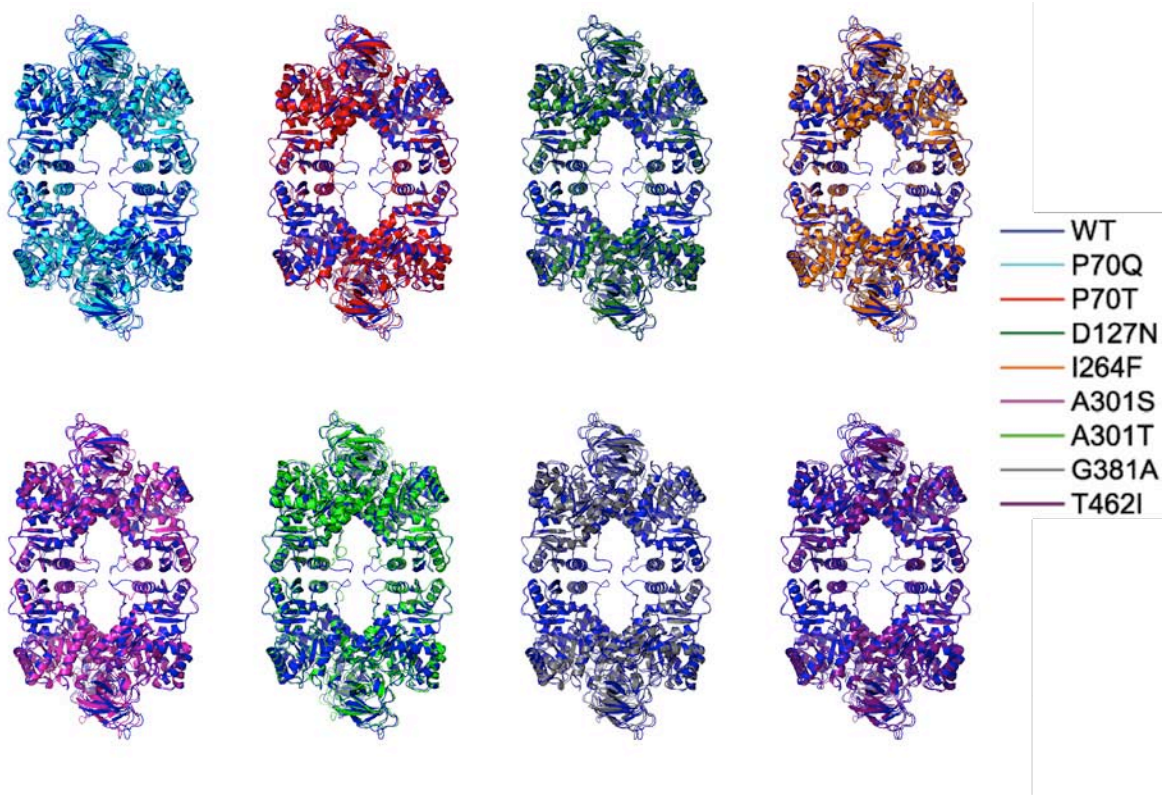

Figure 5.1 Crystal structures of each of the eight evolved enzymes compared to wild-type PK1. Enzymes are aligned by the AC core of all four subunits. Wild-type (blue), P70Q (cyan), P70T (red), D127N (olive), I264F (orange), A301S (magenta), A301T (green), G381A (grey) and T462I (purple).

The RMSD values from the alignments of evolved enzymes to wild-type are compared to the RMSD values for the alignment of unbound and bound A301S enzymes (Section 3.3.3), confirming the evolved enzymes have very little change in the C^{α} backbone position. Superposition of the evolved enzyme structures onto the wild-type provides a C^{α} RMSD fits range from 0.423 to 0.668 Å (Table 5.2). The 1.385 Å RMSD value determined for the alignment of unbound and bound A301S provides a rough idea of the RMSD value expected for a slight conformational change. Thus, it can be concluded that the evolved enzymes have a very similar structural fold to the wild-type enzyme.

Table 5.2 RMSD and interface analysis of wild-type PK1 and eight evolved enzymes. The C^{α} RMSD for each of the evolved enzymes was determined by alignment of the AC cores with wild-type PK1 using PyMOL. Interface analysis was performed using PDBePISA online server.[6]

Enzyme	C^{α} RMSD for AC core domains[a] (Å)	A/A' interface[b] ($Å^2$)	C/C' interface[b] ($Å^2$)
Wild-type	-	1152.2	924.6
P70Q	0.668	1170.3	897.2
P70T	0.443	1192.6	935.3
D127N	0.446	1132.6	935.6
I264F	0.490	1136.0	941.4
A301S	0.447	1124.4	988.0
A301T	0.423	1103.2	954.5
G381A	0.563	1140.3	891.0
T462I	0.562	1165.1	927.7

[a] Calculated using PyMOL
[b] Calculated using PDBePISA[6]

Since the evolved enzymes demonstrated significantly altered allosteric properties compared to the wild-type enzyme, the tetrameric interfaces were carefully assessed to investigate whether the changes to the kinetic properties identified in Chapter Four can be explained by differences in the evolved enzyme interfaces. Analysis of the interface surface areas using PDBePISA[6] provides a surface area calculation for both the A/A' and C/C' interfaces. The interface comparison of wild-type PK1 and the evolved enzymes does not identify any significant changes that could explain the altered kinetic properties (Table 5.2). A more detailed analysis is given is the sections below.

The interfaces between domains and subunits of PK have frequently been described as important for the allosteric regulation of PK enzymes.[7-10] Several studies have mutated residues at the A/A' and C/C' interfaces, resulting in dramatic changes to the enzyme function.[11-14] For example, mutational studies in *E. coli* PK1 have identified a key residue Arg292, as critical for the activation of the enzyme, mutation of this residue completely eliminates enzyme activity.[9, 13] Furthermore, the allosteric activation mechanism proposed in Chapter Three describes the importance of both the domain and subunit interfaces for communicating the allosteric activation signal across the enzyme. The results determine

that FBP binding induces a pathway of disorder between the FBP binding site and the active site, suggesting that the allosteric signal is transferred via conformational flexibility.

5.3 Detailed analysis of crystal structures

Identification of the allosteric mechanism in Chapter Three describes the importance of signal transfer through the wild-type PK1 subunits, from the allosteric site to the active site, over 40 Å away. All of the mutations implicated in this thesis are in positions that could alter the structure and have a significant impact upon enzyme regulation and catalysis. The eight evolved enzymes fall loosely into three different categories based upon their location in the structure: those mutations at or near the active site (P70Q, P70T and D127N), those near the A/A' subunit interface (I264F, A301S and A301T) and those at the allosteric activator binding site (G381A and T462I) (Figure 5.2).

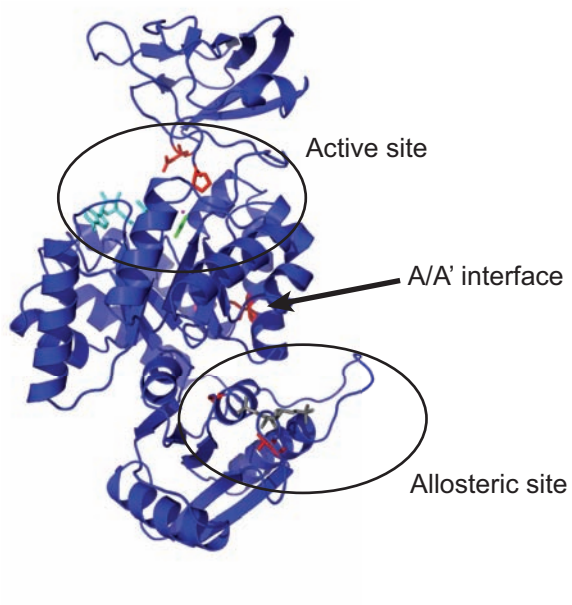

Figure 5.2 Wild-type PK1 subunit displaying the six mutation sites and the ligand binding sites. The structure of the wild-type subunit showing the six mutation sites as red sticks and the active site, A/A' interface and allosteric sites labelled. The FBP is modelled from bound A301S and the suspected substrate/ion binding sites are modelled from PDB ID:3HQO).[9] The bound ligands are shown as sticks and coloured as follows: ATP (cyan), Oxalate (pyruvate mimic; green), FBP (grey), Mg^{2+} (magenta) and K^{+} (orange).

The X-ray crystal structures of wild-type PK1 and the eight evolved enzymes reveal subtle differences between the structures. Could these differences be contributing to the changes found in activity and regulation? The sections below provide a detailed structural analysis of each of the substitution mutations.

5.3.1 Allosteric site mutations show changes that contribute to reduced activator binding

Mapping the allosteric activator, FBP, onto the wild-type PK1 structure reveals that two of the mutated residues are directly involved in FBP binding in the allosteric site (Figure 5.3). Residue G381 forms a hydrogen bond with the 1'-phosphate group of the FBP molecule and residue T462 forms an interaction with the sugar ring of the FBP molecule. The mutation of these residues involved in binding the FBP molecule, may explain the dramatically reduced binding affinity of FBP for the G381A and T462I enzymes (Section 4.3.3.4).

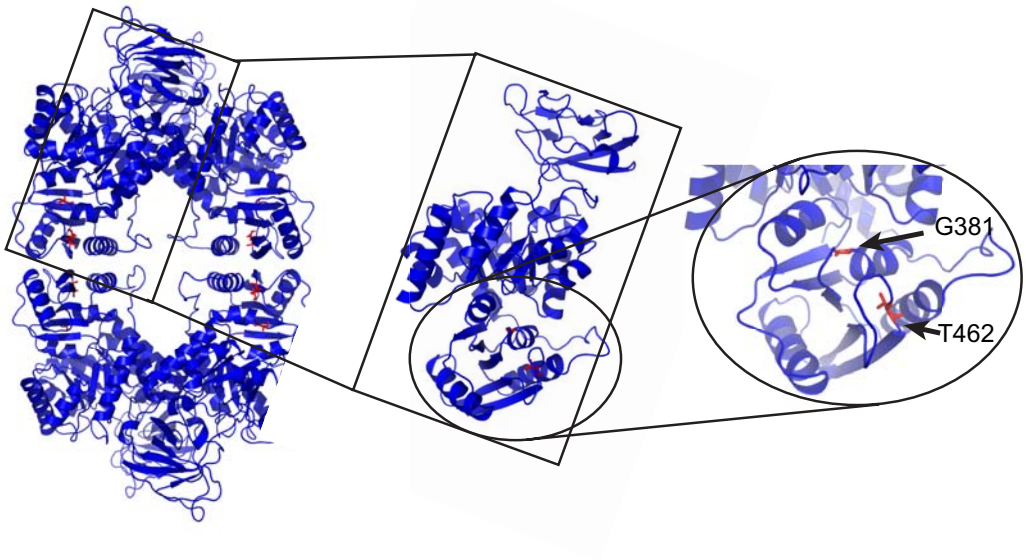

Figure 5.3 Wild-type PK1 displaying the position of the allosteric site mutations. The wild-type structure is shown as a tetramer with first inset showing one subunit. The second inset shows a close up view of the allosteric site mutation positions. The wild-type subunit is coloured blue and the G381 and T462 residues are shown as sticks, labelled and coloured red.

Structural analysis of the G381A enzyme demonstrates a rearrangement of a key loop involved in binding the 1'-phosphate of the FBP molecule. Residue 381 belongs to a stretch of conserved residues (T378−S383) involved in binding the allosteric activator, FBP (Figure 5.4a). Mutation from a glycine to an alanine changes the conformation of the loop region, moving the loop towards the FBP binding site; and if FBP was present it would be in direct contact with the 1'-phosphate of FBP (Figure 5.4b). This is the only enzyme out of eight that shows a rearrangement of this loop region. The remaining seven evolved enzymes display the same conformation as the wild-type, allowing FBP binding to occur. Moreover, G381A is the only evolved enzyme structure without a sulphate bound in the FBP binding pocket, implying that the mutation at residue 381 has reduced the binding affinity of the pocket. This is confirmed by the 105-fold increase in $S_{0.5}^{FBP}$ (Section 4.2, Table 4.3).

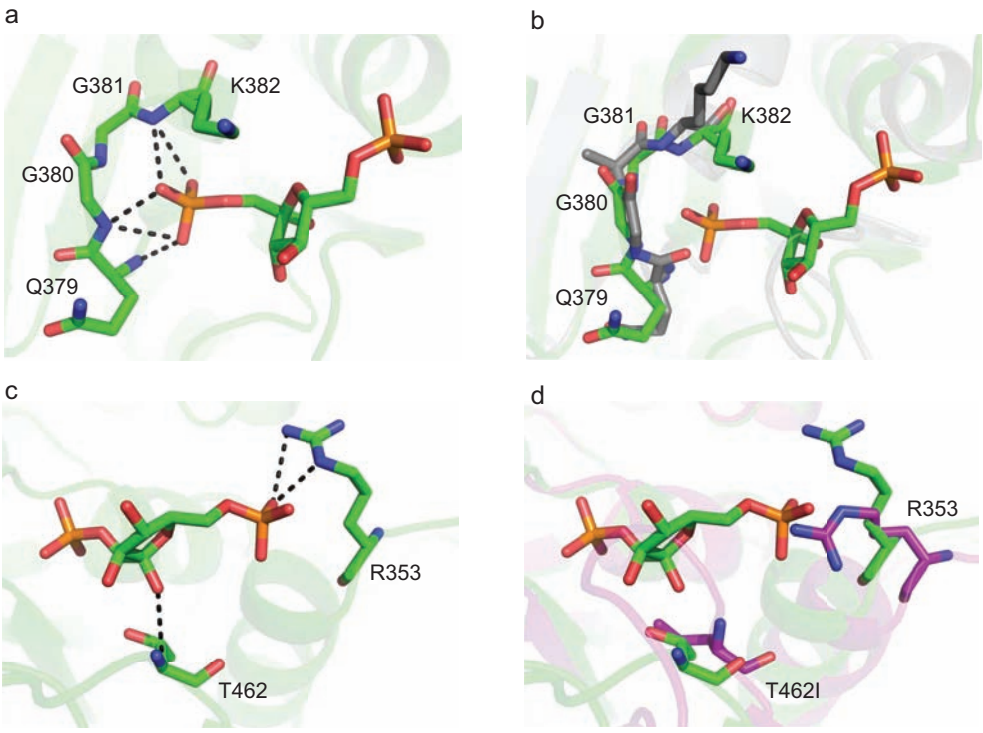

Figure 5.4 **Structure of the allosteric site.** **(a)** Bound A301S structure demonstrating the interactions between FBP and residues Q379, G380, G381 and K382. **(b)** Alignment of bound A301S and G381A showing the slight rearrangement of loop region 378−383 with respect to FBP. **(c)** A301S structure displaying the interactions that form between FBP and residues R353 and T462. **(d)** Allosteric domain alignment of bound A301S and T462I showing the orientation of residue R353 with respect to the FBP molecule. The structures are coloured as follows: A301S (green), G381A (grey), T462I (purple) and FBP (blue). Relevant residues are shown as sticks and labelled. Dashed lines represent interactions.

Next, structural analysis of the T462I structure demonstrates a key change that likely restricts the binding of FBP within the allosteric site. The Thr462 residue is contained within the effector loop (453–462), which is known to be important for binding the FBP molecule. Comparison of the bound and unbound A301S enzymes demonstrate that the presence of FBP causes a structural rearrangement of the effector loop, moving it to create a pocket for FBP binding (Section 3.3.4). The rearrangement places the T462 residue near the FBP molecule, allowing the threonine to form a hydrogen bond with the sugar ring of the FBP molecule (Figure 5.4c).

Mutation of the T462 residue to an isoleucine maintains the main-chain interaction with nearby residue Thr355. Subsequently, the interaction with the sugar ring is lost, reducing the activator binding efficiency. The substitution mutation from threonine to isoleucine removes a hydroxyl group from the polar threonine and introduces hydrophobicity. Based upon analysis of the T462I structure, the pocket surrounding the T462I residue in the unbound form is hydrophobic. Therefore, the hydrophilic nature of the threonine may make driving the effector loop out of the pocket for FBP binding easier. However, the substitution to a hydrophobic isoleucine would decrease effector loop movement because the isoleucine would bury itself in the hydrophobic pocket. Consequently, decreasing FBP binding affinity.

Another observation in the T462I evolved enzyme is that of residue Arg353, which protrudes out towards the FBP binding site. This is unlike all of the other enzymes that are orientated either up or down. It is worth mentioning that although arginine residues are flexible and flip between conformations, the T462I crystallographically averaged conformation places Arg353 in a position that could sterically hinder the binding of FBP's 6'-phosphate (Figure 5.4d).

The loss of a hydrogen bond between residue 462 and the FBP sugar ring, combined with the poor positioning of the Arg353 residue, could explain the dramatic reduction in FBP affinity identified in Section 4.2, Table 4.3.

5.3.2 Mutations at the A/A' interface do not show any significant structural differences

Here, structural analysis of the tetrameric A/A' interfaces determines that the three mutations at the A/A' interface are not displaying any significant differences that could explain the kinetic changes that they produce. Mutation of key residues, I264 and A301 causes a considerable change to the allosteric regulation mechanism of enzymes, I264F, A301T and A301S (Section 4.2 and 4.3). Although residues I264 and A301 are not spatially near the substrate or ligand binding sites (Figure 5.2), the inter-subunit interface interactions are known to strongly influence the allosteric mechanism of PK enzymes.[9, 15] I264F and A301T behave similarly, presenting a dramatic decrease in activity and high $S_{0.5}$ for phosphoenolypruvate (PEP) values compared to the wild-type enzyme, showing a decreased apparent affinity for the substrate, PEP. A structural assessment of the A/A' interface evolved enzymes is used to investigate whether structural changes to the tetrameric interface (around the mutation sites) can explain the dramatically reduced allosteric response identified in the kinetic analysis (Section 4.2 and 4.3).

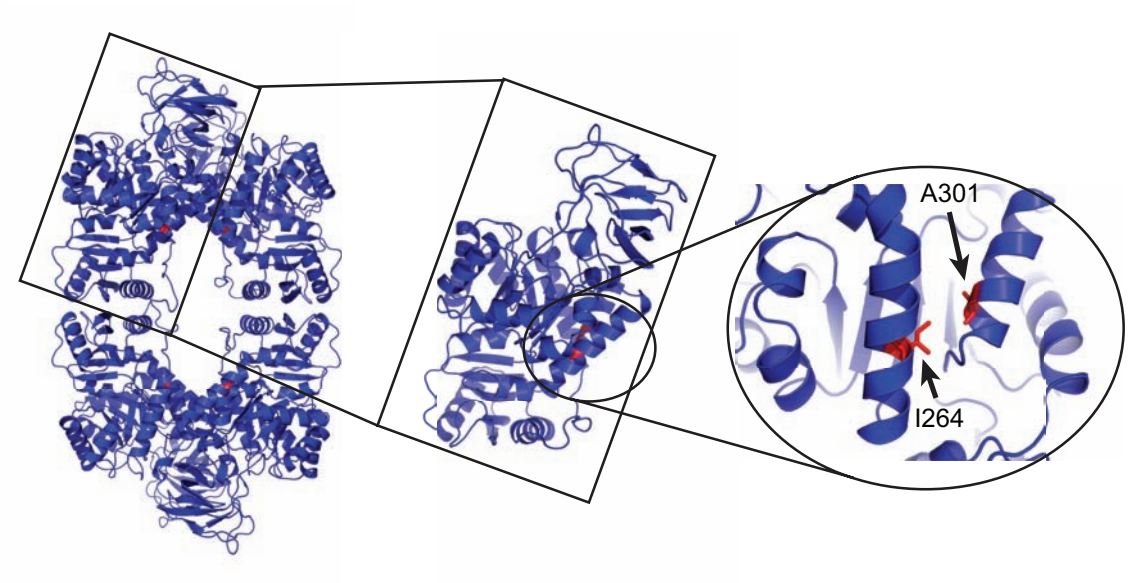

Figure 5.5 Wild-type PK1 subunit displaying the positions of the interface mutations. The wild-type structure is shown as a tetramer with first inset showing one subunit. The second inset shows a close up view of the interface mutation positions. The wild-type subunit is coloured blue and the I264 and A301 residues are shown as sticks, labelled and coloured red.

Analysis of the I264F X-ray structure presented an enzyme with a similar structure and interactions as the wild-type enzyme. Residue Ile264 is located on the Aα6'-helix and forms interactions with Gln260, Cys267 and Ile268 (Figure 5.6a), the mutation to a phenylalanine increases the stability of the helix slightly by introducing a hydrogen bond with Lys261 (Figure 5.6b). The substitution mutation from an isoleucine to a phenylalanine at residue 264 (I264F), slightly changes the backbone bonding within the Aα6'-helix and replaces the hydrophobic isoleucine with a hydrophobic phenylalanine. Although the phenylalanine residue is larger than the isoleucine, structural analysis does not show any steric hindrance within the region surrounding the mutation.

Because there are no significant changes to the structure around the mutation site, except for one additional hydrogen bond, the temperature factors (B-factors) were assessed to compare the flexibility of the mutation site to that of the wild-type enzyme. Comparison of B-factors between the I264F enzyme and the wild-type confirms that the region surrounding the mutation site (Aα6'-helix region) has similar B-factors. Therefore, the I264F mutation does not seem to be changing the flexibility or structure of the Aα6'-helix.

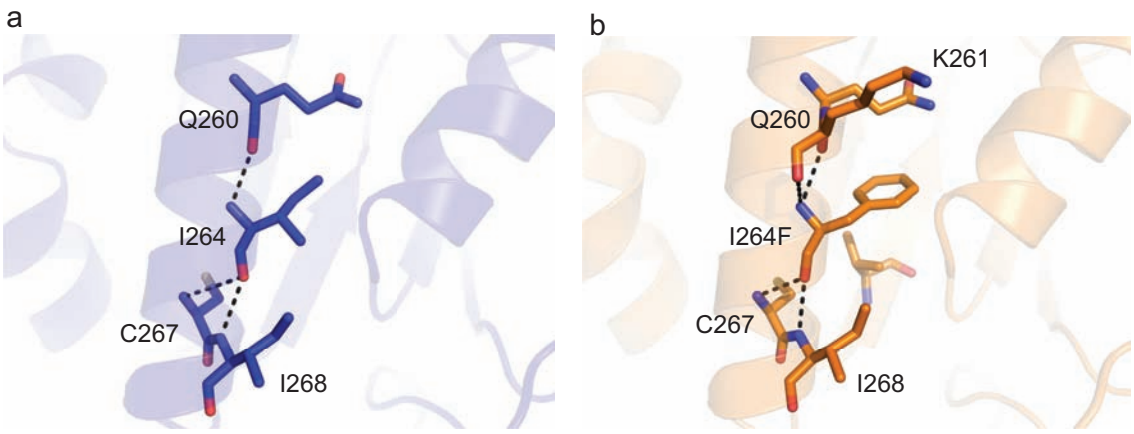

Figure 5.6 **Structure of the Aα6'-helix.** **(a)** Wild-type PK1 (blue) Aα6'-helix displaying the interactions that form between I264 and residues Q260, C267 and I268. **(b)** I264F (orange) Aα6'-helix displaying the interactions that form between I264F and residues Q260, K261, C267 and I268. Relevant residues are displayed as sticks and labelled accordingly. Dashed lines represent interactions.

Structural analysis of the A301 mutated enzymes demonstrates slight changes to the surrounding interactions. Spatially very near the I264F mutation, on the adjacent Aα7'-helix is residue Ala301 and this was mutated to a serine and a threonine, both introducing a

hydroxyl group and a bulkier side chain. Previously residue Ala301 forms interactions with Asp297, Val298 and Thr306 (Figure 5.7a), however the mutation to both serine and threonine introduces additional interactions to residues Gln260 and Gly305 (Figure 5.7b). The additional hydrogen bond between A301S/T and Gln260 would create a stabilised interaction between the Aα6'- and Aα7'-helices.

Next, the B-factors of the A301S and A301T enzymes were compared to the wild-type because the introduced hydrogen bond is expected to alter the structure of this region. Unfortunately, the assessment shows that the two helices (Aα6'- and Aα7'-helices) do not show any significant decrease in flexibility (B-factors) compared to the wild-type.

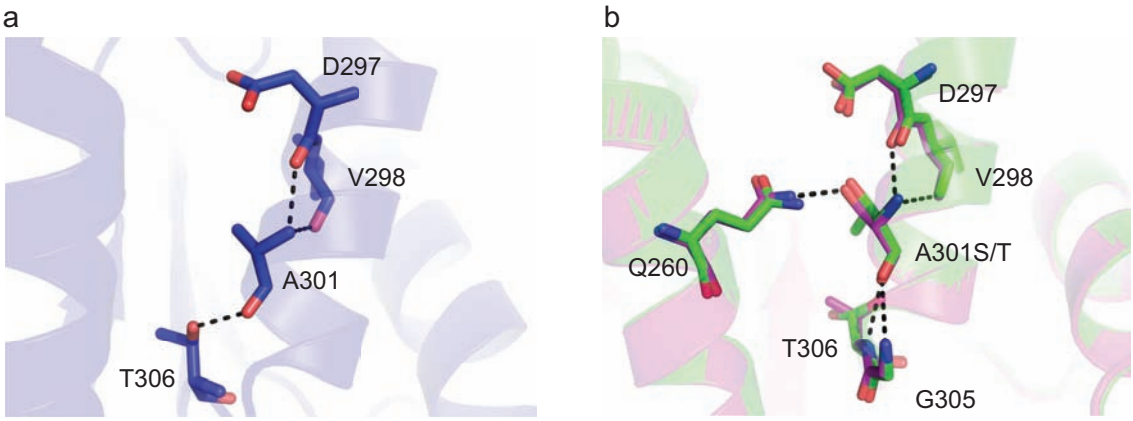

Figure 5.7 **Structure of the Aα7'-helix.** **(a)** Wild-type PK1 (blue) Aα7'-helix displaying the interactions that form between A301 and residues D297, V298 and T306. **(b)** A301S (magenta) and A301T (green) Aα7'-helices displaying the interactions that form between A301S/T and residues Q260, D297, V298, G305 and T306. Relevant residues are displayed as sticks and labelled accordingly. Dashed lines represent interactions.

Despite the dramatically altered activity and allosteric response established in the A/A' interface mutated enzymes, the structure remains similar to wild-type, apart from a series of new hydrogen bond interactions that may strengthen the interface. These enzymes provide a great example of how proteins can alter their 'function' without changing their structure.

5.3.3 Active site mutations have altered interactions compared to wild-type

The structures of the mutated active site enzymes (P70Q, P70T and D127N) were analysed demonstrating some key structural changes that could be contributing to the altered kinetic properties identified in Chapter Four. Mutation of the active site residues changes the activity and activation response of the *E. coli* PK1 enzyme (Sections 4.2 and 4.3). The P70 mutations display a different activity to the wild-type and cooperative activation by PEP, in the presence of the allosteric activator, FBP. On the other hand, the D127N mutation shows a lower activity, but similar activation to the wild-type, with Michaelis-Menten activation in the presence of the allosteric activator. Residues P70 and D127 are located within the active site (Figure 5.8); residue P70 is located on one of the two extended loops between the lid domain and the $(\beta/\alpha)_8$-barrel domain and D127 is located on the underside of the lid domain (Figure 5.8). An assessment of the structural and bonding changes caused by the active site mutations was conducted to rationalise the changes to behaviour found in the three evolved enzymes.

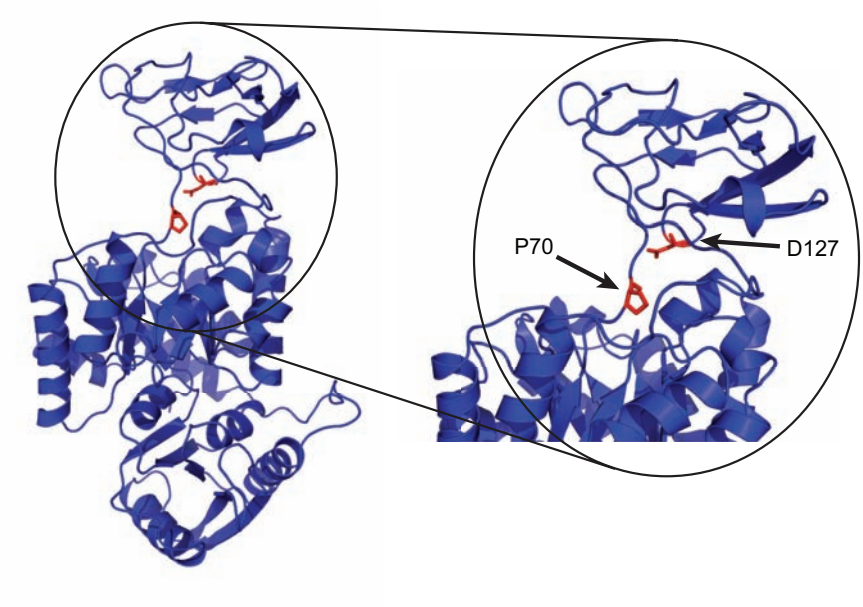

Figure 5.8 Wild-type PK1 subunit displaying the position of the active site mutations. Single subunit structure displaying the positions of the active site mutation positions. Inset shows a close up view of the active site mutation positions. The wild-type subunit is coloured blue and the P70 and D127 residues are shown as sticks, labelled and coloured red.

Structural analysis of the P70 active site mutations demonstrate that the mutations introduce hydrogen bonds between the two extended loops that are responsible for lid opening and closing (Figure 5.9). Previous studies looking at the activation and catalysis of pyruvate kinase, suggest that active site binding events control the movement of the lid domain by closing it over the active site for catalysis.[9, 16, 17] The lid domain moves around a hinge that is created by two proline residues (Pro70 and Pro168) located on the extended loops between the $(\beta/\alpha)_8$-barrel domain and the lid domain. Thus, I predicted that the mutations in the hinge domain would alter the rate of catalysis in these evolved enzymes.

The non-polar Pro70 was mutated to polar residues, glutamine and threonine, in different two replicate populations of *E. coli*. Mutation to a glutamine and to a threonine introduces polarity, which enables new polar interactions to form between the extended loops (hinge regions). The mutation to a glutamine facilitates interactions between Gln70 and the hinge region (Pro168) of the second extended loop connecting domains A and B (Figure 5.9b). The mutation to a threonine introduces new interactions between residue Thr70 and Arg195 of the $\beta_4\alpha_4$-loop (Figure 5.9c). These two enzymes with mutations at residue P70 of the active site show structural changes that could restrict or modify lid opening and closing over the active site. Kinetic analysis determined that the effect of these mutations is on PEP binding within the active site, demonstrated by the reduced $S_{0.5}^{PEP}$ compared to the wild-type enzyme.

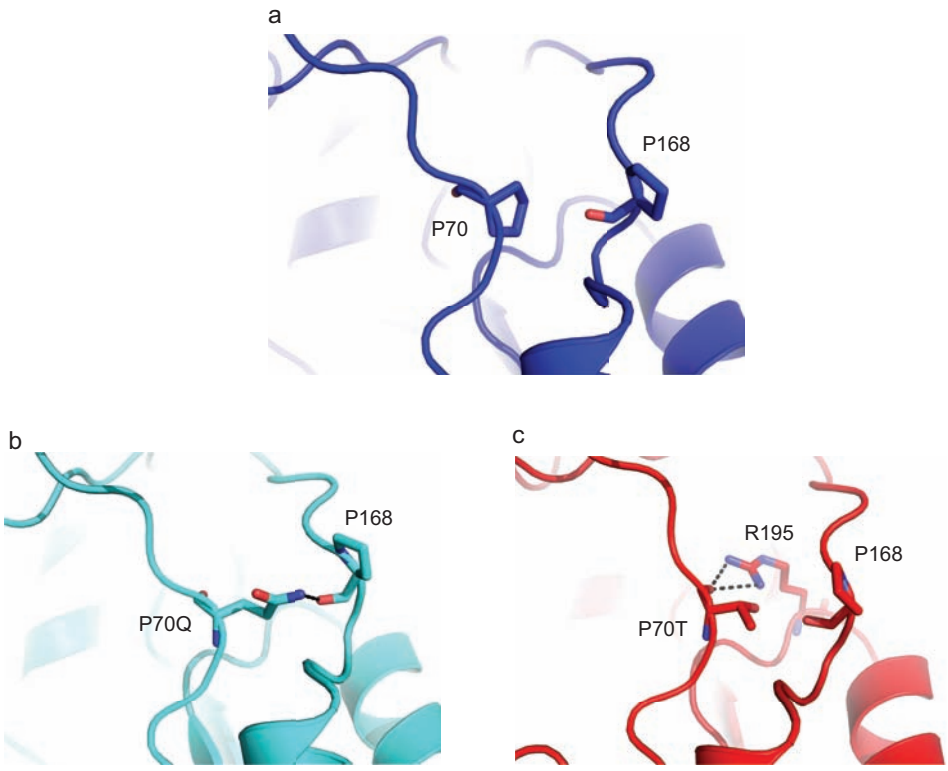

Figure 5.9 Structure of the extended loops between the lid domain and the $(\beta/\alpha)_8$-barrel. (a) Wild-type PK1 structure with the two proline 'hinge' residues (P70 and P168) displayed as sticks. **(b)** P70Q structure displaying the interactions that form between the two proline 'hinge' residues. **(c)** P70T structure displaying the interactions that form between P70T and R195 of loop $\beta_4\alpha_4$. All relevant residues are displayed as sticks (P70, P168 and R195).

Structural analysis of the D127N enzyme demonstrates that the mutation removes the ability of residues Asp127 and Arg292' to form a salt bridge to lock the lid in an open conformation. Residue Asp127 is located on the underside of the lid domain (Figure 5.8) and is proposed to have a critical role in forming a salt bridge with the side chain of Arg292' from the adjacent subunit during the T- to R-state transition (Figure 5.10b).[7] The bound structure of A301S confirms that the *E. coli* PK1 enzyme forms this same interaction between Asp127 and Arg292' when in the active state (Figure 5.10b). Mutating the D127 aspartic acid to an asparagine, removes the negative charge that was associated with the carboxylic group and creates a polar carbomoyl group. Consequently, removal of the negative charge prevents salt bridge formation across the A/A' interface during activation.

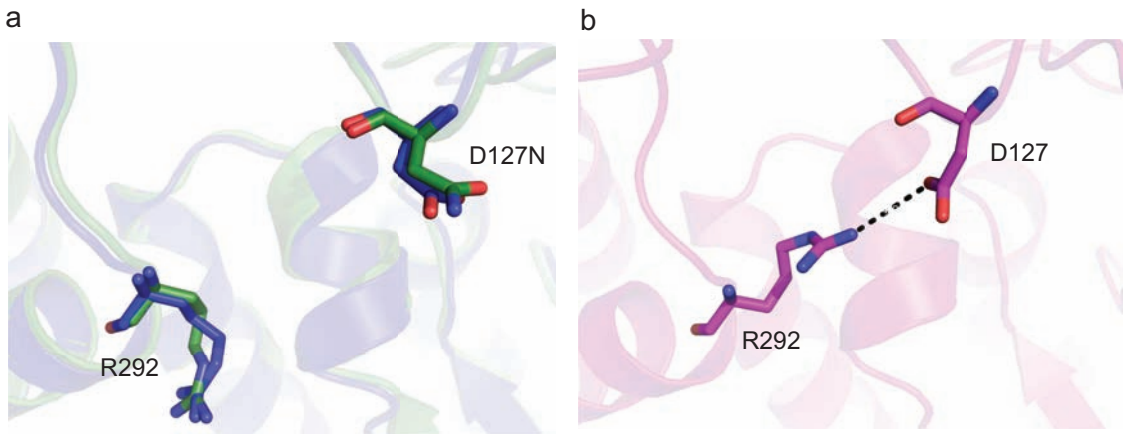

Figure 5.10 Structure of the region surrounding residue D127. (a) Wild-type structure (blue) aligned with the D127N structure (olive). **(b)** Structure of A301S (magenta) showing the interactions that occur between residues D127 and R292 in the bound state.

Structural analysis of the active site mutations identifies small changes in bonding patterns that could have a significant impact upon the efficiency of lid opening and closing. The change in activity caused by these mutations proves that the efficiency of lid opening and closing is important for enzyme catalysis upon substrate binding.[9, 17] Although the P70 mutations are not near the PEP binding site, they do decrease the binding affinity of PEP, which could be due to the mutations altering the lids ability to open and close for catalysis. The D127N mutation has a major effect upon ADP binding and it was suspected that closure of the lid domain may place the residue 127 in contact with bound ADP, thus mutation to the asparagine could alter affinity. However, structural modelling of lid closure from the rabbit M1 PK (PDB ID: 1A5U)[18] with substrates bound shows that residue 127 is not near the ADP binding site when the lid is in a closed conformation, therefore the rationale behind altered ADP binding is unknown.

Overall, X-ray structure analysis confirms that the eight evolved enzymes have retained a conserved three-dimensional structural fold. However, substitution mutations invoke changes that disrupt the electrostatic interactions of mutated residues, resulting in small changes to the structure but major changes to enzyme function.

5.4 Evolved enzymes have the same solution structure as the wild-type

Small angle X-ray scattering provides a powerful method for extracting structural information about proteins in solution. The information gathered, compliments X-ray crystal structures by characterising shape, conformation, flexibly linked domains and folding of proteins in solution.[19] This section employed SAXS to analyse the solution structures of each of the evolved enzymes and compare them to the wild-type to determine whether the evolved enzymes have developed shape or conformational differences to the wild-type in solution. Next, the solution structures of each of the enzymes were compared to their X-ray structures to confirm that the three-dimensional structure is a good representation of what the protein looks like in a solution environment. Finally, SAXS analysis of each of the enzymes is presented in the presence of FBP to determine whether FBP binding causes conformational changes to the proteins and if these changes can be verified using SAXS.

The SAXS data analysis confirms that wild-type PK1 and the eight evolved enzymes have the same solution structure. Scattering patterns for each of the enzymes were obtained from the SAXS data analysis and are presented as radially averaged one-dimensional curves (Figure 5.11). From these curves we can extract important information about the size, general shape and oligomeric state of each of the proteins. Here, the scattering curves of each of the enzymes are overlaid (Figure 5.11) to emphasise the similarities between the nine enzymes (wild-type and eight evolved enzymes). All of the scattering curves are the same shape and align very well, which is consistent with the nine enzymes having the same general shape and oligomeric structure in solution.

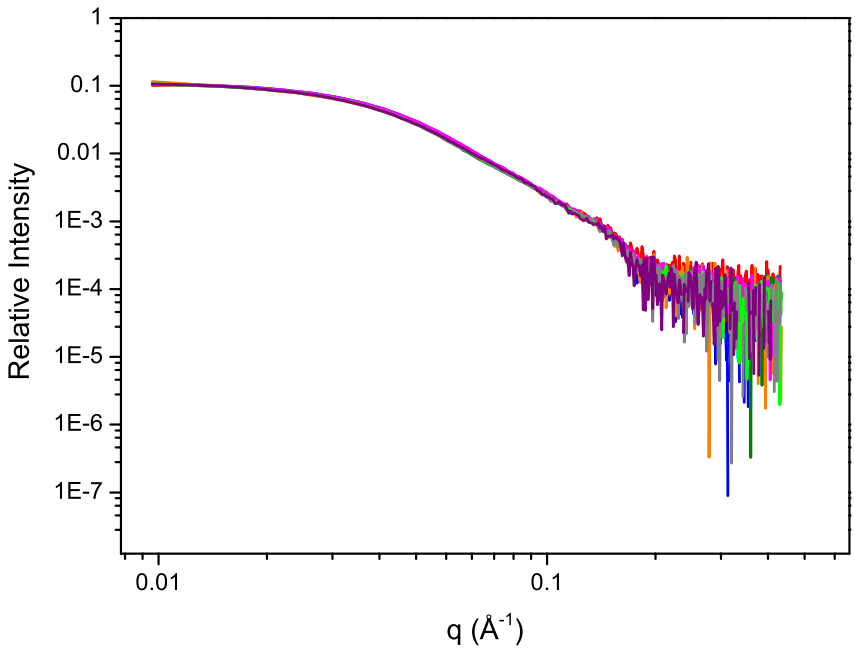

Figure 5.11 SAXS analysis of wild-type PK1 and eight evolved enzymes demonstrating that they all have the same structural fold. Experimental scattering profiles for wild-type and eight evolved enzymes displayed as aligned intensity plots. Enzymes are coloured as follows: wild-type (blue), P70Q (cyan), P70T (red), D127N (olive), I264F (orange), A301S (magenta), A301T (green), G381A (grey) and T462I (purple).

From the presented scattering curves (Figure 5.11), the radius of gyration (R_g), forward scattering intensity ($I(0)$), maximum particle dimensions (D_{max}) and the estimated molecular mass for each of the enzymes was extracted (Table 5.3). The R_g provides a measure of how the mass of a particle is distributed around its centre of mass,[20] and in this case, all of the enzymes have R_g's of between 44 and 46 Å, which confirms that the overall shapes of the proteins are the same. The sizes of the proteins were determined from the D_{max}, which provides a measure of the maximum diameter of the particle. This was then used to estimate the molecular mass of the protein. The results demonstrate that all of the enzymes fall within the maximum dimensions of 135−152 Å, providing mass estimates ranging from 185−193 kDa, which are very close to the 190 kDa estimate of the wild-type in solution.

Table 5.3 Parameters for wild-type PK1 and eight evolved enzymes calculated from SAXS data.
Parameters for each enzyme were determined using *GNOM*[21] and *AUTOPOROD* analyses.[22]

Enzyme	Radius of gyration[a] (Å)	$I(0)$[a]	D_{max}[b] (Å)	Molecular mass[b] (kDa) Calculated for sequence = 200 kDa
Wild-type	44.5 ± 0.12	0.114	141.9	190
P70Q	44.2 ± 0.13	0.127	138.3	187
P70T	44.1 ± 0.22	0.079	135.2	188
D127N	44.8 ± 0.25	0.186	145.6	190
I264F	45.6 ± 0.35	0.077	151.8	185
A301S	44.5 ± 0.16	0.104	145.7	186
A301T	44.3 ± 0.11	0.163	135.6	185
G381A	44.6 ± 0.21	0.091	137.4	193
T462I	44.7 ± 0.29	0.054	145.5	190

[a] Calculated using *GNOM*[21]
[b] Calculated using *AUTOPOROD*[22]

The X-ray crystal structures were then compared to the solution structures, confirming that the *in crystal* structure is consistent with the proteins' *in solution* structure (Figure 5.12). The crystal structures for each of the evolved enzymes were evaluated using *CRYSOL*[23] to determine their theoretical solution scattering, which was then compared to the experimental scattering. The results demonstrate that the lattice structures are a good representation of the enzyme structures in solution.

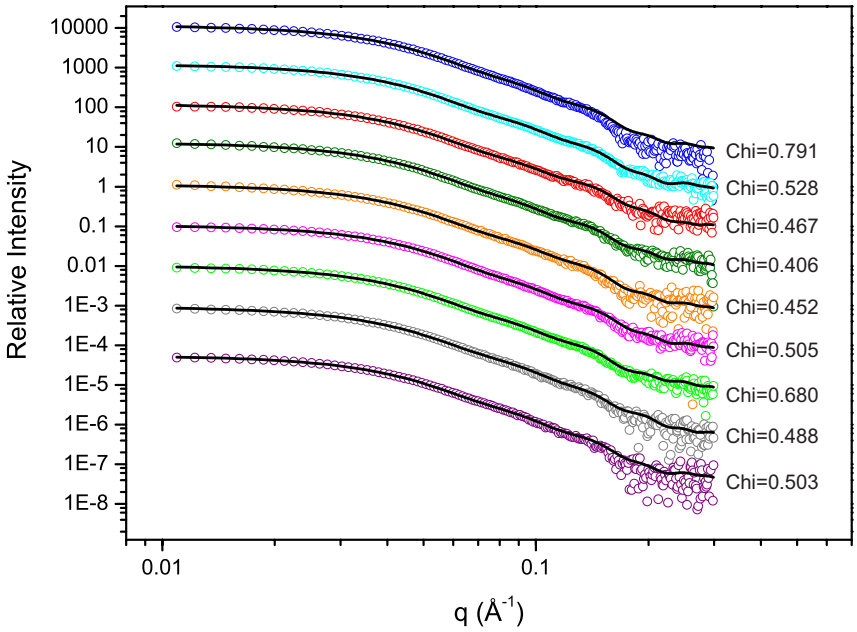

Figure 5.12 SAXS analysis of wild-type PK1 and eight evolved enzymes demonstrating that the crystal structures are a good representation of the structures in solution. Experimental scattering profiles for wild-type and eight evolved enzymes are displayed with the theoretical scattering curves overlaid (black curves) to compare the experimental vs. theoretical. Enzyme experimental curves are coloured as follows: wild-type (blue), P70Q (cyan), P70T (red), D127N (olive), I264F (orange), A301S (magenta), A301T (green), G381A (grey) and T462I (purple).

A comparison of the scattering profiles of each of the evolved enzymes in the presence and absence of FBP demonstrated that FBP binding did not have a large effect on the solution structures of the enzymes (Figure 5.13). While the crystal structures of each of the evolved enzymes are very similar to the wild-type, structural differences may arise upon FBP binding because all of the enzymes (except D127N) show an altered response to FBP. Co-crystallisation and crystal soaking experiments for each of the evolved enzymes have been largely unsuccessful. Therefore, SAXS was used to assess the effect that FBP binding has upon the enzymes structure in solution.

Alignment of the experimental scatter with the scatter in the presence of FBP for each of the enzymes demonstrates that all of the plots align very well, suggesting that FBP binding does not alter the overall structures of the proteins in solution (Figure 5.13). However, we know that this is not the case because the unbound and bound structures of the A301S enzyme (Chapter Three) demonstrate ~5° rotation of subunits, increasing the C^{α} root mean square deviation (RMSD) to 1.385 Å (Section 3.3.3), implying that perhaps the small

variation in conformation is unable to be identified from the 10−50 Å resolution limit of SAXS.[24] To test this, *CRYSOL* was employed to generate the theoretical scattering curves for the A301S bound and unbound structures to see if the conformational changes are large enough to be identified using SAXS (Figure 5.14). The results show that the theoretical scattering curves align very well, which confirms that the conformational changes identified in the crystal structures, are not large enough to be seen using SAXS.

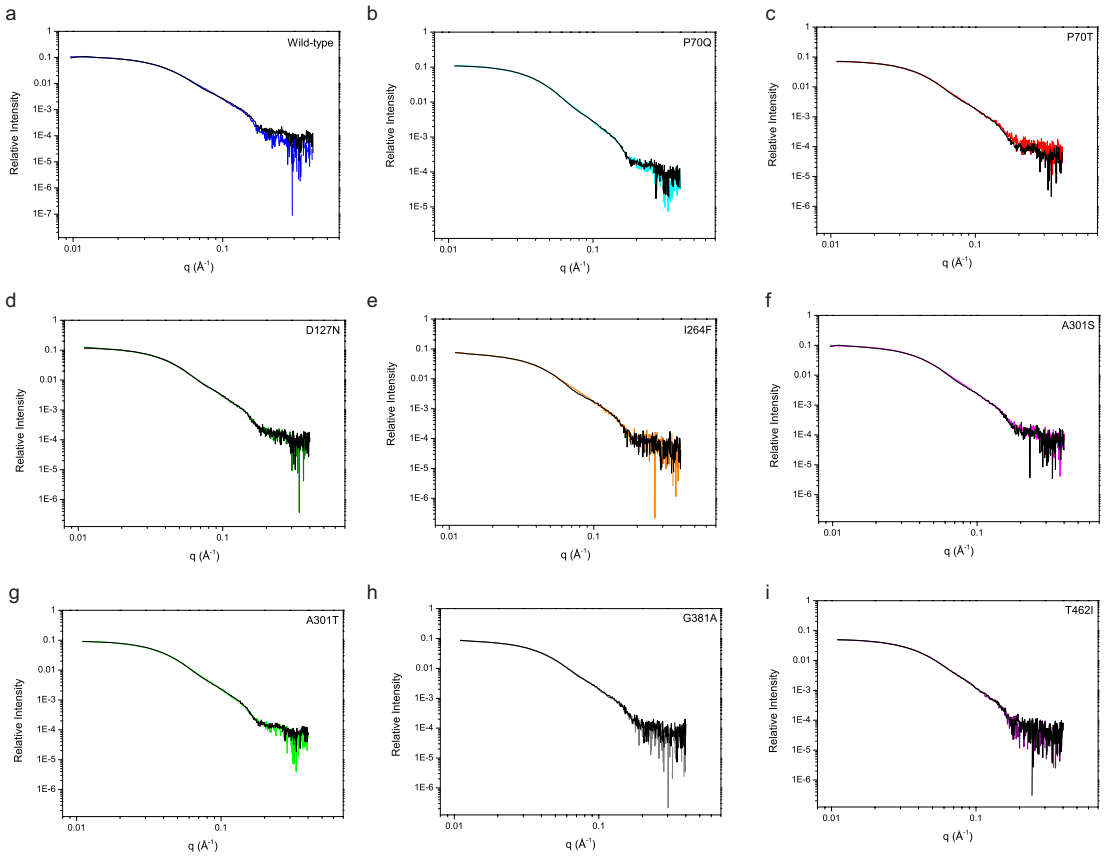

Figure 5.13 SAXS analysis of evolved enzymes in the unbound and bound states. Experimental scattering profiles for the eight evolved enzymes in the presence and absence of FBP. Bound plots are coloured black and unbound plots are coloured by enzyme: **(a)** P70Q (cyan), **(b)** P70T (red), **(c)** D127N (olive), **(d)** I264F (orange), **(e)** A301S (magenta), **(f)** A301T (green), **(g)** G381A (grey), **(h)** T462I (purple).

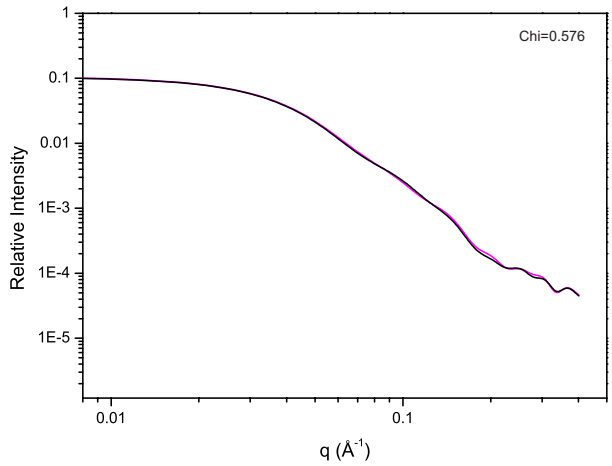

Figure 5.14 Theoretical scattering for unbound and bound A301S demonstrating that the conformational changes are too small to be seen using SAXS. The Chi value for the comparison is 0.576. Unbound A301S is coloured magenta and bound A301S is coloured black.

The theoretical scatter of two different structures was compared to the theoretical scatter of A301S (above) to gauge how much of a structural change is necessary to see a change in the SAXS scatter (Figure 5.15). For this, the theoretical scatter for two different pyruvate kinase structures was obtained; the first is a structurally modified version of A301S depicting a different shaped tetramer with the same molecular weight, and the second is the structure of pyruvate kinase from *Saccharomyces cerevisiae* showing a similar shaped tetramer with a different molecular weight.

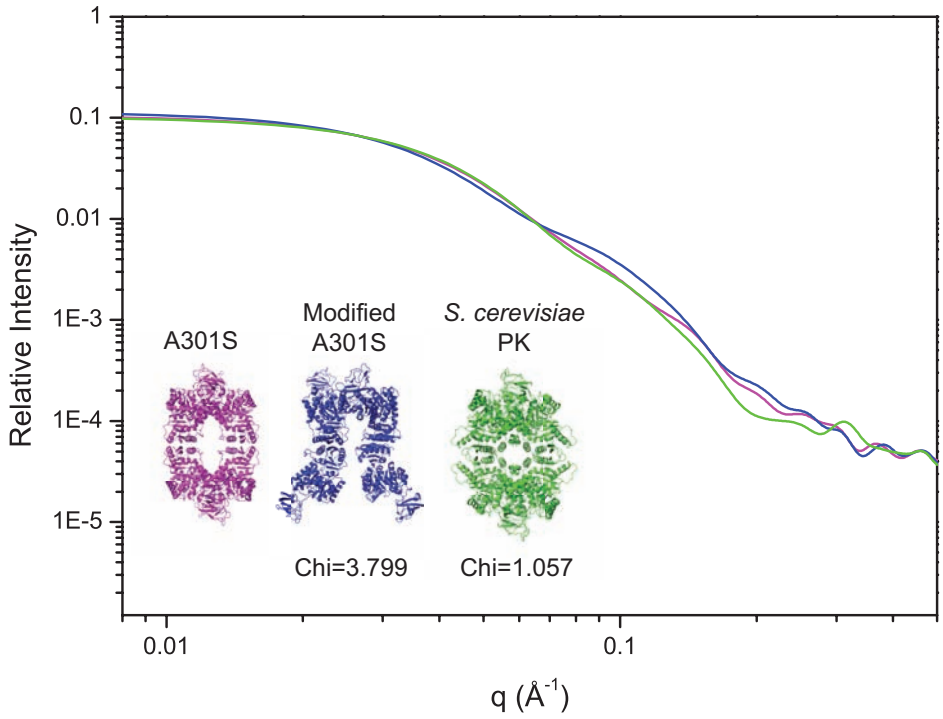

Figure 5.15 Comparison of the theoretical scattering for three different PK structures demonstrating how structural change alters the one-dimensional scattering curve. The three pyruvate kinase structures used for the comparison are: A301S (magenta), modified A301S (blue) and *S. cerevisiae* PK (green).

The results demonstrate that SAXS can differentiate between structural changes in both example PK structures compared to the A301S structure. The comparison determines that altering the shape of the A301S structure has a negative impact upon the fit to the original A301S structure (Chi=3.799). Whereas, the *S. cerevisiae* PK has a reasonably good fit to the original A301S structure (Chi=1.057) because they have a similar shape. These results provide a great example of the magnitude of structural change required to see a difference in the SAXS scatter and confirm that the lack of change found in the theoretical scattering of the unbound and bound A301S structures is not surprising because the changes are too small to be recognised with SAXS.

5.5 Enzymes display substrate binding promiscuity

Structure analysis of the eight evolved enzymes established that the structures are largely the same as the wild-type. However, Chapter Four describes very different kinetic responses from each of the enzymes. Here, serendipitous co-crystallisation and crystal soaks of two of the evolved enzymes (I264F and T462I) provides evidence to suggest that the enzymes have evolved some promiscuity in their substrate binding at the active site. The crystal structures of both enzymes identify foreign molecules bound in the active site, that were not found in the wild-type enzyme. This result suggests that the substrate binding loops have changed in a way that has reduced the enzymes' substrate binding specificity.

Analysis of the I264F crystal structure shows a bis-tris-propane (BTP) molecule bound within the active site of the enzyme (Figure 4.16a, b and c, Chapter Four). The I264F protein formed crystals in a crystallisation condition containing BTP, which subsequently led to BTP binding to substrate binding loops in the active site. It is not uncommon for molecules from the crystallisation media to bind within proteins, however this particular case is different because it is not the first instance of BTP interacting with this particular evolved enzyme. In Chapter Four thermal shift assays determined that I264F was the only enzyme out of eight that displayed a biphasic unfolding pattern in the BTP buffer (Figure 4.10, Chapter Four). This result demonstrates that BTP is binding within the enzyme, causing two major unfolding events (note: BTP was not used in the assay buffer). These interactions of BTP with I264F (but not the other enzymes), confirm that this evolved enzyme has reduced substrate binding specificity.

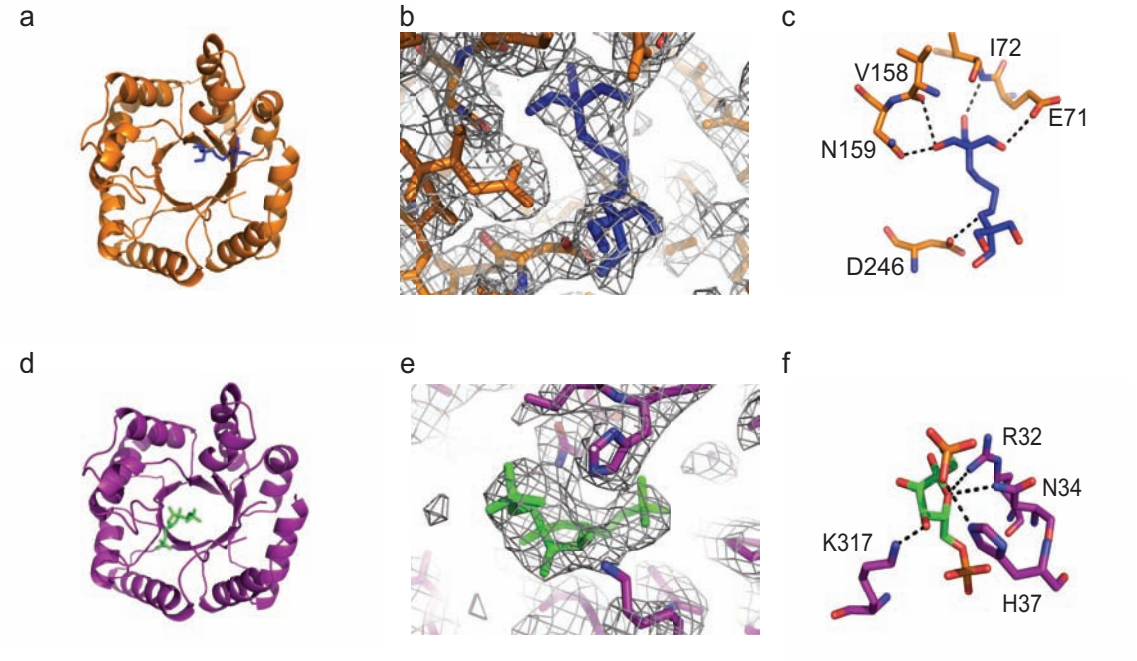

Figure 4.11 Promiscuous binding in the active site of I264F and T462I. I264F (orange) active site with BTP (blue) bound showing: (a) the binding position within the $(\beta/\alpha)_8$-barrel, **(b)** electron density for BTP, and **(c)** interactions formed with relevant residues. **T462I (magenta) active site with FBP (green) bound showing: (d)** the binding position within the $(\beta/\alpha)_8$-barrel, **(e)** electron density FBP, and **(f)** interactions formed with relevant residues.

For the wild-type and A301T enzymes, soaking crystals with FBP results in a cracked crystal – soaking FBP into A301S was successful (Chapter Three – Part 1). Surprisingly, soaking crystals of T462I in FBP (5 mM) did not crack the crystal. The T462I enzyme was soaked in a cryoprotectant containing FBP, with the expectation that it would bind in its allosteric binding pocket in the allosteric domain. However, analysis of the structure determined that the FBP molecule is bound in the active site, close to the proposed ADP binding site (Figures 4.11d, e and f).[9] This finding suggests that the activator-binding pocket has a reduced affinity for FBP (confirmed by the increased $S_{0.5}^{FBP}$ – Chapter Four), and that the substrate binding loops have a reduced substrate binding specificity. Given that FBP binds in the active site, it is unclear why the enzyme is still activated by FBP, as demonstrated by the kinetic analysis.

These crystal structures with 'foreign' molecules bound in the active sites imply that the enzymes have evolved some substrate binding promiscuity, and given the lack of structural differences between the evolved enzymes and the wild-type, it is likely that promiscuity is a result of altered flexibility of the substrate binding loops that surround the active site.

5.6 Discussion

This chapter describes the structural analysis of eight adaptively evolved mutations in the *E. coli* PK1 enzyme. From a long-term evolution experiment, eight single substitution mutations adaptively evolved in the *E. coli* PK1 enzyme, producing a fitness benefit in the low-glucose environment. Functional analysis of these enzymes determined that they all display significantly altered kinetic properties compared to the wild-type, with seven showing a reduced response to the allosteric activator. The significant changes to activity and allosteric response suggest that the structures have changed in a way that would contribute to the altered kinetics.

Parallel evolution − Structural data demonstrate the robustness of the wild-type quaternary structure and structural fold. Whereby, eight substitution mutations can dramatically alter function and allosteric response while preserving the enzyme's structure. The crystal structures of the eight enzymes demonstrate that the evolved enzymes have retained the same structural fold as the wild-type. In addition, solution structure analysis using SAXS confirms that all of the enzymes have the same size and shape as the wild-type in solution. Furthermore, one-dimensional scatter plots from each of the crystal structures determine that they are a good representation of what each of the proteins looks like in solution. These results confirm that the dramatic changes in functional behaviour of the eight evolved enzymes can not be explained by the enzyme structures.

However, the conserved structural fold identified in this chapter provides further evidence to support the parallel evolution of these enzymes. All eight of the mutations have been shown to produce a fitness benefit, as well as a decrease in enzyme activity compared to the wild-type at physiological substrate concentrations. The parallel changes to the evolved enzymes now include the absence of structural change compared to the wild-type enzyme.

Detailed analysis of each of the crystal structures identifies small local changes to the regions surrounding each of the mutation sites. Aside from these small changes, no other changes in the enzymes' three-dimensional structures are found. Although, the substitution mutations in the primary sequence do not change the overall fold of the enzyme, they may alter the order and dynamics within the protein. Local changes to the

charge, polarity and size of amino acids, distorts enzyme electrostatic interactions and can alter the dynamic behaviour, which could promote functional changes.

Rationalising the kinetic responses – Although the structural fold of each of the evolved enzymes has not changed, small changes localised to the individual mutation sites are noted and these are used to rationalise the changes in kinetic behaviours identified in Chapter Four.

The G381 and T462 residues are both involved in binding FBP in the allosteric domain. Unsurprisingly, the G381A and T462I mutations cause a considerable reduction in FBP binding affinity ($S_{0.5}^{FBP}$ of 105-fold and 281-fold, respectively), which can be explained by the mutation of residues 381 and 462 involved in binding FBP, and structural reorientation of the backbone to reduce FBP binding.

Structural assessment of the enzymes with mutations in the A/A' interface helices (I264F, A301S and A301T) show that all three enzymes have increased hydrogen bonding compared to the wild-type. The proposed mechanism of allosteric activation in wild-type involves destabilisation, causing a decoupling of subunits to remove cooperative activation (Chapter Three – Part 2). Following this mechanism, the significant increase in cooperative activation found in I264F and A301T enzymes could be rationalised by increased stability at the A/A' interface, causing a coupling of subunits, thus increasing cooperative activation by PEP.

Analysis of the enzymes with mutations at the active site (P70Q, P70T and D127N) determined two different kinetic behaviours. P70Q shows higher activity and P70T shows lower activity than the wild-type enzyme and both of these mutations were found to have additional hydrogen bonds in the 'hinge' region that controls the movement of the lid domain. The changes to activity could be explained by altered ability of the lid domain to close over the substrates for catalysis, thus altering catalysis and changing the activity of the enzymes. The D127N enzyme displayed major changes to ADP binding, thus it was suspected that lid closure would place residue 127 near the ADP binding site. However, these suspicions were found to be incorrect leaving the rationale behind altered ADP binding unknown.

Promiscuity also suggests altered dynamics − The first evidence for altered dynamics within the enzymes was the identification of 'foreign' molecules bound within the active sites of two of the evolved enzymes. Crystallisation of the I264F enzyme, as well as thermal shift assays in BTP buffer demonstrate that BTP binds within the active site of the enzyme. In addition, a small molecule crystal soak of the T462I enzyme resulted in the activator, FBP, binding in the active site, 40 Å away from its correct binding site in the allosteric domain. Given the lack of change in the crystal structures of the evolved enzymes, it is likely that the binding promiscuity seen here is a result of increased flexibility of substrate binding loops, allowing the active site to bind substrates with different shapes and sizes.

In conclusion, the results confirm that adaptation has not changed the structure − it keeps the fold. These studies demonstrate the robust nature of the *E. coli* PK1 structure, where substitution mutations significantly alter the enzymes function, but have no effect upon the structure of the tetramer. Nevertheless, the dramatic changes to the function may be explained by differences in the dynamic behaviour of the enzymes, which will be addressed in the next chapter.

5.7 References

[1] Ingram, VM. (1957) Gene mutations in human haemoglobin: the chemical difference between normal and sickle cell haemoglobin, *Nature 180*, 326-328.

[2] Zhu, T. (2008) Evolution of pyruvate kinase in the long-term evolution study of *Escherichia coli*: A structure/function study, In *Biological Sciences*, University of Canterbury.

[3] Maiorov, VN, and Crippen, GM. (1994) Significance of root-mean-square deviation in comparing three-dimensional structures of globular proteins, *J. Mol. Biol. 235*, 625-634.

[4] Carugo, O, and Pongor, S. (2001) A normalized root-mean-square distance for comparing protein three-dimensional structures, *Protein Sci. 10*, 1470-1473.

[5] Irving, JA, Whisstock, JC, and Lesk, AM. (2001) Protein structural alignments and functional genomics, *Proteins 42*, 378-382.

[6] Krissinel, E, and Henrick, K. (2007) Inference of macromolecular assemblies from crystalline state, *J. Mol. Biol. 372*, 774-797.

[7] Mattevi, A, Valentini, G, Rizzi, M, Speranza, ML, Bolognesi, M, and Coda, A. (1995) Crystal structure of *Escherichia coli* pyruvate kinase type I: Molecular basis of the allosteric transition, *Structure 3*, 729-741.

[8] Mattevi, A, Bolognesi, M, and Valentini, G. (1996) The allosteric regulation of pyruvate kinase, *FEBS Lett. 389*, 15-19.

[9] Morgan, HP, McNae, IW, Nowicki, MW, Hannaert, V, Michels, PAM, Fothergill-Gilmore, LA, and Walkinshaw, MD. (2010) Allosteric mechanism of pyruvate kinase from *Leishmania mexicana* uses a rock and lock model, *J. Biol. Chem. 285*, 12892-12898.

[10] Morgan, HP, Zhong, W, McNae, IW, Michels, PAM, Fothergill-Gilmore, LA, and Walkinshaw, MD. (2014) Structures of pyruvate kinases display evolutionarily divergent allosteric strategies, *R. Soc. Open. Sci. 1*, 140120.

[11] Lovell, SC, Mullick, AH, and Muirhead, H. (1998) Cooperativity in *Bacillus stearothermophilus* pyruvate kinase, *J. Mol. Biol. 276*, 839-851.

[12] Ikeda, Y, Tanaka, T, and Noguchi, T. (1997) Conversion of non-allosteric pyruvate kinase isozyme into an allosteric enzyme by a single amino acid substitution, *J. Biol. Chem. 272*, 20495-20501.

[13] Valentini, G, Chiarelli, L, Fortini, R, Speranza, ML, Galizzi, A, and Mattevi, A. (2000) The allosteric regulation of pyruvate kinase: A site-directed mutagenesis study, *J. Biol. Chem. 275*, 18145-18152.

[14] Fenton, AW, and Blair, JB. (2002) Kinetic and allosteric consequences of mutations in the subunit and domain interfaces and the allosteric site of yeast pyruvate kinase, *Arch. Biochem. Biophys. 397*, 28-39.

[15] Pendergrass, DC, Williams, R, Blair, JB, and Fenton, AW. (2006) Mining for allosteric information: natural mutations and positional sequence conservation in pyruvate kinase, *IUBMB Life 58*, 31-38.

[16] Zhong, W, Morgan, HP, Nowicki, MW, McNae, IW, Yuan, M, Bella, J, Michels, PA, Fothergill-Gilmore, LA, and Walkinshaw, MD. (2014) Pyruvate kinases have an intrinsic and conserved decarboxylase activity, *Biochem. J. 458*, 301-311.

[17] Fenton, AW, Williams, R, and Trewhella, J. (2010) Changes in small angle X-ray scattering parameters observed upon ligand binding to rabbit muscle pyruvate kinase are not correlated with allosteric transitions, *Biochemistry 49*, 7202-7209.

[18] Larsen, TM, Benning, MM, Rayment, I, and Reed, GH. (1998) Structure of the bis(Mg2+)-ATP-oxalate complex of the rabbit muscle pyruvate kinase at 2.1 A resolution: ATP binding over a barrel, *Biochemistry 37*, 6247-6255.

[19] Putnam, CD, Hammel, M, Hura, GL, and Tainer, JA. (2007) X-ray solution scattering (SAXS) combined with crystallography and computation: defining accurate macromolecular structures, conformations and assemblies in solution, *Q. Rev. Biophys. 40*, 191-285.

[20] Wall, ME. (2012) *Quatitative Biology: From molecular to cellular systems*, CRC Press.

[21] Svergun, DI. (1992) Determination of the regularization parameter in indirect-transform methods using perceptual criteria, *J. Appl. Crystallogr. 25*, 495-503.

[22] Petoukhov, MV, Konarev, PV, Kikhney, AG, and Svergun, DI. (2007) ATSAS 2.1 - towards automated and web-supported small-angle scattering data analysis., *J. Appl. Crystallogr. 40*, s223–s228.

[23] Svergun, D, Barberato, C, and Koch, M. (1995) CRYSOL-a program to evaluate X-ray solution scattering of biological macromolecules from atomic coordinates, *J. Appl. Crystallogr. 28*, 768-773.

[24] Skou, S, Gillilan, RE, and Ando, N. (2014) Synchrotron-based small-angle X-ray scattering of proteins in solution, *Nat. Protoc. 9*, 1727-1739.

5.8 Supplementary

Table S5.1 **X-ray data collection statistics.** Statistical values for the highest resolution shells are given in parentheses.

	Escherichia coli type PK1-P70Q
Data-collection statistics	
Wavelength (Å)	0.9537
Number of images	360
Oscillations (°)	0.5
Space group	$C222_1$
Cell parameters *a*, *b*, *c*, *α*, *β*, γ (Å; º)	73.54, 242, 133.8; 90, 90, 90
Mol/asym. unit	2
Resolution range (Å)	48.47-2.64 (2.77-2.64)
Unique reflections	33,796 (3,236)
Mean I/σ(I)	19.1 (2.5)
Completeness (%)	94.8 (70.1)
R_{merge} †	0.087 (0.631)
Multiplicity	7.2 (6.1)
Refinement details	
Resolution (Å)	2.64
R_{work}/R_{free} ‡ (%)	19.9/24.3
Ramachandran plot, residues in (%)	
Most favoured regions	96.63
Additionally allowed regions	3.16
Disallowed regions	0.22
All-atom clashscore	3.71

	Escherichia coli type PK1-P70T
Data-collection statistics	
Wavelength (Å)	0.9537
Number of images	360
Oscillations (°)	0.5
Space group	$C222_1$
Cell parameters *a*, *b*, *c*, *α*, *β*, γ (Å; º)	76.85, 244.4, 131.8; 90, 90, 90
Mol/asym. unit	2
Resolution range (Å)	44.80-2.10 (2.14-2.10)
Unique reflections	72,220 (4,159)
Mean I/σ(I)	15.8 (2.4)
Completeness (%)	99.4 (93.7)
R_{merge} †	0.080 (0.694)
Multiplicity	5.1 (5.1)
Refinement details	
Resolution (Å)	2.10
R_{work}/R_{free} ‡ (%)	19.3/23.1
Ramachandran plot, residues in (%)	
Most favoured regions	96.85
Additionally allowed regions	2.82
Disallowed regions	0.33
All-atom clashscore	1.71

	Escherichia coli type PK1-D127N
Data-collection statistics	
Wavelength (Å)	0.9537
Number of images	360
Oscillations (°)	0.5
Space group	$P2_1$
Cell parameters *a*, *b*, *c*, β (Å; º)	76.14, 131.6, 129.1; 107.1
Mol/asym. unit	4
Resolution range (Å)	48.80-2.32 (2.36-2.32)
Unique reflections	103,257 (4,814)
Mean I/σ(I)	19.1 (2.5)
Completeness (%)	94.8 (70.1)
R_{merge} †	0.087 (0.631)
Multiplicity	8.2 (1.4)
Refinement details	
Resolution (Å)	2.32
R_{work}/R_{free} ‡ (%)	21.1/25.9
Ramachandran plot, residues in (%)	
Most favoured regions	96.80
Additionally allowed regions	3.04
Disallowed regions	0.16
All-atom clashscore	8.46

	Escherichia coli type PK1-I264F
Data-collection statistics	
Wavelength (Å)	0.9537
Number of images	360
Oscillations (°)	0.5
Space group	$C222_1$
Cell parameters *a*, *b*, *c*, α, β, γ (Å; º)	74.87, 244.9, 134.3; 90, 90, 90
Mol/asym. unit	2
Resolution range (Å)	48.98-2.88 (3.04-2.88)
Unique reflections	162,311 (23,320)
Mean I/σ(I)	12.5 (2.8)
Completeness (%)	99.9 (99.4)
R_{merge} †	0.149 (0.623)
Multiplicity	5.7 (5.7)
Refinement details	
Resolution (Å)	2.88
R_{work}/R_{free} ‡ (%)	18.4/24.0
Ramachandran plot, residues in (%)	
Most favoured regions	96.10
Additionally allowed regions	3.80
Disallowed regions	0.11
All-atom clashscore	3.12

	Escherichia coli type PK1-A301S
Data-collection statistics	
Wavelength (Å)	0.9537
Number of images	360
Oscillations (°)	0.5
Space group	$P2_1$
Cell parameters *a*, *b*, *c*, *α*, *β*, γ (Å; º)	129.3, 74.47, 240.8; 90.00, 90.04, 90.00
Mol/asym. unit	8
Resolution range (Å)	48.17-2.00 (2.03-2.00)
Unique reflections	305,954 (14,348)
Mean I/σ(I)	10.2 (1.2)
Completeness (%)	98.4 (93.8)
R_{merge} †	0.087 (0.631)
Multiplicity	7.7 (7.3)
Refinement details	
Resolution (Å)	2.00
R_{work}/R_{free} ‡ (%)	18.0/20.3
Ramachandran plot, residues in (%)	
Most favoured regions	94.47
Additionally allowed regions	4.81
Disallowed regions	0.72
All-atom clashscore	14.17

	Escherichia coli type PK1-A301T
Data-collection statistics	
Wavelength (Å)	0.9537
Number of images	360
Oscillations (°)	0.5
Space group	$C222_1$
Cell parameters *a*, *b*, *c*, *α*, *β*, γ (Å; º)	75.22, 247.07, 130.71; 90, 90, 90
Mol/asym. unit	2
Resolution range (Å)	130.71-2.01 (2.12-2.01)
Unique reflections	80,638 (10,818)
Mean I/σ(I)	13.6 (2.8)
Completeness (%)	98.9 (92.3)
R_{merge} †	0.094 (0.499)
Multiplicity	7.0 (5.1)
Refinement details	
Resolution (Å)	2.01
R_{work}/R_{free} ‡ (%)	14.9/19.8
Ramachandran plot, residues in (%)	
Most favoured regions	97.64
Additionally allowed regions	1.93
Disallowed regions	0.43
All-atom clashscore	2.36

	Escherichia coli type PK1-G381A
Data-collection statistics	
Wavelength (Å)	0.9537
Number of images	360
Oscillations (°)	0.5
Space group	$P2_1$
Cell parameters *a*, *b*, *c*, *α*, *β*, γ (Å; º)	76.4, 131.4, 129.4; 90, 107.2, 90
Mol/asym. unit	4
Resolution range (Å)	48.84-2.45 (2.50-2.45)
Unique reflections	82,083 (2,766)
Mean I/σ(I)	22.1 (2.2)
Completeness (%)	91.6 (56.5)
R_{merge} †	0.028 (0.466)
Multiplicity	3.4 (2.2)
Refinement details	
Resolution (Å)	2.45
R_{work}/R_{free} ‡ (%)	22.1/26.5
Ramachandran plot, residues in (%)	
Most favoured regions	93.49
Additionally allowed regions	6.01
Disallowed regions	0.49
All-atom clashscore	8.23

	Escherichia coli type PK1-T462I
Data-collection statistics	
Wavelength (Å)	0.9537
Number of images	360
Oscillations (°)	0.5
Space group	$C222_1$
Cell parameters *a*, *b*, *c*, *α*, *β*, γ (Å; º)	74.68, 247.4, 130; 90, 90, 90
Mol/asym. unit	2
Resolution range (Å)	48.09-2.25 (2.31-2.25)
Unique reflections	57,553 (4,433)
Mean I/σ(I)	11.4 (2.0)
Completeness (%)	100 (100)
R_{merge} †	0.117 (0.984)
Multiplicity	7.4 (7.5)
Refinement details	
Resolution (Å)	2.25
R_{work}/R_{free} ‡ (%)	18.5/23.3
Ramachandran plot, residues in (%)	
Most favoured regions	96.20
Additionally allowed regions	3.70
Disallowed regions	0.11
All-atom clashscore	3.00

Chapter Six

Adaptive evolution fine-tunes protein dynamics

Part 1 – Evolved enzymes have different dynamics

This chapter uses specialised dynamic techniques to identify and describe the importance of dynamics for the catalysis and regulation of *Escherichia coli*'s pyruvate kinase type 1 (PK1) activity. Firstly, Part 1 of this chapter uses molecular dynamics simulations to identify dynamic differences between the wild-type and the evolved enzyme, A301T. Next, hydrogen-deuterium exchange (HDX) experiments were employed 'globally' to provide information regarding the overall flexibility of whole proteins, confirming that the overall dynamics of each of the evolved enzymes is different to the wild-type. Additional localised dynamic analyses were used to distinguish site-specific regions with varying degrees of conformational flexibility in four of the evolved enzymes. The results identify differences in conformational flexibility of key regions of the evolved proteins compared to the wild-type. These analyses suggest that adaptive evolution may occur through natural selection for enzymes with different dynamics.

6.1 Introduction

Having established that the dramatic changes to the kinetic behaviour of the evolved enzymes (Chapter Four) can not be explained by the structure (Chapter Five), I hypothesise that the kinetic and allosteric responses are a result of altered conformational dynamics. This chapter describes dynamic analyses that firstly test whether the evolved enzymes have different dynamic behaviours to the wild-type and secondly, whether dynamics can explain the altered allosteric responses.

Although the X-ray crystal structures provided an atomic resolution model for each of the evolved enzymes (Chapter Five), information regarding the conformational fluctuations of the enzymes was limited to B-factor analyses only. This chapter uses molecular dynamics simulations combined with HDX to show that the evolved enzymes have different dynamic behaviours to the wild-type. Molecular dynamics simulations demonstrated differences in dynamics between the wild-type and A301T enzymes by monitoring the root-mean-square fluctuation (RMSF) of atoms over time. Whereas, time-resolved electrospray ionisation mass spectrometry coupled to hydrogen-deuterium exchange (TRESI-MS/HDX) experimentally assessed the dynamics of each of the evolved enzymes showing differences in overall dynamics compared to the wild-type.

To identify site-specific changes in dynamics between the evolved enzymes and the wild-type, TRESI-MS/HDX was implemented for the study of function-related conformational changes. This was peformed on the millisecond to second timescale for four of the evolved enzymes and comparisons were made to the wild-type enzyme.[1-4] The rapid labelling time enabled characterisation of intrinsically disordered regions of proteins (weak α-helices and β-sheets) whose conformational flexibility (‘breathing motion’) results in rapid exchange of hydrogens with deuterium from the solvent. Rigid regions of protein (strong secondary structure segments) mostly exist in an ‘exchange-incompetent’ state, where amide protons are occupied by hydrogen bonds. However, these regions can experience transient ‘breathing motions’ which briefly disrupt the amide hydrogen bonds and provide solvent contact for isotope exchange.[5-7] Here, the results demonstrate that each of the evolved enzymes show different localised dynamics compared to the wild-type and to each other, confirming that natural selection has selected for mutations that alter the

dynamics of enzymes. But have the altered dynamics contributed to the different allosteric responses?

For years, it has been accepted that changes in enzyme structures are not induced by an allosteric binding event, but are an artefact of a higher proportion of the population existing in that conformational state.[8] However, because proteins are inherently dynamic molecules, existing as an ensemble of conformations constantly sampling conformational substates,[9, 10] recent studies have determined that the binding of an allosteric ligand can trigger a shift in the relative occupancy of states, increasing how often a given (activated or inhibited) state is sampled.[11, 12] Therefore, allostery can be described as a ligand binding event causing a change at the substrate binding site via alteration of the structure and/or dynamics of the enzyme.[8, 13]

Dynamics have been shown to play a key role in enzyme function, with many enzymes displaying dynamic responses to binding events, with no obvious conformational changes to the structure.[8] Mutations in the PDZ (second postsynaptic density-95/discs large/zonula occludens-1) domain of the human tyrosine phosphatase 1E protein demonstrated significant changes in binding, altered dynamic effects and no conformational change, suggesting that the mutated residues are important for transmitting the dynamic signal through the domain for binding.[14] Moreover, Popovych *et al.* demonstrated that allostery can be mediated exclusively by changes in protein dynamics without any conformational change.[15] These studies emphasise the importance of conformational flexibility for transmitting the allosteric activation signal between distant sites on a protein.

Here, localised dynamic measurements determine that the evolved enzymes have different dynamic responses to allosteric activation, compared to the wild-type. Dynamic analyses of the evolved enzymes in the absence and presence of the allosteric activator fructose-1,6-bisphosphate (FBP), identifiy changes to the conformational flexibility of key regions within the protein, suggesting the enzymes have evolved different allosteric activation mechanisms. This chapter provides evidence to suggest that natural selection has not only selected for enzymes with altered dynamics (Part 1), but it has used altered dynamics to change allostery (Part 2).

6.2 Molecular dynamics simulations identify dynamic differences between A301T and wild-type

The molecular dynamics simulations described in this section were carried out by collaborators, Ben Porebski and Ashley Buckle (Monash University, Melbourne) using the wild-type and A301T X-ray crystal structures that were presented in Chapters Two and Five. Molecular dynamics simulations were employed (Section 8.8) to evaluate the dynamic potential of the wild-type and A301T enzymes, and the results determine that the enzymes have key differences in their dynamic behaviour.

Initial analysis of the wild-type and A301T enzyme simulations is presented as a RMSF plot of each subunit in the tetramer (Figure 6.1). Comparison of the RMSF plots for wild-type and A301T enzymes demonstrate that the prominent fluctuations are occuring around the A301 mutation site (Figure 6.1). A more detailed analysis of the molecular dyanmics simulations can be found below in Sections 6.2.1 to 6.2.3.

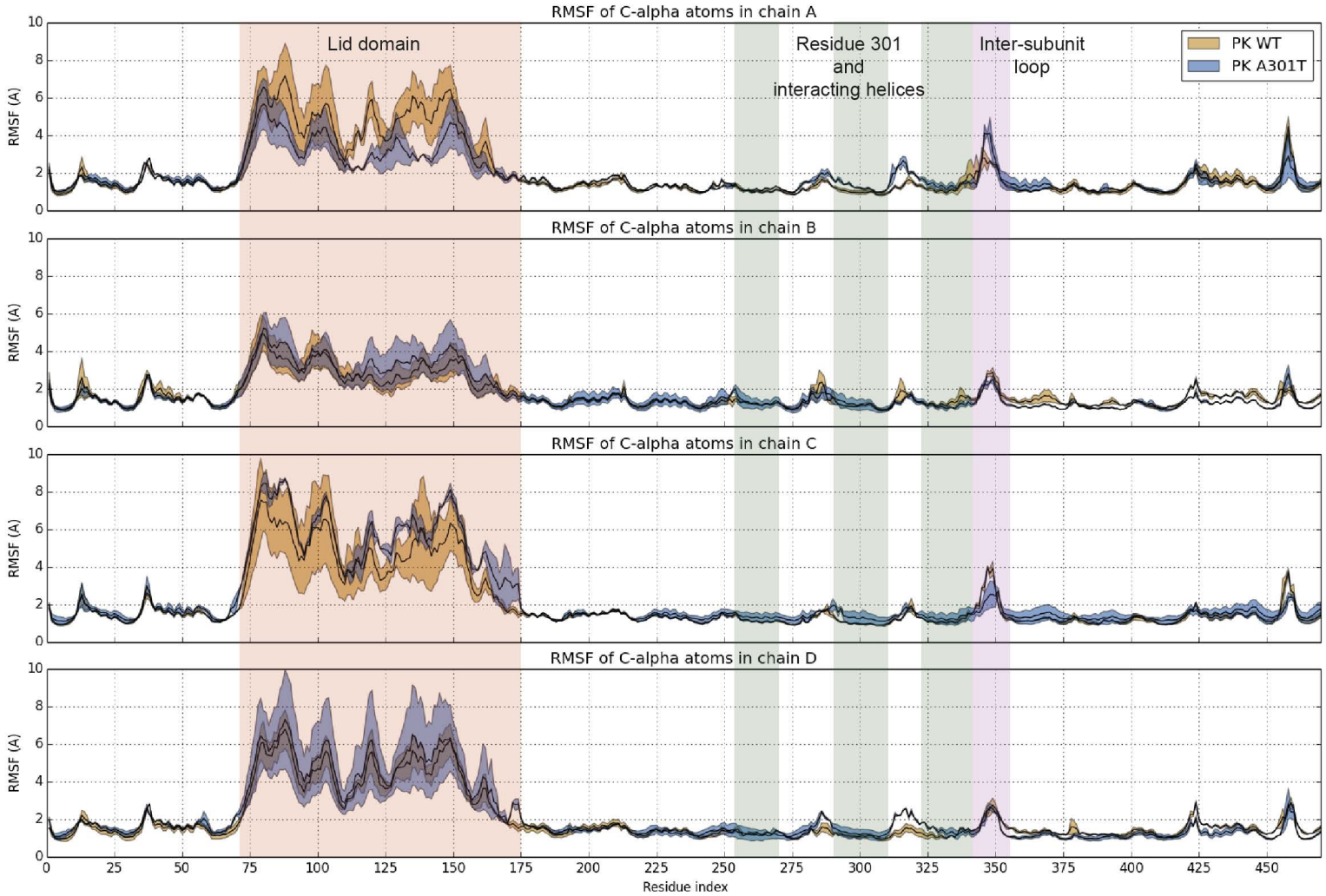

Figure 6.1 RMSF plot of wild-type and A301T simulations, showing mean RMSF averaged over the two simulation replicates (black line), as well as the min/max fluctuations. Each of the subunits is shown separately. The lid domain is highlighted in red, residue 301 and surrounding destabilised helices are highlighted in green and the disordered loop highlighted in purple.

6.2.1 Increased fluctuation of two helices near the A301T mutation site

Initial assessment of the two enzymes demonstrated slight dynamic differences in the structural regions surrounding the A301 mutation site (Figure 6.2). There are three α-helices around the A301 mutation site: the first is the helix containing residue A301 (Aα7'-helix), the second is the Aα6'-helix (Val253−Ala270) and the third is the Aα8'-helix (Pro321−Val338). The analysis determines that the Aα6'- and Aα7'-helices show slight increases in dynamic fluctuation, which can also be seen in Figure 6.1.

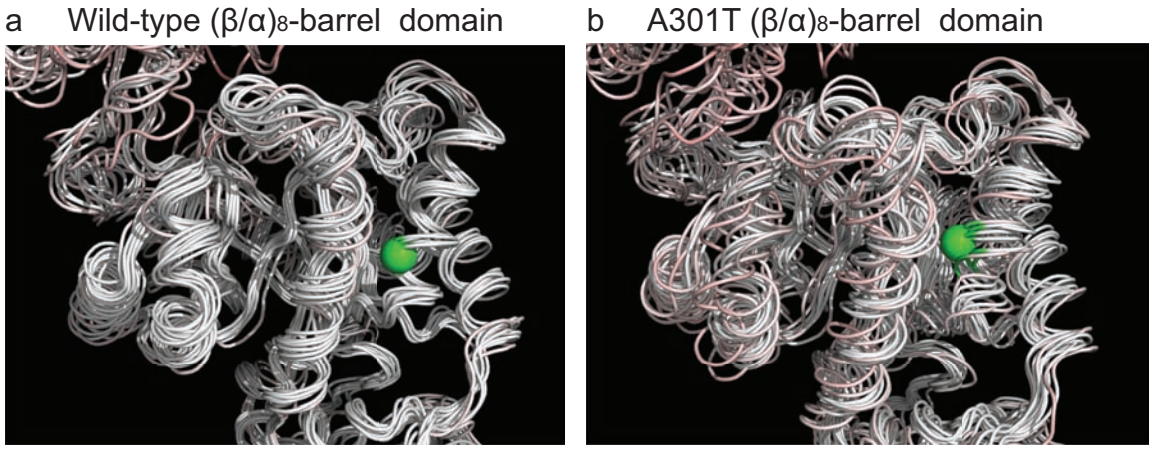

Figure 6.2 Simulation trajectory of the region surrounding residue A301 (green sphere) showing increased fluctuation in the A301T enzyme compared to the wild-type. Snapshots were taken every 50 ns over a 500 ns timespan. The snapshots are aligned and residues are coloured based upon their deviation from the mean, with white being 0 Å and red being >6 Å.

The observed fluctuations are likely a result of introduced rotations caused by the mutation from an alanine to a threonine. In the wild-type enzyme, the slightly hydrophobic A301 residue is situated in a hydrophobic environment that has the potential for rotation into a solvated polar environment. The mutation from hydrophobic alanine to polar threonine would increase the potential for rotation of the helix containing the threonine residue, increasing dynamic fluctuations of the region.

6.2.2 Disordered loop is contracted in the A301T enzyme

Next, the molecular dynamics simulations were assessed for changes in the FBP binding region because kinetic analyses determined that the A301T enzyme has reduced FBP binding affinity compared to the wild-type (Chapter Four). The results show that the mobile loop (344−354) connecting the $(\beta/\alpha)_8$-barrel domain (A-domain) to the allosteric domain (C-domain) is contracted in the A301T enzyme compared to the wild-type (Figure 6.3). In the wild-type crystal structure, the distance between opposing mobile loops is 6.4 Å, whereas, the distance is 16.5 Å in the A301T enzyme. Not only are the mobile loops of A301T contracted in the structure, but they are also contracted throughout the 500 ns of simulation, suggesting that mutation to residue A301 at the A/A' interface has altered the dynamics at the distant allosteric domain.

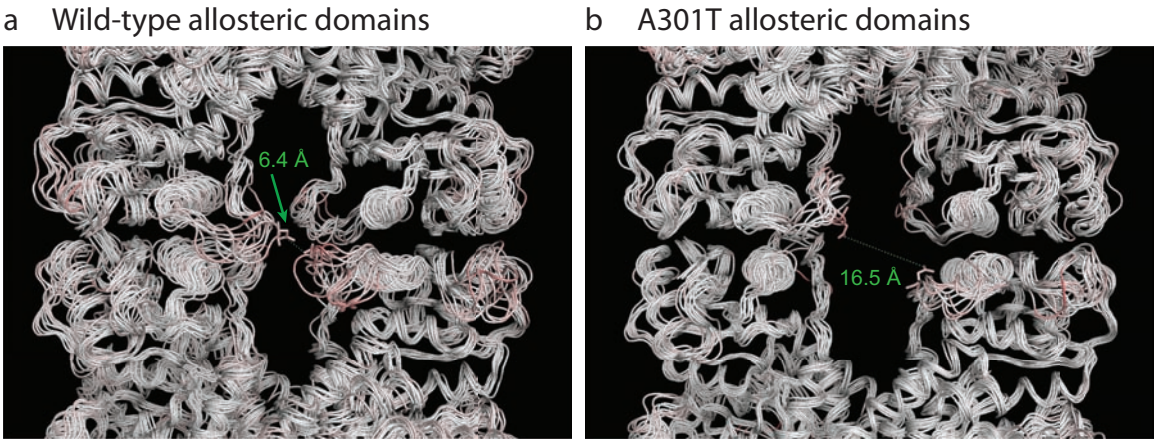

Figure 6.3 Simulation trajectory of the allosteric domains showing the mobile loop is contracted in the A301T enzyme compared to the wild-type. Snapshots were taken every 50 ns over a 500 ns timespan. The snapshots are aligned and residues are coloured based upon their deviation from the mean, with white being 0 Å and red being >6 Å.

Analysis of the allosteric domains of the enzymes suggested that the contraction of the mobile loop in the A301T enzyme could be reducing the FBP binding affinity. The molecular dynamics simulations demonstrate that the mobile loop in the A301T enzyme contracts inwards towards the FBP binding site and due to the charge associated with the loop, this action could sterically or electrically frustrate the binding of FBP within the activator binding pocket.

6.2.3 Lid domains are closer together in A301T compared to wild-type

Finally, the molecular dynamics simulations of the active site regions were analysed to determine whether dynamic fluctuations can explain the reduced PEP binding affinity in the A301T enzyme compared to the wild-type (Chapter Four). In the duplicate simulations and in all four subunits, there is a prominent difference in the dynamics of the lid domains (B-domains) (Figure 6.4) between the A301T and wild-type enzymes. The lid domains of the A301T enzyme are very close together in a conformation that may restrict PEP binding within the active site of the enzyme.

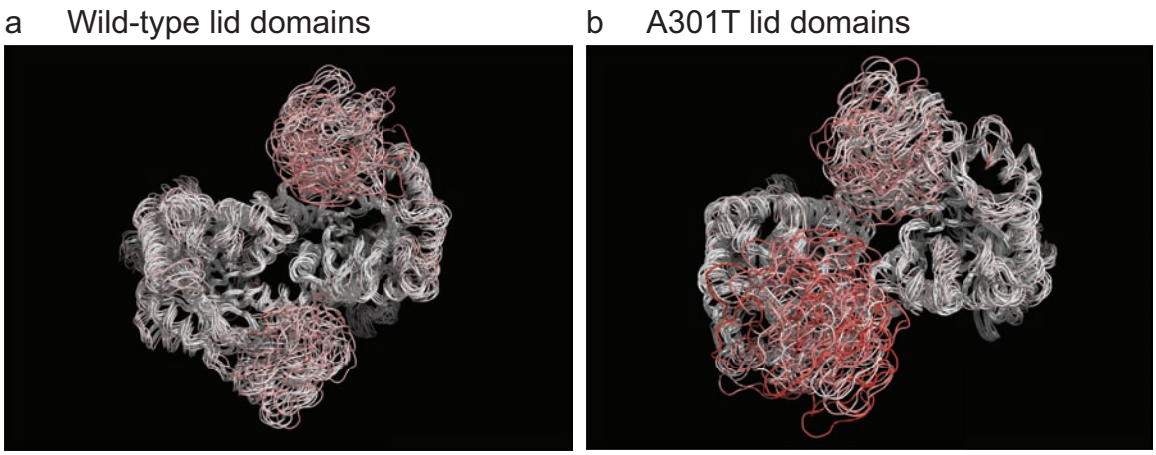

Figure 6.4 Simulation trajectory of lid domains showing the lids of opposing subunits are closer together in the A301T enzyme compared to the wild-type. Snapshots were taken every 50 ns over a 500 ns timespan. The snapshots are aligned and residues are coloured based upon their deviation from the mean, with white being 0 Å and red being >6 Å.

Molecular dynamics simulations of the wild-type and A301T enzymes determine key differences in the dynamics between the two enzymes. Unfortunately, the remaining seven evolved enzymes were not able to be simulated because of the time and computational memory required to run the simulations. Instead, experimental measures (HDX-MS) were used to measure the dynamics of each of the enzymes and these will be described below in Section 6.3.

6.3 Global dynamics of evolved enzymes is altered compared to the wild-type enzyme

To evaluate the overall conformational dynamics of each of the evolved enzymes, global HDX was measured as a time-course (14 ms to 1.5 s) and compared to the wild-type *E. coli* PK1 enzyme. The global HDX data for A301S that is presented here was collected by Peter Liuni (York University, Toronto) because I ran out of time and protein sample during my visit to Canada.

Using HDX to expose the enzymes to deuterium resulted in isotopic exchange of the unprotected backbone hydrogen atoms for deuterium atoms.[5] As deuterium is double the mass of hydrogen, the mass change was monitored as a time-course to show the shift in deuterium exchange over time. The data was fit to an exponential function (Section 3.7) generating kinetic plots of the overall deuterium exchanged into each enzyme (Figure 6.5).

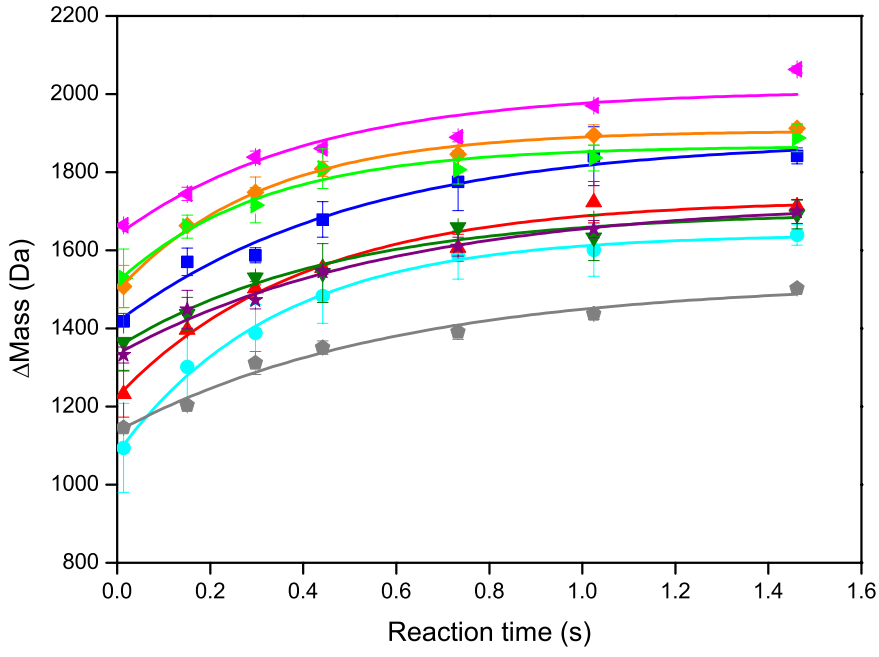

Figure 6.5 Global deuterium exchange kinetics of wild-type PK1 and eight evolved enzymes. The global HDX kinetics were measured for wild-type (blue), P70Q (cyan), P70T (red), D127N (olive), I264F (orange), A301S (magenta), A301T (green), G381A (grey) and T462I (purple). Kinetic data were fit using a single exponential non-linear regression analysis ($y=y0 + a(1-e^{-kt})$).[1] Error bars represent the standard error of the mean (SEM) of three technical replicates.

The global deuterium exchange kinetics (Figure 6.5) provided information regarding side chain flexibility, overall structuredness and rate of conformational sampling of each of the enzymes. These three key pieces of information have been analysed and described below in Sections 6.3.1 to 6.3.3.

6.3.1 Burst phase of exchange in proteins is different

The global kinetic plot demonstrates that all of the enzymes have differences in flexibility and solvent accessibility of 'fast-exchangers'. The burst phase of deuterium exchange (before 14 ms) describes the flexibility of 'fast-exchangers', which are largely the side chain protons with some backbone amide protons.[16] Side chains and solvent accessible amide protons exchange rapidly because they are solvent accessible, thus allowing contact with the deuterated solution for exchange. Amide protons that are inaccessible to solvent or are occupied in stable hydrogen bonds (secondary structures) must experience distortion of local structure to allow solvent access for exchange, therefore their exchange is slower.[17]

The global kinetic plot (Figure 6.5) shows that at the first time point (14 ms) each of the enzymes has a different Δmass, suggesting that the enzymes have different 'burst phases' of deuterium uptake. The A/A' interface evolved enzymes (I264F, A301S and A301T) show the highest burst phase of any of the enzymes, i.e. the largest amount of deuterium exchange within the first 14 ms of the experiment. There is no trend in 'burst phase' among the remaining enzymes, however the variability indicates different solvent accessibility of 'fast exchangers' between the enzymes.

6.3.2 Amplitude of deuterium exchange is different

Assessment of the global kinetic plots (Figure 6.5) confirms the prediction that the enzymes have differences in their conformational flexibility compared to the wild-type enzyme. The maximum amount (amplitude) of deuterium exchanged into each enzyme was varied: G381A displays the lowest amount of exchange (~Δ1500 Da at 1.4 s) suggesting that it is the most structured protein, and A301S shows the highest exchange (~Δ2000 Da at 1.4 s), implying it is the most unstructured of the nine enzymes analysed.

One result common to the site of mutation, is that all three mutations at the A/A' interface appear to have more conformational flexibility than the wild-type enzyme. The I264F, A301S and A301T enzymes all have a higher amplitude of deuterium exchange at the pleateu of 1.4 s. This result suggests that mutations to the A/A' interface can have a negative impact upon overall amide protection by increasing the number of unprotected amide hydrogens contacting and exchanging with the deuterated solvent.

6.3.3 Rate of deuterium uptake is different

Finally, initial rate analysis determined that each of the evolved enzymes have varying rates of deuterium exchange compared to the wild-type enzyme. The initial rate of deuterium exchange was extrapolated from the exponential fit to the kinetic data, and this is displayed below as a bar graph (Figure 6.6).

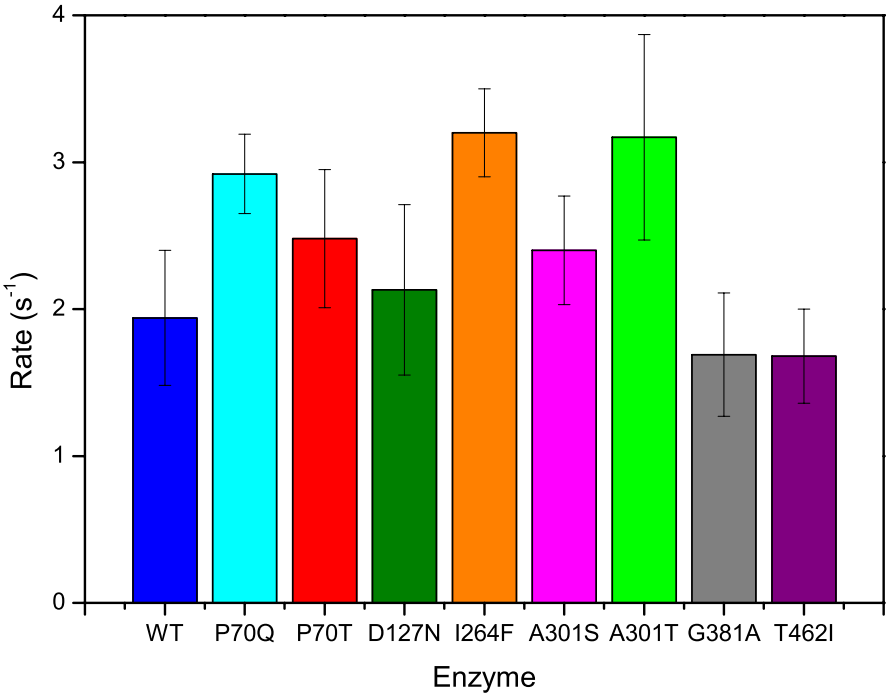

Figure 6.6 Rate of global deuterium exchange for wild-type PK1 and eight evolved enzymes. The rate of global HDX was measured for wild-type (blue), P70Q (cyan), P70T (red), D127N (olive), I264F (orange), A301S (magenta), A301T (green), G381A (grey), and T462I (purple). The rate was derived by fitting the kinetic data using a single exponential non-linear regression analysis ($y=y0 + a(1-e^{-kt})$).[1] Error bars represent the SEM of three technical replicates.

The rate of deuterium uptake into a protein is dependent upon the globally averaged dynamic conformational sampling of the protein over time – if a protein explores its conformational space rapidly, then it will have a higher rate of deuterium uptake and vice versa.

Figure 6.6 displays the rate of deuterium uptake derived from the global HDX kinetic plots for wild-type and the eight evolved enzymes. The wild-type enzyme acts as a reference for comparison with the evolved enzymes and has a deuterium uptake rate of $1.9 \pm 0.5\ s^{-1}$. The two enzymes with mutations at the allosteric site (G381A and T462I) display similar uptake rates of $1.7 \pm 0.4\ s^{-1}$ and $1.7 \pm 0.3\ s^{-1}$, respectively. These uptake rates are slightly lower than the wild-type, suggesting they have a decreased rate of conformational sampling compared to the wild-type enzyme. Two A/A' interface mutations, I264F and A301T produce high rates of global conformational sampling, exhibited by deuterium uptake rates of $3.2 \pm 0.3\ s^{-1}$ and $3.2 \pm 0.7\ s^{-1}$, respectively. There are no other trends between rate of deuterium uptake and mutation position, but the key piece of information here is that the enzymes have different rates of conformational sampling compared to the wild-type and to each other.

There is no obvious correlation between the global dynamic behaviour of the enzymes and their functional behaviour identified in Chapter Four. Nevertheless, the global deuterium exchange profiles confirm that the single substitution mutations in each enzyme alters the overall conformational flexibility, demonstrating differences in how structured/protected the enzymes are and how 'fast' they explore conformational space.

6.4 Site-specific analysis of conformational flexibility

The results of this chapter provide evidence to support the idea that evolution by natural selection has selected for enzymes with altered dynamics. In Section 6.3, it was established that all of the evolved enzymes have different overall structuredness and dynamics. Here, TRESI-MS/HDX was implemented to investigate the dynamics of site-specific regions of the evolved enzymes to identify differences that may help to explain how the enzymes function so differently while maintaining the same structure. In this

section, TRESI-MS/HDX measures the conformational flexibility of specific regions of four of the eight evolved enzymes and compares them to the wild-type. Unfortunately, these localised experiments were limited to four of the eight evolved enzymes because of time restraints.

The A301S, P70T, T462I and A301T enzymes were chosen for analysis based upon their functional behaviour observed in Chapter Four, where each was chosen from one of the four groups identified in Figure 4.5, Section 4.3. The groups were separated based upon the enzymes response to activators, PEP and FBP, to provide a dynamic example for each observed functional behaviour.

- Group one enzymes are P70T and D127N – these enzymes have a lower activity than wild-type and have a $S_{0.5}^{PEP/FBP}$ of less than 0.5 mM.
- Group two enzymes are I264F and A301T – these enzymes have a lower activity than wild-type and have a $S_{0.5}^{PEP/FBP}$ of more than 0.5 mM.
- Group three enzymes are G381A and T462I – these enzymes have a higher activity than wild-type and have a $S_{0.5}^{PEP/FBP}$ of more than 0.5 mM.
- Group four enzymes are P70Q and A301S – these enzymes have a higher activity than wild-type and have a $S_{0.5}^{PEP/FBP}$ of less than 0.5 mM.

The localised TRESI-MS/HDX experiments were carried out on P70T (Group one), A301T (Group two), T462I (Group three) and A301S (Group four) and compared to the wild-type in Sections 6.4.1 to 6.4.4 below.

6.4.1 Pattern of dynamics is altered in the evolved enzymes

The TRESI-MS/HDX experiments utilised a continuous protein-deuterium mixing device which provided rapid labelling times of 59 ms to 1 s. The on-chip digestion and electrospray resulted in an effective system, providing >50% sequence coverage with an average spatial resolution of 10 amino acids for each enzyme. A comparison of the exchange profiles of the wild-type and evolved enzymes uncovers regions that have significant changes in local backbone dynamics (Figure 6.7). The localised HDX data for A301S was collected by Shaolong Zhu (York University, Toronto) because I ran out of time and protein sample during my visit to Canada.

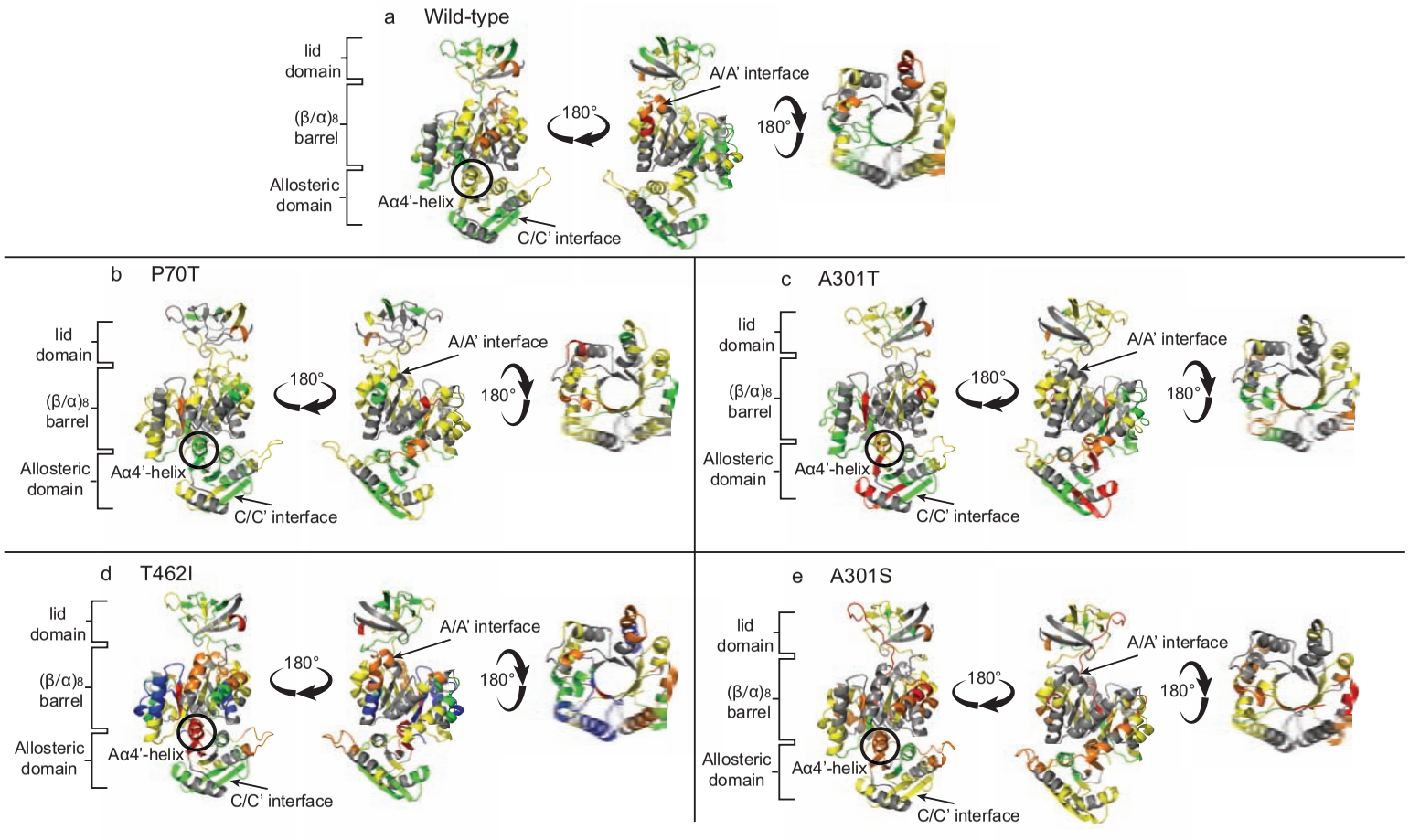

Figure 6.7 Average deuterium exchange mapped and colour-coded onto the structures of wild-type and four evolved enzymes, P70T, A301T, T462I and A301S. Images view both sides of the subunit and looking down the $(\beta/\alpha)_8$-barrel of **(a)** Wild-type, **(b)** P70T, **(c)** A301T, **(d)** T462I and **(e)** A301S. The colour spectrum indicates the level of exchange: blue to red; low to high exchange, respectively. The grey regions were not identified in the HDX experiment. The Aα4'-helix (residues 398−408) at the A/C domain interface is circled in black.

Analysis of the deuterium exchanged into each of the proteins shows differences in the conformational flexibility of key structural regions, which are discussed further in sections 6.4.1.1 to 6.4.1.4.

6.4.1.1 Tetrameric interfaces are similar between wild-type and evolved enzymes

Evaluation of the tetrameric interfaces of each enzyme determined that the dynamics of both interfaces are similar between the wild-type and evolved enzymes (Figure 6.7). The importance of the tetrameric interfaces has been well stated throughout the pyruvate kinase (PK) literature, with studies demonstrating that the A/A' and C/C' interfaces are critical for enabling subunit rotations upon activation by FBP.[18-21] Here, the deuterium exchange in the peptides at the tetrameric interfaces was analysed to determine whether the single substitution mutations have altered the conformational flexibility of the A/A' and C/C' interfaces.

The final β-strand of each subunit forms the C/C' interface and this presented a deuterium exchange range of 21−40% in the wild-type, P70T, T462I and A301T enzymes. However, the A301S enzyme shows a slightly higher exchange for this peptide of 41−60%, suggesting a slight increase in conformational flexibility at the C/C' interface.

Comparison of the A/A' interfaces demonstrates similar exchange levels in the measured enzymes, with wild-type and T462I both showing 61−80% deuterium exchange and P70T showing slightly reduced exchange of 41−60%. The A301S and A301T enzymes have been excluded from the A/A' interface analysis because the peptides that form this interface were not identified in the experiment.

6.4.1.2 A/C domain interfaces vary between wild-type and evolved enzymes

The A/C domain interface of each enzyme was analysed, demonstrating variability amongst the wild-type and evolved enzymes (Figure 6.7). Structural studies of several PK enzymes have led to two possible activation mechanisms that both describe a significant involvement of the A/C domain interface for conformational change upon FBP binding. Moreover, the results in Chapter Three − Part 1 showed strong evidence to suggest that disorder at the A/C domain interface is important for transferring the activation signal from the allosteric site to the active site. Since the evolved enzymes show significant differences in their activation response with no change in structure, it is important that the

conformational flexibility of the A/C domain interface be analysed to identify any differences that may be contributing to the altered kinetic responses.

The peptides at the A/C domain interface of the wild-type act as a reference for comparison with the evolved enzymes and they show moderate exchange in the 41−60% range, which is the same as the A301T enzyme. The P70T enzyme displays a lower exchange (21−40%) than the wild-type, suggesting decreased conformational flexibility. However, the A301S and T462I enzymes show increased exchange of the A/C domain interface, demonstrating increased conformational flexibility. The A301S enzyme displays 61−80% deuterium exchange at the A/C domain interface and T462I shows an even bigger increase in exchange of 81−100%. The proposed allosteric activation mechanism in Chapter Three − Part 2 involves disorder at the inter-domain interface to send the activation signal. Therefore, the significant increase in disorder of the A/C domain interface seen here in response to mutations, especially T462I, could imply that the activation signal can be transferred without the need for FBP binding.

6.4.1.3 Significant variability in substrate binding loops of wild-type and evolved enzymes

Analysis of the active sites of the wild-type and four evolved enzymes shows significant variability in conformational flexibility of the substrate binding loops (Figure 6.7). Structural studies in Chapter Five suggested that the enzymes have evolved substrate binding promiscuity because two of the enzymes (I264F and T462I) were found to bind foreign molecules in their active sites. Here, deuterium exchange analyses were used to investigate the conformational flexibility of substrate binding loops to see if the flexibility of these loops can be identified and quantified, and to determine whether the other evolved enzymes show a similar behaviour.

The deuterium exchange results demonstrate a significant amount of variability in the conformational flexibility of the substrate binding loops. The substrate binding loops of the wild-type enzyme show moderate exchange of approximately 21−60%. Similarly, the A301S, P70T and A301T enzymes also display moderate exchange within the 21−60% region. However, they each show increased flexibility (61−80%) in at least one of their substrate binding loops. The T462I enzyme shows different behaviour to the other enzymes, with two substrate binding loops showing only 1−20% exchange, suggesting they are much more stabilised compared to the other four enzymes. Kinetic analyses in Chapter Four suggest that the enzymes have evolved altered flexibility of substrate binding

loops, allowing the active site to bind substrates with different shapes and sizes. Here, the exchange results confirm this prediction by showing variability in the conformational flexibility of these loops.

6.4.1.4 Allosteric activator binding sites are similar between wild-type and evolved enzymes

Finally, the dynamics of the FBP binding site is explored for the wild-type and evolved enzymes and shows that they have similar deuterium exchange, corresponding to a similar level of conformational flexibility. Measuring the dynamics at the allosteric FBP binding site is important because the evolved enzymes all demonstrate different FBP binding affinities to the wild-type (Chapter Four) and since the structures are similar (Chapter Five), it is likely that these differences are caused by altered flexibility. Here, the focus is on the flexibility of the allosteric domain, which is where the FBP molecule binds to allosterically activate the enzyme.

The results determine that the allosteric domain of the wild-type enzyme displays moderate exchange of 21−60%. Similarly, three of the evolved enzymes, A301S, P70T and T462I also show moderate deuterium exchange (21−60%) in the allosteric domain, suggesting that the flexibility within this domain is similar between the enzymes. However, the A301T enzyme shows a significant increase in deuterium exchange in part of the allosteric domain. Although the region with high exchange (81−100%) is not involved in FBP binding, it is still interesting that this section of the domain is very conformationally flexible.

Analysis of the wild-type enzyme in the presence and absence of FBP (Chapter Three Part 2) shows siginificant deuterium exchange changes upon the addition of FBP. Therefore, in Part 2, the effect of FBP presence upon these four evolved enzymes will be discussed and compared to the wild-type results to establish how the dynamic response to FBP has changed.

6.5 Summary of Part 1

The results presented here provide strong evidence that dynamics play a key role in mediating enzyme function. Here, dynamic analyses using a combination of computational and experimental techniques confirm that the eight enzymes have evolved significant changes to their overall dynamic behaviour, as well as changes to the conformational flexibility of key structural regions within the proteins.

Molecular dynamics simulations identifiy significant differences in the structural fluctuations of the A301T enzyme compared to the wild-type. Molecular dynamics simulations were implemented using the X-ray structures of the wild-type and A301T enzymes to measure the RMSF of atoms over time. As expected, the region surrounding the mutation site displayed altered dynamics compared to the wild-type, with the A301T mutation introducing disorder at the tetrameric A/A' interface. In addition, the analysis showed that mutation of the A/A' interface residue altered the conformational flexibility of the distant activator binding region, and lid domain. This result demonstrates that the changes are not limited to the mutation site.

Hydrogen-deuterium exchange experiments confirmed that all of the enzymes have evolved different overall structuredness and rates of conformational sampling compared to the wild-type enzyme. Conformational flexibility facilitates the structural changes neccesary for conformational sampling, allowing proteins to fluctuate between different conformers which have different binding affinities for the substrates and ligand.[10, 22, 23] The differences in flexibility of the evolved enzymes suggests that they have altered conformational behaviour to the wild-type, which is likely contributing to the changed functional behaviours. Adding to this idea, localised TRESI-MS/HDX analysis showed varying degrees of conformational flexibility in key regions of the wild-type and evolved enzymes. Overall, the HDX results provide strong evidence that the conformational flexibility of the evolved *E. coli* PK1 enzymes has changed compared to the wild-type.

Although the dynamic analyses presented here confirm that the evolved enzymes have altered conformational flexibility compared to the wild-type, the results do not explain why the enzymes have altered allosteric responses to the activator, FBP. It is therefore important that dynamic information is gathered in the presence of FBP to identify changes

to conformational flexibility that are induced by the binding of the activator. Part 2 of this chapter uses TRESI-MS/HDX to investigate the dynamic response to FBP in these four evolved enzymes. The dynamic response will then be compared to the wild-type to determine whether the altered activation response is a result of an altered allosteric mechanism.

Chapter Six

Adaptive evolution fine-tunes dynamics

Part 2 – Dynamics are important for allostery

Having established that the dynamics of each of the evolved *E. coli* PK1 enzymes is different, additional dynamic analyses were implemented to assess the effect of allosteric activation by FBP upon conformational flexibility. The results determined that flexibility changes were not limited to the region surrounding the FBP binding site, but were found right across the enzyme. The dynamic response of each of the evolved enzymes was then compared to the wild-type to assess whether the mechanism of allosteric activation has changed. The allosteric activation-induced conformational flexibility in Part 2 of this chapter provides evidence to suggest that natural selection has selected for dynamics that alter enzyme allostery.

6.6 Activation-induced dynamics is altered in the evolved enzymes

Time-resolved electrospray ionisation mass spectrometry coupled to hydrogen deuterium exchange was implemented to investigate allosteric activation induced site-specific changes to enzyme conformational flexbility of four of the evolved enzymes. As mentioned in Part 1, the localised experiments were limited to four of the eight evolved

enzymes because of time restraints. The A301S, P70T, T462I and A301T enzymes were chosen for analysis based upon their functional behaviour observed in Chapter Four, where each was chosen from one of the four groups identified in Figure 4.5, Section 4.3 – Group one = P70T, Group two = A301T, Group three = T462I and Group four = A301S.

Each of the enzymes were analysed in the absence and presence of allosteric activator, FBP, to identify any changes in conformational flexibility caused by allosteric activation. The dynamic responses to FBP were then compared with the wild-type to determine whether the evolved enzymes have altered allosteric activation mechanisms compared to the wild-type.

In this section the proposed allosteric activation mechanism for the wild-type enzyme (Chapter Three – Part 2) is summarised to establish a reference for comparison with the evolved enzymes. The wild-type summary is followed by a description of the dynamic changes induced by FBP binding in four of the evolved enzymes.

6.6.1 Summary of proposed allosteric activation mechanism for wild-type PK1

Chapter Three – Part 2 concludes that the allosteric signal between the allosteric site and the active site is sent via a series of destabilisation events, producing increased conformational sampling of active site loops. The binding of allosteric activator, FBP, causes a significant amount of destabilisation across the enzyme. This result was confirmed using both global and localised deuterium exchange analyses. Here the exchange changes in the wild-type enzyme are restated (Figure 6.8) for easy comparison with the evolved enzymes.

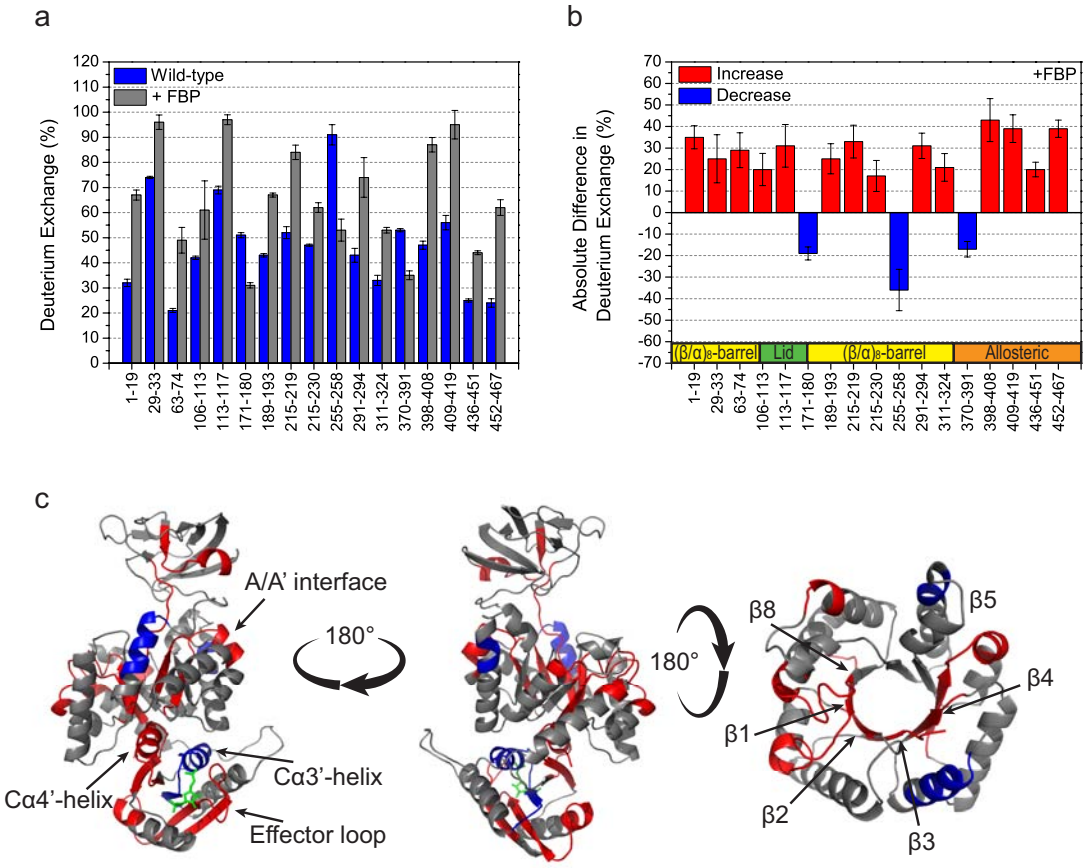

Figure 6.8 Change in average deuterium exchange between the unbound and bound wild-type PK1. **(a)** Amount of deuterium exchange in peptides derived from unbound (blue) and FBP bound (grey) wild-type PK1. **(b)** Absolute differences (>15%) in deuterium exchange are plotted as an increase (red) or a decrease in exchange (blue) when in the presence of FBP. **(c)** Absolute differences (>15%) are mapped onto the wild-type subunit as an increase (red) or a decrease in exchange (blue). The allosteric activator FBP (green stick) has been modelled into the structure to show the binding position based upon the bound structure of A301S. Only peptides with a difference of >15% normalised deuterium exchange are plotted. Data represent an average of triplicate runs and error bars represent the SEM.

The destabilisation events include:

1) The presence of FBP destabilises the effector loop and causes a structural rearrangement, displacing it to allow binding.

2) The FBP then forms interactions with the Cα3'-helix, increasing the stability of the helix and weakening an interaction between the loop preceding Cα3'- and the Cα4'-helix.

3) Destabilisation of the Cα4'-helix results in destabilisation of the inter-domain interface that links the allosteric domain (C-domain) and the $(\beta/\alpha)_8$-barrel (A-domain) within the monomer.

4) Altered interactions of the destabilised Cα4'-helix at the interface between the A- and C-domains and loops $\alpha_2\beta_2$ and $\alpha_3\beta_3$ result in destabilised β-strands following the αβ-loops, consequently producing a more conformationally flexible $(\beta/\alpha)_8$-barrel core. This destabilisation is consistent with the β-strands being involved in allosteric signal transfer through the core of the $(\beta/\alpha)_8$-barrel, to the active site.

5) The signal transfer through the core of the $(\beta/\alpha)_8$-barrel destabilises the substrate binding loops at the active site. I propose that the active site loops then sample a greater number of conformations, some of which facilitate binding of the substrate and catalytic ions. This theory is supported by studies directly assessing the correlation between flexibility and binding, which demonstrated that increased loop flexibility does enhance ligand affinity.[24]

6) The destabilisation of the tetrameric interfaces (A/A' and C/C') decouples the monomers attenuating the PEP homotropic allosteric signal between active sites, explaining why FBP binding blocks the PEP allosteric mechanism.

Now that the wild-type allosteric activation mechanism has been re-stated, the dynamic response of the four evolved enzymes is measured for comparison the with wild-type.

6.6.2 Group one – P70T

Kinetic, structural and dynamic analysis of the P70T evolved enzyme has demonstrated various differences to the wild-type enzyme. Kinetic analysis determined that P70T displays a lower maximal activity to the wild-type enzyme, and has a slight increase in cooperative binding of both activators, PEP and FBP (Chapter Three). The absence of structural differences between the wild-type and P70T enzyme implies that something else has changed to alter the kinetic behaviour. Dynamic analyses (Section 6.3) confirmed that the conformational flexibility has changed. The altered dynamics result was taken one-step further by showing that the P70T enzyme also displays an altered dynamic response to the allosteric activator, FBP. The dynamic response to FBP binding was measured by mapping the deuterium exchange from peptides of unbound and bound P70T (Figure 6.9).

Analysis of Figure 6.9 presents a similar exchange profile between the unbound and bound P70T enzyme, suggesting that FBP binding does not have a significant effect upon the conformational flexibility of structural regions within the enzyme.

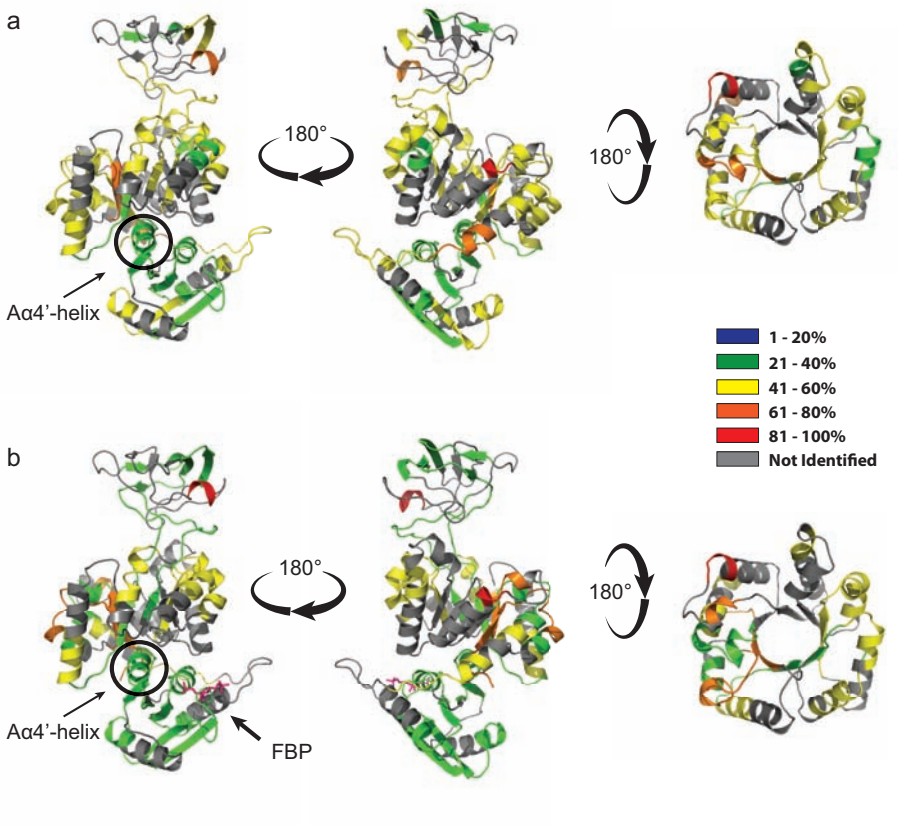

Figure 6.9 Average deuterium exchange mapped and colour-coded onto the P70T structure. **(a)** Unbound P70T viewing both sides of the subunit and looking down the $(\beta/\alpha)_8$-barrel. **(b)** P70T with the allosteric activator, FBP (magenta), modelled into the structure (based upon bound A301S) viewing both sides of the subunit and looking down the $(\beta/\alpha)_8$-barrel. The grey regions were not identified in the HDX experiment. The suspected pivot point (Aα4'-helix, residues 398−408) is circled in black. Only peptides that were identified in both experiments (with and without FBP) are displayed.

Next, the difference in exchange between the unbound and bound P70T were mapped to clearly show the specific regions of protein that have been dynamically altered as a response to FBP binding (Figure 6.10). The differences were mapped as either an increase or decrease of deuterium exchange upon FBP binding, displaying only those peptides that exhibited >5% change in absolute deuterium exchange.

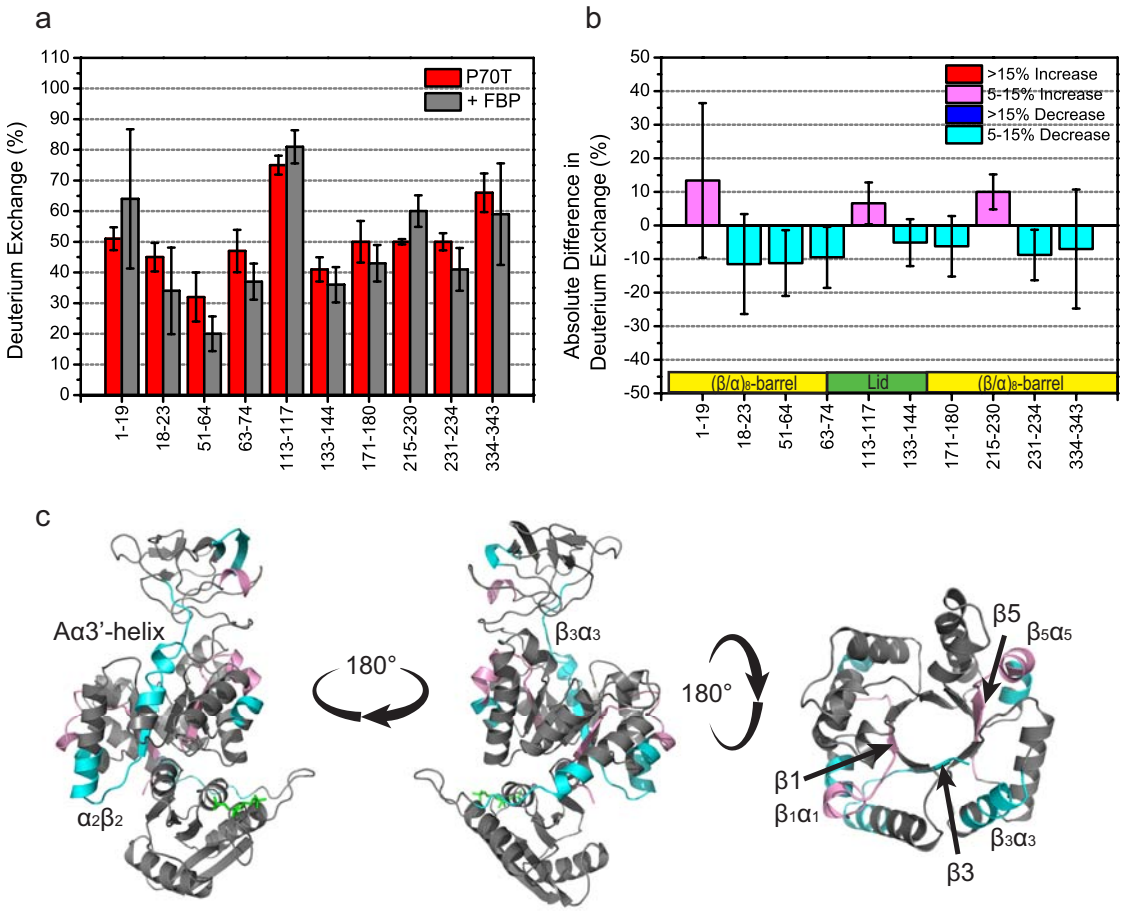

Figure 6.10 Change in average deuterium exchange between the unbound and bound P70T peptides. Displaying only those peptides with >5% change between unbound and bound P70T forms. **(a)** Amount of deuterium exchange in peptides derived from unbound (red) and FBP bound (grey) P70T. **(b)** Absolute differences in deuterium exchange (>5%) are plotted on a bar graph as increases or decreases. **(c)** Absolute differences (>5%) are mapped onto the P70T subunit as high increases (>15%, red), low increases (5−15%, pink), high decreases (>15%, blue) and low decreases in exchange (5−15%, cyan). The allosteric activator FBP (green stick) has been modelled into the structure to show the binding position based upon the bound structure of A301S. Data represent an average of triplicate runs and error bars represent SEM.

6.6.2.1 Stabilisation of the (β/α)$_8$-barrel fold

Unlike the wild-type PK1 enzyme, FBP binding to the allosteric domain of P70T produced an 11% decrease in deuterium exchange of the $\alpha_2\beta_2$-loop (residues 51−64) at the N-terminal end of the $(\beta/\alpha)_8$-barrel. The role of this loop in the activation mechanism is unknown but the N-terminal loops of $(\beta/\alpha)_8$-barrel proteins are said to be important for stabilising the $(\beta/\alpha)_8$-barrel fold.[25]

6.6.2.2 Signalling the P70T catalytic site for activation

The changes in conformational flexibility within the $(\beta/\alpha)_8$-barrel were plotted to identify dynamic changes in the region between the allosteric binding site and the active site. Any changes in this region would suggest that they might be involved in the transfer of the allosteric activation signal between these sites. The results show that FBP binding causes small increases in deuterium exchange in two βα-loops and their preceding β-strands within the core of the $(\beta/\alpha)_8$-barrel. Loop $\beta_1\alpha_1$ (1−19) shows a 13% increase and loop $\beta_5\alpha_5$ (215−230) shows a 10% increase in deuterium exchange, determining that there is some disorder occurring between the allosteric site and active site.

The deuterium exchange results demonstrate that FBP binding only causes a small number of changes, suggesting that P70T has a weak dynamic response to FBP binding.

6.6.3 Group two – A301T

Kinetic analysis of the A301T enzyme determined that it had a lower maximal activity than the wild-type and more cooperative binding of both PEP and FBP. Moreover, A301T was shown to have an extremely low PEP binding affinity in the absence of FBP. The affinity is so low that without FBP it is inactive at physiologically relevant substrate concentrations (PEP concentrations <0.2 mM).[26, 27] The considerable change in activation response and substrate binding could not be explained by the structure, which was essentially the same as the wild-type. The only structural difference that could offer any explanation was the additional hydrogen bonds in the helix at the A/A' interface. Increased hydrogen bonds would increase stability, which could couple the subunits for cooperative activation by PEP. Dynamic analyses determined significant differences in the dynamics of the enzyme, suggesting that altered dynamics may explain the kinetic behaviour.

Here, the A301T enzyme's dynamic response to FBP was measured, confirming that it displays an altered dynamic response to the allosteric activator, FBP. The response to FBP binding was measured by mapping the deuterium exchange from peptides of unbound and bound A301T (Figure 6.11).

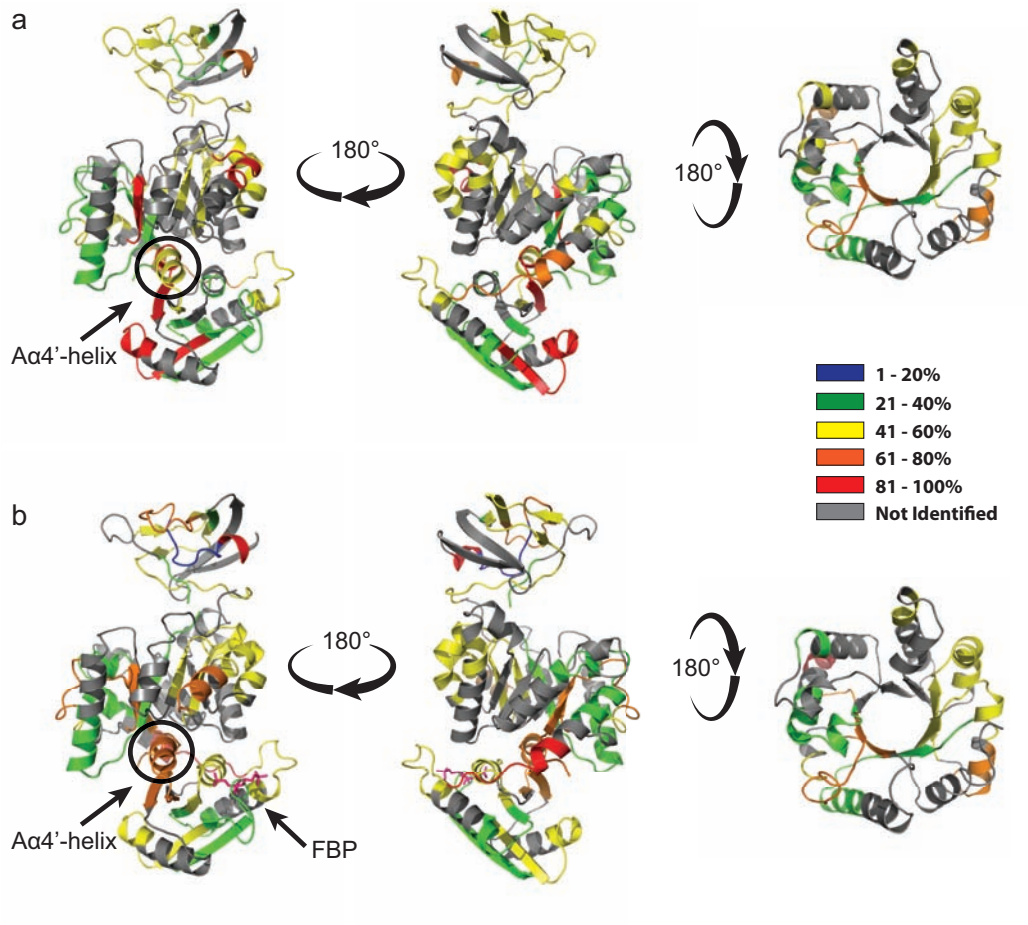

Figure 6.11 Average deuterium exchange mapped and colour-coded onto the A301T structure. **(a)** Unbound A301T viewing both sides of the subunit and looking down the $(\beta/\alpha)_8$-barrel **(b)** A301T with the allosteric activator, FBP (magenta), modelled into the structure (based upon bound A301S) viewing both sides of the subunit and looking down the $(\beta/\alpha)_8$-barrel. The grey regions were not identified in the HDX experiment. The suspected pivot point (Aα4'-helix, residues 398−408) is circled in black. Only peptides that were identified in both experiments (with and without FBP) are displayed.

Initial analysis of the deuterium exchange in the unbound and bound A301T enzyme identified significant differences in exchange that verify that FBP binding has a considerable effect upon the conformational flexibility of the enzyme (Figure 6.11).

The difference in exchange between the unbound and bound A301T were then mapped to establish specific regions of protein that have been dynamically altered as a response to FBP binding (Figure 6.12). The differences were mapped as either an increase or decrease upon FBP binding, displaying only those peptides that exhibited >5% change in absolute deuterium exchange.

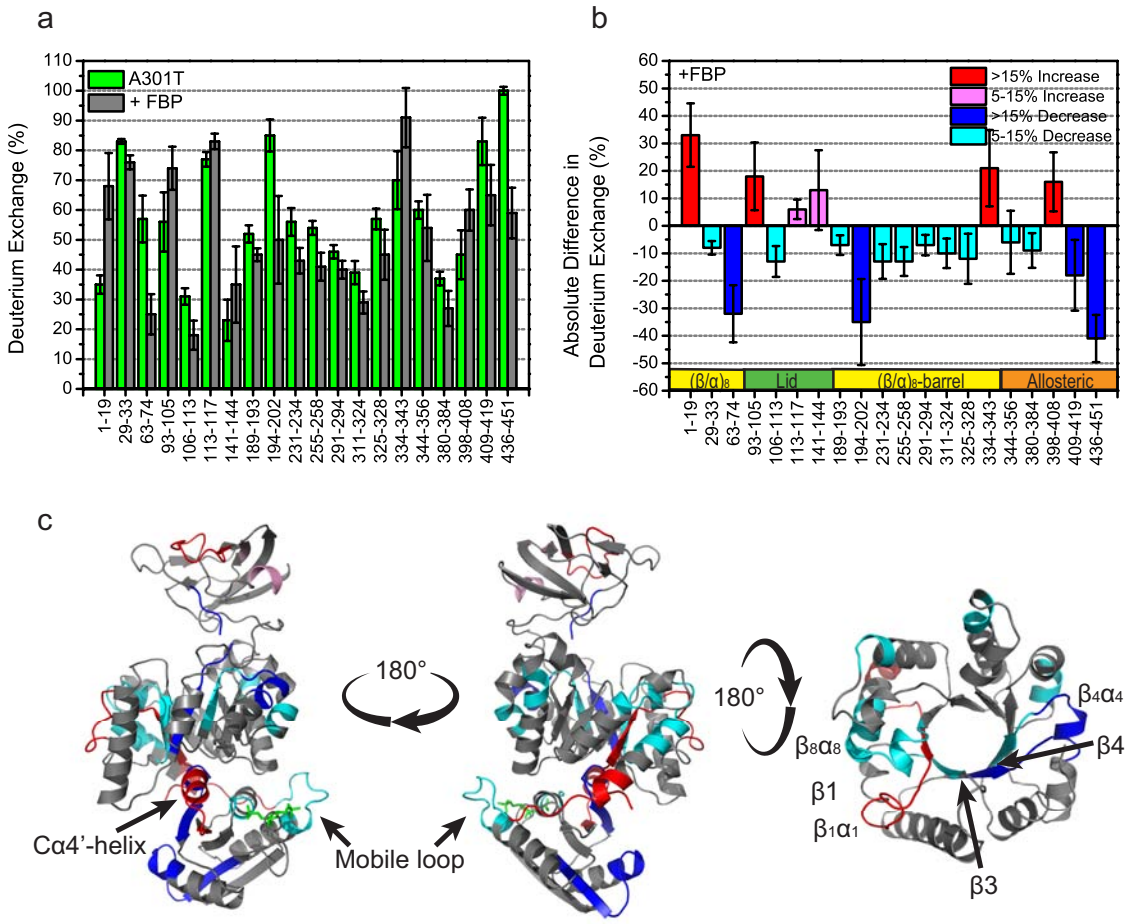

Figure 6.12 Change in average deuterium exchange between the unbound and bound A301T peptides. Displaying only those peptides with >5% change between unbound and bound A301T forms. **(a)** Amount of deuterium exchange in peptides derived from unbound (green) and FBP bound (grey) A301T. **(b)** Absolute differences in deuterium exchange (>5%) are plotted on a bar graph as increases or decreases. **(c)** Absolute differences (>5%) are mapped onto the A301T subunit as high increases (>15%, red), low increases (5−15%, pink), high decreases (>15%, blue) and low decreases in exchange (5−15%, cyan). The allosteric activator FBP (green stick) has been modelled into the structure to show the binding position based upon the bound structure of A301S. Data represent an average of triplicate runs and error bars represent SEM.

6.6.3.1 Dynamic changes to the allosteric domain upon FBP binding

Deuterium exchange in the allosteric activator binding domain was assessed to determine the effect of FBP binding upon conformational flexibility of the domain. FBP binding within the allosteric site of A301T induced a 16% increase in deuterium exchange of the Cα4'-helix (residues 398−408) due to destabilisation of the A/C inter-domain interface, similar to wild-type PK1.

6.6.3.2 Signalling the A301T catalytic site for activation

The $(\beta/\alpha)_8$-barrel was examined to identify changes in conformational flexibility that could be associated with allosteric signal transfer through the $(\beta/\alpha)_8$-barrel to the active site. It was found that FBP binding caused decreased deuterium uptake of β-strands Aβ2 (29−33, -8%), Aβ3 (63−74, -32%) and Aβ4 (189−193, -6%) located in the core of the $(\beta/\alpha)_8$-barrel. The decreased flexibility through the barrel core is inconsistent with the wild-type results, which show increased flexibility through this region. Conversely, the 33% increase in exchange of Aβ1 (residues 1−19) shows that there is some conformational flexibility within the core.

6.6.3.3 The tetrameric C/C' and A/A' interfaces are altered upon FBP binding

Examination of the A/A' and C/C' tetrameric interfaces show the opposite response to FBP binding as the wild-type. FBP binding causes a small decrease in flexibility of both subunit interfaces, whereas the wild-type demonstrated significant increases in flexibility upon FBP binding. The A/A' interface (residues 291−294) exhibited a 7% decrease in deuterium exchange, supporting the structural analysis in Chapter Five (Section 5.3.2). In addition, the C/C' interface decreased by 4%, indicating a coupling of the tetrameric interfaces upon FBP binding.

Overall the deuterium exchange results for A301T present an enzyme with less conformational flexibility in the presence of FBP. This is the opposite to wild-type, which shows increased dynamics upon FBP binding.

6.6.4 Group three – T462I

Kinetic analysis of T462I described an enzyme with a higher maximal activity than wild-type and increased cooperative binding of PEP and FBP. The mutation at the FBP binding site was shown to significantly reduce FBP binding affinity, which left the enzyme almost completely unresponsive to allosteric activation by FBP. Structural and dynamic analyses determined that the lack of activation response to FBP is due to structural changes at the FBP binding site, reducing FBP binding. In addition, increased flexibility of substrate binding loops may be responsible for FBP binding within the active site of the enzyme (at low FBP concentrations), rather than the allosteric site.

Here, the dynamic response to FBP of the T462I enzyme is investigated, confirming that not only does the enzyme have altered conformational flexibility, but it also displays an altered dynamic response to the allosteric activator, FBP. The response to FBP binding is measured by mapping the deuterium exchange from peptides of unbound and bound T462I (Figure 6.13).

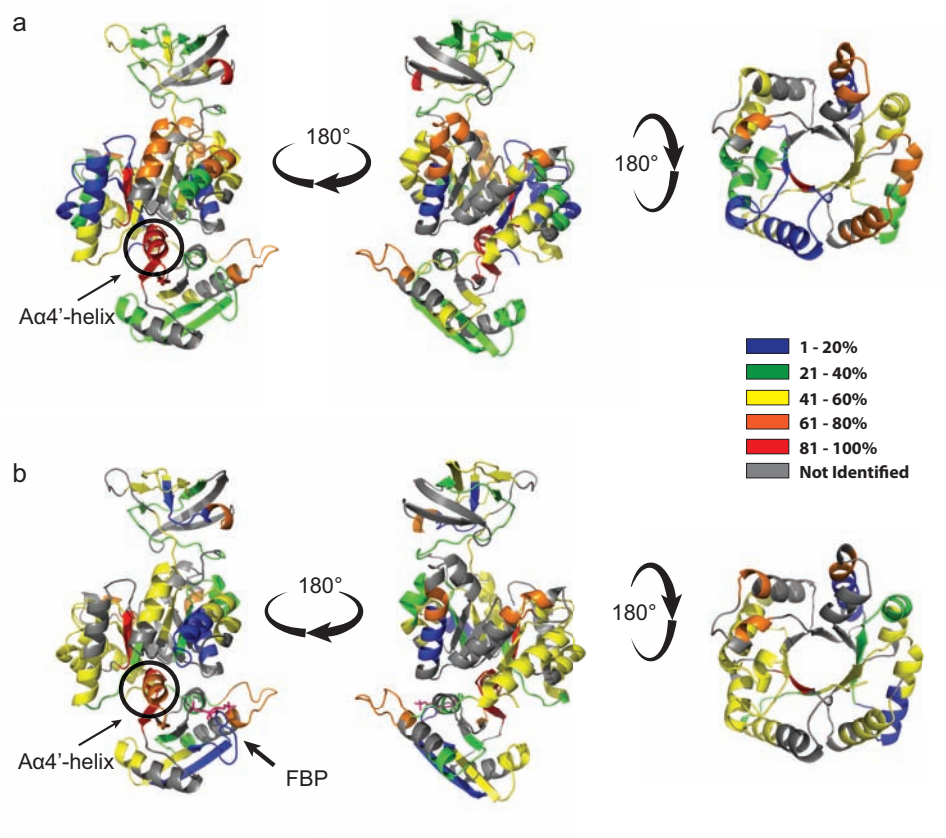

Figure 6.13 Average deuterium exchange mapped and colour-coded onto the T462I structure. **(a)** Unbound T462I viewing both sides of the subunit and looking down the $(\beta/\alpha)_8$-barrel. **(b)** T462I with the allosteric activator, FBP (magenta), modelled into the structure (based upon bound A301S) viewing both sides of the subunit and looking down the $(\beta/\alpha)_8$-barrel. The grey regions were not identified in the HDX experiment. The suspected pivot point (Aα4'-helix, residues 398−408) is circled in black. Only peptides that were identified in both experiments (with and without FBP) are displayed.

Initial analysis of the deuterium exchange in the unbound and bound T462I enzyme identified significant differences that prove that FBP binding has a considerable effect upon the conformational flexibility of the enzyme (Figure 6.13).

The mapped differences in exchange between the unbound and bound T462I establish that specific regions of protein are dynamically altered as a response to FBP binding (Figure 6.14). The differences were mapped as either an increase or decrease upon FBP binding, displaying only those peptides that exhibited >5% change in absolute deuterium exchange.

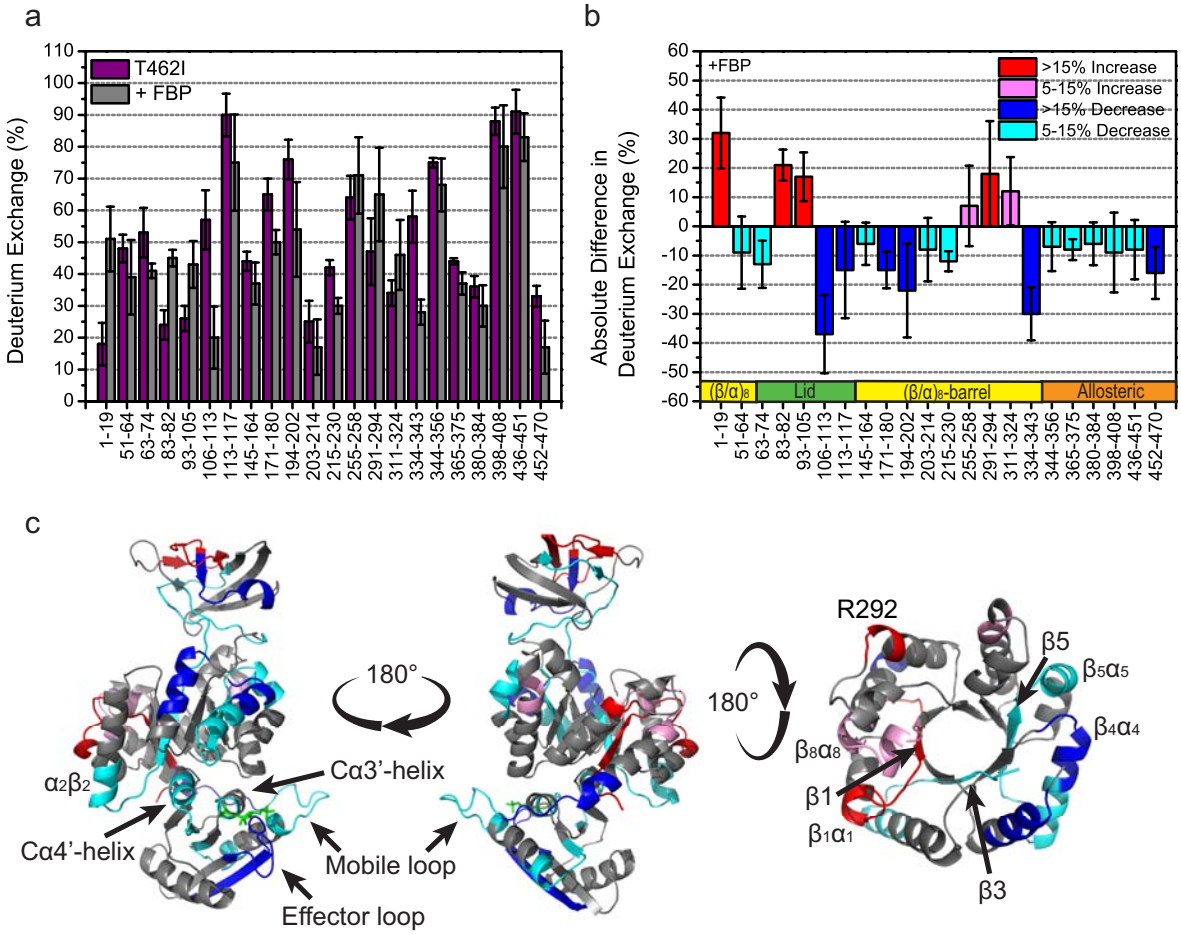

Figure 6.14 Change in average deuterium exchange between the unbound and bound T462I peptides. Displaying only those peptides with >5% change between unbound and bound T462I forms. **(a)** Amount of deuterium exchange in peptides derived from unbound (purple) and FBP bound (grey) T462I. **(b)** Absolute differences in deuterium exchange (>5%) are plotted on a bar graph as increases or decreases. Absolute differences (>5%) are mapped onto the T462I subunit as high increases (>15%, red), low increases (5−15%, pink), high decreases (>15%, blue) and low decreases in exchange (5−15%, cyan). The allosteric activator FBP (green stick) has been modelled into the structure to show the binding position based upon the bound structure of A301S. Data represent an average of triplicate runs and error bars represent SEM.

6.6.4.1 Dynamic changes to the allosteric domain upon FBP binding

First, the allosteric activator binding domain was examined to assess how FBP binding affects its conformational flexibility. The results presented in Figure 6.14 show that the T462I enzyme has the complete opposite response to FBP binding compared to the wild-type. This was not unexpected because the T462I enzyme was found to bind FBP in the active site, rather than the allosteric site (at low concentrations). Here, the presence of FBP has caused the allosteric C-domain to become more stabilised, which means that the enzyme is much more flexible in the absence of FBP. Notably, FBP binding casues the stabilisation of the Cα4'-helix region (residues 398−408, -9%) that forms the inter-domain interface between the allosteric domain (C-domain) and the $(\beta/\alpha)_8$-barrel domain (A-domain). This is surprising as the wild-type, A301S and P70T enzymes all showed a destabilisation of this region, presumably to transfer the activation signal between C- and A-domains, to the active site.

6.6.4.2 Signalling the T462I catalytic site for activation

The changes in conformational flexibility associated with the $(\beta/\alpha)_8$-barrel domain were traced to understand the mechanism by which FBP binding within the active site affects catalysis at the active site. The results determined that two of the three identified β-strands in the core of the $(\beta/\alpha)_8$-barrel show decreased deuterium exchange; Aβ3, -9% and Aβ5, -12%. The decrease of disorder through the $(\beta/\alpha)_8$-barrel core is inconsistent with the signal transfer mechanism proposed for wild-type, which may explain why 2mM of FBP binding to T462I has a reduced ability to increase substrate binding at the active site, demonstrated by the similar $S_{0.5}^{PEP}$ values with (2.36 ± 0.05 mM) and without (5.5 ± 0.1 mM) 2mM of FBP (Section 4.2.2). However, two of the three βα loops that were found to bind FBP in the active site showed increased conformational flexibility. Aβ1 and $\beta_1\alpha_1$-loop (residues 1−19) show a significant increase in deuterium exchange of 32%, and loop $\beta_8\alpha_8$ displayed a 12% increase in exchange, proving that some destabilisation of β-strands and substrate binding loops is occuring.

6.6.4.3 The tetrameric C/C' and A/A' interfaces are altered upon FBP binding

Measurements of the deuterium exchange changes at the A/A' and C/C' tetrameric interfaces demonstrated different dynamic behaviour to the wild-type. The wild-type enzyme presents with a destabilisation of both tetrameric interfaces upon FBP binding. Here, the T462I enzyme displays a different behaviour, whereby the C/C' interface is stabilised (residues 452−470, -16% deuterium exchange), indicating an increase in

protection caused by increased hydrogen bond formation at this interface. On the other hand, the A/A' tetrameric interface (residues 291−294) shows an 18% increase in deuterium exchange, suggesting decoupling of two of the four subunits.

The deuterium exchange results for T462I present an enzyme with less conformational flexibility in the presence of FBP, this is the opposite to wild-type, which showed increased dynamics upon FBP binding.

6.6.5 Group four – A301S

The deuterium exchange data for A301S was collected by Shaolong Zhu (York University, Toronto) because I ran out of time and protein sample during my visit to Canada.

Kinetic, structural and dynamic analysis of the A301S evolved enzyme has demonstrated various differences to the wild-type enzyme. Kinetic analysis determined that A301S has a higher activity than the wild-type, with a slight increase in cooperative binding of PEP and FBP (Chapter Three). Although the structure of A301S was indistinguishable from the wild-type, the significant differences in dynamics suggest that altered conformational flexibility may be changing the way the enzyme functions. X-ray crystal structures of A301S in the unbound and bound states determined that FBP binding did cause subunit rotations. However, structural differences within the subunits were hard to identify from the B-factors. Here, the dynamic response to FBP binding was measured by mapping the deuterium exchange from peptides of unbound and bound A301S (Figure 6.15).

Initial analysis of Figure 6.15 shows key differences in the extent of exchange in the allosteric domain near where the FBP molecule binds, and some changes in the substrate binding loops at the top of the $(\beta/\alpha)_8$-barrel between bound and unbound A301S. These differences confirm that FBP binding is altering the conformational flexibility of the A301S enzyme.

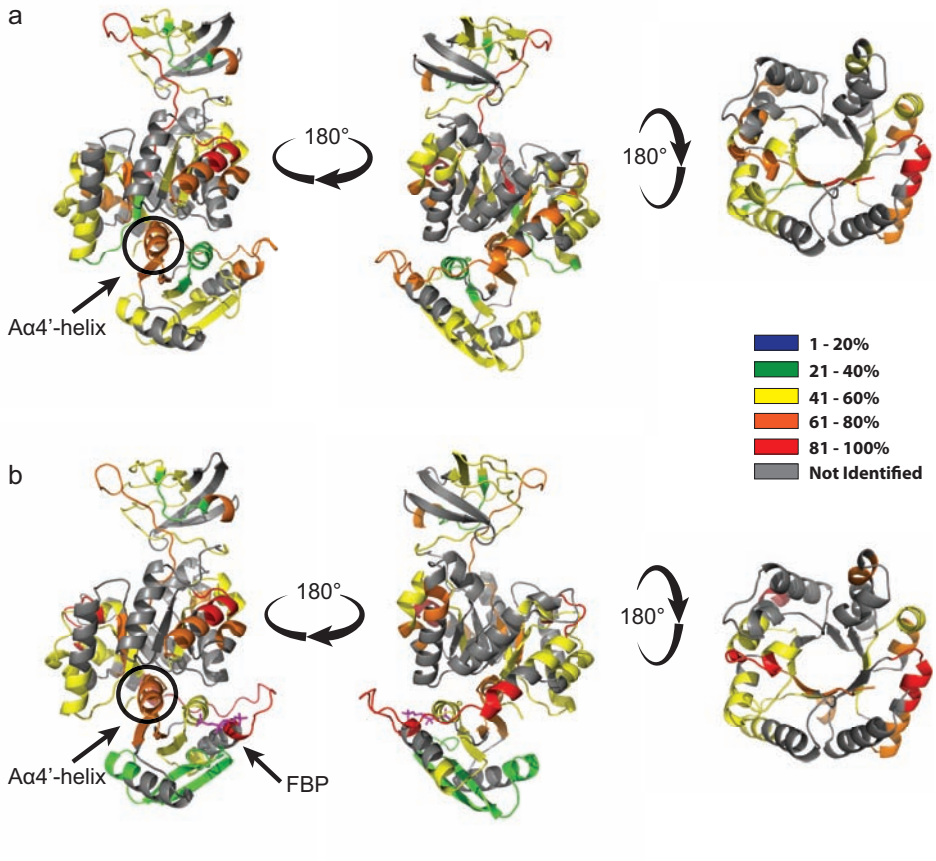

Figure 6.15 Average deuterium exchange mapped and colour-coded onto the A301S structure. **(a)** Unbound A301S viewing both sides of the subunit and looking down the $(\beta/\alpha)_8$-barrel. **(b)** A301S with the allosteric activator, FBP, bound viewing both sides of the subunit and looking down the $(\beta/\alpha)_8$-barrel. The grey regions were not identified in the HDX experiment. The suspected pivot point (Aα4'-helix, residues 398−408) is circled in black. Only peptides that were identified in both experiments (with and without FBP) are displayed.

Next, the difference in exchange between the unbound and bound A301S were mapped to clearly show the specific regions of protein that have been dynamically altered as a response to FBP binding (Figure 6.16). The differences were mapped as either an increase or decrease upon FBP binding, displaying only those peptides that exhibited >5% change in absolute deuterium exchange.

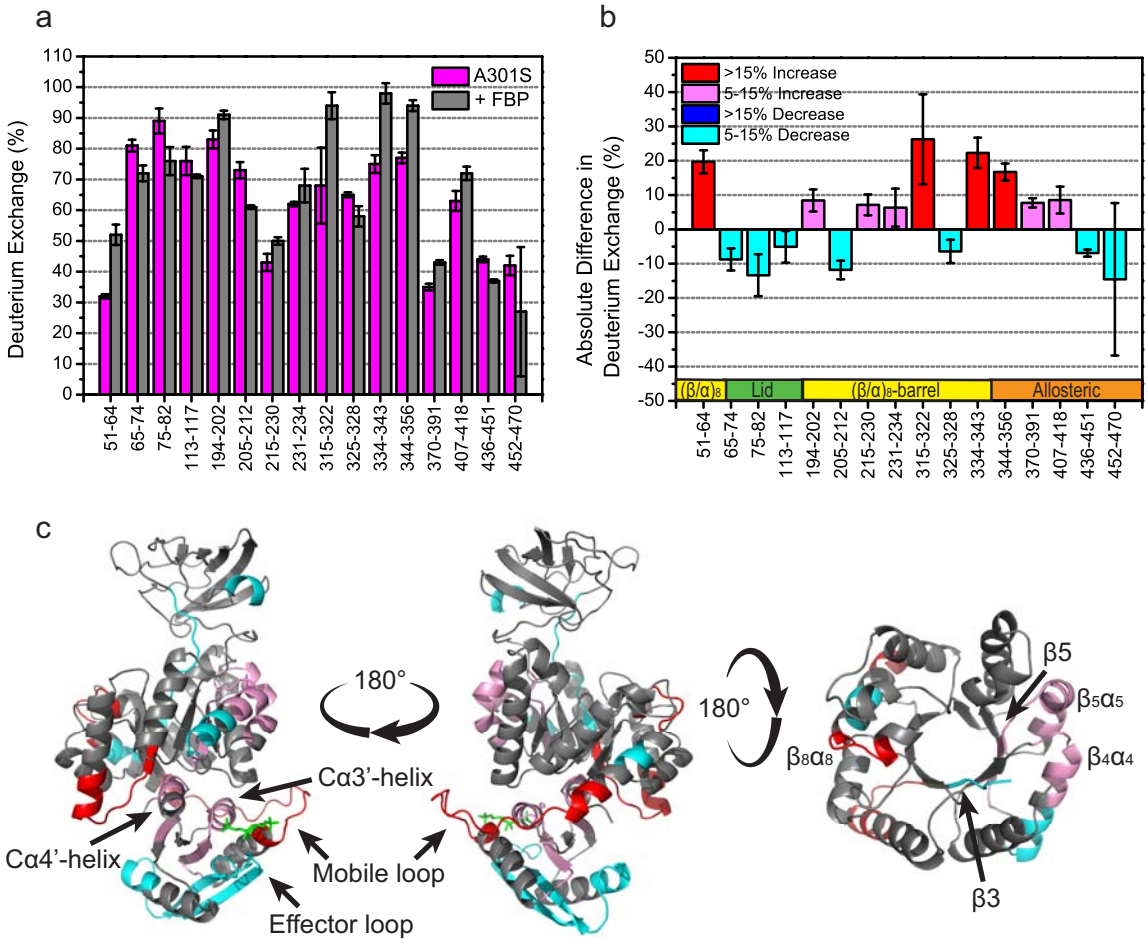

Figure 6.16 Change in average deuterium exchange between the unbound and bound A301S peptides. Displaying only those peptides with >5% change between unbound and bound A301S forms. **(a)** Amount of deuterium exchange in peptides derived from unbound (magenta) and FBP bound (grey) A301S. **(b)** Absolute differences in deuterium exchange (>5%) are plotted as increases or decreases. Absolute differences (>5%) are mapped onto the A301S subunit as high increases (>15%, red), low increases (5−15%, pink), high decreases (>15%, blue) and low decreases in exchange (5−15%, cyan). The allosteric activator FBP (green stick) has been modelled into the structure to show the binding position based upon the bound structure of A301S. Data represent an average of triplicate runs and error bars represent SEM.

6.6.5.1 FBP binding decouples the A301S A/C inter-domain interface

FBP binding to A301S triggered similar responses to that found in the wild-type. It showed a destabilisation of the Cα4'-helix that forms the A/C inter-domain interface (residues 407−418, +9% exchange), and a destabilisation of the $\alpha_2\beta_2$-loop (residues 51−64, +18% exchange) that connects the Cα4'-helix to the $(\beta/\alpha)_8$-barrel domain. The A/C inter-domain contacts are largely mediated by the Cα4'-helix. Therefore decoupling this helix and the surrounding region is consistent with the wild-type results, and with the 'domain

and subunit rotation' activation model proposed by Mattevi (1995).[20] The mobile loop that extends between the $(\beta/\alpha)_8$-barrel domain and the allosteric domain (sequential peptides 334−343 and 344−356) show 22% and 16% increases, respectively. These increases in deuterium uptake upon FBP binding, disagree with the decrease in disorder identified in the bound A301S B-factor plot.

6.6.5.2 Signalling the A301S catalytic site for activation

The changes in conformational flexibility associated with the active site $(\beta/\alpha)_8$-barrel domain were mapped to find the link between FBP binding and increased substrate binding in the active site. Similar to the wild-type, FBP binding generated disorder of structural regions between the allosteric site and the active site, including β-strands and substrate binding loops. Two β-strands in the core of the barrel, Aβ3 (residues 51−64) and Aβ5 (residues 215−230), display increased deuterium exchange of 18% and 7% respectively. Also, three substrate binding loops, $\beta_4\alpha_4$, (194−202, 8%) $\beta_5\alpha_5$ (215−230, 7%) and $\beta_8\alpha_8$ (315−322, 26%) in the active site of A301S display increased deuterium exchange. The increased exchange suggests that FBP binding in the allosteric site can affect substrate binding over 40 Å away. The destabilisation of substrate binding loop $\beta_8\alpha_8$ (residues 315−322) supports the B-factor plot of the A301S bound structure (Section 3.3.3), which shows an increase in disorder of this loop region with FBP bound.

6.6.5.3 The A301S tetrameric C/C' interface is altered upon FBP binding

One significant difference in the A301S exchange results compared to wild-type are the changes to the C/C' subunit interfaces. Unlike the wild-type enzyme which shows a significant increase in deuterium exchange for residues 452−467, the A301S enzyme displays a 14% decrease in deuterium exchange, suggesting an increase in stability of the effector loop and β-strand at the C/C' interface.

Overall, these results confirm that the binding of FBP alters the conformational flexibility of various structural regions within the A301S enzyme, providing similar changes to those identified in the wild-type enzyme.

6.7 Discussion of evolved enzyme allosteric mechanisms

Part 1 of this chapter demonstrates that the dynamics of each of the evolved enzymes are different to the wild-type and Part 2 shows that the evolved enzymes display key differences in their dynamic responses to FBP. The following section will describe a proposed mechanism of allosteric activation for each of the evolved enzymes in the context of their kinetic behaviours.

6.7.1 Allosteric activation mechanism of P70T

The deuterium exchange was analysed in the P70T enzyme to try and identify the allosteric activation mechanism for this evolved enzyme. It was difficult to identify a mechanism for this enzyme because the deuterium exchange was very similar with and without FBP. In addition, this enzyme had the lowest number of peptides identified in both unbound and bound states. Although the data is limited, it generally indicates destabilisation through the centre of the $(\beta/\alpha)_8$-barrel and increased stability on the outside of the $(\beta/\alpha)_8$-barrel. The interpreted results suggest that the following scheme results in allosteric activation of the evolved P70T enzyme upon FBP binding:

1) The presence of FBP does not cause any significant change to the disorder of peptides within the allosteric binding site.
2) FBP binding increases the flexibility of two β-strands within the core of the barrel, which could be involved in transferring the allosteric activation signal between the FBP binding site and the active site.
3) Peptides from four different α-helices around the outside of the $(\beta/\alpha)_8$-barrel show increased stabilisation, suggesting a tightening of these helices.
4) The only two βα loops to show a change in exchange upon FBP binding, show an increase suggesting that these two loops become more flexible and increase conformational sampling when FBP is present. Increased conformational sampling of loops $\beta_5\alpha_5$ and $\beta_1\alpha_1$ likely increases the number of conformations that will facilitate substrate and catalytic ion binding for catalysis.

5) Finally, the extended loop that connects the lid domain to the $(\beta/\alpha)_8$-barrel domain showed a 10% decrease in deuterium exchange. This result is consistent with the P70T mutation forming additional hydrogen bonds to loop $\beta_4\alpha_4$, decreasing available amide protons and locking the lid in one conformation.

Overall, the proposed mechanism for the P70T enzyme is incomplete because of the restricted results for this enzyme. However, the changes that are seen suggest that destabilisation events transfer the activation signal between the allosteric site and the active site to increase substrate binding.

6.7.2 Allosteric activation mechanism of A301T

The deuterium exchange changes for the A301T enzyme upon FBP binding demonstrate an activation mechanism very different to that of the wild-type enzyme, with FBP binding inducing decreased flexibility in most of the enzyme. The kinetics for this enzyme have shown a considerable increase in cooperative activation by PEP, in the presence of FBP, along with increased stability at the A/A' interface suggesting coupling of subunits. Also, FBP binding dramatically increased the binding affinity of PEP. Therefore changes in the PEP binding loops were expected, but this was not observed in this experiment. Nevertheless, the interpreted results suggest that the following scheme results in allosteric activation of the evolved A301T enzyme upon FBP binding:

1) Binding of FBP decreases deuterium exchange in the Cα1'- and Cα3'-helices because they form hydrogen bonds with the FBP molecule decreasing the number of amide protons available for exchange with the deuterated solvent.
2) FBP binding destabilises the Cα4'-helix causing a disruption of the inter-domain interface that links the allosteric domain (C-domain) and the $(\beta/\alpha)_8$-barrel domain (A-domain).
3) Following the stabilised domain interface, FBP binding causes a stabilisation of three β-strands within the core of the $(\beta/\alpha)_8$-barrel, demonstrating a tightening of the $(\beta/\alpha)_8$-barrel core.

4) The stabilised β-strands subsequently lead to stabilised substrate binding loops. Loops $\beta_3\alpha_3$, $\beta_4\alpha_4$ and $\beta_8\alpha_8$ show decreased flexibility upon FBP binding, suggesting decreased conformational sampling, which may be a result of the enzyme stabilising a particular conformation that is well suited to binding substrate.
5) The C/C' tetrameric interface in this enzyme shows a 4% decrease in deuterium exchange, while the A/A' interface demonstrated a 7% decrease in deuterium exchange. These results suggest that FBP binding decreases the flexibility of both tetrameric interfaces, suggesting coupling of subunits. This result explains the increased cooperative activation of the enzyme, supporting structural data, which showed increased hydrogen bonding within helices at the A/A' interface (Section 5.3.2).

Overall FBP binding to the A301T enzyme causes a variety of changes that demonstrate an activation mechanism involving increased stability of the allosteric site, β-strands within the $(\beta/\alpha)_8$-barrel core, and subunit interfaces. However, a considerable destabilisation of the A/C domain interface may allow domain rotations, similar to Mattevi's proposed model.[20, 21]

6.7.3 Allosteric activation mechanism of T462I

The deuterium exchange results for the T462I enzyme with and without FBP show very different results to the wild-type, with FBP binding causing decreased flexibility for most of the enzyme. Structural analyses have demonstrated that at low FBP concentrations, FBP preferentially binds in the active site of the enzyme rather than the allosteric site, and that FBP has very little activation effect upon the enzyme. It is therefore not surprising that the deuterium exchange results present an activation mechanism very different to that of the wild-type enzyme. The interpreted results suggest that the following scheme results in allosteric activation of the evolved T462I enzyme upon FBP binding:

1) The presence of 2 mM FBP results in a slight decrease in $S_{0.5}^{PEP}$ (Section 4.2.2), suggesting that FBP is able to bind to the allosteric site of the enzyme and cause some allosteric activation. FBP binding results in decreased flexibility of the allosteric binding site, demonstrating a more structured domain.

2) FBP binding also causes decreased flexibility of the A/C domain interface, suggesting a decrease in domain movement.
3) Following the stabilised domain interface, FBP binding causes a stabilisation of β-strands within the core of the $(\beta/\alpha)_8$-barrel and the α-helices around the outside of the $(\beta/\alpha)_8$-barrel, demonstrating a tightening of the entire $(\beta/\alpha)_8$-barrel.
4) Although the deuterium exchange results show that FBP binding creates a more structured allosteric domain and catalytic domain, two substrate binding loops become more flexible. Loops $\beta_1\alpha_1$ and $\beta_8\alpha_8$ are destabilised for increased conformational sampling, increasing the number of conformations that may bind substrates and catalytic ions (and FBP).
5) Finally, there was a 16% decrease in exchange at the C/C' tetrameric interface, but an 18% increase in the peptide making up the A/A' tetrameric interface. These changes suggest that FBP binding initiates some flexibility in the A/A' interface, allowing rotations, however the C/C' interface is rigid.

Overall, the deuterium exchange results show a much more flexible protein in the absence of FBP. The proposed mechanism of allosteric activation for the T462I enzyme includes stabilisation of the allosteric and catalytic domains, but a destabilisation of substrate binding loops, increasing conformational sampling for substrate and catalytic ion binding.

6.7.4 Allosteric activation mechanism of A301S

The deuterium exchange changes in the A301S enzyme upon FBP binding support a similar allosteric activation model to that proposed for the wild-type enzyme, whereby FBP binding transmits an activation signal via structural disorder between the FBP binding site and the active site. The interpreted results suggest that the following scheme results in allosteric activation of the evolved A301S enzyme upon FBP binding:

1) The presence of FBP stabilises the effector loop, which is confirmed to be involved in binding the FBP molecule in the bound A301S structure.
2) There is then a destabilisation of the Cα3'- and Cα4'-helices, causing a disruption of the inter-domain interface that links the allosteric domain (C-domain) and the $(\beta/\alpha)_8$-barrel domain (A-domain).

3) The destabilisation at the A/C interface causes the destabilisation of $\alpha_2\beta_2$, as well as two of the four identified β-strands within the core of the $(\beta/\alpha)_8$-barrel domain. This destabilisation is consistent with the β-strands being involved in allosteric signal transfer through the core of the $(\beta/\alpha)_8$-barrel, to the active site
4) Destabilisation of the β-strands consequently destabilises two substrate binding loops (loops $\beta_4\alpha_4$ and $\beta_5\alpha_5$) at the top of the $(\beta/\alpha)_8$-barrel, near the PEP and Mg^{2+} binding sites. The decreased order within these active site loops is expected to allow them to sample a greater number of conformations, some of which will facilitate the binding of substrate and catalytic ions.
5) Finally, FBP binding causes a stabilisation of the β-sheet at the C/C' interface suggesting that the conformational change upon FBP binding (Chapter Three – Part 1) may decrease the occupancy of amide protons within this region. However, data for this peptide have large error bars so it is difficult to assess how true this stabilisation is.

Overall the proposed mechanism supports that proposed by Mattevi *et al*., where FBP binding causes domain and subunit rotations.[20, 21] The results also support the proposed model for the wild-type enzyme which extends Mattevi's model by describing how FBP binding promotes substrate binding at the active site over 40 Å away.

6.8 Discussion

The results presented in this chapter provide evidence that evolution by natural selection has selected for *E. coli* PK1 enzymes with altered function and dynamics but the same structure. Eight single substitution mutations were adaptively evolved in the *E. coli* PK1 enzyme, and all of these evolved enzymes display a fitness benefit compared to the wild-type. Comparative studies of the wild-type and evolved enzymes demonstrated that the mutations have altered enzyme function but the structure remaines the same. Here, dynamic analyses using a combination of computational and experimental techniques demonstrate that the eight evolved enzymes display significant changes in their conformational flexibility.

To gain a deeper understanding of how the conformational flexibility affects the enzymes' functional behaviour, the dynamics upon allosteric activation by FBP were analysed to justify the functional changes identified in Chapter Four. The results demonstrate a variety of responses to FBP binding across the four evolved enzymes. Major changes were identified in the β-strands within the core of the $(\beta/\alpha)_8$-barrels, and at the domain and tetrameric interfaces of the enzymes. Overall, the four evolved enzymes exhibited reduced allosteric activation responses to FBP binding compared to the wild-type. This result could be explained by a reduced signal transfer through the β-strands, between the allosteric site and the active site. Also, the coupling of subunits (rather than the uncoupling found in wild-type) caused by FBP binding could explain the positive cooperativity for PEP binding displayed in all four enzymes, where PEP binding to one subunit increases the affinity for PEP molecules at subsequent subunits.

It is easy to over analyse the complex deuterium exchange results for each of the enzymes, however, the semantics are not important. The important message is that natural selection has selected for enzymes with altered dynamics, which results in the enzymes having altered allosteric responses. For years conformational flexibility has been described as important for elliciting the allosteric response, in the absence and presence of structural changes.[13] Allostery is a signal induced by the binding of an effector at one site and the transfer of that signal to a distant site for activation.[9, 23, 28] Allosteric signals can be transferred over long distances using changes in the mean conformation (enthalpic contribution) and/or by changes in the dynamic fluctuations around a mean conformation (entropic contribution).[15, 29]

The *E. coli* PK1 study presented here describes a protein that has adaptively evolved allostery by leaving the backbone structure unchanged, but by altering the enzymes conformational flexibility. Similarly, there are several similar cases of this in the literature; one such case investigated the adaptive response of organisms to high altitude hypoxia. Comparative studies in animal and human haemoglobin mutants demonstrated that single substitution mutations were capable of changing the allosteric equilibrium constants between bound (oxy) and unbound (deoxy) states. In the bar-headed goose example, natural selection selected for mutations that shifted the allosteric equilibrium in favour of the oxygenated haemoglobin conformation by disrupting contacts at the intersubunit interface, introducing conformational flexibility.[30] Another example of an

enzyme with altered function and dynamics without any change in structure is the catabolite activator protein. 3',5'-cyclic adeosine monophosphate binds to catabolite activator protein and alters the motions of residues at a distant site, without changing the proteins structural conformation.[15] This example emphasises the importance of conformational flexibility for transmitting the allosteric signal between distant sites on a protein.

The HDX data presented in this chapter confirms that the enzymes have evolved different overall dynamics It also demonstrates that the enzymes have evolved changes to the conformational flexibility of specific regions which contribute to the altered allosteric activation responses. In other words, adaptive evolution has fine-tuned protein dynamics to alter allostery.

6.9 References

[1] Resetca, D, Haftchenary, S, Gunning, PT, and Wilson, DJ. (2014) Changes in signal transducer and activator of transcription 3 (STAT3) dynamics induced by complexation with pharmacological inhibitors of Src homology 2 (SH2) domain dimerization, *J. Biol. Chem. 289*, 32538-32547.

[2] Rob, T, and Wilson, DJ. (2009) A versatile microfluidic chip for millisecond time-scale kinetic studies by electrospray mass spectrometry, *J. Am. Soc. Mass Spectrom. 20*, 124-130.

[3] Liuni, P, Rob, T, and Wilson, DJ. (2010) A microfluidic reactor for rapid, low-pressure proteolysis with on-chip electrospray ionization, *Rapid Commun. Mass Spectrom. 24*, 315-320.

[4] Resetca, D, and Wilson, DJ. (2013) Characterizing rapid, activity-linked conformational transitions in proteins via sub-second hydrogen deuterium exchange mass spectrometry, *FEBS J. 280*, 5616-5625.

[5] Konermann, L, Pan, J, and Liu, YH. (2011) Hydrogen exchange mass spectrometry for studying protein structure and dynamics, *Chem. Soc. Rev. 40*, 1224-1234.

[6] Balasubramaniam, D, and Komives, EA. (2013) Hydrogen-exchange mass spectrometry for the study of intrinsic disorder in proteins, *Biochim. Biophys. Acta 1834*, 1202-1209.

[7] McAllister, RG, and Konermann, L. (2015) Challenges in the interpretation of protein h/d exchange data: a molecular dynamics simulation perspective, *Biochemistry 54*, 2683-2692.

[8] Tsai, CJ, del Sol, A, and Nussinov, R. (2008) Allostery: absence of a change in shape does not imply that allostery is not at play, *J. Mol. Biol. 378*, 1-11.

[9] Boehr, DD, Nussinov, R, and Wright, PE. (2009) The role of dynamic conformational ensembles in biomolecular recognition, *Nat. Chem. Biol. 5*, 789-796.

[10] Kerns, SJ, Agafonov, RV, Cho, YJ, Pontiggia, F, Otten, R, Pachov, DV, Kutter, S, Phung, LA, Murphy, PN, Thai, V, Alber, T, Hagan, MF, and Kern, D. (2015) The energy landscape of adenylate kinase during catalysis, *Nat. Struct. Mol. Biol. 22*, 124-131.

[11] Tsai, CJ, and Nussinov, R. (2014) A unified view of "how allostery works", *PLoS Comput. Biol. 10*, e1003394.

[12] Motlagh, HN, Wrabl, JO, Li, J, and Hilser, VJ. (2014) The ensemble nature of allostery, *Nature 508*, 331-339.

[13] Tsai, CJ, Del Sol, A, and Nussinov, R. (2009) Protein allostery, signal transmission and dynamics: a classification scheme of allosteric mechanisms, *Mol. Biosyst. 5*, 207-216.

[14] Fuentes, EJ, Gilmore, SA, Mauldin, RV, and Lee, AL. (2006) Evaluation of energetic and dynamic coupling networks in a PDZ domain protein, *J. Mol. Biol. 364*, 337-351.

[15] Popovych, N, Sun, S, Ebright, RH, and Kalodimos, CG. (2006) Dynamically driven protein allostery, *Nat. Struct. Mol. Biol. 13*, 831-838.

[16] Rob, T, Liuni, P, Gill, PK, Zhu, S, Balachandran, N, Berti, PJ, and Wilson, DJ. (2012) Measuring dynamics in weakly structured regions of proteins using microfluidics-enabled subsecond H/D exchange mass spectrometry, *Anal. Chem. 84*, 3771-3779.

[17] Zhou, B, and Zhang, ZY. (2007) Application of hydrogen/deuterium exchange mass spectrometry to study protein tyrosine phosphatase dynamics, ligand binding, and substrate specificity, *Methods 42*, 227-233.

[18] Morgan, HP, Zhong, W, McNae, IW, Michels, PAM, Fothergill-Gilmore, LA, and Walkinshaw, MD. (2014) Structures of pyruvate kinases display evolutionarily divergent allosteric strategies, *R. Soc. Open. Sci. 1*, 140120.

[19] Morgan, HP, McNae, IW, Nowicki, MW, Hannaert, V, Michels, PAM, Fothergill-Gilmore, LA, and Walkinshaw, MD. (2010) Allosteric mechanism of pyruvate kinase from *Leishmania mexicana* uses a rock and lock model, *J. Biol. Chem. 285*, 12892-12898.

[20] Mattevi, A, Bolognesi, M, and Valentini, G. (1996) The allosteric regulation of pyruvate kinase, *FEBS Lett. 389*, 15-19.

[21] Mattevi, A, Valentini, G, Rizzi, M, Speranza, ML, Bolognesi, M, and Coda, A. (1995) Crystal structure of *Escherichia coli* pyruvate kinase type I: Molecular basis of the allosteric transition, *Structure 3*, 729-741.

[22] Ma, B, Tsai, CJ, Haliloglu, T, and Nussinov, R. (2011) Dynamic allostery: linkers are not merely flexible, *Structure 19*, 907-917.

[23] Marsh, JA, and Teichmann, SA. (2014) Protein flexibility facilitates quaternary structure assembly and evolution, *PLoS Biol. 12*, e1001870.

[24] Bauer, F, and Sticht, H. (2007) A proline to glycine mutation in the Lck SH3-domain affects conformational sampling and increases ligand binding affinity, *FEBS Lett. 581*, 1555-1560.

[25] Urfer, R, and Kirschner, K. (1992) The importance of surface loops for stabilizing an eightfold βα barrel protein, *Protein Sci. 1*, 31-45.

[26] Xu, YF, Amador-Noguez, D, Reaves, ML, Feng, XJ, and Rabinowitz, JD. (2012) Ultrasensitive regulation of anapleurosis via allosteric activation of PEP carboxylase, *Nat. Chem. Biol. 8*, 562-568.

[27] Bennett, BD, Kimball, EH, Gao, M, Osterhout, R, Van Dien, SJ, and Rabinowitz, JD. (2009) Absolute metabolite concentrations and implied enzyme active site occupancy in *Escherichia coli*, *Nat. Chem. Biol. 5*, 593-599.

[28] Weinkam, P, Chen, YC, Pons, J, and Sali, A. (2013) Impact of mutations on the allosteric conformational equilibrium, *J. Mol. Biol. 425*, 647-661.

[29] Wand, AJ. (2001) Dynamic activation of protein function: a view emerging from NMR spectroscopy, *Nat. Struct. Biol. 8*, 926-931.

[30] Storz, JF, and Moriyama, H. (2008) Mechanisms of hemoglobin adaptation to high altitude hypoxia, *High. Alt. Med. Biol. 9*, 148-157.

Chapter Seven

Discussion – Molecular adaptation of an allosteric enzyme

7.1 Introduction

The molecular mechanisms underlying enzyme adaptation are not well understood. Key to a better understanding of molecular adaptation for proteins is a full account of the relationship between altered alleles (genotype) and the resulting physiological properties (phenotype) that allows a population to move towards a phenotype that best fits the present environment (adaptation).[1, 2] This connection, which describes how adaptive mutations in a gene facilitate beneficial phenotypic changes, is often left undetermined due to the difficulties involved in investigating molecular mechanisms in complex systems.[3, 4] Phillips[5] described this as a 'chasm' in evolutional biology: "*We are caught between molecular knowledge in the absence of adaptive context and ecological context in the absence of molecular details. One view of the modern challenge to understanding the genetics of adaptation is the need to span this chasm – to be able to move freely from sequence to phenotype to ecological context and, more importantly, to be able to test specific hypotheses at each of these levels."* The work described in this thesis bridges the 'chasm' with a case study of the molecular changes underlying adaptive evolution in an allosteric enzyme. This is the first study that I know of to characterise adaptive changes in an allosteric enzyme, where the adaptive changes have been mapped from organismal fitness, to enzyme function, to enzyme structure, and to enzyme dynamics.

The challenges involved in studying adaptation were recognised early on, with Lewontin stating that "*it has proved remarkably difficult to get compelling evidence for changes in enzymes brought about by selection, not to speak of adaptive changes*".[6] For years studying adaptive evolution relied on comparative studies of living organisms, supplemented with data of descendants from fossil records.[7] Now, laboratory-based evolutionary experiments with microorganisms enable the study of adaptation in real-time. Adaptation is the process by which species evolve to gain, lose or modify their functional features to increase their survival in fluctuating environments.[8] As emphasised by the quotes above, it is important to determine which features are driving the evolutionary process by studying the molecular mechanisms underlying adaptation.[3, 4]

Behe recently surveyed the results of all of the evolutionary laboratory experiments that were performed using microorganisms between 1970 and 2010, and concluded that loss-of-function or modification-of-function seemed to dominate adaptation.[3] Assessment of the long-term evolution experiment by Lenksi determined that his twelve evolved *E. coli* populations demonstrated both losses and modifications of function. The repeated mutation of four genes (*pyk*F, *nad*R, *pbp*A-*rod*A and *hok*B/*sok*B) at different sites suggested decreased protein function, which was described as adaptation by functional modification.[3, 9] In addition, adaptive mutations in the MalT protein were shown to reduce the activity of the maltose regulon, consistent with a loss of function of the MalT transcriptional activator.[2, 3]

The research presented here focuses on the series of mutations that were identified in *pyk*F as 'modification-of-function' mutations, which we (Fen Peng[10] and I) have demonstrated to be adaptive. These mutations were selected for under a low-glucose selection pressure in Lenski's long-term evolution experiment. All twelve replicate populations in the evolution experiment developed substitution mutations in the *pyk*F gene. Across these twelve populations, eight different substitution mutations were found and fitness analyses determined that all of the non-synonymous mutations produce a parallel fitness advantage for the host *E. coli*. The parallel changes at the genotypic and phenotypic level raises the question of whether the resulting evolved *E. coli* pyruvate kinase type 1 (PK1) enzymes also show a parallel change in function.

A recent study carried out by Xu *et al*.,[11] investigated the adaptation of *E. coli* to changing access to carbon, i.e. the response of *E. coli* to switches between glucose and no carbon. The results demonstrated that *E. coli* rapidly turns off phosphoenolpyruvate (PEP) consumption upon glucose removal by reducing the activity of the PEP carboxylase enzyme that uses PEP to produce oxaloacetate for the citric acid cycle. The resulting accumulated PEP is used to quickly import glucose by reducing the lag time when it becomes re-available.[9, 11] Based upon this study, I hypothesised that *E. coli* PK1 will respond in a similar way, whereby the substitution mutations lower the catalytic activity of the enzyme, increasing PEP build-up for rapid uptake of glucose upon reintroduction (i.e. in Lenski's evolution experiment this is when the populations are diluted into fresh media).

The aim of this thesis, as discussed in Chapter One, has been to investigate the eight evolved *E. coli* PK1 enzymes to determine the molecular mechanisms underlying adaptive evolution. The aim was to provide answers to key questions: 1) What is the mechanism of allosteric activation in *E. coli* PK1? (Chapter Three). 2) Have the adaptive mutations altered the function of the enzymes? Is this change in enzyme function parallel? What is being selected for? (Chapter Four). 3) Have the structures of the evolved enzymes changed to alter the function? (Chapter Five), or 4) Has natural selection selected enzymes with altered dynamics? (Chapter Six).

7.2 Allosteric activation is mediated by conformational flexibility

The mechanism of *E. coli* PK1 allosteric activation is not well understood, in part because a structure of the FBP bound enzyme has not been reported. Moreover, my own (and others) efforts to crystallise this bound structure was unsuccessful. [12-14] The wild-type enzyme is heterotropically activated upon fructose-1,6-bisphosphate (FBP) binding in its allosteric site and increasing PEP binding affinity at the active site in the same subunit 40 Å away.[14-16] Moreover, FBP binding also alters the response to PEP: in the absence of FBP the enzyme is cooperative with respect to PEP concentration (sigmoidal response curve), but in the presence of FBP a classic Michaelis-Menten

response is obtained.[13, 14, 16, 17] A careful kinetic study of the wild-type enzyme, verifies that my recombinant *E. coli* PK1 enzyme behaves in the same way as reported by others.[14]

I tested two proposed models for pyruvate kinase (PK) allostery, and further, report a novel allosteric mechanism for *E. coli* PK1. Structural analysis combined with hydrogen-deuterium exchange studies determined that the allosteric signal is transferred by a series of dynamic changes between the allosteric site and the active site, 40 Å away. During this investigation, the first known structure of an *E. coli* PK1 enzyme with FBP bound was solved. The structure of the evolved A301S enzyme identified FBP bound in the allosteric site of the enzyme and confirmed that FBP binds in a similar position to other PK isozymes.[18-20] The FBP bound structure began to describe a mechanism for allosteric activation that is similar to the mechanism described by Morgan *et al*.,[18, 19] which included a ~5° rotation of subunits. Further structural analysis of the FBP bound A301S identified altered tetrameric interfaces, a structural rearrangement of the effector loop, and increased flexibility of three substrate binding loops in the active site of the enzyme.

Next, deuterium exchange analyses demonstrated that FBP binding to wild-type PK1 causes an increase in overall flexibility of the enzyme. The deuterium exchange analysis was then taken a step further to identify site-specific regions of the protein that were more or less flexible upon FBP binding. The result is consistent with the structural rearrangement of the effector loop, showing that this loop becomes very disordered upon FBP binding. In addition, FBP binding resulted in destabilisation of the FBP binding site, inter-domain (A/C) interface, tetrameric interfaces (A/A' and C/C'), β-strands within the $(\beta/\alpha)_8$-barrel core and substrate binding loops within the active site. The destabilised regions as a result of FBP binding identifies a pathway for signal transfer via destabilisation, from the allosteric site, through the $(\beta/\alpha)_8$-barrel core to the active site for the purpose of increasing substrate-binding affinity.

My proposed allosteric mechanism supports the domain rotation model of activation,[16, 21] whereby FBP binding alters both domain and subunit rotations to induce the heterotropic activation mechanism. The results suggest that FBP binding in the allosteric domain decouples the subunits via destabilisation and provokes active site loops to sample a greater number of conformations, some of which facilitate

binding of the substrate and catalytic ions, thus creating heterotropic activation within the subunit. With this said, I would presume that homotropic activation would not show the same destabilisation of tetrameric interfaces because decoupling subunits would remove the ability to transfer the activation signal between subunits. Instead, the signal transfer might be viewed as a destabilisation pathway between active sites of different subunits. However, further investigation would be required to follow up this presumption.

The key result of this section of work is that I have shown that protein dynamics is important for the catalytic and regulatory function of *E. coli* PK1. The results presented are consistent with the description of proteins as dynamic molecules, fluctuating between conformational states, towards which the favoured states can be shifted by an allosteric event.[22-24] The interpreted results provide a valid mechanism of allosteric activation for wild-type PK1 to act as a reference for comparison with the evolved PK1 enzymes.

7.3 *E. coli* PK1 enzyme has evolved functional, but not structural differences

7.3.1 Function is adapted

The role of PK is to regulate the conversion of glucose to pyruvate by catalysing the final step in the glycolytic pathway, creating adenosine triphosphate (ATP) and pyruvate from adenosine diphosphate (ADP) and PEP.[14, 16, 25] It is therefore not surprising that a severe change in environment, such as glucose-limitation, results in the selection and fixation of beneficial mutations in an enzyme involved in glucose metabolism. It is, however, surprising that PK is the only enzyme in the glycolytic pathway that is altered, which suggests that, in a low glucose environment, PK is more important for regulating glycolysis than first thought (most text books and literature consider phosphofructokinase as the key regulatory step).[26]

In Lenski's evolution experiment, all twelve populations had mutations in the *pyk*F-coding region. However, in two cases the mutations led to the deletion of large

portions of the protein, including much of the active site, and are very likely to be loss-of-function mutations. The other ten populations contained point mutations at a tetrameric interface, in the allosteric binding domain, or close to the active site. Given that the loss-of-function deletion mutations provide a fitness benefit, others had proposed that all of the mutations in *E. coli* PK1 were complete loss-of-function mutations, similar to the deletions (Lenski personal communication).[3, 9] This, in part, led to the hypothesis that the mutations in *E. coli* PK1 serve to increase the availability of PEP to stimulate glucose import, particularly during the lag phase growth.[9] A similar hypothesis was proposed by Travisano and Lenski in the early stages of the evolution experiment. They found a correlated fitness response of the first 2,000 generations of *E. coli,* suggesting that glucose transport mechanisms are targets of selection, i.e. adaptive mutations affect the phosphotransferase system.[27] These hypotheses reason that the mutations in *E. coli* PK1 have a reduced activity and a shorter lag time for rapid glucose import into cells. Under low-glucose conditions, a reduced *E. coli* PK1 activity would reduce PEP flux to pyruvate, and allow the PEP concentration to build up. Since the phosphotransferase system utilises PEP for the transport of glucose into the cell, the accumulated PEP provides a benefit for glucose uptake. Once glucose is reintroduced into the media, the accumulated PEP drives the phosphotransferase-mediated glucose uptake into the cells.[9, 11, 28]

Functional studies (Chapter Four) confirmed, however, that all eight enzymes with non-synonymous mutations are functional (and some are considerably more active at saturating substrate concentrations). Studies by Fen Peng confirmed that the enzymes are functional *in vivo* by showing that the deletion genotypes have a lower fitness benefit (~5%) compared to the point mutations (~10%), see Figure 1.3, Chapter One. If the deletions and point mutations have the same functional effect then we would expect the same fitness effect in otherwise isogenic backgrounds. The mutations could be very unstable, thus mimicking the deletions *in vivo*; however, I have demonstrated that each retains a high thermal stability (55−65 °C compared to the wild-type enzyme of 62 °C, Figure 4.10, Chapter Four). Lastly, proteomics studies[2] and DNA expression arrays[29] demonstrated that the evolved enzymes express at a similar level as the wild-type enzyme.

The results demonstrate two separate adaptive trajectories, both of which are beneficial in the low glucose environment: 1) deletion of (or part of) the gene, and 2) modification of the gene that leads to a functional, yet modified enzyme. The second trajectory is favoured (i.e. substitution mutations occur in ten of twelve populations), and this is consistent with the increased fitness benefit caused by the evolved enzymes (~10%) over the deletion (~5%).[10] However, given that a deletion is only one of many possible ways that the function of a protein can be deleted (i.e. frame shift mutations), and that there is estimated to be ~100 mutations at each coding position of the protein across 20,000 generations, it is surprising that non-synonymous mutations occur as frequently as they do. One explanation for this is that most loss-of-function mutations provide an overall fitness loss, due to protein misfolding or non-compatible interactions and are therefore not retained in the population. Another explanation is that there are reversions in the population, i.e. a deletion occurs, which is reverted and replaced shortly after by a point mutation. What is clear is that the two trajectories have quite different consequences for the evolution of the enzyme and in the low glucose environment are not easily inter-convertible.

The evolved enzymes have altered kinetic properties compared to the wild-type PK1 enzyme, and even more surprisingly, are very different from one another. However, kinetic analyses demonstrated that all of the evolved enzymes have one feature in common: they have a lower activity than the wild-type at physiological PEP concentrations (0.08−0.12 mM in the stationary phase, which was measured in the ancestor strain with the evolved PK1 mutations, which is in accordance with the 0.16 mM reported by Xu *et al*.,[11] and the 0.18 mM reported by Bennet *et al*.[30]). This result is consistent with a parallel metabolic consequence across the twelve populations, where natural selection has selected for adapted enzymes with a lower activity than the wild-type at low PEP concentrations. This result is also consistent with the hypothesis that lower catalytic activity decreases PEP flux through the citric acid cycle, enabling the accumulation of PEP, which in turn initiates rapid glucose import when glucose is reintroduced.[9, 11]

Not only has evolution selected for a lower activity (at physiological PEP concentrations), but it has done so by adapting the FBP allosteric mechanism. The wild-type enzyme has a Michaelis-Menten response to PEP when in the presence of

allosteric activator FBP (Figure 2.5, Chapter 2), producing a rectangular hyperbola curve. This is proposed to be caused by increased dynamics at the A/A' interface which decouples the adjacent active sites, preventing cooperative PEP binding in the presence of FBP (Section 3.6). In contrast to the wild-type enzyme, kinetic studies of the evolved enzymes with respect to PEP and the presence of FBP, found that all of the evolved enzymes (except D127N) show a sigmoidal PEP activation curve. Therefore, PEP cooperativity occurs even when FBP is bound—this is a new feature of the evolved enzymes. The sigmoidal response has the effect of lowering the activity at low PEP concentrations where the $S_{0.5}^{PEP}$ is similar to the wild-type, which is the case in three evolved enzymes (P70Q, P70T and A301S) that occur in five of the twelve populations. In four further evolved enzymes (I264F, A301T, G381A and T462I) the $S_{0.5}^{PEP}$ is also higher (decreased substrate affinity). For the D127N enzyme, the activity is lower because the affinity of ADP is decreased and the k_{cat} is decreased (Table 4.1, Chapter Four), but the PEP affinity and response is very similar to the wild-type enzyme—this is the only evolved enzyme to behave in this way.

Thus, I conclude that while the functional effect is likely to be parallel (i.e. lower activity at low PEP concentrations), and this is what is acted upon by natural selection, the mechanism by which this is achieved is different (not parallel):

1) deletion of a functional gene product (two populations);
2) D127N (one population), which has a lower k_{cat} and decreased ADP affinity;
3) P70Q, P70T and A301S (five populations), which have similar PEP affinity to the wild-type, but now have PEP cooperativity in the presence of FBP; and
4) I264F, A301T, G381A, and T642I (four populations), which have both a lower affinity for PEP and have PEP cooperativity in the presence of FBP.

Lastly, all of the point mutations have a higher fitness than the deletion mutation, suggesting that some additional feature of these enzymes is improving fitness beyond PEP accumulation to aid glucose import. I note that all of the evolved enzymes have a decreased affinity to FBP compared to the wild-type enzyme (wild-type = 0.010 ± 0.007 mM, D127N = 0.017 ± 0.003 mM, other point mutations = 0.1−2.8 mM; Table 4.3, Chapter Four). On one hand this is surprising, given that many of the mutations are distant from the FBP binding site. On the other hand, it probably reflects the dynamic nature of the enzyme. Given that the concentration of FBP at the stationary

phase in the ancestor strain and the ancestor with the evolved *E. coli* PK1 enzymes was found to be ~1.1−1.8 mM, most of the evolved enzymes would be every sensitive to small changes in FBP concentrations. Whereas the wild-type PK1 is fully activated when the FBP concentration is 1 mM (100-fold greater than the $S_{0.5}^{FBP}$ of 0.01 mM), the evolved enzymes (except D127N) will be more sensitive to changes in FBP concentration since their $S_{0.5}^{FBP}$ (0.1−2.8 mM) is within the intracellular FBP concentration range (1.1−1.8 mM) in the stationary phase. This leads to the proposal that the evolved enzymes are able to better regulate glycolysis in response to changes in FBP, fine-tuning the interplay between energy production and glucose import.

7.3.2 Structural fold is conserved

Overall the results confirm that natural selection has selected for enzymes with a taylored activity and an altered activation mechanism compared to the wild-type. However, structure analyses determined that the *in crystal* and *in solution* structures of all eight evolved enzymes remain the same. The robustness of the wild-type quaternary structure and fold in the eight evolved enzymes provides further evidence to support parallel adaptive evolution in *E. coli* PK1, i.e. all of the evolved enzymes have a preserved structure.

A detailed analysis of each of the crystal structures identified small local changes to the evolved enzymes' residue conformations and interactions; however, no other changes to the enzymes' three dimensional structures could be identified. However, local changes to the charge, polarity and size of amino acids, can distort the enzymes electrostatic interactions and alter the dynamic behaviour, promoting functional differences.

The first evidence for altered dynamics within the enzymes was the identification of 'foreign' molecules bound within the active sites of two of the evolved enzymes.[8] Crystallisation of the I264F enzyme, as well as thermal shift assays in Bis-Tris Propane buffer demonstratated that Bis-Tris Propane binds to substrate binding loops within the active site of the enzyme. In addition, a small molecule crystal soak of the T462I enzyme resulted in FBP being bound in the active site, 40 Å away from its correct binding site in the allosteric domain. These results suggest that although the crystal structures of the enzymes are unchanged, the substrate binding promiscuity is

likely a result of increased flexibility of substrate binding loops, which allow the active site to bind substrates with different shapes and sizes.

As described previously, adapatation is the process whereby species gain, lose or modify function to enhance survival in changing environments. The I264F and T462I enzyme results presented here, like many others, support the idea that promiscuous activities create a 'biochemical leakiness', which is exploitable for gain-of-function.[31-33] Studies by Seffernick *et al*. proposed that selection acted upon the substrate binding promiscuity of the melamine deaminase (TriA) and atrazine chlorohydrolase (AtzA) enzymes in *pseudomonas* strains (98% sequence identity), to enable them to catalyse different reactions in different pathways.[31] Another study was successful in generating new enzyme activities in crytochrome P450 enzymes due to their mutational robustness and ability to accept new substrates.[34] These two examples, along with the substrate binding promiscuity identified in two of the evolved PK1 enzymes, demonstrates adaptation by exploitation of substrate binding promiscuity.

The results presented demonstrate the robust nature of the *E. coli* PK1 structure, where substitution mutations completely alter the enzymes' kinetic behaviour and allosteric response, but have no effect upon enzyme structure. However, selection for substrate binding promiscuity in two of the evolved enzymes suggested that the evolved enzymes have different dynamics. It is possible that changes in dynamics are mediating the altered kinetic behaviours of the evolved enzymes, because proteins must move to carry out their functional role.

7.4 Selection for altered dynamics

Having established that the considerable differences in functional behaviour of the evolved *E. coli* PK1 enzymes cannot be explained by the structure; dynamic analysis techniques were employed to determine whether dynamics could explain the altered functional behaviour. The key role that dynamics plays in enzyme function is supported by several studies, including those by Fuentes *et al*.[35] Fuentes *et al*., demonstrated that mutations in the PDZ (second postsynaptic density-95/discs large/zonula occludens-1) domain of the human tyrosine phosphatase 1E protein causes altered ligand binding and protein dynamics, with no change to the structure or

protein conformation.[36] Here, computational and experimental dynamic analyses determined that all of the evolved enzymes have differences in their conformational flexibility compared to the wild-type enzyme.

The relationship between protein dynamics and protein evolution has emerged as an important field, because dynamics are inherent for function, i.e. proteins must move to function. One evolutionary study investigated the dynamic-function relationship of cold-adaptation in an elastase enzyme. Molecular dynamics simulation results demonstrate the role of changes in flexibility of key loops involved in enzyme catalysis for organisms adapted to hot or cold environments.[37, 38] The time required for adaptive evolution and the difficulties involved in dynamically characterising a protein indicates there is a huge gap in the literature concerning the evolutionary connection between dynamics and function.[38] The scarcity of research investigating this relationship establishes a niche for the following results.

Molecular dynamics simulations monitored the root-mean-square fluctuation of the atoms in the wild-type and evolved A301T enzymes, demonstrating differences in the fluctuations between the two proteins. Next, the experimental dynamics results using time-resolved electrospray ionisation coupled to hydrogen-deuterium exchange (TRESI-MS/HDX) showed that all of the evolved enzymes have altered conformational flexibility and differences in how 'fast' they explore conformational space compared to the wild-type. These results provide evidence to suggest that evolution by natural selection has selected for enzymes with altered dynamics.

Not only has natural selection selected for enzymes with altered dynamics, but it has used altered dynamics to change the allostery of the enzyme. Deuterium exchange analysis of the evolved enzymes, demonstrates that allosteric activation by FBP binding, causes a change in the dynamics of the enzymes. Since enzymes exist in an ensemble of conformations, the change in dynamics upon activation suggests that FBP binding induces a shift in the conformational selection of the enzymes.[22, 39, 40] This shift increases how often the enzyme samples the active state by lowering its activation energy.[24, 40, 41] In addition, the dynamic response to activation of each of the evolved enzymes is altered compared to the wild-type enzyme. This result provides dynamic evidence demonstrating that natural selection has selected for

enzymes with an altered response to FBP binding, i.e. adaptation has altered the allosteric activation mechanism by changing the dynamic response to FBP binding.

7.5 Summary

In the case of Lenski's long-term evolution experiment, the adaptations in *E. coli* PK1 serve to increase the availability of PEP for glucose import. The molecular adaptation that achieved this is either a deletion of the gene product, or subtle changes to the function of the gene product. In the later case, the activity of the enzyme is reduced at low PEP concentrations, and the affinity of the enzyme for the allosteric activator (FBP) is fine-tuned to match the concentration of FBP in the cell at the point of serial dilution.

From a molecular perspective, whereas the adaptive mutations in *E. coli* PK1 significantly alter the catalytic activity and allosteric regulation of the enzyme; the structural fold of the evolved enzymes remains conserved. Instead, molecular dynamics studies (simulations and hydrogen-deuterium exchange) demonstrate that the dynamics of the evolved enzymes have changed compared to the wild-type. In addition, localised hydrogen-deuterium exchange analyses determined that the evolved enzymes have different dynamic responses to allosteric activation compared to the wild-type. Conformational flexibility is an important and general underlying molecular cause of adaptation in enzymes—adaptive evolution has fine-tuned protein dynamics to alter allostery.

7.6 References

[1] Ostrowski, EA, Woods, RJ, and Lenski, RE. (2008) The genetic basis of parallel and divergent phenotypic responses in evolving populations of *Escherichia coli*, *Proc. Biol. Sci. 275*, 277-284.

[2] Pelosi, L, Kühn, L, Guetta, D, Garin, J, Geiselmann, J, Lenski, RE, and Schneider, D. (2006) Parallel changes in global protein profiles during long-term experimental evolution in *Escherichia coli*, *Genetics 173*, 1851-1869.

[3] Behe, MJ. (2010) Experimental evolution, loss-of-function mutations, and "the first rule of adaptive evolution", *Q. Rev. Biol. 85*, 419-445.

[4] Golding, GB, and Dean, AM. (1998) The structural basis of molecular adaptation, *Mol. Biol. Evol. 15*, 355-369.

[5] Phillips, PC. (2005) Testing hypotheses regarding the genetics of adaptation, *Genetica 123*, 15-24.

[6] Lewontin, RC. (1978) Adaptation, *Sci. Am. 239*, 212-218, 220, 222 passim.

[7] Elena, SF, and Lenski, RE. (2003) Evolution experiments with microorganisms: the dynamics and genetic bases of adaptation, *Nat. Rev. Genet. 4*, 457-469.

[8] Hottes, AK, Freddolino, PL, Khare, A, Donnell, ZN, Liu, JC, and Tavazoie, S. (2013) Bacterial adaptation through loss of function, *PLoS Genet 9*, e1003617.

[9] Woods, R, Schneider, D, Winkworth, CL, Riley, MA, and Lenski, RE. (2006) Tests of parallel molecular evolution in a long-term experiment with *Escherichia coli*, *Proc. Natl. Acad. Sci. U. S. A. 103*, 9107-9112.

[10] Peng, F. (2015) Molecular basis of adaptive evolution of pyruvate kinase in *Escherichia coli*, In *Biology and Biochemistry*, University of Houston.

[11] Xu, YF, Amador-Noguez, D, Reaves, ML, Feng, XJ, and Rabinowitz, JD. (2012) Ultrasensitive regulation of anapleurosis via allosteric activation of PEP carboxylase, *Nat. Chem. Biol. 8*, 562-568.

[12] Boiteux, A, Markus, M, Plesser, T, Hess, B, and Malcovati, M. (1983) Analysis of progress curves. Interaction of pyruvate kinase from *Escherichia coli* with fructose 1,6-bisphosphate and calcium ions, *Biochem. J. 211*, 631-640.

[13] Speranza, ML, Valentini, G, and Malcovati, M. (1990) Fructose-1,6-bisphosphate-activated pyruvate kinase from *Escherichia coli.* Nature of bonds involved in the allosteric mechanism, *Eur. J. Biochem. 191*, 701-704.

[14] Valentini, G, Chiarelli, L, Fortini, R, Speranza, ML, Galizzi, A, and Mattevi, A. (2000) The allosteric regulation of pyruvate kinase: A site-directed mutagenesis study, *J. Biol. Chem. 275*, 18145-18152.

[15] Monod, J, Wyman, J, and Changeux, JP. (1965) On the nature of allosteric transitions: a plausible model, *J. Mol. Biol. 12*, 88-118.

[16] Mattevi, A, Valentini, G, Rizzi, M, Speranza, ML, Bolognesi, M, and Coda, A. (1995) Crystal structure of *Escherichia coli* pyruvate kinase type I: Molecular basis of the allosteric transition, *Structure 3*, 729-741.

[17] Fenton, AW, and Blair, JB. (2002) Kinetic and allosteric consequences of mutations in the subunit and domain interfaces and the allosteric site of yeast pyruvate kinase, *Arch. Biochem. Biophys. 397*, 28-39.

[18] Morgan, HP, McNae, IW, Nowicki, MW, Hannaert, V, Michels, PAM, Fothergill-Gilmore, LA, and Walkinshaw, MD. (2010) Allosteric mechanism of pyruvate kinase from *Leishmania mexicana* uses a rock and lock model, *J. Biol. Chem. 285*, 12892-12898.

[19] Morgan, HP, Zhong, W, McNae, IW, Michels, PAM, Fothergill-Gilmore, LA, and Walkinshaw, MD. (2014) Structures of pyruvate kinases display evolutionarily divergent allosteric strategies, *R. Soc. Open. Sci. 1*, 140120.

[20] Jurica, MS, Mesecar, A, Heath, PJ, Shi, W, Nowak, T, and Stoddard, BL. (1998) The allosteric regulation of pyruvate kinase by fructose-1,6-bisphosphate, *Structure 6*, 195-210.

[21] Mattevi, A, Bolognesi, M, and Valentini, G. (1996) The allosteric regulation of pyruvate kinase, *FEBS Lett. 389*, 15-19.

[22] Ma, B, Tsai, CJ, Haliloglu, T, and Nussinov, R. (2011) Dynamic allostery: linkers are not merely flexible, *Structure 19*, 907-917.

[23] Kerns, SJ, Agafonov, RV, Cho, YJ, Pontiggia, F, Otten, R, Pachov, DV, Kutter, S, Phung, LA, Murphy, PN, Thai, V, Alber, T, Hagan, MF, and Kern, D. (2015) The energy landscape of adenylate kinase during catalysis, *Nat. Struct. Mol. Biol. 22*, 124-131.

[24] Tsai, CJ, and Nussinov, R. (2014) A unified view of "how allostery works", *PLoS Comput. Biol. 10*, e1003394.

[25] Muirhead, H, Clayden, D, Barford, D, Lorimer, C, Fothergill-Gilmore, L, Schiltz, E, and Schmitt, W. (1986) The structure of cat muscle pyruvate kinase, *EMBO J. 5*, 475-481.

[26] Berg, J, Tymoczko, J, and Stryer, L (2002) *Biochemstry*, 5th Edition ed., W H Freeman, New York.

[27] Travisano, M, and Lenski, RE. (1996) Long-term experimental evolution in *Escherichia coli*. IV. Targets of selection and the specificity of adaptation, *Genetics 143*, 15-26.

[28] Schneider, D, Duperchy, E, Coursange, E, Lenski, RE, and Blot, M. (2000) Long-term experimental evolution in *Escherichia coli*. IX. Characterization of insertion sequence-mediated mutations and rearrangements, *Genetics 156*, 477-488.

[29] Cooper, TF, Rozen, DE, and Lenski, RE. (2003) Parallel changes in gene expression after 20,000 generations of evolution in *Escherichia coli*, *Proc. Natl. Acad. Sci. U. S. A. 100*, 1072-1077.

[30] Bennett, BD, Kimball, EH, Gao, M, Osterhout, R, Van Dien, SJ, and Rabinowitz, JD. (2009) Absolute metabolite concentrations and implied enzyme active site occupancy in *Escherichia coli*, *Nat. Chem. Biol. 5*, 593-599.

[31] Seffernick, JL, de Souza, ML, Sadowsky, MJ, and Wackett, LP. (2001) Melamine deaminase and atrazine chlorohydrolase: 98 percent identical but functionally different, *J. Bacteriol. 183*, 2405-2410.

[32] Jensen, RA. (1976) Enzyme recruitment in evolution of new function, *Annu. Rev. Microbiol. 30*, 409-425.

[33] Copley, SD. (2014) An evolutionary perspective on protein moonlighting, *Biochem. Soc. Trans. 42*, 1684-1691.

[34] Jung, ST, Lauchli, R, and Arnold, FH. (2011) Cytochrome P450: taming a wild type enzyme, *Curr. Opin. Biotechnol. 22*, 809-817.

[35] Fuentes, EJ, Gilmore, SA, Mauldin, RV, and Lee, AL. (2006) Evaluation of energetic and dynamic coupling networks in a PDZ domain protein, *J. Mol. Biol. 364*, 337-351.

[36] Tsai, CJ, del Sol, A, and Nussinov, R. (2008) Allostery: absence of a change in shape does not imply that allostery is not at play, *J. Mol. Biol. 378*, 1-11.

[37] Papaleo, E, Riccardi, L, Villa, C, Fantucci, P, and De Gioia, L. (2006) Flexibility and enzymatic cold-adaptation: a comparative molecular dynamics investigation of the elastase family, *Biochim. Biophys. Acta 1764*, 1397-1406.

[38] Liberles, DA, Teichmann, SA, Bahar, I, Bastolla, U, Bloom, J, Bornberg-Bauer, E, Colwell, LJ, de Koning, AP, Dokholyan, NV, Echave, J, Elofsson, A, Gerloff, DL, Goldstein, RA, Grahnen, JA, Holder, MT, Lakner, C, Lartillot, N, Lovell, SC, Naylor, G, Perica, T, Pollock, DD, Pupko, T, Regan, L, Roger, A, Rubinstein, N, Shakhnovich, E, Sjolander, K, Sunyaev, S, Teufel, AI, Thorne, JL, Thornton, JW, Weinreich, DM, and Whelan, S. (2012) The interface of protein structure, protein biophysics, and molecular evolution, *Protein Sci. 21*, 769-785.

[39] Dellus-Gur, E, Elias, M, Caselli, E, Prati, F, Salverda, ML, de Visser, JA, Fraser, JS, and Tawfik, DS. (2015) Negative Epistasis and Evolvability in TEM-1 beta-Lactamase--The Thin Line between an Enzyme's Conformational Freedom and Disorder, *J. Mol. Biol. 427*, 2396-2409.

[40] Motlagh, HN, Wrabl, JO, Li, J, and Hilser, VJ. (2014) The ensemble nature of allostery, *Nature 508*, 331-339.

[41] Smock, RG, and Gierasch, LM. (2009) Sending signals dynamically, *Science 324*, 198-203.

Chapter Eight

Experimental procedures

8.1 Molecular biology techniques

The protocols and methods from this section were adapted from "Molecular cloning: a laboratory manual" 4th Edition.[1]

8.1.1 Sterilisation technique

All culture procedures were carried out on a bench cleaned with 70% ethanol, next to a blue flamed Bunsen burner. The nichrome loop was sterilised using both 70% ethanol and the blue bunsen flame before each use. A sterile control plate was made with every bacterial streak to ensure no contamination was present. All Luria Bertani (LB) media were prepared using sterile, filtered double distilled water (ddH_2O), followed by sterilisation in the autoclave at 121 °C for 15 minutes before use, along with any equipment involved in the handling of bacterial cultures.

8.1.2 Bacterial strains and plasmids

Two bacterial strains were used in this study. *Escherichia coli* XL-1 Blue strain was used for mutagenesis and as a storage strain. *E. coli* BL21 (DE3) strain provides a high level of protein expression and easy induction; therefore this strain was used for protein expression and purification.

The *pyk*F gene had been previously cloned into a pBluescript II KS+ vector, forming pGV5A and this was donated by Professor Mattevi.[2]

8.1.3 Media preparation

A ready-to-use powder LB base was purchased through Invitrogen and prepared by mixing 20 g LB powder per litre of distilled water (dH_2O) to give a 2% w/v medium. Bacto-agar was dissolved in the LB media to a final concentation of 1.5%. Following autoclaving, when the agar cooled to around 50 °C, ampicillin was added to a final concentration of 100 µg/mL. The agar media was mixed by gentle swirling. Approximately 20 mL of the media was poured into each Petri dish under sterile conditions. The plates were left for around 30 minutes to cool before being wrapped in glad wrap and stored at 4 °C for up to one month.

8.1.4 Antibiotics

Antibiotics are used to selectively eliminate bacteria that do not contain an antibiotic resistance gene. The *E. coli* bacterial cells were transformed with plasmids carrying the ampicillin resistance gene, therefore ampicillin was the selective antibiotic used for this study. 1000× concentration ampicillin stocks were prepared by adding 100 mg of ampicillin to 1 mL of ddH_2O. The ampicillin stocks were then filtered through a 0.22 µm Millipore syringe driven filter unit and stored in 1 mL aliquots at -20 °C for up to 1 year.

8.1.5 Inoculation of bacterial culture

Bacteria from a frozen glycerol stock solution were streaked onto LB + ampicillin plates using a flame-sterilised nichrome wire loop. The quadrant dilution streak technique was used to obtain well-isolated single colonies. The plate was then incubated at 37 °C overnight. A single colony from the isolation plate was used to inoculate a 100 mL starter culture of LB media containing 100 µg/mL ampicillin. This 100 mL pre-culture was placed in a 37 °C incubator with moderate shaking (160 rpm) overnight. The pre-culture (10 mL) was then used to inoculate 1 L of LB media containing 100 µg/mL of ampicillin and incubated at 37 °C with shaking (160 rpm) overnight.

8.1.6 Preparation of glycerol stocks for storage

An aliquot (1.5 mL) from an overnight culture was centrifuged at 13,000 × g, 5 min. The supernatant was removed and the pellet was re-suspended in 500 µL of fresh LB medium. 50% glycerol was then added (50% v/v, 500 µL) and mixed gently before being snap cooled in liquid nitrogen and stored in the -80 °C freezer.

8.1.7 Plasmid miniprep by PureLink® Quick Plasmid kit

A PureLink® Quick Plasmid Miniprep kit was used to isolate high quality plasmid DNA from an overnight pre-culture of *E. coli* cells. The 8 step centrifugation purification procedure was used to isolate the DNA, steps include:

1. Harvest
2. Resuspend
3. Lyse
4. Precipitate
5. Bind
6. Wash and remove ethanol
7. Elute
8. Recover

8.1.8 Transformation of BL21 (DE3) cells

Aliquots of competent cells (100 µL) were gently thawed on ice. DNA (2 µL) was transferred to the competent cells and the transformation reactions were incubated on ice for 20 minutes. The reaction was heat pulsed at 42 °C for 90 seconds and then put on ice for 2 minutes. Super optimal broth (400 µL) with catabolic repressor (SOC) media was added to the reaction and incubated at 37 °C for 1 hour with shaking. The reaction mixture (100 µL and 400 µL) was plated on separate agar plates containing ampicillin and incubated over night at 37 °C.

8.2 General biochemistry methods

Unless otherwise stated, all enzymes were kept on ice or at 4 °C to reduce denaturation or inactivation during manipulation. All enzymes were aliquoted (100 µL, 1 - 5 mg/mL) and routinely stored in 1 mM ethylenediaminetetraacetic acid (EDTA), 2 mM β-mercaptoethanol and 10 mM Tris pH 7.5 at 4 °C at -80 °C.

8.2.1 Growth and over-expression of wild-type PK1 and evolved enzymes

8.2.1.1 Growth

Frozen glycerol stocks of *E. coli* BL21 (DE3) cells containing pGV5A and its derivatives were streaked onto LB and ampicillin plates and incubated at 37 °C overnight. For each strain, a single isolated colony was used to inoculate a 100 mL LB broth and ampicillin pre-culture which was grown overnight with shaking at 37 °C. This pre-culture (10 mL) was then used to inoculate 1 L of LB broth and ampicillin. The 1 L culture was incubated at 37 °C with shaking for 3–5 hours until it reached an optical density at 600 nm (OD_{600}) of 0.6−0.8. At this time isopropylthio-β-D-galactoside (IPTG) was added to the culture to a final concentration of 1 mM, to induce protein expression. The culture was then left overnight in the shaking incubator to allow protein expression to continue. The cultures were put on ice to cool to 4 °C to reduce any protease activity. The cells were harvested by centrifugation at 5,000 × g at 4 °C, 10 min. The supernatant was discarded and the cell pellet was resuspended in crude extract buffer (Table 8.1) and centrifuged again to wash off any residual LB. Finally, the washed cell pellet was suspended in 40−80 mL of cold crude extract buffer.

Table 8.1 Crude extract buffer conditions.

Crude extract buffer	1 mM EDTA 2 mM β-mercaptoethanol 10 mM Tris, pH 8.5 at 4 °C 100 mM KCl 10 mM $MgCl_2$

8.2.1.2 Preparation of cell free crude extract by ultrasonication

Cells resuspended in crude extract buffer were sonicated for 5 minutes using the UP2005 Ultrasonic Processor in cycles of 0.5 second bursts followed by 0.5 second pauses. Sonication was performed on ice with an amplitude of 70%. The lysed cells were then spun in a centrifuge at 20,000 × g for 20 minutes at 4 °C to precipitate the cell debris. The pellet was discarded and the supernatant containing soluble protein was collected and filtered through a 0.45 μm Millipore syringe driven filter unit.

8.2.2 Purification of wild-type PK1 from *E. coli* BL21 (DE3)

The protocol for the purification of *E. coli* PK1 from BL21 (DE3) was adapted from the procedure used by Mattevi and colleagues.[3] This procedure involved three purification steps: anion-exchange chromatography, hydrophobic interaction chromatography and size exclusion chromatography to obtain pure and active enzymes.

8.2.2.1 Anion-exchange chromatography

The cell free crude extract was loaded on to a Q-Sepharose anion-exchange column (GE Healthcare) with a bed volume of 20 mL. The column had been washed (1 M NaCl or KCl buffer) and pre-equilibrated with three column volumes of anion-exchange buffer A (Table 8.2) until the A_{280} nm ultraviolet (UV) absorbance flat lined and the required pH of 8.5 was reached. The protein sample was then injected into the column, followed by a wash with 100–200 mL of buffer A at 3 mL/min to remove any unbound proteins and DNA. The enzyme was eluted with Q-Sepharose buffers A and B (Table 8.2) with an increasing salt gradient (100−500 mM KCl) over 60 minutes. Eluted fractions were collected and the UV peaks were tested for protein using sodium dodecyl sulfate poly acrylamide gel electrophoresis (SDS-PAGE) gel (Section 8.2.3). The fractions with the highest levels of protein were pooled for the next purification step.

Table 8.2 Anion-exchange buffer conditions.

Q-Sepharose buffer A	1 mM EDTA 2 mM β-Mercaptoethanol 10 mM Tris, pH 8.5 at 4 °C 100 mM KCl
Q-Sepharose buffer B	1 mM EDTA 2 mM β-Mercaptoethanol 10 mM Tris, pH 8.5 at 4 °C 500 mM KCl

8.2.2.2 Hydrophobic interaction chromatography

The Phenyl-Sepharose column (GE Healthcare; bed volume 20 mL) was washed and equilibrated with three column volumes of Phenyl-Sepharose buffer A until a pH of 7.5 was reached (Table 8.3). The protein solution was then prepared by adding $(NH_4)_2SO_4$ to a final concentration of 1.17 M to the pooled anion-exchange fractions to encourage a hydrophobic interaction with the column. The protein solution was injected onto the column and washed through with three column volumes of buffer A. The enzyme was then eluted with a gradient of decreasing $(NH_4)_2SO_4$ concentration (1.17-0 M) over 30 minutes. Again, the eluted fractions with high UV absorbance were run on an SDS-PAGE gel and those with the most protein were pooled for the final purification step.

Table 8.3 Phenyl-Sepharose buffer conditions.

Phenyl-Sepharose buffer A	1 mM EDTA 2 mM β-Mercaptoethanol 50 mM Tris, pH 7.5 at 4 °C 100 mM KCl 1.17 M $(NH_4)_2SO_4$
Phenyl-Sepharose buffer B	1 mM EDTA 2 mM β-Mercaptoethanol 50 mM Tris, pH 7.5 at 4 °C 100 mM KCl

8.2.2.3 Size exclusion chromatography

Buffer containing 10 mM Tris (pH 7.5, 4 °C), 1 mM EDTA and 2 mM β-mercaptoethanol was used to equilibrate a HiLoad 16/600 Superdex 200 gel filtration column (GE Healthcare; bed volume 120 mL). The pooled fractions from the previous purification step were concentrated to 2 mL using a 30 kDa molecular weight cutoff centricon (Millipore). The protein was injected onto the gel filtration column and eluted by washing through with up to 150 mL of the size exclusion buffer. Nano-Drop measurements (Section 8.2.4.1) of the eluted fractions with the highest UV absorbance were taken and the fractions that were found to have the highest protein concentration were pooled for storage.

8.2.3 NuPAGE® Sodium dodecyl sulphate polyacrylamide gel electrophoresis

Samples for SDS-PAGE were prepared according to the conditions outlined in Table 8.4, and heated at 70 °C for 10 minutes. A SDS-PAGE gel chamber was set up with a NuPAGE® (Life Technologies) precast 4–12% gradient Bis-Tris gel containing 10 × 1.0 mm wells. Both the inner and outer buffer chambers were filled with 3-(N-morpholino)-propanesulfonic acid (MOPS) SDS running buffer (see Table 8.5). 5 µL of BioRad Precison Plus Protein™ WesternC™ Standards (10–250 kDa) was loaded into the first well of the gel and 10 µL of each sample was loaded into the remaining required wells. Electrophoresis was run at 200 V (constant) for 50 minutes. The SDS-PAGE gel was then stained with SimplyBlue ™ safestain (Invitrogen). The gel was then photographed in the CHEMI GENIUS^2 bio-imaging system (Syngene).

Table 8.4 Conditions for preparation of sample for SDS-PAGE gel electrophoresis.

Reagent	Volume (µL)
Protein Sample	5
NuPAGE® LDS Sample Buffer (4x)	2.5
NuPAGE® Reducing Agent (10x)	1
ddH_2O	1.5
Total Volume	10

Table 8.5 NuPAGE MOPS SDS running buffer conditions.

Reagent	Concentration (mM)
MOPS	50
Tris Base	50
EDTA	1.025
SDS	3.465

8.2.4 Determination of protein concentration

8.2.4.1 Nano-Drop spectrophotometry

The approximate concentration of protein was quantitated using a Nano-Drop ND-1000-v3.5 UV-Vis spectrophotometer and the appropriate molar extinction coefficient of the protein at 280 nm (calculated from the amino acid sequence using ExPASy ProtParam tool).[4] From this, absoption was converted to protein concentration using Beer's law.

8.2.4.2 Bio-Rad protein assay

Accurate concentration measurements of solubilised protein were determined using the Bio-Rad Protein Assay, which was based on the method of Bradford.[5] The Bio-Rad microtiter plate protocol was used at each purification step to monitor the changes in concentration during protein purification. Five dilutions (0, 0.062, 0.125, 0.25 and 0.5 mg/mL) of bovine serum albumin (BSA) protein standard were prepared within the linear range of the assay (0.05–0.5 mg/mL). The protein solution (10 µL) was added to 200 µL of Coomassie dye reagent (Bio-Rad) in each microplate well. The microplate was mixed thoroughly with shaking, followed by incubation at room temperature for exactly 5 minutes to allow the dye to bind to the protein. Absorbance at 595 nm was measured in a SpectraMax M-series Multi-Mode Microplate reader spectrophotometer and a linear standard curve was created. This same procedure was followed for measuring protein samples and the absorbances were compared to the standard curve to give accurate protein concentration readings. All samples were blanked against a solution containing 10 µL of ddH_2O and 200 µL of coomassie dye reagent. Concentrations of protein samples were measured in triplicate.

8.3 Kinetics

8.3.1 Lactate dehydrogenase coupled activity assay

The LDH coupled assay[6] was used to test the activity of protein fractions collected at each purification step. The LDH coupled reaction is illustrated below in Figure 8.1.

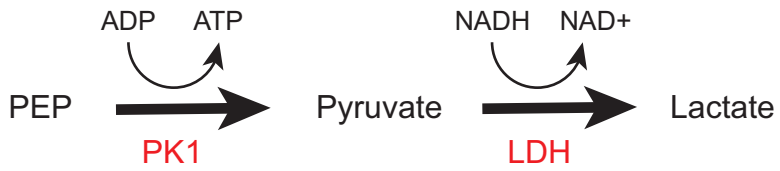

Figure 8.1 LDH coupled reaction. The reaction catalysed by *E. coli* PK1 produces pyruvate which reacts with NADH via LDH catalysis to produce oxidised NAD^+ and lactate.

The reagents and concentrations required to make up the *E. coli* PK1 assay solution are presented in Table 8.6.

Table 8.6 Conditions for preparation of *E. coli* PK1 assay mixture.

	[Initial] (mM)	Volume (µL)	[Final] (mM)
HEPES (pH 7.5)	1000	100	100
KCl	500	100	50
$MgCl_2$	100	100	10
PEP	100	20	2
ADP	100	20	2
FBP	100	20	2
NADH	6	20	0.12
LDH		20	22 (units/cell)
ddH_2O		580	
Total		980	

The assay mixture was incubated for 12 minutes at 37 °C in the Cary 100 Bio UV-VIS spectrophotometer (Varian, Agilent Technologies, Palo Alto, USA), giving an initial absorbance of about 0.72 at 340 nm. The reaction was initiated by the addition of 20 µL of protein sample from the eluted fractions. The activity was measured by monitoring the oxidation of NADH as a decrease in absorbance at 340 nm. The decrease in NADH absorbance is due to the LDH catalysing a reaction between NADH and pyruvate to form NAD^+ and lactate. 1 unit of *E. coli* PK1 activity (U) was found to oxidise 1 µmole NADH per second per mg of protein.

8.3.2 Steady-state kinetic analysis of wild-type PK1 and evolved enzymes

Steady-state kinetic analysis of the enzymes was carried out using the same LDH coupled assay method as used for the enzyme activity test (Section 8.3.1.). The reaction mixture contained 100 mM HEPES at pH 7.5, 50 mM KCl, 10 mM $MgCl_2$, 0.12 mM NADH, 22 unit/mL LDH and varying concentrations of fructose-1,6-bisphosphate (FBP), phosphoenolpyruvate (PEP) and adenosine diphosphate (ADP). Firstly, enzyme activity was determined with saturating ADP (as determined in the ADP titrations) and varying concentrations of PEP, with and without FBP. Secondly, the enzymatic activity was measured with saturating PEP (as determined in the PEP titrations) and varying concentrations of ADP, with and without FBP.

Finally, FBP titrations were carried out using limiting substrate concentrations determined in the previous four assay conditions – I264F and A301T FBP titrations contained 10 mM PEP and ADP, and wild-type PK1 and the remaining six evolved enzymes contained 2 mM PEP and ADP. Each reaction mixture was incubated at 37 °C for 12 minutes to enable the reaction mixture to reach temperature. The reaction was initiated by the addition of 20 µL enzyme, bringing the total reaction volume to 1 mL.

8.3.3 Kinetic analysis using alternative substrate

Steady-state kinetic analysis of *E. coli* PK1 was carried out using the substrate GDP in place of ADP. These assays were performed using the same method as Section 8.3.2.

8.3.4 Data analysis

All kinetic assays were duplicated and the intial rate data were processed and analysed using the program OriginPro (Origin Lab, version 8.5.1). The Hill cooperativity model (Equation 8.1)[7] was fit to the data to determine the various V_{max}, $S_{0.5}$ and n_H parameters.

Hill cooperativity model: $$V_0 = \frac{(k_{cat}[S]^n)}{(S_{0.5}{}^n) + ([S]^n)}$$ **(Equation 8.1)**

k_{cat}	Turnover number
$[S]$	Substrate concentration
$S_{0.5}$	Substrate concentration when half of the V_{max} is reached
V_0	Initial velocity
n_H	Hill coefficient

8.4 Biophysical methods

8.4.1 Mass spectrometry for mass measurement

Mass spectrometry (MS) sample preparation for mass determination (hydrogen-deuterium exchange MS will be described in Section 8.7) typically involves desalting the protein out of its buffer and into water or ammonium bicarbonate. *E. coli* PK1 and the evolved enzymes were prepared by dilution to 1 mg/mL with ddH_2O to minimise detection of the background buffer constituents. The samples were then directly injected into the maXis 3G UHR-Qq-TOF MS (Bruker Daltonik GmbH, Bremen, Germany) coupled to a Dionex Ultimate 3000 LC system (ThermoFisher), followed by injection of a calibrant, ESI-L Low Concentration Tuning Mix (Agilent Technologies).

The resulting data was processed using Compass software (Bruker Daltonik GmbH, Bremen, Germany)

The mass/charge (m/z) distribution was used to estimate the molecular weight of each sample by using the following equation:

$$m/z = \frac{(MM + nH^{+})}{n} \qquad \textbf{(Equation 8.2)}$$

m/z	mass-to-charge
MM	molecular mass
n	integer number on the ion
H	mass of a proton = 1.008 Da

8.4.2 Differential scanning

DSF was performed using the Bio-Rad iQ™5 Multicolour Real-Time PCR Detection System, with methods based upon those from Morgan and colleagues.[8] Solutions of Sypro® Orange protein gel stain (20 µL, 50x concentrate) and protein (80 µL, 0.4−0.6 mg/mL) were added to the wells of a 96-well thick-wall PCR plate (Bio-Rad). The plates were sealed with optical quality sealing tape (Bio-Rad) and heated in an iQ™5 Multicolor Real-Time PCR Detection System from 20 to 100 °C, with 10 second fluorescence measurements taken in 0.5 °C increments.

The fluorescence was plotted as a function of temperature, generating a sigmoidal shaped curve.[9] The inflection point of the transition curve (T_m) is calculated using an equation such as the Boltzmann equation:

$$Y = \frac{LL + (UL - LL)}{1 + \exp((T_m - x) / a)} \qquad \textbf{(Equation 8.3)}$$

LL	minimum intensities
UL	maximum intensities
a	slope of the curve within T_m

8.5 Small angle X-ray scattering

8.5.1 Sample preparation and detection

Protein was purified following the purification protocol in Section 8.2.2, producing >95% pure protein (as judged on SDS-PAGE gel) (Section 8.2.3). The protein was then concentrated to 10 mg/mL using a 30 kDa molecular weight cutoff centricon (Millipore). The SAXS detector is very sensitive, so freezing was avoided and the protein was kept on ice at all times during preparation.

A 5 ml size exclusion column was equilibrated with the exact buffer that the proteins were purified in (10 mM Tris, pH 7.5, 4 °C and 1 mM EDTA and 2 mM β-mercaptoethanol). Protein samples (~10 mg/mL, 50 μL) were auto loaded onto the column and shot with a monochromatic beam of X-rays (camera length 1600 mm), the scatter was detected on a 2D detector and produced a diffraction pattern. Data collection required two measurements: one of the protein solution, and one of the buffer background solution. The 2D detected scatter intensities created by the protein were produced by subtracting the buffer scattering profile from the protein scattering profile. The buffer-subtraction was carried out using *SCATTERBRAIN* (written and provided by the Australian Synchrotron; available at http://www.synchrotron.org.au/), creating the starting point for the analysis of the protein SAXS data.

8.5.2 Data analysis

Data quality was confirmed using *GUINIER* analysis, which plots the buffer-subtracted profile as a guinier curve (ln(I)) versus q^2.

Next, *PRIMUS* Qt from the ATSAS package[10] was used to form a trial P(r) function from the substrated scatter. The *GNOM* program generated the Fourier transform and balanced the smoothness of the trial P(r) function with the goodness of the fit to the data and provided the first estimate of the maximum dimension of the proteins (D_{max}). Finally, the *CRYSOL*[11] program was used to form an overlay of the scatter with the crystal structure PDB data.[12]

8.5.3 Protein with ligand preparation

Preparation of protein for SAXS detection with ligand were performed in a similar way to Section 8.5.1. However, 2 mM FBP was added to both the protein after purification and the purification buffer. All other aspects of the data collection and analysis were the same.

8.6 X-ray crystallography

8.6.1 Crystallisation

8.6.1.1 Crystallisation of the wild-type PK1 enzyme

Crystallisation was conducted using a 10 mg/mL preparation of wild-type enzyme in 10 mM Tris (pH 7.5, 4 °C), 2 mM β-mercaptoethanol and 1 mM EDTA. Crystal growth was carried out using the hanging drop vapour diffusion method and a reservoir solution of 16% (w/v) PEG 8000, 10 mM $MgSO_4$, 10 mM KCl, 100 mM MES/NaOH (pH 6.2), 0.02% (w/v) NaN_3.[12] The following conditions within the drop were varied for optimisation: 1.7–2.2 µL of reservoir solution and 2 µL or 2.5 µL of protein solution. The plates were equilibrated against 1 mL of reservoir solution in 24-well Linbro plates (Hampton Research) at 8 °C and 20 °C. Co-crystallisation was also attempted, with some of the drops containing 2 mM FBP or PEP. Co-crystallisation was unsuccessful, however, and soaking crystals with the allosteric activator, FBP, lead to the immediate cracking of the crystals.

8.6.1.2 Crystallisation of the evolved enzymes

Crystallisation trials were carried out for each of the evolved enzymes using a 8–12 mg/mL preparation of enzyme in 10 mM Tris (pH 7.5, 4 °C), 2 mM β-mercaptoethanol and 1 mM EDTA. Four different crystal screens were selected for the crystal growth trials: PACT premier™, JCSG plus™, Morpheus™ and Clear Strategy™ Screen I (Molecular Dimensions). The sitting-drop vapour diffusion crystal screen set up was carried out using a protein crystallisation robot at the University of Canterbury or the Collaborative Crystallisation Centre (C3) in Melbourne Australia, creating droplets consisting of 300 nL protein + 300 nL reservoir and 150 nL protein + 150 nL reservoir, respectively. All four of the crystal screens produced numerous hits (signs of crystallinity) with precipitation and

crystals forming in several wells from plates incubated at both 8 and 20 °C. Details of the crystallisation conditions of each of the crystal structures described in Chapter Three and Five are shown in Table 8.7 below.

Table 8.7 Crystallisation conditions for each crystal structure solved in this study.

Protein	Screen	Well No.	Buffer/Salt/Ligands	Precipitant	pH
P70Q	Morpheus	E2	0.12 M Ethylene glycol 0.1 M Buffer System 1*	30% EDO_P8K**	6.5
P70T	Morpheus	H3	0.1 M Amino acids 0.1 M Buffer System 1*	30% GOL_P4K***	6.5
D127N	Morpheus	D3	0.12 M Alcohols 0.1 M Buffer System 1*	30% GOL_P4K***	6.5
I264F	PACT	F6	0.2 M Sodium formate 0.1 M BTP	20% w/v PEG 3350	6.5
A301S	PACT	D4	0.1 M MMT buffer	25% w/v PEG 1500	7.0
A301T	PACT	B2	0.1 M MIB buffer	25% w/v PEG 1500	5.0
G381A	Morpheus	H3	0.1 M Amino acids 0.1 M Buffer System 1*	30% GOL_P4K***	6.5
T462I	Morpheus	D2	0.12 M Alcohols 0.1 M Buffer System 1*	30% EDO_P8K**	6.5
T462I + ligand	Morpheus	C2	0.09 M NPS 0.1 M Buffer System 1*	30% EDO_P8K**	6.5

Mixes of buffer systems and precipitants used:

*Buffer System 1: 1 M Imidazole, MES (acid) at pH 6.5, 20 °C

**EDO_P8K: 60 % Ethylene glycol, PEG 8000

***GOL_P4K: 60 % Glycerol, PEG 4000

8.6.2 X-ray data collection and processing

Diffraction data for all *E. coli* PK1 crystals were collected on MX1 or MX2 beamlines at the Australian Synchrotron, Victoria, Australia. The crystals were mounted onto nylon loops before being briefly soaked in a cryoprotectant solution containing the reservoir solution of the drop they were crystallised in (Table 8.7). Crystals were then flash cooled in liquid nitrogen and mounted onto either the MX1 or MX2 beamline's goniometer in a cold nitrogen stream at 110 K. The detector was positioned approximately 240−320 mm

(slight variation with beamline) from the crystal and images were taken in 0.5° steps for at least a 180° pass, with an exposure time of 1 s.

Multiple data sets were collected on all of the protein crystals available from the different drops and collected diffraction was generally 2 Å–3.1 Å. Co-crystallisation was attempted where possible by soaking the crystals in a cryo-protectant solution containing 2 mM of substrate or ligand (FBP, PEP, ADP or GDP). The co-crystallisation often led to crystal cracking, however it was successful on a few occasions. The datasets were processed and evaluated using *XDS*[13] and the resulting reflections were scaled and merged using *AIMLESS*[14] from the *CCP4* program suite.[15]

8.6.3 Structure determination and refinement

All crystal structures were solved by molecular replacement, intially performed using *PHASER*[16] from the *CCP4* suite of programs,[15] using the structure of *E.coli* PK1 as a search model (PDB ID: 1PKY).[12] All relevant data-collection and processing parameters for wild-type PK1 and eight evolved enzymes are provided in Sections 2.5 and 5.8. Initial rounds of refinement were carried out in *REFMAC5*[17] from the *CCP4* program suite. Space group and data quality analysis were assessed using *XTRIAGE* from the *PHENIX* package.[18] Manual refinement in *COOT* was combined with simulated annealing and subsequent iterative adjustments using *REFINE* from the *PHENIX* package[18] to produce a strong structural model of the wild-type PK1. Each model was examined residue-by-residue in *COOT* and addition and/or deletion of atoms was carried out based upon the presence of sufficient electron density. The refinement output was monitored for a decrease in both the R_{factor} and R_{free} over the refinement cycles. Ligands and water molecules were manually modelled into the observed electron density using *COOT*. The crystallographic R_{factors} provided a means to follow the model improvement throughout the refinement process.

Structure determination of all subsequent protein crystals was carried out using the same procedure as above. However, the new wild-type PK1 structural model, 4YNG, was used for molecular replacement in place of 1PKY.

8.7 Time-resolved electrospray ionisation mass spectrometry coupled to hydrogen-deuterium exchange

The TRESI-MS/HDX experiment described in this section required engineering of a protein-deuterium mixing device and a microfluidic chip. A detailed description of the device preparation is provided below.

8.7.1 Protein preparation

Purified protein was desalted using 2 mL Zeba spin desalting columns (Thermo Scientific), followed by overnight buffer exchange into a 200 mM ammonium acetate buffer (pH 6.9) using a Slide-A-Lyzer mini dialysis device (10 kDa MWCO; Thermo Scientific).

8.7.2 Rapid protein-deuterium mixing device design

The rapid continuous flow protein-deuterium mixing devices (Figure 8.1)[19-22] were modified from Wilson and Konnerman and fabricated according to the following methods:

8.7.2.1 Global

A stainless steel metal capillary (Outside diameter (OD.) 203 μm, Interior diameter (ID.) 101 μm; McMaster-Carr, Aurora, OH, USA) was cut to a length of 220 mm. A 2 mL mixture consisting of 25% nitric acid and 75% hydrochloric acid was passed through the metal capillary via syringe to erode and enlarge the capillaries inner diameter. The metal capillary was immediately washed with 10 mL ddH_2O to prevent any further corrosion, followed by polishing of both ends of the capillary using 2000 grit sand paper to open them. The internal diameter was calculated (111.2 μm) by measuring the back pressure on a high pressure liquid chromatography (HPLC) pump (1 mL/min, 100% acetonitrile). The stainless steel capillary was then fit to a 3.5 cm long (ID. 230 μm) fluoroethylene polymer sleeve (Upchurch Scientific, Oak Harbor, WA, USA) and attached to a three-way T-union. The top of the source housing was then modified to accept the three-way T-union (Upchurch Scientific, Oak Harbor, WA, USA).

A 40 cm long polyimide coated glass capillary (OD. 109 µm, ID. 40 µm; Polymicro Technologies, Phoenix, AZ, USA) was passed through the newly eroded metal capillary and sealed using a CO_2-powered laser (Versa-Laser^{TM} engraving device; Universal Laser, Scottsdale, AZ, USA). A notch was cut 2 mm in from the sealed end and the open end of the glass capillary was passed through the T-union and connected to a syringe (syringe 1, protein) via a LuerLock fitting. A second 40 cm long glass capillary (OD. 167 µm, ID. 98 µm) was attached to syringe 2 (deuterium) in the same manner as syringe 1, while the other end was connected to the T-union.

8.7.2.2 Localised

Fabrication of the protein-deuterium mixing device for localised experiments was the same but without eroding the metal capillary, therefore localised experiments had a longer minimum reaction time.

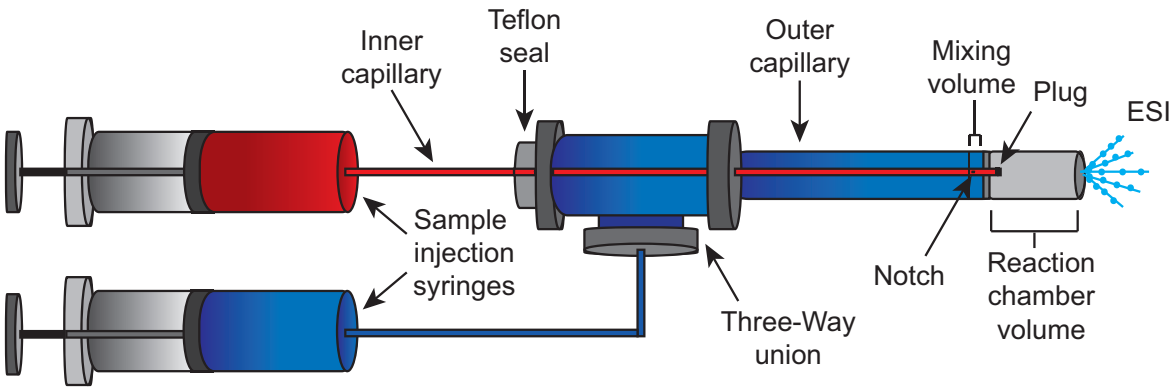

Figure 8.1 Schematic of the microfluidic rapid mixing device for time-resolved electrospray ionisation mass spectrometry coupled to hydrogen-deuterium exchange experiments. Schematic depiction of the capillary-based protein-deuterium rapid mixing device with adjustable reaction chamber volume.[19-22]

8.7.3 Global HDX

8.7.3.1 TRESI-MS experiments

The global rapid continuous flow protein-deuterium mixing device was interfaced to a Waters Synapt G1 mass spectrometer (Waters, Milford, MA, USA). The instrument was operated in positive ion mode with optimal running conditions of +4900 V to +5200 V source voltage.

Fluids were introduced into the device using Harvard 11+ infusion pumps (Holliston, MA). Protein and D_2O were introduced to the protein-deuterium mixing device in a (1:3 ratio) and these followed a laminar flow pattern until they reach the notch, where they were mixed. Flow rates of 1 μL/min for protein solution and 3 μL/min of D_2O were able to achieve labeling times of 13.6 ms to 1.5 s. The reaction time was adjusted by changing the position of the mixing capillary within the channel by pulling the mixing capillary back increasing the dead space after mixing, thus increasing the reaction time (Figure 8.1).

8.7.3.2 Global data analysis

All mass spectrometry spectra analyses were carried out using the MassLynx MS software, version 5.5.0 (Waters, Milford, MA, USA). Deuterium uptake was calculated based upon the change in mass over time from non-deuterated protein. Deuterium exchange kinetics were plotted over time and fit to an exponential function: $y=y0 + a(1-e^{-kt})$.[22]

8.7.4 Localised HDX

8.7.4.1 Microfluidic device preparation

The microfluidic channel design was generated based upon a protocol by Rob *et al.*[23] in CorelDraw X3 (Corel Co., Ottawa, ON, Canada) and lasered onto blank pre-cut polymethyl methacrylate (PMMA) substrate with dimensions (8.9 cm x 3.8 cm x 0.3 cm; Professional Plastics, Fullterton, CA, USA). Three channels and a pepsin digestion well (32 mm x 5 mm, 0.01 mm; volume = 1.6 μL) were engraved into the PMMA substrate using a 30 W CO_2 Versa-Laser™ engraving device (Universal Laser, Scottsdale, AZ, USA) as shown below in Figure 8.2.

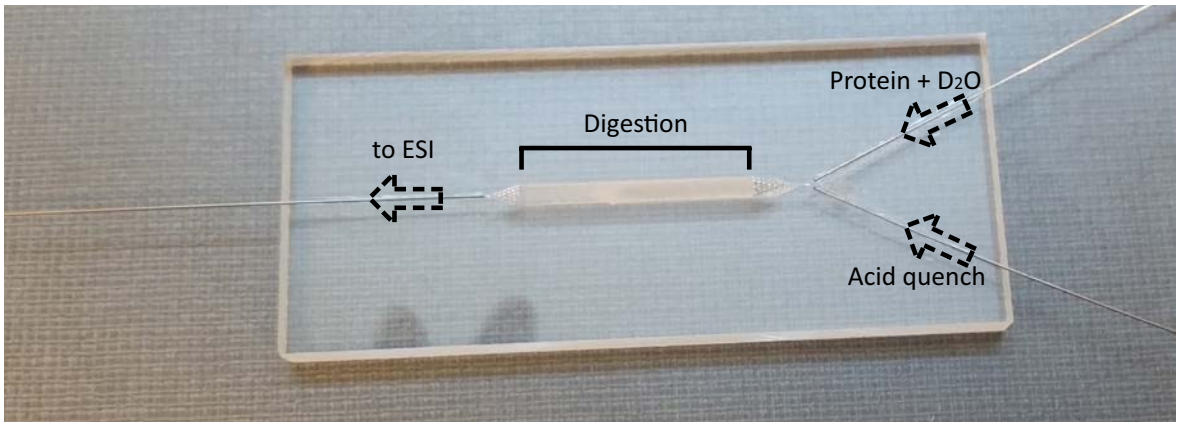

Figure 8.2 The microfluidic chip for site-specific hydrogen-deuterium exchange experiments. The capillary-based protein-deuterium rapid mixing device (Figure 8.1) was integrated onto the microfluidic chip for localised analysis. The input and output capillaries and the digestion well are labelled.

A protein microfluidic channel was created by passing a polyimide coated glass capillary (OD. 153 μm, ID. 75 μm; Polymicro Technologies, Phoenix, AZ, USA) through a 12 cm long stainless steel metal capillary (OD. 318 μm, ID. 158.75 μm). The distal end of the glass capillary was sealed with fused silica by cutting with high laser power and a notch was cut 2 mm from the sealed end. The distal end of the glass capillary was then pulled back until it was flush with the metal capillary and soldered into one of the proximal channels on the PMMA substrate. The proximal end of the mixing channel was pressure-fit into polytetrafluoroethylene (PTFE) tubing and connected to a T-union which created the entrance for both the protein and D_2O. Two metal capillaries (OD. 400 μm, ID. 200 μm; Small Parts, Inc., Miramar, FL, USA) were soldered into the distal and the remaining proximal channel of the device using a soldering iron. Glass capillaries were passed through the metal capillaries prior to soldering to prevent blockages and these were removed once the metal capillaries were firmly held in place. The proximal capillary served as the inlet and was connected to the high-voltage power supply of the mass spectrometer, while the distal capillary served as the ESI source.

A piece of silica was cut to fit the engraved PMMA substrate to create a liquid-tight seal around the reaction well. Pepsin agarose (~15 mg) was spread over the digestion 'well' and activated using 1 M HCl. A second blank PMMA substrate was used as a cover over top of the silica seal. The chip and cover were placed in a custom built clamp (LAC Machine & Tooling Limited, ON, Canada) to pressure-seal the microfluidic device (Figure 8.3).

Figure 8.3 The assembled microfluidic chip for site-specific hydrogen-deuterium exchange experiments. The capillary-based protein-deuterium rapid mixing device (Figure 8.1) was integrated onto the microfluidic chip (Figure 8.2) for localised analysis. The input and output capillaries are labelled.

8.7.4.2 ESI coupled proteolytic experiments

The microfluidic chip was interfaced with a modified QSTAR Elite hybrid quadrupole time-of-flight (QqTOF) mass spectrometer (Sciex, MDS Analytical Technologies, Concord, ON). The instrument was operated in positive ion mode with optimal running conditions of +4600 V to +5000 V source voltage.

Fluids were introduced into the device using Harvard 11+ infusion pumps (Holliston, MA). Protein and D_2O were introduced to the protein-deuterium mixing device channel in a 1:3 ratio and these followed a laminar flow pattern until they reach the notch, where they were mixed for base catalysed reaction (deuteration). Flow rates of 1 μL/min for protein solution and 3 μL/min of D_2O were able to achieve labeling times of 59 ms to 3 s. The reaction time was adjusted by changing the position of the mixing capillary within the channel; pulling the mixing capillary back increased the dead space after mixing, thus increasing the reaction time. Flow from the mixing capillary immediately contacted the

flow of 12.5% acetic acid (8 µL/min) from the acid channel within the microfluidic chip, resulting in immediate reaction quenching by reduction of pH to ~2.6 (acid catalysed reaction). The protein-D_2O-acid mix then continued to flow across the pepsin beads where pepsin digestion occurred and out through the distal ESI source capillary. Voltage was applied to the capillary creating a gas 'spray' of peptides which was detected on the QqTOF-MS. The samples were scanned over the 400–1500 m/z range.

8.7.4.3 Peptide identification

The resulting digests of each of the proteins were analysed using the FindPept tool on the ExPASy Proteomics server (Swiss Institute of Bioinformatics, Basel, Switzerland). The search field was set to pepsin (Porcine A) as the digestive enzyme at pH >2, with a mass tolerance of ± 0.5 Da. Confirmation of any ambiguous peptides was carried out using collision-induced dissociation (CID), involving peptide fragmentation and identification of product ions using mass spectrometry.

8.7.4.4 Localised data analysis

All mass spectrometry spectra analyses were carried out using the mMass software, version 5.5.0.[24] Deuterium uptake was computed using software for isotopic distribution analysis (Centre for Research in Mass Spectrometry, York University, ON, Canada), and normalised to the maximum deuterium uptake of 75%. Deuterium exchange kinetics were plotted over time and fit to an exponential function: $y=y0 + a(1-e^{-kt})$.[22] Protein structures were rendered using PyMOL (The PyMOL Molecular Graphics System, Version 1.7.x, Schrödinger, LLC).

8.8 Molecular dynamics simulations

Molecular dynamics simulations were carried out by collaborators, Ben Porebski and Ashley Buckle (Monash University, Melbourne) using the X-ray crystal structures of wild-type and A301T that were solved in this study (Chapers Two and Five).

Molecular dynamics simulations were carried out on prepared systems of wild-type PK1 and the respective A301T structures in a tetrameric biological assembly. Missing atoms, side chains and residues were rebuilt using Modeller V. 9.12.[25] In each instance, 50 models were generated and the lowest DOPE (Discrete Optimized Protein Energy) scoring

model was selected. Chain termini were capped with neutral groups (acetyl and methylamide) and residues were protonated as per their states in pH 7.

Completed structures were solvated in a rectangular simulation box with a minimum distance between any protein atom and the box wall being 10 Å. System charges were neutralised with respective sodium or chloride counter ions. Protein and ions were modelled using the CHARMM 36 force field.[26] Water was modelled using the 3-particle TIP3P force field.[27] All bonds involving hydrogen atoms were constrained to their equilibrium lengths with the SHAKE algorithm.[28] The resulting systems were subjected to at least 10,000 steps of energy minimisation to remove any clashes, followed by an equilibration protocol. During equilibration, harmonic positional restraints of 10 *k*cal/mol/Å^2 were applied to the protein backbone atoms, pressure was kept at 1 atm using Berendsen algorithm[29] and the temperature was increased from -260 °C to 27 °C as a linear function of time over the course of 1.2 ns, with Langevin temperature coupling. Relaxation times for temperature and pressure were 0.5 ps. Subsequently, the restraints were removed and a 5 ns simulation was performed at constant isotropic pressure of 1 atm and temperature of 27 °C. Electrostatic interactions were computed using an 8 Å cut-off radius and the Particle Mesh Ewald method for long-range interactions.[30] All molecular dynamics simulations (equilibration and production) were carried out under periodic boundary conditions.

Production simulations were carried out in the isothermal-isobaric ensemble. Temperature was kept at 300 K using the Langevin thermostat with a collision frequency of 2 ps, whilst Berendsen pressure coupling was used to maintain the pressure at 1 atm with a 2 ps relaxation time. The simulation time step was 2 fs and snapshots were taken every 100 ps. Simulations were run in duplicate with NAMD 2.9 for 500 ns.[31]

8.9 References

[1] Green, MR, and Sambrook, J. (2012) *Molecular Cloning: A Laboratory Manual*, 4th ed., Cold Spring Harbor Laboratory Press.

[2] Mattevi, A, Rizzi, M, and Bolognesi, M. (1996) New structures of allosteric proteins revealing remarkable conformational changes, *Curr. Opin. Struct. Biol. 6*, 824-829.

[3] Mattevi, A, Bolognesi, M, and Valentini, G. (1996) The allosteric regulation of pyruvate kinase, *FEBS Lett. 389*, 15-19.

[4] Gasteiger, E, Gattiker, A, Hoogland, C, Ivanyi, I, Appel, RD, and Bairoch, A. (2003) ExPASy: The proteomics server for in-depth protein knowledge and analysis, *Nucleic Acids Res. 31*, 3784-3788.

[5] Bradford, MM. (1976) A rapid and sensitive method for the quantitation of microgram quantities of protein utilizing the principle of protein-dye binding, *Anal. Biochem. 72*, 248-254.

[6] Malcovati, M, and Valentini, G. (1982) AMP- and fructose 1,6-bisphosphate-activated pyruvate kinases from *Escherichia coli*, *Methods Enzymol. 90*, 170-179.

[7] Hill, A. (1910) The possible effects of the aggregation of the molecules of haemoglobin on its dissociation curves, *J. Phys. 40*, i-vii.

[8] Morgan, HP, McNae, IW, Nowicki, MW, Hannaert, V, Michels, PAM, Fothergill-Gilmore, LA, and Walkinshaw, MD. (2010) Allosteric mechanism of pyruvate kinase from *Leishmania mexicana* uses a rock and lock model, *J. Biol. Chem. 285*, 12892-12898.

[9] Niesen, FH, Berglund, H, and Vedadi, M. (2007) The use of differential scanning fluorimetry to detect ligand interactions that promote protein stability, *Nat. Protoc. 2*, 2212-2221.

[10] Konarev, PV, Volkov, VV, Sokolova, AV, Koch, MHJ, and Svergun, DI. (2003) PRIMUS: a Windows PC-based system for small-angle scattering data analysis, *J. Appl. Crystallogr. 36*, 1277-1282.

[11] Svergun, D, Barberato, C, and Koch, M. (1995) CRYSOL-a program to evaluate X-ray solution scattering of biological macromolecules from atomic coordinates, *J. Appl. Crystallogr. 28*, 768-773.

[12] Mattevi, A, Valentini, G, Rizzi, M, Speranza, ML, Bolognesi, M, and Coda, A. (1995) Crystal structure of *Escherichia coli* pyruvate kinase type I: Molecular basis of the allosteric transition, *Structure 3*, 729-741.

[13] Kabsch, W. (2010) Xds, *Acta Crystallogr. D Biol. Crystallogr. 66*, 125-132.

[14] Evans, P. (2005) Scaling and assessment of data quality, *Acta Crystallogr. D Biol. Crystallogr. 62*, 72-82.

[15] Winn, MD, Ballard, CC, Cowtan, KD, Dodson, EJ, Emsley, P, Evans, PR, Keegan, RM, Krissinel, EB, Leslie, AGW, and McCoy, A. (2011) Overview of the CCP4 suite and current developments, *Acta Crystallogr. D Biol. Crystallogr. 67*, 235-242.

[16] McCoy, AJ, Grosse-Kunstleve, RW, Adams, PD, Winn, MD, Storoni, LC, and Read, RJ. (2007) Phaser crystallographic software, *J. Appl. Crystallogr. 40*, 658-674.

[17] Murshudov, GN, Vagin, AA, and Dodson, EJ. (1997) Refinement of macromolecular structures by the maximum-likelihood method, *Acta Crystallogr. D Biol. Crystallogr. 53*, 240-255.

[18] Adams, PD, Afonine, PV, Bunkóczi, G, Chen, VB, Davis, IW, Echols, N, Headd, JJ, Hung, L-W, Kapral, GJ, and Grosse-Kunstleve, RW. (2010) PHENIX: a comprehensive Python-based system for macromolecular structure solution, *Acta Crystallogr. D Biol. Crystallogr. 66*, 213-221.

[19] Wilson, DJ, and Konermann, L. (2003) A capillary mixer with adjustable reaction chamber volume for millisecond time-resolved studies by electrospray mass spectrometry, *Anal. Chem. 75*, 6408-6414.

[20] Rob, T, Liuni, P, Gill, PK, Zhu, S, Balachandran, N, Berti, PJ, and Wilson, DJ. (2012) Measuring dynamics in weakly structured regions of proteins using microfluidics-enabled subsecond H/D exchange mass spectrometry, *Anal. Chem. 84*, 3771-3779.

[21] Resetca, D, and Wilson, DJ. (2013) Characterizing rapid, activity‐linked conformational transitions in proteins via sub‐second hydrogen deuterium exchange mass spectrometry, *FEBS J. 280*, 5616-5625.

[22] Resetca, D, Haftchenary, S, Gunning, PT, and Wilson, DJ. (2014) Changes in signal transducer and activator of transcription 3 (STAT3) dynamics induced by complexation with pharmacological inhibitors of Src homology 2 (SH2) domain dimerization, *J. Biol. Chem. 289*, 32538-32547.

[23] Rob, T, and Wilson, DJ. (2009) A versatile microfluidic chip for millisecond time-scale kinetic studies by electrospray mass spectrometry, *J. Am. Soc. Mass Spectrom. 20*, 124-130.

[24] Strohalm, M, Kavan, D, Novak, P, Volny, M, and Havlicek, V. (2010) mMass 3: a cross-platform software environment for precise analysis of mass spectrometric data, *Anal. Chem. 82*, 4648-4651.

[25] Eswar, N, Webb, B, Marti-Renom, MA, Madhusudhan, MS, Eramian, D, Shen, MY, Pieper, U, and Sali, A. (2007) Comparative protein structure modeling using MODELLER, *Curr Protoc Protein Sci Chapter 2*, Unit 2 9.

[26] Huang, J, and MacKerell, AD, Jr. (2013) CHARMM36 all-atom additive protein force field: validation based on comparison to NMR data, *J. Comput. Chem. 34*, 2135-2145.

[27] Jorgensen, W, Chandrasekhar, J, Madura, J, Impey, R, and Klein, M. (1983) Comparison of simple potential functions for simulating liquid water., *J. Chem. Phys. 79*, 926-911.

[28] Lippert, RA, Bowers, KJ, Dror, RO, Eastwood, MP, Gregersen, BA, Klepeis, JL, Kolossvary, I, and Shaw, DE. (2007) A common, avoidable source of error in molecular dynamics integrators, *J. Chem. Phys. 126*, 046101.

[29] Berendsen, H, Postma, J, van Gunsteren, W, DiNola, A, and Haak, J. (1984) Molecular dynamics with coupling to an external bath, *J. Chem. Phys. 81*, 3684.

[30] Darden, T, York, D, and Pedersen, L. (1993) Particle mesh Ewald: An N·log(N) method for Ewald sums in large systems., *J. Chem. Phys. 98*, 10089.

[31] Phillips, JC, Braun, R, Wang, W, Gumbart, J, Tajkhorshid, E, Villa, E, Chipot, C, Skeel, RD, Kale, L, and Schulten, K. (2005) Scalable molecular dynamics with NAMD, *J. Comput. Chem. 26*, 1781-1802.